AD-A184 856 EXPERIMENTAL STUDY OF THE FLUID MECHANICS OF UNSTEADY TURBULENT BOUNDARY LAYERS(U) STANFORD UNIV CA THERMOSCIENCES DIV G J BRERETON ET AL MAY 87 TF-29 1/3

UNCLASSIFIED ARO-19976 4-EG DAAG29-83-K-0056 F/G 20/4 NL

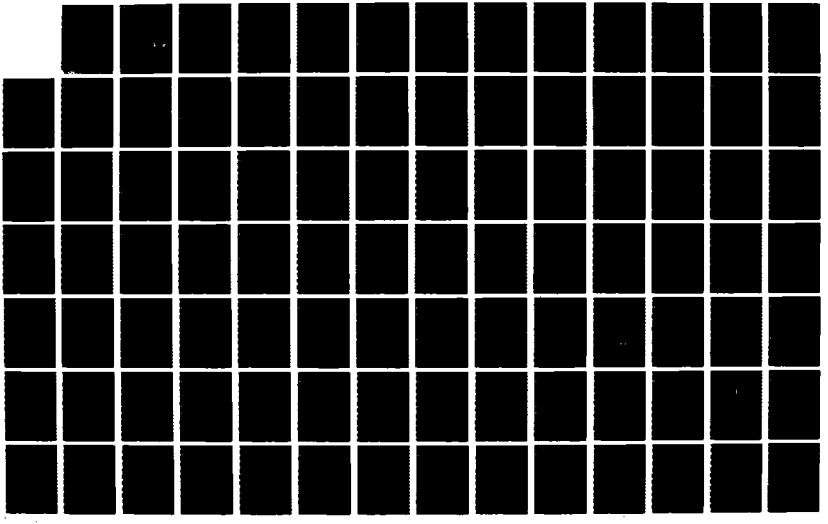

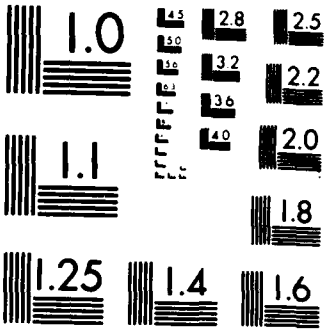

(2)

EXPERIMENTAL STUDY OF THE FLUID MECHANICS OF UNSTEADY TURBULENT BOUNDARY LAYERS

by

G. J. Brereton
and
W. C. Reynolds

Prepared with the support of the
Army Research Office
under Contract DAAG 29-83-K-0056

Report TF-29

Thermosciences Division
Department of Mechanical Engineering
Stanford University
Stanford, California 94305

May 1987

REPORT DOCUMENTATION PAGE

1a. REPORT SECURITY CLASSIFICATION Unclassified	1b. RESTRICTIVE MARKINGS
2a. SECURITY CLASSIFICATION AUTHORITY	3. DISTRIBUTION/AVAILABILITY OF REPORT Approved for public release; distribution unlimited.
2b. DECLASSIFICATION/DOWNGRADING SCHEDULE	
4. PERFORMING ORGANIZATION REPORT NUMBER(S)	5. MONITORING ORGANIZATION REPORT NUMBER(S) ARO 19976.4-EG
6a. NAME OF PERFORMING ORGANIZATION Stanford University 6b. OFFICE SYMBOL (If applicable)	7a. NAME OF MONITORING ORGANIZATION U. S. Army Research Office
6c. ADDRESS (City, State, and ZIP Code) Stanford, CA 94305	7b. ADDRESS (City, State, and ZIP Code) P. O. Box 12211 Research Triangle Park, NC 27709-2211
8a. NAME OF FUNDING/SPONSORING ORGANIZATION U. S. Army Research Office 8b. OFFICE SYMBOL (If applicable)	9. PROCUREMENT INSTRUMENT IDENTIFICATION NUMBER DAAG29-83-K-0056
8c. ADDRESS (City, State, and ZIP Code) P. O. Box 12211 Research Triangle Park, NC 27709-2211	10. SOURCE OF FUNDING NUMBERS PROGRAM ELEMENT NO. / PROJECT NO. / TASK NO. / WORK UNIT ACCESSION NO.

11. TITLE (Include Security Classification)
Experimental Study of the Fluid Mechanics of Unsteady Turbulent Boundary Layers

12. PERSONAL AUTHOR(S)
G. J. Brereton and W. C. Reynolds

13a. TYPE OF REPORT	13b. TIME COVERED	14. DATE OF REPORT (Year, Month, Day)	15. PAGE COUNT
Final	FROM 3/7/83 TO 6/1/86	May 1987	240

16. SUPPLEMENTARY NOTATION
The view, opinions and/or findings contained in this report are those of the author(s) and should not be construed as an official Department of the Army position, policy, or decision, unless so designated by other documentation.

17 COSATI CODES		
FIELD	GROUP	SUB-GROUP

18. SUBJECT TERMS (Continue on reverse if necessary and identify by block number)
Fluid Mechanics, Boundary Layers, Turbulent Boundary Layers, Turbulence Modelers, Free-Stream Unsteadiness, Fluid Motion

19. ABSTRACT (Continue on reverse if necessary and identify by block number)

An experimental study of the effects of forced, free-stream unsteadiness on turbulent boundary layers was undertaken in an effort to characterize the nature of such flows and to provide guidance for turbulence modelers. A turbulent boundary layer, which had developed under steady, constant-pressure conditions, was locally subjected to a range of frequencies of sinusoidal free-stream unsteadiness. The response of the boundary layer to these free-stream effects was studied through simultaneous

20. DISTRIBUTION/AVAILABILITY OF ABSTRACT ☐ UNCLASSIFIED/UNLIMITED ☐ SAME AS RPT. ☐ OTIC USERS	21. ABSTRACT SECURITY CLASSIFICATION Unclassified
22a. NAME OF RESPONSIBLE INDIVIDUAL	22b. TELEPHONE (Include Area Code) / 22c. OFFICE SYMBOL

20. ABSTRACT CONTINUED

measurements of the u and v components of the velocity field, using a two-color laser-Doppler anemometer.

To focus on the distinct behaviors of the deterministic and time-averaged fields of flow, the equations of fluid motion were reformulated according to a triple decomposition of velocity and pressure into: (*i*) a time-averaged measure, (*ii*) a deterministic or organized, unsteady measure, and (*iii*) a turbulent measure.

EXPERIMENTAL STUDY OF THE FLUID MECHANICS

OF

UNSTEADY TURBULENT BOUNDARY LAYERS

by

G. J. Brereton

and

W. C. Reynolds

Prepared with the support of the

Army Research Office

under Contract DAAG 29-83-K-0056

Report TF-29

Thermosciences Division

Department of Mechanical Engineering

Stanford University

Stanford, California 94305

May 1987

Acknowledgements

The authors gratefully acknowledge the financial support of the Army Research Office under contract DAAG 29-83-K-0056.

They wish to extend special thanks to Professors B. Cantwell and J. Koseff, and to Dr. L. Carr, for reviewing the manuscript and providing constructive criticism. The contributions of several present and former members of the Thermosciences Division are also greatly appreciated. They include:

Professors J. Johnston and J. Eaton, for their advice, suggestions, and their continued interest in this study.

Drs. A. Naqwi and R. Barlow for sharing their expertise in optical matters.

Dr. R. Jayaraman for his key contributions to earlier phases of this study.

Mrs. A. Ibaraki, Ms. C. Mortensen, Mr. R. Dodge and Mr. K. Marshall for their secretarial and administrative assistance throughout the course of the project.

Mr. R. Birch and Mr. L. Johal for lending their skills to the fabrication of equipment for the experiments.

The first author would also like to acknowledge the generosity of the United States–United Kingdom Educational Commission in supporting a year of his residence at Stanford under a Fulbright-Hays Travel and Maintenance grant.

Abstract

An experimental study of the effects of forced, free-stream unsteadiness on turbulent boundary layers was undertaken in an effort to characterize the nature of such flows and to provide guidance for turbulence modelers. A turbulent boundary layer, which had developed under steady, constant-pressure conditions, was locally subjected to a range of frequencies of sinusoidal free-stream unsteadiness. The response of the boundary layer to these free-stream effects was studied through simultaneous measurements of the u and v components of the velocity field, using a two-color laser-Doppler anemometer.

To focus on the distinct behaviors of the deterministic and time-averaged fields of flow, the equations of fluid motion were reformulated according to a triple decomposition of velocity and pressure into: (*i*) a time-averaged measure, (*ii*) a deterministic or organized, unsteady measure, and (*iii*) a turbulent measure.

Experimental results of this study confirmed that the time-averaged behavior of the flow was largely invariant with frequency of forced unsteadiness and similar to that of steady flow under the corresponding mean conditions. However, the dynamic responses of the velocity and turbulence fields to forced unsteadiness were strongly dependent on frequency. While the dynamic response of the streamwise velocity appeared to be well described in terms of variation between asymptotic high- and low-frequency forms of the momentum equation, considerations of the unsteady energy budgets were necessary to characterize the dynamic turbulence response. Inter-component transfer of turbulent kinetic energy was identified as an important feature of the dynamic response of the turbulence field. When normalized by the local anisotropy of the dynamic turbulent stress tensor, the time scale of inter-component energy transfer was invariant with the frequency of forced unsteadiness and similar in size to the value expected in steady flow under comparable mean conditions.

Table of Contents

List of Tables

List of Figures

Nomenclature

Roman Symbols

A	Amplitude of oscillation of the free-stream velocity, at the end of the test section.
a, b	General variables of unsteady, turbulent, fluid flow.
C	Constant of Coles' mean velocity function.
C_f	Friction coefficient.
D_c	Boundary-layer thickness deduced from fitting Coles' mean velocity function to a profile (see §5.1).
f	General time-dependent variable of turbulent fluid flow (§2.1).
f	Frequency.
H	Shape factor.
k	Turbulent kinetic energy.
L	Length of the test section.
ℓ	Mixing length.
ℓ_S	Dimensionless parameter for unsteady flow, representative of the Stokes-layer thickness. It is defined as: $\sqrt{2\nu/\omega}$.
ℓ_S^+	Dimensionless parameter for unsteady flow, $\sqrt{2u_\tau^2/(\nu\omega)}$.
N	Number of elements, usually in a summation.
n	General integer variable.
P	Mean pressure.
p	Pressure.
p'	Turbulent pressure fluctuation.
q^2	Twice the turbulent kinetic energy.
Re	Reynolds number.

Re_{δ_2}	Momentum-thickness Reynolds number.
S_X	Strouhal number based on streamwise distance, defined as: $\omega X/U_0$.
S_δ	Strouhal number based on local boundary-layer thickness, defined as: $\omega X/U_0$.
t	Time.
t_0	Reference time.
U	Streamwise mean velocity.
U_c	Streamwise mean velocity for convection of eddies.
U_0	Mean velocity in the free stream, at the entrance to the test section.
U_i	Component of the mean velocity vector.
u_i	Component of the velocity vector.
u_τ	Friction velocity.
u', v', w'	Streamwise, normal and spanwise components of the turbulent velocity fluctuations.
u	Velocity vector.
V	Normal mean velocity.
W	Spanwise dimension of the test section.
X	Streamwise distance along the test section.
X'	Fractional streamwise distance along the test section.
x	Streamwise coordinate.
x, y	Position vectors.
y	Normal coordinate.
y^+	Normal coordinate in wall units.
Z	Spanwise distance from the centerline of the test section.
z	Spanwise coordinate.

Greek Symbols

Δt	Time increment.
δ	Boundary-layer thickness.
$\delta(\ \ )$	Estimate of the uncertainty in a quantity (Appendix E).
δ_1	Displacement thickness.
δ_2	Momentum thickness.
ϵ	Dissipation of turbulent kinetic energy.
η	Kolmogoroff length scale.
η	General transformation characteristic.
κ	Von-Karman constant in Coles' mean velocity function.
κ	Half angle of intersection of two laser beams.
λ	Wavelength.
ν	Kinematic viscosity.
ν_t	Eddy viscosity.
ξ	General transformation characteristic.
ρ	Density.
τ	Period of an organized, unsteady event.
υ	Kolmogoroff velocity scale.
$\phi_{n,f}$	Phase of the nth Fourier mode of the periodic function f.
Ω_i	Component of the mean vorticity vector.
ω	Angular velocity.
ω_i	Component of the vorticity vector.
ω_i'	Component of the vector of turbulent vorticity fluctuations.
ω^+	Dimensionless parameter for unsteady flow, defined as: $\omega\nu/u_\tau^2$.

Other Symbols

$\overline{\quad}$	Average over time.
$\langle \quad \rangle$	Average performed at the same phase in each of a series of periodic events.
$\tilde{\quad}$, $\overline{\quad}$	Deterministic or periodic component of an unsteady quantity.
$\hat{\quad}_n$	Amplitude of the nth Fourier mode of a quantity.
$\lvert \quad \rvert$	Modulus of a quantity.
∞	The free-stream value of a quantity, when used as a subscript.
$'$	Derivative of a quantity, when used as a superscript (Appendix D).

1. Introduction

Scientific study of *sinuous* or turbulent fluid mechanics has been actively pursued since the pioneering work of Osborne Reynolds in the 1880's. A century of experiments and analyses have yielded many *laws*, revealed new phenomena and formulated engineering techniques with which to attempt prediction of fluid behavior. Yet the fundamental understanding of turbulence remains incomplete.

The original methods of mathematical analysis and experimental investigation are now augmented by computational prediction of fluid flow. However, restrictions on computer size and on the lengths of time required for calculations are such that it is unlikely that the complete differential equations governing viscous fluid behavior could be solved, for complex turbulent flows at high Reynolds numbers, for many years to come. Compromises must therefore be made and solutions are sought to equations rendered less complex, using techniques of averaging and simplifying assumptions and approximations. Through experimental investigation, information lost in averaging may be supplied, the validity of assumptions may be tested and the use of approximation may be substantiated. In this way, interaction between experiment, analysis, and computation leads to better understanding of the phenomenon of turbulence.

New heights of sophistication in experimental techniques have been brought about by innovations in instrumentation and by the ease with which computers may be utilized to perform repetitive functions with great speed. The advent of the laser-Doppler anemometer has made non-intrusive, instantaneous measurement of fluid velocities practicable in experiments. Moreover computers may be programmed to both sample data and actively vary and control the conditions of the experiment itself. These developments make possible study of a class of flows formerly thought too complex for detailed experimental investigation — organized unsteady turbulent flows.

1.1 Motivation

Unsteady, turbulent, boundary-layer flows are the class of wall-bounded turbulent flows in which the bulk fluid undergoes some well-defined, time-dependent motion relative to the wall. Common examples of organized, unsteady, relative motion include:

(*i*) the moving boundary in a nominally stationary bulk fluid, as in Stokes' treatise on the motion of pendulums in a viscous fluid (Stokes 1851) or the flow of air over the rotors of a helicopter in forward flight,

(*ii*) the stationary wall bounding a mainstream undergoing some kind of organized unsteadiness — the kind of flow found between stator blades downstream of a rotary stage in an axial compressor.

In this study, an experimental investigation into the behavior of a turbulent, boundary-layer flow undergoing sinusoidal mainstream unsteadiness is carried out. Measurements of the response of the boundary layer to different frequencies of forced mainstream unsteadiness are made in an effort to provide deeper insights into the nature of turbulence under unsteady conditions and to generate target data against which computer-prediction schemes might be compared and refined.

The ultimate goal of this field of research is both understanding of and accurate prediction of unsteady flowfields in situations ranging from flow over accelerating airfoils to blood flow through the heart.

1.2 Experimental Studies

Summaries of experimental studies of unsteady turbulent flow are now presented. To focus on research most relevant to the present work, the material of this section is restricted to developing turbulent boundary-layer flows and to fully-developed turbulent channel and pipe flows.

Unsteady Turbulent Boundary-Layer Experiments

The effects of imposed, organized unsteadiness on turbulent boundary layers have been under experimental and theoretical study for some time. In 1959, Karlsson reported the results of an experiment conducted under mean, zero-pressure-gradient conditions, in which sinusoidal variations in mainstream velocity were imposed upon a free stream of otherwise constant mean velocity. Through measurements of streamwise components of velocity, he found that the mean values of unsteady velocity within the boundary layer were unaffected by either amplitude or frequency of the imposed perturbation field, although he noted slight differences between the mean quasi-steady velocity profile and the corresponding steady one. He also reported that the near-wall perturbation velocity always led the free stream, in agreement with the laminar analysis of Lighthill (1954).

The imposition of an oscillating core velocity in a diffuser enabled Schachenmann & Rockwell (1976) to extend experimental study of unsteady turbulent boundary layers to flows, the mean pressure gradients of which were adverse. In surveys of the streamwise component of velocity, their hot-wire anemometer measurements exhibited no effects of unsteadiness in mean unsteady profiles or momentum or displacement thicknesses over a range of frequencies. Amplitudes and phases of the fluctuating component of velocity were strongly dependent on the Strouhal number of the unsteady flow.

Cousteix and his co-workers have studied unsteady flows with a view to developing prediction methods. Their preliminary results (Cousteix *et al.* 1977) were from a wind-tunnel experiment in which oscillation in the main stream was induced in the form of a travelling wave. Using hot-wire and cross-wire anemometers, they made measurements at a single frequency of oscillation of streamwise velocity, correlation coefficient, Reynolds stresses and the probability density functions for the streamwise turbulence measure. At this frequency of imposed unsteadiness, the correlation coefficient appeared almost constant throughout each unsteady cycle,

approximately at its expected value in the corresponding steady turbulent boundary layer.

In later experiments, they studied unsteady flows of both mean-zero and mean-adverse gradients in pressure, with particular emphasis placed on extensive streamwise documentation of the flow. In regions where reverse flow was anticipated, a laser-Doppler anemometer was used for velocity measurements. The mainstream oscillation was again generated as a travelling wave along the core flow of the wind tunnel. They reported strong spatial periodicity in the phase and amplitude of integral parameters such as momentum thickness, displacement thickness and shape factor. While the mean unsteady flow was in good agreement with the corresponding steady flow, the phase and amplitude of the unsteady component of velocity underwent continued development in the streamwise direction and no tendency towards an asymptotic shape was observed. These results were presented and discussed in detail in their later review (Cousteix & Houdeville 1983).

A more recent work (Cousteix & Houdeville 1985) included measurements of skin friction, and amplitudes and phases of wall shear stress in unsteady flow. A heated-element gauge was used to deduce these measurements, a satisfactory frequency response having been obtained by the positioning of the element of the gauge above a cavity in the test surface. They measured advances in phase (relative to the perturbing flow) significantly greater than the asymptotic value suggested by quasi-laminar analysis for high frequency unsteadiness. They also reported near-wall data from different experiments to be well grouped when plotted against an unsteady dimensionless parameter based on kinematic viscosity, frequency of unsteadiness and mean friction velocity.

The studies of Patel (1977) and Kenison (1977) concerned wind-tunnel experiments in which low frequencies of unsteadiness were imposed on boundary layer flows in the form of a longitudinal travelling wave. Hot-wire anemometers were used to deduce streamwise measures of velocity. In Patel's zero-pressure-gradient experiment, he reported a welcome insensitivity in measures of the mean flow to

systematically varied frequencies of unsteadiness. Measurements across the boundary layer of phase lag (relative to the wave motion of the main flow) and amplitude of oscillation in velocity were strongly dependent on the wave's frequency. Peak amplitude and phase lag grew with increased frequency, but no spatial periodicity in any measurements was reported. Kenison's study dealt with a flow of mean-adverse gradient in pressure; his data indicated a monotonic increase in phase lag across the boundary layer, with increased downstream distance (and static pressure in the free stream).

In an earlier experiment in the facility used for this study, Jayaraman *et al.* (1982) performed a detailed investigation into the effects of locally imposed free-stream unsteadiness on a turbulent boundary layer. The mainstream condition was one of a mean-adverse pressure gradient, the strength of which increased with downstream distance. Upstream of the region where unsteadiness was imposed, an almost steady turbulent boundary layer developed under zero-pressure-gradient conditions. Thus the study was not complicated by history effects due to unsteady laminar boundary-layer development and unsteady transition. They reported streamwise velocity measurements made with a laser-Doppler anemometer in a water-tunnel experiment. Careful validation of the upstream development and spanwise uniformity of the flow was carried out and the measured and prescribed unsteady fields of flow were in good agreement. Their turbulence measurements over the inner quarter of the flat-plate, constant-pressure boundary layer were somewhat lower than those of Klebanoff (1955) and this discrepancy was attributed to Reynolds-number effects. However, the measurements of the present investigation, made under almost identical conditions, did not suffer from this shortcoming and so it was thought to be a single anomalous result in their study.

Their experiments covered a wide range of Strouhal number through systematic variation of the imposed frequency and amplitude. They found an expected insensitivity of the time-averaged flow to imposed unsteadiness and identified two asymptotic regimes for the periodic velocity field — an inertial regime at low Strouhal num-

bers and a regime dominated by the pressure gradient for high Strouhal numbers. At high frequencies, the unsteady velocity field was compared with the quasi-laminar Stokes solution. While results for the phase were generally in good agreement, the measured amplitudes of the perturbation velocity were consistently smaller than the analytic predictions, though of similar shape.

Brereton *et al.* (1985) investigated the effects of abrupt changes in mainstream velocity on the same turbulent boundary layer, in a closely related study. In the facility used by Jayaraman *et al.* (1982), the response of an initially steady, zero-pressure-gradient, turbulent boundary layer to an abrupt decrease in free-stream velocity was monitored through measurements of streamwise components of the velocity field. When the flow had reached its equilibrium state under the new, adverse-pressure-gradient conditions, the mainstream velocity underwent a rapid increase to restore conditions of constant pressure. The complementary response of the boundary layer to this abrupt change was then recorded. The dynamic response of streamwise velocity measures to abrupt, ramp-like changes in free-stream velocity was in good agreement with the analytic solution of the Stokes equation describing those changes. In the subsequent relaxations to equilibrium states, the changes in integral parameters such as momentum and displacement thickness decayed almost exponentially to their asymptotic values, which were reached in about two "times of flight" of the free stream.

Ramaprian and his co-workers have conducted a wide range of experiments in unsteady boundary-layer flows and pipe flows. Measurements of streamwise velocity and Reynolds stresses were made with laser-Doppler anemometers in oil and water flows. In a time-mean, constant-pressure flow, Menendez & Ramaprian (1983) studied the development of a periodic turbulent boundary layer. They found that the imposed unsteadiness accelerated the streamwise spatial development of the mean condition of the outer part of the boundary layer, while it had little affect on the inner layer. At large Reynolds numbers, the expected agreement between mean unsteady values and the corresponding steady ones was approached. The thickness

of the unsteady layer over which viscous effects were significant was characterized by the ratio of the mean friction velocity to the frequency of perturbation, in agreement with the findings of Ramaprian & Tu (1982). Measurements of the shear stress at the wall were made with a heat-flux gauge and were of similar amplitude to those measured under the corresponding quasi-steady conditions.

Ramaprian & Menendez (1983) also characterized unsteady turbulent flows by the sizes of three time scales, corresponding to the frequency of oscillation, an outer scale based on the friction velocity and boundary-layer thickness, and an inner scale based on friction velocity and kinematic viscosity. Moreover they found some agreement between features of unsteady-flow experiments conducted under different conditions, when compared within regimes bounded by ranges of these time scales.

Unsteady Turbulent Pipe-Flow Experiments

In a study of oscillatory, fully-developed pipe flow (Ramaprian & Tu 1979), the imposed unsteadiness was at a frequency near the estimated turbulent burst frequency in the equivalent steady pipe flow. The authors noted that the turbulence intensities generally appeared "frozen" at their time-averaged state throughout the unsteady cycle. They deduced values of shear stress from measured velocity profiles and found that the shear stress was also "frozen" beyond the equivalent quasi-laminar Stokes layer. Within this layer, the shear stress followed the mainstream oscillations, with a lag in phase.

Using an electro-chemical probe, Mao & Hanratty (1985) made measurements of the wall shear in unsteady turbulent pipe flow. Their measures of the phase and amplitude of the oscillating wall shear were well grouped when plotted as functions of the ratio of length scales proposed by Binder and his co-workers. In common with velocity-field measurements of Binder *et al.* (1981) and Jayaraman *et al.* (1982) near the wall, they reported amplitudes of wall shear which were noticeably lower than those predicted by quasi-laminar theory for perturbations at high frequencies.

Unsteady Turbulent Channel-Flow Experiments

In one of the first efforts directed towards the needs of turbulence modeling for unsteady flow, Acharya & Reynolds (1975) investigated the effects on fully-developed channel flow of sinusoidal unsteadiness imposed on the through-flow rate. A hot-wire anemometer was used to make measurements of mean and fluctuating components of streamwise velocity and turbulence across the flowfield. Using a cross-wire, measurements were made of the wall-normal velocity components and of Reynolds stresses, although the size and orientation of the probe precluded near-wall measures being taken. Little deviation was found between the mean unsteady measures of velocity, turbulence and Reynolds stress profiles, and the equivalent steady flow profiles. Differing thicknesses of Stokes layer — the near-wall region which accommodates unsteady effects of differing magnitude to the asymptotic unsteady free-stream values — were reported for the unsteady values of streamwise velocity and turbulence, and were attributed to effects of turbulence dynamics.

Binder & Kueny (1981) studied the problem of an unsteady, turbulent, fully-developed channel flow, with particular emphasis placed on taking measurements in the near-wall region. They used a laser-Doppler anemometer to make measurements of streamwise velocity components in a water flow and achieved extremely high spatial resolution through beam expansion. At high frequencies of imposed unsteadiness, the amplitude and phase of the velocity oscillations behaved as in quasi-laminar Stokes flow. At lower frequencies, this behavior was still observed for the amplitude but not the phase of the unsteady velocity component. The mean characteristics of the flow were unaffected by the forced oscillation in the through-flow rate.

They proposed as a characteristic parameter, for unsteady flows in the near-wall region, the ratio of the Stokes-layer-thickness parameter to the viscous length scale of the mean unsteady flow (the ratio of kinematic viscosity to the deduced friction velocity). The usefulness for characterization of unsteady flows of a Strouhal number

alone, based on a frequency, and outer length and velocity scales, was discounted; measurements at the same Strouhal number under varied experimental conditions may have had markedly different boundary-layer histories.

Later experiments were conducted at sufficiently large amplitudes of imposed oscillation in the through-flow rate that reverse flow was encountered at the wall (Binder *et al.* 1985). Measurements of the instantaneous wall shear were made using a hot-film gauge. Because of the directional insensitivity of this device, corrections were applied to deduce the values of wall shear where reverse flow was suspected (Pedley 1976). They reported measures of mean, oscillating and turbulent components of wall shear for systematic variations in frequency of oscillation, mean through-flow rate and amplitude of oscillation of through-flow rate. Their measurements were well grouped when plotted as functions of the ratio of Stokes-layer-thickness parameter to viscous length scale.

1.3 Computational Predictions

Acharya & Reynolds (1975) tested models for fully-developed turbulent channel flow in parallel with their experimental investigation. They chose to predict the mean and unsteady fields of flow separately, in the spirit of the commonly used triple decompositions of unsteady turbulent values of velocity and pressure. In computing the behavior of the mean flow, the equations were closed by solving the turbulent kinetic energy equation, modeling its unknown terms as functions of the turbulent kinetic energy. The Reynolds-stress tensor was modeled in terms of the turbulent kinetic energy and the mean strain rate. A formulation of the Prandtl-energy model was used to deduce the eddy viscosity. While this model predicted the mean velocity field accurately, discrepancies between computed and measured turbulence were as high as 20%.

In their attempts to calculate the unsteady behavior of the flow, they used a model which related the unsteady Reynolds stress to the unsteady velocity gradient through the mean eddy viscosity, and a model which allowed no dissipation of turbulent kinetic energy in the unsteady field; both performed poorly. Through decomposition of the turbulent kinetic energy equation into its unsteady counterpart, the "one equation" approach used to predict the mean flow was adopted and again the performance was poor. They concluded that a successful model would have to incorporate the dynamics of the Reynolds stresses, through inclusion of field equations which adequately represented the pressure-strain terms.

Another parallel study of an unsteady flow and prediction of its behavior was undertaken by Cook *et al.* (1985). In predicting their streamwise hot-wire measurements in an unsteady turbulent boundary layer in a wind tunnel, they used two scalar eddy-viscosity models. The quasi-steady Cebeci-Smith model was algebraic in form. A mixing-length expression was employed near the wall and Van Driest's function smoothed the transition to a constant outer value of eddy viscosity. The Glushko model used a differential equation to describe transport of turbulent kinetic energy in conjunction with an algebraic scale equation. It was considered the simplest model that explicitly included time dependence in the turbulence field, as distinct from the mean velocity field. The results of the Cebeci-Smith model were generally in better agreement with measurements than the Glushko model. The authors concluded that, at low frequencies of oscillation, the Cebeci-Smith turbulence model performed reasonably well.

In common with several other researchers, Menendez & Ramaprian (1982) tested simple, quasi-steady, turbulence-closure schemes on unsteady boundary-layer data sets. While their models, based on mixing length and on the Prandtl-energy model with prescribed length scale, enjoyed reasonable success in low-frequency calculations, at high frequencies they could not predict the dynamics of turbulence properties.

Launder and his co-workers predicted the pipe-flow experiments of Ramaprian & Tu (1981) using a number of k–ϵ schemes (Kebede *et al.* 1985). In an effort to improve upon earlier reliance on Boussinesq stress-strain relations, they proposed a set of rate equations for the modeling of the Reynolds stresses. Difficulties were encountered in achieving results independent of the size of time step, although as many as 2880 per cycle were tried. The results of this scheme were superior to those of Tu & Ramaprian (1983), who used an eddy-viscosity model (a phase-averaged form of the Prandtl-energy model) in a one-equation closure. They were also generally inferior to the predictions of the k–ϵ scheme used with an eddy-viscosity model. In conclusion, the authors speculated that the equation for ϵ computed an excessively varying length scale and so compensated for errors introduced by the Boussinesq stress-strain relation.

Blondeaux & Colombini (1985) obtained results in good agreement with the data of Tu & Ramaprian (1983) in their prediction of oscillating pipe flow. They extended Saffman's turbulence model, based on field equations for pseudo-energy and pseudo-vorticity, to cope with unsteady flows. The Reynolds stresses were expressed in terms of the ensemble-averaged strain tensor through an effective viscosity, which in turn was deduced from the ratio of pseudo-energy to pseudo-vorticity. They reported that the peak unsteady velocity coincided with the part of the cycle in which production played a fundamental role. During other parts of the cycle, dissipative effects, along with convective and diffusive effects, prevailed. They commented that mixing-length models would generally not be adequate for prediction of unsteady flows and that, for this particular calculation, the notion of a balance between production and dissipation terms did not seem appropriate. They further remarked that, for their study, the idea of instantaneous logarithmic laws applying to the unsteady flow seemed unrealistic.

Recently, Wilcox has applied a multi-scale turbulence model (Wilcox 1986) to the flow investigated in the experiments of Jayaraman *et al.* (1982) — the boundary layer in a mean-adverse pressure gradient, with an imposed, sinusoidal, free-

stream disturbance, the amplitude of which increased with streamwise distance. When compared with results of the low-amplitude experiment, predicted values of the mean, unsteady velocity and the phase and amplitude of the deterministic, streamwise, fluid velocity were in good agreement for all frequencies of imposed unsteadiness (Wilcox 1987). However, in attempts to predict the results of the high-amplitude experiment, separation was predicted prematurely — this shortcoming was thought to be due to the use of boundary-layer approximations in the prediction program, rather than limitations in the turbulence model. When the prediction technique was used for a flow, the most adverse condition of which was slightly less severe than that of Jayaraman's high-amplitude experiments, good agreement between prediction and experiment was found.

1.4 Objectives

To judge from recent computations of unsteady flows (Kebede *et al.* 1985, Blondeaux & Colombini 1985), progress has been made in extending sophisticated prediction techniques to the most readily modeled of unsteady flows — fully-developed turbulent pipe flow undergoing sinusoidal variations in through-flow rate. In the course of this progress, the need for more unsteady turbulent data sets of high accuracy and detail has been expressed frequently. Measurements of more than one component of the velocity field are scarce in the variety of experiments which have been conducted in nominally one- and two-dimensional flows. This shortage has limited the possibilities of making comparisons between measured and modeled quantities such as Reynolds stresses and turbulent kinetic energies; often the only clues to the performance of a scheme are provided by mean and unsteady profiles of streamwise velocity and turbulence measures. Therefore reliable experimental measurements of multiple components of the velocity field in unsteady flows are needed to provide suitable target data for turbulence modelers.

The unknown effects of different boundary-layer histories on unsteady developing turbulent flows have both complicated the comparison of results of different experiments, and hindered correct interpretation of unsteady turbulent behavior. In unsteady developing turbulent flows, this behavior can only be properly studied if the influence of upstream effects (for example, unsteady transition to turbulence, or growth of a boundary layer from a leading edge under unsteady conditions) is known to be either insignificant or absent. To date, no studies of the influence of such upstream effects have been reported. Hence experimental studies of flows with well defined upstream or initial conditions are desirable for the purposes of comparison with the results of turbulence models.

With the advent of the laser-Doppler anemometer, researchers have the capability of making non-intrusive, instantaneous measurements of several components of velocity in a fluid. However, when used for simultaneous measurement of multiple components of velocity, successful application of this measurement technique requires careful consideration to be given to the attributes of the particular experiment; it therefore requires thorough qualification *in situ* to assure accurate results.

This study was undertaken in an effort to fulfill some of these needs and had the following objectives:

(*i*) To make accurate measurements of two components of the velocity field, simultaneously, in an unsteady flowfield, for the purpose of identifying the influence on statistical and structural turbulence measures of organized unsteadiness.

(*ii*) To optimize the performance of a laser-Doppler anemometer for the particular experimental conditions and test it rigorously to assure the trustworthiness of subsequent measurements.

(*iii*) To make these measurements over a wide range of frequencies, in the absence of upstream effects.

The apparatus of Jayaraman *et al.* (1982) matched these requirements and the flow studied was one of local, sinusoidal, free-stream unsteadiness imposed on a boundary

layer in a mean-adverse pressure gradient. The boundary layer would develop under steady, constant-pressure conditions. The value of performing experiments in a flow of mean-adverse pressure gradient is evident through the need to control boundary-layer separation in decelerating flows. A better understanding of the effects on turbulence of organized unsteadiness might help to explain the role which imposed unsteadiness might play.

2. Mathematical Foundations

The mathematical framework within which the results of this study are to be examined is presented in this chapter. Although some of the material is found in earlier works on periodic turbulent flow (*e.g.* Hussain & Reynolds 1970), much of it was developed for the purposes of this particular study and so is included here in the interests of completeness.

Analysis of turbulent fluid flow is usually carried out through decomposition of the velocity and pressure into their mean and turbulent components. The well-known Reynolds-averaging technique is then employed to deduce separate equations of motion for the mean and turbulent fields; the formation of these equations is a frequent point of departure for more sophisticated forms of analysis. An unsteady turbulent flow, the unsteadiness of which is organized, may be analyzed in a similar manner through an extra stage of decomposition and an additional averaging process. These procedures result in equations of fluid motion in mean, turbulent, and organized unsteady fields and are described in the following sections. A Cartesian tensor notation is used in which repeated indices in Roman letters follow the Einstein summation convention; repeated indices in Greek letters are not intended to be summed. The meanings of the symbols are given in the nomenclature.

2.1 Decomposition and Averaging

It is useful to decompose a time-dependent, turbulent variable, $f(\mathbf{x},t)$, into three components (Hussain & Reynolds 1970):

$$f(\mathbf{x},t) = \overline{f}(\mathbf{x}) + \widetilde{f}(\mathbf{x},t) + f'(\mathbf{x},t). \tag{2.1.1}$$

The quantity $\overline{f}(\mathbf{x})$ represents the mean or time-averaged value of $f(\mathbf{x},t)$ and $f'(\mathbf{x},t)$ is its turbulent component. The deterministic component, the contribution attributed to the organized unsteady motion, is $\widetilde{f}(\mathbf{x},t)$. This triple decomposition

has become the norm for analysis of turbulent flows with an organized kind of unsteadiness.

Separation of the term $f(\mathbf{x},t)$ into its component parts is achieved through two averaging procedures. If the unsteady phenomenon is of a periodic nature, the concept of a *phase average* is especially helpful; it is the average of the quantity $f(\mathbf{x},t)$ when taken at the same point, or phase, in a record of many cycles. Formally, this operation is defined as:

$$\langle f(\mathbf{x},t)\rangle = \lim_{N\to\infty} \frac{1}{N} \sum_{n=0}^{N-1} f(\mathbf{x},t+n\tau) \ ,$$

where τ is the period of the cycle; τ may be prescribed or it may be deduced from a Fourier transformation of $f(\mathbf{x},t)$ — hence the requirement that the unsteadiness be organized. This operation serves to remove the contributions of the uncorrelated turbulent component, $f'(\mathbf{x},t)$. It follows that:

$$\langle f(\mathbf{x},t)\rangle = \overline{f}(\mathbf{x}) + \widetilde{f}(\mathbf{x},t) \qquad \text{and} \qquad f'(\mathbf{x},t) = f(\mathbf{x},t) - \langle f(\mathbf{x},t)\rangle.$$

The second stage of separation is carried out by the familiar time average:

$$\overline{f}(\mathbf{x}) = \lim_{N\to\infty} \frac{1}{N} \sum_{n=0}^{N-1} f(\mathbf{x},t_0+n\Delta t) \qquad \text{where} \qquad N\Delta t \gg \tau.$$

Considering the two operations together, it follows that:

$$\overline{\langle f(\mathbf{x},t)\rangle} = \overline{f}(\mathbf{x}) \qquad \text{and} \qquad \widetilde{f}(\mathbf{x},t) = \langle f(\mathbf{x},t)\rangle - \overline{\langle f(\mathbf{x},t)\rangle}.$$

This time-averaging procedure removes the contribution of the deterministic component, $\widetilde{f}(\mathbf{x},t)$, which is uncorrelated with the mean value of the variable, $\overline{f}(\mathbf{x})$. Thus the operations of phase averaging and time averaging allow deduction of the turbulent component $f'(\mathbf{x},t)$, the deterministic component $\widetilde{f}(\mathbf{x},t)$, and the mean component $\overline{f}(\mathbf{x})$ from the variable, $f(\mathbf{x},t)$.

2.2 Basic Equations

The equations of motion for an organized, unsteady, incompressible flow may be formulated by applying the decomposition and the averaging processes of the previous section to the equations describing the flow of an incompressible Newtonian fluid of constant viscosity, namely:

the continuity equation,
$$\frac{\partial u_k}{\partial x_k} = 0 \,, \tag{2.2.1}$$

and the momentum equation,
$$\frac{\partial u_i}{\partial t} + \frac{\partial}{\partial x_k}(u_k u_i) = -\frac{1}{\rho}\frac{\partial p}{\partial x_i} + \nu \frac{\partial^2 u_i}{\partial x_k \partial x_k} \,. \tag{2.2.2}$$

Following (2.1.1), the velocity and pressure are decomposed such that:

$$u_i = U_i + \tilde{u}_i + u_i' \qquad \text{and} \qquad p = P + \tilde{p} + p' \,, \tag{2.2.3}$$

where $U_i = \overline{u}_i$, $\tilde{u}_i = \langle u_i \rangle - \overline{u}_i$, $P = \overline{p}$ and $\tilde{p} = \langle p \rangle - \overline{p}$.

After substituting (2.2.3) into (2.2.1), the phase- and time-averaging processes are performed and yield:

$$\frac{\partial U_k}{\partial x_k} = 0 \,, \quad \frac{\partial \tilde{u}_k}{\partial x_k} = 0 \,, \quad \frac{\partial u_k'}{\partial x_k} = 0 \,. \tag{2.2.4}$$

These are the equations of continuity for the mean, deterministic, and turbulent velocity fields respectively.

The corresponding equations of momentum may be developed in a similar manner. The velocity and pressure are decomposed as in (2.2.3) and substituted into (2.2.2), yielding:

$$\frac{\partial}{\partial t}(U_i + \widetilde{u}_i + u_i') + \frac{\partial}{\partial x_k}\Big[(U_k + \widetilde{u}_k + u_k')(U_i + \widetilde{u}_i + u_i')\Big] =$$

$$-\frac{1}{\rho}\frac{\partial}{\partial x_i}(P + \widetilde{p} + p') + \nu\frac{\partial^2}{\partial x_k \partial x_k}(U_i + \widetilde{u}_i + u_i') \; . \qquad (2.2.5)$$

Phase averaging (2.2.5), to remove the uncorrelated turbulent quantities, results in the equation:

$$\frac{\partial \widetilde{u}_i}{\partial t} + \frac{\partial}{\partial x_k}\Big(U_k U_i + U_k \widetilde{u}_i + \widetilde{u}_k U_i + \widetilde{u}_k \widetilde{u}_i + \langle u_k' u_i' \rangle\Big) =$$

$$-\frac{1}{\rho}\frac{\partial}{\partial x_i}(P + \widetilde{p}) + \nu\frac{\partial^2}{\partial x_k \partial x_k}(U_i + \widetilde{u}_i) \; . \qquad (2.2.6)$$

Time averaging either (2.2.5) or (2.2.6), to remove the quantities uncorrelated with the mean ones, yields the momentum equation for the mean field:

$$\frac{\partial}{\partial x_k}(U_k U_i) + \frac{\partial}{\partial x_k}(\overline{u_k' u_i'} + \overline{\widetilde{u}_k \widetilde{u}_i}) = -\frac{1}{\rho}\frac{\partial P}{\partial x_i} + \nu\frac{\partial^2 U_i}{\partial x_k \partial x_k} \; . \qquad (2.2.7)$$

To deduce the deterministic momentum equation, (2.2.7) is subtracted from (2.2.6) and the result is:

$$\frac{\partial \widetilde{u}_i}{\partial t} + \frac{\partial}{\partial x_k}(U_k \widetilde{u}_i + \widetilde{u}_k U_i + \widetilde{u_k' u_i'} + \widetilde{\widetilde{u}_k \widetilde{u}_i}) = -\frac{1}{\rho}\frac{\partial \widetilde{p}}{\partial x_i} + \nu\frac{\partial^2 \widetilde{u}_i}{\partial x_k \partial x_k} \; . \qquad (2.2.8)$$

The expression $\overline{(\quad)}$ has the same meaning as $\widetilde{(\,)}$ and denotes the deterministic measure, $\langle\langle \quad \rangle\rangle - \overline{(\quad)}$; thus $\overline{\widetilde{u}_k\widetilde{u}_i} = \widetilde{u}_k\widetilde{u}_i - \overline{\widetilde{u}_k\widetilde{u}_i}$.

Finally, the turbulent momentum equation may be formulated by subtracting (2.2.6) from (2.2.5):

$$\frac{\partial u_i'}{\partial t}+\frac{\partial}{\partial x_k}\Big(U_k u_i'+\widetilde{u}_k u_i'+u_k' U_i+u_k'\widetilde{u}_i+u_k' u_i'-\langle u_k' u_i'\rangle\Big) = -\frac{1}{\rho}\frac{\partial p'}{\partial x_i}+\nu\frac{\partial^2 u_i'}{\partial x_k \partial x_k} \ . \quad (2.2.9)$$

It is customary to rearrange the mean and deterministic momentum equations, (2.2.7) and (2.2.8), so that the Reynolds stresses are displayed as terms on the right-hand side. Their final form is then:

$$\frac{\partial}{\partial x_k}(U_k U_i) = -\frac{1}{\rho}\frac{\partial P}{\partial x_i} - \frac{\partial}{\partial x_k}(\overline{u_k' u_i'} + \overline{\widetilde{u}_k\widetilde{u}_i}) + \nu\frac{\partial^2 U_i}{\partial x_k \partial x_k} \ , \quad (2.2.10)$$

$$\frac{\partial \widetilde{u}_i}{\partial t} + \frac{\partial}{\partial x_k}(U_k\widetilde{u}_i + \widetilde{u}_k U_i) = -\frac{1}{\rho}\frac{\partial \widetilde{p}}{\partial x_i} - \frac{\partial}{\partial x_k}(\overline{\widetilde{u_k' u_i'}} + \overline{\widetilde{u}_k\widetilde{u}_i}) + \nu\frac{\partial^2 \widetilde{u}_i}{\partial x_k \partial x_k} \ . \quad (2.2.11)$$

Since the density of the fluid, ρ, is assumed uniform throughout the field, the term *Reynolds stress* is used somewhat liberally here to describe turbulent inertial tensors such as $\overline{u_k' u_i'}$ or its deterministic counterpart. It would be more correctly used in reference to apparent turbulent-stress tensors, *i.e.* $-\rho\overline{u_k' u_i'}$.

2.3 Time-Averaged Energy Equations

The dependence of the mean, deterministic, and turbulent fields upon one another may be studied in terms of energy transfer. Although energy equations are

only manipulations of the equations of momentum and introduce no new information, they allow a clearer interpretation of the relationship between the various fields of flow, in terms of measurable quantities. Therefore sets of kinetic-energy equations relating these three fields are developed to describe the mean energy-transfer process. The time-averaged Reynolds-stress equation is closely related to this set of energy equations and is developed here too.

To determine the set of kinetic-energy equations describing mean energy transfer, differential equations for the mean squares of U_i , $\widetilde{u}_i$ and u'_i are formulated. As it would not be possible to measure all three components of velocity in this study, the corresponding equations for the "energy" of each component of the velocity field are sought. The equation for $U_\alpha U_\alpha$ is formed by multiplying (2.2.10), with $i = \alpha$, by U_α and rearranging to give:

$$\frac{\partial}{\partial x_k}\Big(U_k\frac{U_\alpha U_\alpha}{2}\Big) = -\frac{U_\alpha}{\rho}\frac{\partial P}{\partial x_\alpha} - \frac{\partial}{\partial x_k}(U_\alpha\overline{u'_k u'_\alpha} + U_\alpha\overline{\widetilde{u}_k\widetilde{u}_\alpha}) + \nu\frac{\partial}{\partial x_k}\Big(U_\alpha\frac{\partial U_\alpha}{\partial x_k}\Big)$$

$$+ \overline{u'_k u'_\alpha}\frac{\partial U_\alpha}{\partial x_k} + \overline{\widetilde{u}_k\widetilde{u}_\alpha}\frac{\partial U_\alpha}{\partial x_k} - \nu\frac{\partial U_\alpha}{\partial x_k}\frac{\partial U_\alpha}{\partial x_k} \ . \qquad (2.3.1)$$

The mean kinetic-energy equation for $\widetilde{u}_\alpha\widetilde{u}_\alpha$ is found by multiplying (2.2.11), with $i = \alpha$, by $\widetilde{u}_\alpha$ and then time averaging the result. Subsequent rearrangement yields:

$$\frac{\partial}{\partial x_k}\Big(U_k\frac{\overline{\widetilde{u}_\alpha\widetilde{u}_\alpha}}{2}\Big) + \frac{\partial}{\partial x_k}\Big(\overline{\widetilde{u}_k\frac{\widetilde{u}_\alpha\widetilde{u}_\alpha}{2}}\Big) = -\overline{\frac{\widetilde{u}_\alpha}{\rho}\frac{\partial\widetilde{p}}{\partial x_\alpha}} - \frac{\partial}{\partial x_k}(\overline{\widetilde{u}_\alpha u'_k u'_\alpha}) + \nu\frac{\partial}{\partial x_k}\Big(\overline{\widetilde{u}_\alpha\frac{\partial\widetilde{u}_\alpha}{\partial x_k}}\Big)$$

$$+ \overline{u'_k u'_\alpha\frac{\partial\widetilde{u}_\alpha}{\partial x_k}} - \overline{\widetilde{u}_k\widetilde{u}_\alpha}\frac{\partial U_\alpha}{\partial x_k} - \nu\overline{\frac{\partial\widetilde{u}_\alpha}{\partial x_k}\frac{\partial\widetilde{u}_\alpha}{\partial x_k}} \ . \qquad (2.3.2)$$

The $u'_\alpha u'_\alpha$ equation which completes this set is formed by multiplying (2.2.9), with $i = \alpha$, by u'_α and time averaging the result. The outcome of these operations is the equation:

$$\frac{\partial}{\partial x_k}\Big(U_k\overline{\frac{u'_\alpha u'_\alpha}{2}}\Big) + \frac{\partial}{\partial x_k}\Big(\widetilde{u}_k\overline{\frac{u'_\alpha u'_\alpha}{2}}\Big) + \frac{\partial}{\partial x_k}\Big(\overline{u'_k\frac{u'_\alpha u'_\alpha}{2}}\Big) = -\overline{\frac{u'_\alpha}{\rho}\frac{\partial p'}{\partial x_\alpha}}$$

$$+\nu\frac{\partial}{\partial x_k}\Big(\overline{u'_\alpha\frac{\partial u'_\alpha}{\partial x_k}}\Big) - \overline{u'_k u'_\alpha\frac{\partial \widetilde{u}_\alpha}{\partial x_k}} - \overline{u'_k u'_\alpha}\frac{\partial U_\alpha}{\partial x_k} - \nu\overline{\frac{\partial u'_\alpha}{\partial x_k}\frac{\partial u'_\alpha}{\partial x_k}} \ . \qquad (2.3.3)$$

The accompanying mean Reynolds-stress equation is formed by:

(*i*) multiplying (2.2.9) by u'_j,

(*ii*) replacing the subscript i by j in (2.2.9) and multiplying by u'_i,

(*iii*) adding the results of (*i*) and (*ii*),

(*iv*) time averaging the result of (*iii*).

Rearrangement of the resultant expression gives:

$$\frac{\partial}{\partial x_k}(U_k\overline{u'_i u'_j}) + \frac{\partial}{\partial x_k}(\overline{\widetilde{u}_k u'_i u'_j}) + \frac{\partial}{\partial x_k}(\overline{u'_k u'_i u'_j}) = -\overline{\frac{u'_j}{\rho}\frac{\partial p'}{\partial x_i}} - \overline{\frac{u'_i}{\rho}\frac{\partial p'}{\partial x_j}}$$

$$+\nu\frac{\partial}{\partial x_k}\Big(\overline{u'_j\frac{\partial u'_i}{\partial x_k}} + \overline{u'_i\frac{\partial u'_j}{\partial x_k}}\Big) - \overline{u'_k u'_j\frac{\partial \widetilde{u}_i}{\partial x_k}} - \overline{u'_k u'_i\frac{\partial \widetilde{u}_j}{\partial x_k}}$$

$$-\overline{u'_k u'_j}\frac{\partial U_i}{\partial x_k} - \overline{u'_k u'_i}\frac{\partial U_j}{\partial x_k} - 2\nu\overline{\frac{\partial u'_i}{\partial x_k}\frac{\partial u'_j}{\partial x_k}} \ . \qquad (2.3.4)$$

The *production* terms in the equations for mean kinetic energies are of particular interest. Each of the time-averaged equations for the mean, deterministic and turbulent energies contain two such terms. The term $\overline{u'_k u'_\alpha}(\partial U_\alpha/\partial x_k)$ appears, with opposite sign, in (2.3.1) and (2.3.3). It serves to exchange kinetic energy between the mean and turbulent fields, as in the corresponding steady flow (see, for

example, Tennekes & Lumley, §3.2). The $\overline{\tilde{u}_k \tilde{u}_\alpha}(\partial U_\alpha / \partial x_k)$ term represents the product of mean shear and the mean correlation between components of deterministic velocity. Its appearance, with opposite sign, in (2.3.1) and (2.3.2) indicates its ability to transfer energy between the mean and deterministic fields. Mean kinetic energy is exchanged between the deterministic and turbulent fields by the quantity $\overline{u'_k u'_\alpha (\partial \tilde{u}_\alpha / \partial x_k)}$, which is positive in (2.3.2) and negative in (2.3.3). Examination of the time-averaged Reynolds-stress equation, (2.3.4), reveals terms closely related to the energy-production terms of (2.3.3). The behavior of these three energy-production terms may help to explain, in a time-averaged sense, the relationship between steady or quasi-steady flow, organized (deterministic) unsteadiness and unorganized unsteadiness (turbulence).

The corresponding equations for the squares of the mean, deterministic and turbulent components of vorticity may be developed using the methods of this section. They contain a similar system of production terms which relate the equations for each field. However, because of the appreciable uncertainties involved, deduction of these quantities from experimental measurements was not attempted in this study and the presentation of the equations here would serve little purpose.

2.4 Deterministic Energy Equations

Whereas the operations of the previous section resulted in equations for time-averaged energy transfer, in this section the equations describing periodic exchange of energy are devised. During an unsteady cycle, this deterministic or organized component of energy fluctuates about its mean value of zero. Energy associated with the square of the mean component of velocity clearly plays no part in this process; it is independent of time. Therefore a set of two kinetic-energy equations is developed to describe the deterministic energy contents of the turbulent and deterministic velocity fields. The accompanying Reynolds-stress equation is also formed.

The equations for the deterministic energy budgets of $\widetilde{\widetilde{u}_\alpha \widetilde{u}_\alpha}$ and $\widetilde{u'_\alpha u'_\alpha}$ are formulated as follows. The energy equation for $\widetilde{\widetilde{u}_\alpha \widetilde{u}_\alpha}$ is the result of:

(i) multiplying (2.2.11), with $i = \alpha$, by $\widetilde{u}_\alpha$,

(ii) phase averaging the result,

(iii) subtracting from the result of (ii), the time average of (i), *i.e.* (2.3.2).

These operations yield the equation:

$$\frac{\partial}{\partial t}\left(\widetilde{\frac{\widetilde{u}_\alpha \widetilde{u}_\alpha}{2}}\right) + \frac{\partial}{\partial x_k}\left(U_k \widetilde{\frac{\widetilde{u}_\alpha \widetilde{u}_\alpha}{2}}\right) + \frac{\partial}{\partial x_k}\left(\widetilde{\widetilde{u}_k \frac{\widetilde{u}_\alpha \widetilde{u}_\alpha}{2}}\right) = -\widetilde{\frac{\widetilde{u}_\alpha}{\rho}\frac{\partial \widetilde{p}}{\partial x_\alpha}}$$

$$- \frac{\partial}{\partial x_k}\left(\widetilde{\widetilde{u}_\alpha \widetilde{u'_k u'_\alpha}} - \widetilde{u}_\alpha \overline{\widetilde{u}_k \widetilde{u}_\alpha}\right) + \nu \frac{\partial}{\partial x_k}\left(\widetilde{\widetilde{u}_\alpha \frac{\partial \widetilde{u}_\alpha}{\partial x_k}}\right) + \widetilde{u'_k u'_\alpha \frac{\partial \widetilde{u}_\alpha}{\partial x_k}}$$

$$- \widetilde{\widetilde{u}_k \widetilde{u}_\alpha}\frac{\partial U_\alpha}{\partial x_k} - \overline{\widetilde{u}_k \widetilde{u}_\alpha}\frac{\partial \widetilde{u}_\alpha}{\partial x_k} - \overline{u'_k u'_\alpha}\frac{\partial \widetilde{u}_\alpha}{\partial x_k} - \nu \widetilde{\frac{\partial \widetilde{u}_\alpha}{\partial x_k}\frac{\partial \widetilde{u}_\alpha}{\partial x_k}} \quad . \qquad (2.4.1)$$

The $\widetilde{u'_\alpha u'_\alpha}$ equation may be formed by multiplying (2.2.9), with $i = \alpha$, by u'_α , phase averaging the result and subtracting from it (2.3.3). The result of these manipulations is:

$$\frac{\partial}{\partial t} + \frac{\partial}{\partial x_k}\left(U_k \widetilde{\frac{u'_\alpha u'_\alpha}{2}}\right) + \frac{\partial}{\partial x_k}\left(\widetilde{\widetilde{u}_k \frac{u'_\alpha u'_\alpha}{2}}\right) + \frac{\partial}{\partial x_k}\left(\widetilde{u'_k \frac{u'_\alpha u'_\alpha}{2}}\right) = -\widetilde{\frac{u'_\alpha}{\rho}\frac{\partial p'}{\partial x_\alpha}}$$

$$+ \nu \frac{\partial}{\partial x_k}\left(\widetilde{u'_\alpha \frac{\partial u'_\alpha}{\partial x_k}}\right) - \widetilde{u'_k u'_\alpha}\frac{\partial \widetilde{u}_\alpha}{\partial x_k} - \widetilde{u'_k u'_\alpha}\frac{\partial U_\alpha}{\partial x_k} - \nu \widetilde{\frac{\partial u'_\alpha}{\partial x_k}\frac{\partial u'_\alpha}{\partial x_k}} \quad . \qquad (2.4.2)$$

Finally, the deterministic Reynolds-stress equation is formed by:

(*i*) multiplying (2.2.9) by u'_j,

(*ii*) replacing the subscript i by j in (2.2.9) and multiplying by u'_i,

(*iii*) adding the results of (*i*) and (*ii*),

(*iv*) subtracting from the phase average of (*iii*), the time average of (*iii*), *i.e.* (2.3.4).

The resultant expression is:

$$\frac{\partial}{\partial t}(\widetilde{u'_i u'_j}) + \frac{\partial}{\partial x_k}(U_k \widetilde{u'_i u'_j}) + \frac{\partial}{\partial x_k}(\widetilde{\widetilde{u}_k u'_i u'_j}) + \frac{\partial}{\partial x_k}(\widetilde{u'_k u'_i u'_j}) = -\widetilde{\frac{u'_j}{\rho}\frac{\partial p'}{\partial x_i}} - \widetilde{\frac{u'_i}{\rho}\frac{\partial p'}{\partial x_j}}$$

$$+ \nu \frac{\partial}{\partial x_k}\left(\widetilde{u'_j \frac{\partial u'_i}{\partial x_k}} + \widetilde{u'_i \frac{\partial u'_j}{\partial x_k}}\right) - \widetilde{u'_k u'_j \frac{\partial \widetilde{u}_i}{\partial x_k}} - \widetilde{u'_k u'_i \frac{\partial \widetilde{u}_j}{\partial x_k}}$$

$$- \widetilde{u'_k u'_j}\frac{\partial U_i}{\partial x_k} - \widetilde{u'_k u'_i}\frac{\partial U_j}{\partial x_k} - 2\nu \widetilde{\frac{\partial u'_i}{\partial x_k}\frac{\partial u'_j}{\partial x_k}} \quad . \qquad (2.4.3)$$

The organized, unsteady, equations of kinetic energy, (2.4.1) and (2.4.2), have a common production term, $\widetilde{u'_k u'_\alpha (\partial \widetilde{u}_\alpha / \partial x_k)}$; it appears with opposite sign in each equation. This term describes the transfer of energy back and forth between the deterministic and turbulent fields about a mean value of zero. The amplitude of this quantity, relative to its mean value, $\overline{u'_k u'_\alpha (\partial \widetilde{u}_\alpha / \partial x_k)}$, is especially interesting. If it were larger, it would imply that, at times during an unsteady cycle, there is net energy transfer from the unorganized field to the organized field.

Deterministic equations for the squares of vorticity may also be developed in the manner outlined in this section. They also reveal a vorticity-production term relating the $\widetilde{\omega}_\alpha \widetilde{\omega}_\alpha$ and $\widetilde{\omega'_\alpha \omega'_\alpha}$ fields. However, the uncertainties involved in deducing this term from measurements are considerable and this shortcoming detracts from the usefulness of inclusion of the relevant equations here.

Development of the equations of fluid motion into these decomposed forms allows unsteady, turbulent flow to be studied according to its behavior in each of the three distinct fields of the decomposition. Time-averaged and dynamic responses of the boundary-layer flow to forced free-stream unsteadiness may then be deduced through experimental measurement of pertinent terms of the relevant equations. Through these measurements, important quantities may be identified, the existence of asymptotic forms of behavior may be examined and the suitability of turbulence models may be considered.

3. Experimental Considerations

Detailed descriptions of the facility and its measurement system are given in this chapter. The measurement system comprised a two-component laser-Doppler anemometer which was used to make simultaneous measurements of the u and v components of the velocity field. This instrument is becoming more widely used for non-intrusive, instantaneous measurements of fluid velocity and so the rationale for selection of a reliable, high-resolution measurement system for this study is given. Careful consideration is also given to the use of a mini-computer for control of the flow and for data acquisition and processing, as aspects of its performance influenced the methodologies for making different kinds of measurements under steady and unsteady conditions.

3.1 Experimental Facility

The experiments were performed in the closed-loop water tunnel used by Jayaraman *et al.* (1982). In this facility, organized unsteadiness could be imposed locally upon a turbulent boundary layer which had developed under steady, zero-pressure-gradient conditions. This feature was important for several reasons:

(*i*) It allowed the conditions upstream of the point of introduction of unsteadiness to be prescribed and documented (which could then serve as initial conditions in target-data sets for turbulence modelers).

(*ii*) It allowed study of the effects of unsteadiness on a turbulent boundary layer, without regard for any complicating factors due to transition to turbulence under unsteady conditions.

(*iii*) It allowed study of the influence of unsteadiness, in isolation from history effects associated with the initiation of the boundary layer. Had the boundary layer grown from a leading edge in an already unsteady flow, the unsteady

leading-edge vorticity would have been convected downstream and interacted with vorticity generated through local unsteadiness. It would then have been difficult to separate unsteady effects due to the local unsteadiness from those related to conditions at the leading edge.

Illustrations of the closed-loop water tunnel are given in Figures 3.1 and 3.2. The sump was filled with water through filters rated at five microns, to remove any particles of undesirably large size. Water was pumped from the sump to a constant-head tank; the water level in the tank was precisely maintained by an overflow weir, some 3.4 meters above the point of exit from the water tunnel to the sump. From the tank, water flowed down to the inlet of a two-dimensional contraction, via a honeycomb section and three taut screens of 70% porosity; the contraction ratio was 20:1. Boundary layers were bled off on all walls at the contraction exit, where it smoothly joined a horizontal duct of rectangular cross-section (0.15 meters in height and 0.35 meters in width). This duct was the *development section* of the tunnel, in which a new, turbulent, boundary layer was allowed to develop for 2.0 meters along the top wall, under steady, constant-pressure conditions; it was tripped by a strip of sand-paper glued to the top wall.

The bottom wall of the development section contained porous sections at twelve evenly spaced intervals. Flow through these sections was controlled by valves, which were set to permit sufficient fluid to be removed so that a constant free-stream velocity was maintained and growth of a boundary layer on the bottom wall was prevented. Thus a steady, zero-pressure-gradient, turbulent boundary layer developed on the top wall. At the end of this section, splitter plates protruded from the side walls of the tunnel so that boundary layers on these walls would be removed; the width of the tunnel was then reduced to 0.30 meters, the spacing between the splitter plates. Here the turbulent boundary layer was characterized by a Reynolds number (based on momentum thickness) of 3200; it had developed in a flow with a constant free-stream velocity of 0.74 meters/second.

The part of the tunnel immediately downstream of the development section was the *test section*. Here the free-stream velocity was varied so that unsteady effects on the top-wall boundary layer could be studied. Water which entered the test section could exit to the sump by either of two routes. Some could be bled off through the porous bottom wall of the test section and then reach the sump via a gate valve (Figure 3.3). The remainder passed through to the *recovery section* and flowed through its bottom wall and the gate valve before discharge to the sump. The proportions of the flow which exited by each route were governed by the position of the gate valve. The sum of the areas presented by the gate valve to the exiting flows was constant so that, regardless of its position, the through-flow rate and the pressure drop across the valve would not vary. By design, the pressure drop across the gate valve was the primary resistance to flow through the entire apparatus. Thus, although movement of the gate valve allowed dynamic control of the bleed rate through the porous bottom wall of the test section, the total through-flow rate, and hence the development-section flow, was essentially unaffected.

The porosity of the bottom wall of the test section was provided by uniformly spaced holes over a length of 0.61 meters. The hole size was chosen so that the drop in pressure across the holes would be large, relative to the change in static pressure in the flow along the test section, but small compared to the pressure drop across the gate valve. Consequently, when the gate valve was positioned to allow flow through these holes, the result was a nearly linear decrease in free-stream velocity along the test section. By moving the gate valve back and forth in a sinusoidal manner, oscillations in free-stream velocity were induced with amplitude increasing in proportion to distance along the test section. One limiting position of the gate valve was that at which no flow was allowed through the bottom wall of the test section — hence no pressure gradient in the test section. The other limiting position was chosen as that of the greatest desired adverse-pressure gradient. In this way, with minimal disturbance to the flow in the development section, oscillation of the gate valve produced sinusoidal unsteadiness in the test section. The amplitude of

oscillation of the free-stream velocity was almost linearly proportional to distance along the test section, as was the streamwise decrease in the mean value of free-stream velocity. In Figure 3.4 the desired distributions in free-stream velocity during an unsteady cycle is shown. A scotch-yoke mechanism driven by motor (Figure 3.3) was built onto the gate valve to produce its sinusoidal motion. Frequencies of unsteadiness as high as 2.0 cycles/second could be imposed on the test-section flow through precise control of the motor's speed.

The recovery section was smoothly joined to the end of the test section. It consisted of a channel of rectangular section followed by a tapered duct with a porous bottom wall, of the same design as the bottom wall of the test section. All fluid which entered the recovery section passed through its bottom wall and returned to the sump via the gate valve.

The development, test and recovery sections were constructed from plexiglass and were transparent. Thus the flow was readily accessible by optical means and non-intrusive measurements of fluid velocity could be made using a laser-Doppler anemometer.

3.2 Velocity Measurement System

The velocity data presented in this study were obtained using a three-beam, two-color, laser-Doppler anemometry system and an overview of this measurement technique is given in Appendix B. The system was assembled primarily from TSI modular components mounted on a custom-made optical breadboard, which straddled the water tunnel in the manner shown in Figure 3.5. The breadboard was attached to a framework which also held the laser, its power supply and some electrical instrumentation. The framework was supported by a trolley, the wheels of which rested on I-beams running the length of the facility. The linkage between the framework and the trolley was a pair of linear bearings, which allowed lateral movement of the framework. Thus the measurement system could be moved along

the length of the water tunnel and across its span. A third degree of freedom was provided in the direction normal to the top wall of the tunnel, the direction in which boundary-layer profiles would be taken.

Precise controlled movement in the vertical plane of all the optics, the breadboard and an argon-ion laser was not considered a feasible option. Therefore the degree of freedom in the wall-normal direction was achieved through simultaneous movement of both the final mirror and lens of the transmitting optics, and the mirror and collimating lens of the receiving optics (Figure 3.5); the position of the laser and the remainder of the transmitting and receiving optics was fixed, relative to the breadboard. Each mirror-and-lens combination was mounted on a linear slide, the lead screws of which were linked by shafts and gears, and driven by a small stepping motor.

Correct operation of this traversing system required that beams of laser light travelling from the transmitting optics to the mirror on the right slide (Figure 3.5) were parallel to the direction of motion of the slide. The same provision applied to scattered light leaving the lens of the left slide. The location of the slides, in precisely spaced holes on the optical breadboard, assured that their motion was parallel. Careful alignment of the transmitted beams, relative to the holes of the breadboard, ensured they were parallel to the slides. By selection of a lens of correct focal length, and by precise placement of this lens on the traversing stage of the receiving optics, scattered light focused by the lens was collimated. Thus the bulk of the transmitting and receiving optics remained stationary on the breadboard, while two traversing stages, each comprising a mirror and lens mounted on a slide, could be moved to position the measuring volume at the desired location in the boundary layer. Details of the components of the traversing system are given in Table 3.1.

A three-beam, laser-Doppler anemometer was assembled, with coincident interference patterns of blue and green light aligned with the u and v components of fluid velocity respectively. The mode of operation was chosen as forward scatter,

TABLE 3.1

Traversing System Components

Item	Specifications	No.
Stepping motor	Slo-Syn, M093-FC07	1
Translator	Slo-Syn, ST101	1
Linear slide	Velmex Unislide, A4012B, 20 tpi	2
Gear drive	Boston, RA 631	2

15° off axis, to take advantage of the strength of light scattered in this direction and the reduced requirement for laser power. Off-axis collection of scattered light also offered the opportunity to improve spatial resolution in velocity measurements through the use of a small pinhole in the field-stop module, positioned at the front of the fixed receiving-optics train. Moreover, this field-stop system prevented stray transmitted light, reflected or scattered from sources other than the measuring volume, reaching the remainder of the receiving optics. The intensity of power in the probe volume was increased by expanding the diameter and increasing the separation of the beams before focusing them; the beams subsequently intersected with waists of reduced size, concentrating the power in the transmitted beams within a smaller volume. The optical system comprised the components listed in Table 3.2. The positions of the components on the optical breadboard are shown in Figure 3.5.

Since the scattered light had to be separated by dichroic means, the risk of cross-talk was reduced through the inclusion of a frequency-separation scheme. The Bragg cell, used to shift the blue beam in frequency, was driven at the standard 40 megahertz. The cell which shifted the green beam was driven at 38 megahertz; this frequency was generated by making a small change in the configuration of the frequency-selection electronics in the driver module. The bandwidths of the frequency spectra in the u and v components of velocity corresponded to less than 200 kilohertz, for the velocity scales in this flow and the optical parameters of the system. Consequently, spurious signals of blue scattered light, which passed through the color filters of the receiving optics for green scattered light, were around 2

TABLE 3.2

Optical Components of the Measurement System

Item	Description	Specifications
1	Argon-ion laser	Lexel series 75, 300 milliwatts
2	Beam collimator	TSI 9108
3,4	Mirror	Newport 10D10 DM.2
5	Rotating polarization mount	TSI 9178-1
6	Beam splitter	TSI 9115-1X
7	Dichroic color separator	TSI 9112
8,9	Bragg cell	TSI 9182-12, 9182-11
10,11	Beam steering module	TSI 9175
12	Beam spacer	TSI 9114-22
13	Rotating mount	TSI 9179
14	Mirror	Newport 20D10 DM.2
15	Beam expander	TSI 9189
16	Mirror	Newport 60D10 DM.2
17	Lens	TSI 9169-450
18	Mirror	Newport 40D10 DM.2
19	Lens	TSI 9167-500
20	Field-stop module	TSI 9143
21	Dichroic color separator	TSI 9144
22,23	Color filter	TSI 9158, 9159
24	Optical breadboard	Newport XA-35, custom-made

megahertz higher in frequency; they could then be removed easily through electrical frequency filtering. Similarly, contaminant green light, in the receiving optics for blue scattered light, was about 2 megahertz lower in frequency and could be eliminated by band-pass filtering.

After color separation, the scattered light was channeled to photo-multiplier tubes. The resultant electrical signals were downmixed in frequency, band-pass filtered and routed to frequency trackers. The effective frequency shift (the difference between the frequency at which the Bragg cell was driven and the downmix frequency) was chosen as 200 kilohertz, the frequency at which stationary particles would then appear to scatter light. The bandwidths of the tracked signals would then lie between about 200 and 400 kilohertz and the best use would be made of the

TABLE 3.3

Operational Frequencies in the Measurement System

	Green Channel v	Blue Channel u
Shift frequency	38.0 megahertz	40.0 megahertz
Downmix frequency	37.8 megahertz	39.8 megahertz
Effective shift frequency	200 kilohertz	200 kilohertz
High-pass filter	100 kilohertz	100 kilohertz
Low-pass filter	500 kilohertz	500 kilohertz
Tracker range	$2 \rightarrow 500$ kilohertz	$2 \rightarrow 500$ kilohertz

range of operation of the trackers for which their voltage output was most sensitive to changes in Doppler frequency. The operational frequencies of the measurement system are presented in Table 3.3.

Given an input signal at some frequency, the output of a tracker is an analog voltage. The frequency–voltage characteristic of a tracker is highly linear so that fluid velocity may be related to voltage through two calibration constants — a voltage offset, corresponding to zero velocity, and a voltage–velocity slope. By downmixing the electrical signal generated to drive the Bragg cell, a signal oscillating at the effective shift frequency was formed. This signal could be tracked perfectly and the tracker's voltage output at this frequency corresponded to its voltage offset at zero velocity. The second calibration constant, describing the voltage–velocity slope, was found from simple optical considerations and from the tracker's frequency–voltage characteristic and verified by independent measurement with a pitot probe.

The success of trackers as frequency analyzers depends upon the rate at which data are supplied to them and the rate at which the input frequency changes in magnitude. If the data rate can be considered continuous (*i.e.* an order of magnitude greater than the Kolmogoroff frequencies, the highest frequencies of the flow) and the slew rate of the tracker is fast enough to follow all changes in input frequency, then the frequency-following electronics should continually track the data signal. The tracker may then provide a continuous, analog, voltage output, proportional to

TABLE 3.4

Signal Conditioning Equipment

Instrument	Specifications
Photo-multiplier system	TSI 9162, 9165
Frequency-shift system	TSI 9186
High-pass filter	TSI 10095
Low-pass filter	Krohn-Hite 3202
Frequency tracker	TSI 1090-1A
Signal conditioner	TSI 1057

the instantaneous fluid velocity. This kind of output signal is most desirable in an unsteady flow as it greatly simplifies the sampling strategy — data can be sampled when desired. An alternative scheme, for sparse data, is to wait for it to arrive, identify it by the time at which it was detected and sort the data accordingly — a function which digital instruments such as counters are well-equipped to perform. The signal-processing and frequency-analyzing equipment is specified in Table 3.4. It is demonstrated in the next chapter that trackers could be used with confidence in these experiments.

A three-beam system, with coincident measuring volumes of blue and green light, may be used with several different orientations of its beams. A commonly used arrangement (Figure 3.6) aligns the probe volume of one color to measure the velocity components $(u+v)/\sqrt{2}$ and the other to measure $(u-v)/\sqrt{2}$ (for the idealized case of perfect beam orientation and alignment); a small contribution of w is necessarily included in each measure too. If the half angle of the beams is sufficiently small, so that the w measure is negligible, this arrangement is analogous to the cross-wire of hot-wire anemometry. Although measurements may be made to within a beam diameter of the top wall with this method, it has its drawbacks. In shear flows, v is often much smaller than u. Consequently the deduction of v, as the difference between two much larger numbers, may suffer from uncertainty through rounding errors.

TABLE 3.5

Optical Parameters

	Green Channel v	Blue Channel u
Beam wavelength, in air	514.5 nm	488.0 nm
Beam half angle, in air	$3.58° \pm 0.06°$	$3.70° \pm 0.06°$
Beam half angle, in water	$2.68° \pm 0.04°$	$2.76° \pm 0.04°$
Length of probe volume	~ 1.5 mm	~ 1.5 mm
Diameter of probe volume	~ 0.15 mm	~ 0.15 mm
Fringe spacing	$4.12\ \mu\text{m} \pm 0.07\ \mu\text{m}$	$3.78\ \mu\text{m} \pm 0.07\ \mu\text{m}$
Effective frequency shift	200 kilohertz	200 kilohertz
Effective fringe velocity	-0.824 m/s ± 0.014 m/s	-0.756 m/s ± 0.012 m/s
Velocity equivalent of A/D bit	0.503 mm/s	0.461 mm/s

An alternative orientation requires the interference patterns of each color to be aligned with the u and v components of velocity respectively (the standard four-beam system). This arrangement (Figure 3.7) precludes measurements being taken near the wall; the limiting distance is determined by the span of the tunnel and the half angle of intersection of the beams. Although the half angle might be reduced, it would only result in a longer probe volume with a reduced concentration in optical power and hence scattered light of weaker intensity.

For a nominally two-dimensional flow, in which values of $\overline{w}$ should be small, the three-beam system discussed above was adapted to make measurements of u and v. The arrangement of Figure 3.6 was first rotated through 45°. The final mirror and lens of the transmitting optics were then repositioned so that the two-color beam travelled through the center of the lens, along its optical axis (in practice this alignment was easily achieved by adjustment of the mirror so that the reflection back from the tunnel walls was coincident with the forward path of the beam). The blue and green beams then formed interference patterns aligned with the velocity components, u plus a small contribution from w, and v plus some contamination of w (Figure 3.10). In shear flows, it is far more important that measurements of v do not include small contributions from u than it is that u measurements

contain a little of the v component. Therefore alignment of the optics was carried out by first ensuring perfect coincidence of the interference patterns, and then by making slight adjustments in the rotation of the transmitting-optics train, until the $\overline{v}$ measurements were correct (*i.e.* the green interference pattern was insensitive to any contribution from u). Details of the alignment technique, which were specific to the components of this system, are presented in Appendix C.

This optical arrangement was considered the best compromise within the constraints of the experiment. The $\overline{u}$ and $\overline{v}$ measures would both contain a small amount of $\overline{w}$, but, in this nominally two-dimensional flow, $\overline{w}$ should be negligible. That measurements of u' and v' would contain contributions from w' was of greater concern; all these quantities are usually of the same order of magnitude. A further compromise therefore had to be made between reducing the half angles of the intersecting beams, to minimize undesired contributions of w', and keeping the length of the probe volume sufficiently small, so that scattered light retained an acceptable level of power. The optical parameters of the operational system are displayed in Table 3.5. Although perfect measurement of u and v was not possible, this optical arrangement did allow near-wall measurements to be made where, without compromise, they might not be made at all. The accuracy with which measurements were made with this system, in a steady, zero-pressure-gradient, turbulent boundary layer, is treated in the next chapter.

3.3 Control, Data Acquisition and Processing

Experiments were conducted under the control of a laboratory mini-computer, a MINC-11 with an LSI-11/2 processor. It was programmed to acquire data and perform control functions related to the operation of the experiment through the interface systems listed in Table 3.6. A limited amount of data processing was also possible, but all memory-intensive data reduction was carried out after transfer to a VAX 11/750.

When experiments were conducted under steady conditions, data from the trackers were sampled through the analog input system, at a rate controlled by the programming of the real-time clock. If time-averaged quantities were desired, running averages of the sampled data (or of squares or cross products of the sampled data) were maintained throughout the measurement period. When a record of instantaneous values of velocity was required (*i.e.* for subsequent spectral analysis), this information was transferred to a diskette during the sampling process. Boundary-layer profiles were taken by programmed movement of the measuring volume between periods of data acquisition; this movement was achieved by driving a stepping motor via the parallel digital output system.

Experiments conducted under unsteady conditions required more complex programming and more sophisticated equipment — the frequency of oscillation of the gate valve (Figure 3.3) was to be controlled and data were to be sampled at many discrete times during each unsteady cycle. To perform these functions, the absolute position of the gate valve had to be known. Therefore an optical encoder, with digital output, was fitted to the free end of the d.c. motor shaft, which drove the scotch-yoke mechanism. By monitoring the parallel digital input system, the angular position of the gate valve could be determined to an accuracy of ten bits at any instant. The least significant bit was fed to a Schmitt trigger of the real-time clock; on the rising of this bit (512 times per shaft revolution) the ensuing trigger was used to initiate a sample of velocity data at 512 discrete times during each cycle. Synchronization of sampling with the 0° position of the shaft was achieved by monitoring the parallel digital input from the encoder, until the pre-penultimate position was reached; the next rise of the least significant bit corresponded to 0°. The controller of the d.c. motor drove it at a speed almost directly proportional to an analog input voltage. This input voltage was supplied through the analog output system of the mini-computer; it was systematically varied until monitoring of the shaft-encoder position indicated that the desired frequency of oscillation had been reached. Thus, through control of the speed of oscillation of the gate

TABLE 3.6

LSI-11/2 Interface Systems

System	Specifications
Programmable real-time clock	Data Translation 2769, 2 Schmitt triggers
Analog input system	Data Translation 2762-DI-PG, 12 bit, 16 channels
Analog output system	Data Translation 2766, 12 bit, 4 channels
Parallel digital input/output	Data Translation 2768, 16 bit input, 16 bit output

valve and feedback of its position, unsteady experiments could be performed under mini-computer control.

The limited memory of this computer (64 kilobytes) placed constraints upon the size of program which could be executed and the amount of data which could be retained in memory. To take velocity data while controlling oscillations of the gate valve, the computer was programmed to:

(*i*) time the shaft encoder over several revolutions,

(*ii*) proceed to (*iii*) if the oscillation frequency was correct; otherwise trim the voltage output to the motor controller in proportion to the error and return to (*i*),

(*iii*) synchronize with the position of the shaft encoder,

(*iv*) sample and store velocity data over four cycles,

(*v*) time the shaft encoder over a revolution,

(*vi*) update stored averages of the various velocity measures, at each phase in the cycle, and return to (*iii*) if the frequency of oscillation was correct; otherwise discard data and return to (*i*).

In a typical experiment, velocity measurements might be made at 512 discrete, evenly spaced times in an unsteady cycle. To achieve reliable measures of phase-averaged quantities, data would be ensemble averaged over 500 such cycles. The range in frequency, attainable with this apparatus, was from 0.1 hertz to 2 hertz and a thorough investigation into frequency effects could require measurements to

be made at ten frequencies in this range. These considerations translated to a time requirement of several hours per data point. A reasonably well resolved profile of an unsteady boundary layer would require over thirty data points and hence around a week of continuous data acquisition. To avoid uncertainty due to changing fluid viscosity over long periods of time, water from the sump was pumped through a chiller, which was energized whenever the water temperature exceeded its prescribed value by 0.1°C.

A small amount of data processing was necessary before storage. Instantaneous values of u and v were measured at each of 512 discrete times per cycle and, from these quantities, their instantaneous squares and cross product, uu, vv and uv, were calculated. At each discrete phase, averages of u, v, uu, vv and uv were continually updated in memory throughout the 500 ensembles. On completion of the desired number of ensembles at a specific frequency of oscillation, at a prescribed position in the boundary layer, the 512 phase averages for each of $\langle u \rangle$, $\langle v \rangle$, $\langle uu \rangle$, $\langle vv \rangle$ and $\langle uv \rangle$ were transferred from memory to diskette.

Subsequent processing, often after completion of the experiment, was carried out according to the decomposition of (2.2.3):

$$U = \overline{\langle u \rangle} \ , \quad \tilde{u} = \langle u \rangle - \overline{\langle u \rangle} \ , \quad V = \overline{\langle v \rangle} \ , \quad \tilde{v} = \langle v \rangle - \overline{\langle v \rangle} \ ,$$

$$\langle u'u' \rangle = \langle uu \rangle - \langle u \rangle \langle u \rangle \ , \quad \langle v'v' \rangle = \langle vv \rangle - \langle v \rangle \langle v \rangle \ , \quad \langle u'v' \rangle = \langle uv \rangle - \langle u \rangle \langle v \rangle \ ,$$

$$\overline{u'u'} = \overline{\langle u'u' \rangle} \ , \quad \widetilde{u'u'} = \langle u'u' \rangle - \overline{\langle u'u' \rangle} \ , \quad \overline{v'v'} = \overline{\langle v'v' \rangle} \ , \quad \widetilde{v'v'} = \langle v'v' \rangle - \overline{\langle v'v' \rangle} \ ,$$

$$\overline{u'v'} = \overline{\langle u'v' \rangle} \ , \quad \widetilde{u'v'} = \langle u'v' \rangle - \overline{\langle u'v' \rangle} \ .$$

3.4 Experimental Plan

Both the time requirements for making measurements of unsteady profiles and the constraints on computer memory placed limits upon the scope of these experiments. As noted in the previous section, measurements would be restricted to phase-averaged values of $\langle u \rangle$, $\langle v \rangle$, $\langle uu \rangle$, $\langle vv \rangle$ and $\langle uv \rangle$ at 512 evenly spaced times during each unsteady cycle.

To judge from the results of Jayaraman *et al.* (1982), measures which varied with the imposed frequency of unsteadiness did so smoothly — when quantities such as the amplitude of the phase-conditioned displacement thickness were plotted against Strouhal number, no pronounced peaks or troughs were observed. For this study, seven frequencies of unsteadiness were considered sufficient and they were chosen as: 0.1, 0.2, 0.5, 0.8, 1.0, 1.6 and 2.0 hertz.

The time-averaged, free-stream velocity in the test section would decrease linearly in proportion to distance along it. The unsteady mainstream flow was to vary in a sinusoidal manner, with its amplitude increasing with distance along the test section, as described in §3.1. The test-section flow could then be expressed as:

$$U_\infty = U_0(1 - AX') \qquad \text{and} \qquad \tilde{u}_\infty = U_0 AX' \cos \omega t \ , \tag{3.4.1}$$

where U_0 is the steady, free-stream velocity along the development section and A is its amplitude of oscillation at the end of the test section, expressed as a fraction of U_0. Also, X' is defined as the dimensionless distance along the test section (of length L).

Measurements were to be taken at one amplitude of unsteadiness and the "high" amplitude value of A ($\simeq 20\%$), used by Jayaraman *et al.* (1982), was chosen. At this amplitude, good signal-to-noise ratio was obtained in deterministic measurements; when deduced by the phase-conditioning techniques of §2.1, deterministic measures

were of a large enough size to be discerned clearly. At this value of A, during the parts of the unsteady cycle when the adverse-pressure gradient was strongest, separation would take place in the equivalent steady flow (in which the detached layer would grow to the height of the channel — no longer a wall flow bounded by a free stream). The imposition of free-stream unsteadiness at frequencies as low as 0.1 hertz, however, was sufficient to ensure that the flow remained attached throughout the cycle.

This finding is partly explained by considering the role of the term $\partial(\overline{\tilde{u}_k\tilde{u}_i})/\partial x_k$ in the mean x-momentum equation (2.2.10) when applied in the free stream. For the boundary conditions of this study, forced free-stream oscillation at any non-zero frequency resulted in a free-stream measure of $\partial(\overline{\tilde{u}_k\tilde{u}_i})/\partial x_k$, the effect of which was to reduce the mean-adverse pressure gradient from its truly quasi-steady value. Therefore, while measurements of the true quasi-steadily-varying flow were not possible, the dynamic response of the turbulent boundary layer to imposed, organized unsteadiness could be studied with good signal-to-noise ratio and under conditions which might help to clarify the role which unsteadiness could play in the control of boundary-layer separation.

An extensive survey of the streamwise variation of the flow within the test section was not considered necessary for the purposes of this study; from the analyses of Appendix D, it would seem that the spatial periodicity observed by Cousteix & Houdeville (1983) and Karlsson (1959) would not be expected in this flow. Time-averaged and phase-conditioned measurements would therefore be made at the beginning of the test section ($X' = 0.0$) and at two locations within the test section ($X' = 0.45$ and $X' = 0.63$). Measurements made at the entrance to the test section could provide initial conditions, were the downstream results to be used as target data by turbulence modelers. These measurements, ostensibly taken under steady inlet conditions, would also be useful for contrasting against those taken further downstream in unsteady flow. For reference purposes, parameters describing the

TABLE 3.7

Steady Flow Conditions at $X' = 0.0$

Boundary-Layer Parameter	Initial Value
Free-stream velocity (U_0)	740 mm/sec
Boundary-layer thickness (D_c)	39.9 mm
Displacement thickness (δ_1)	6.8 mm
Momentum thickness (δ_2)	4.7 mm
Shape factor (H)	1.44
Momentum-thickness Reynolds number (Re_{δ_2})	3190
Friction coefficient (C_f)	3.02×10^{-3}
Kinematic viscosity (ν)	1.1×10^{-6} m^2/sec
Temperature	62° F

steady turbulent boundary layer at the entrance to the test section are given in Table 3.7.

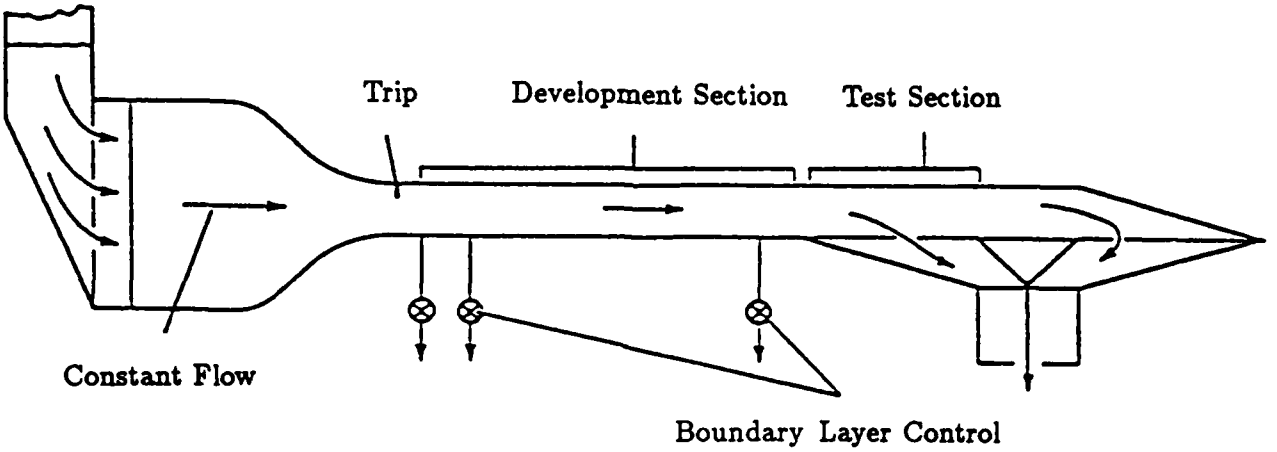

Figure 3.1 Closed-loop water tunnel.

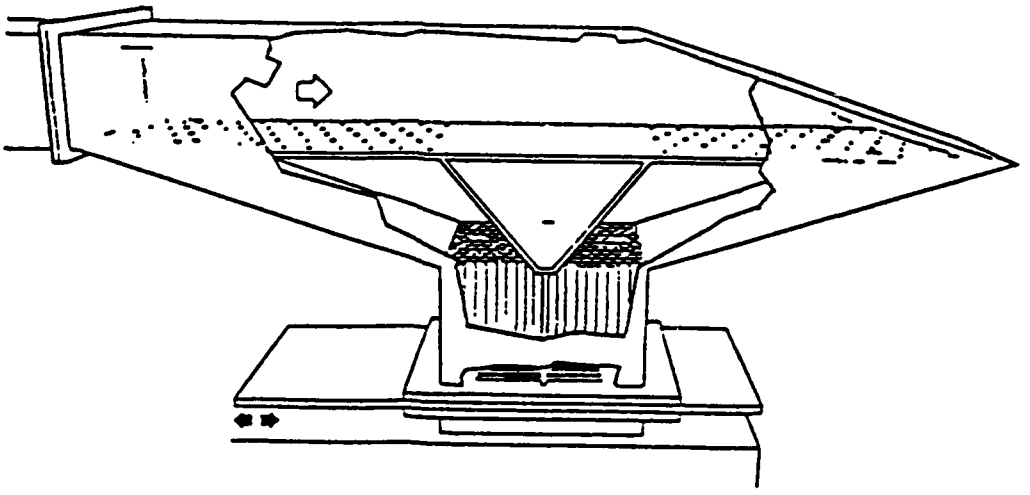

Figure 3.2 Tunnel test section.

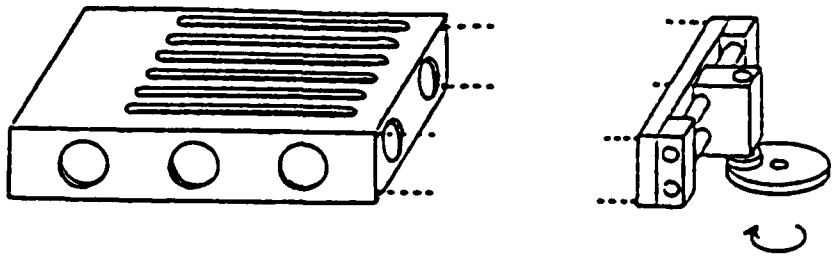

Figure 3.3 Gate valve and scotch-yoke mechanism.

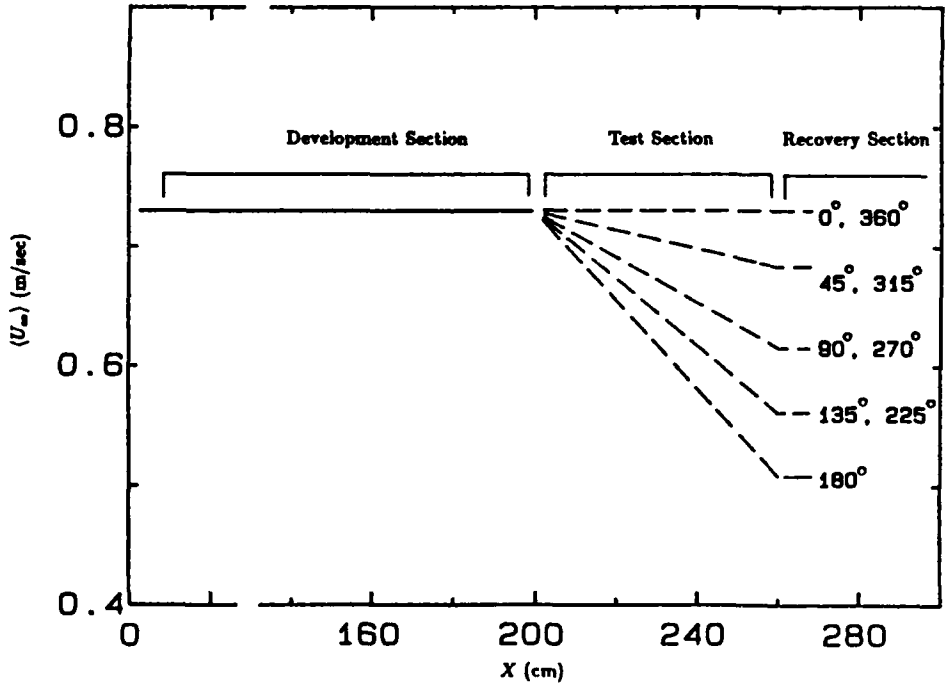

Figure 3.4 Distribution of free-stream velocity in the apparatus.

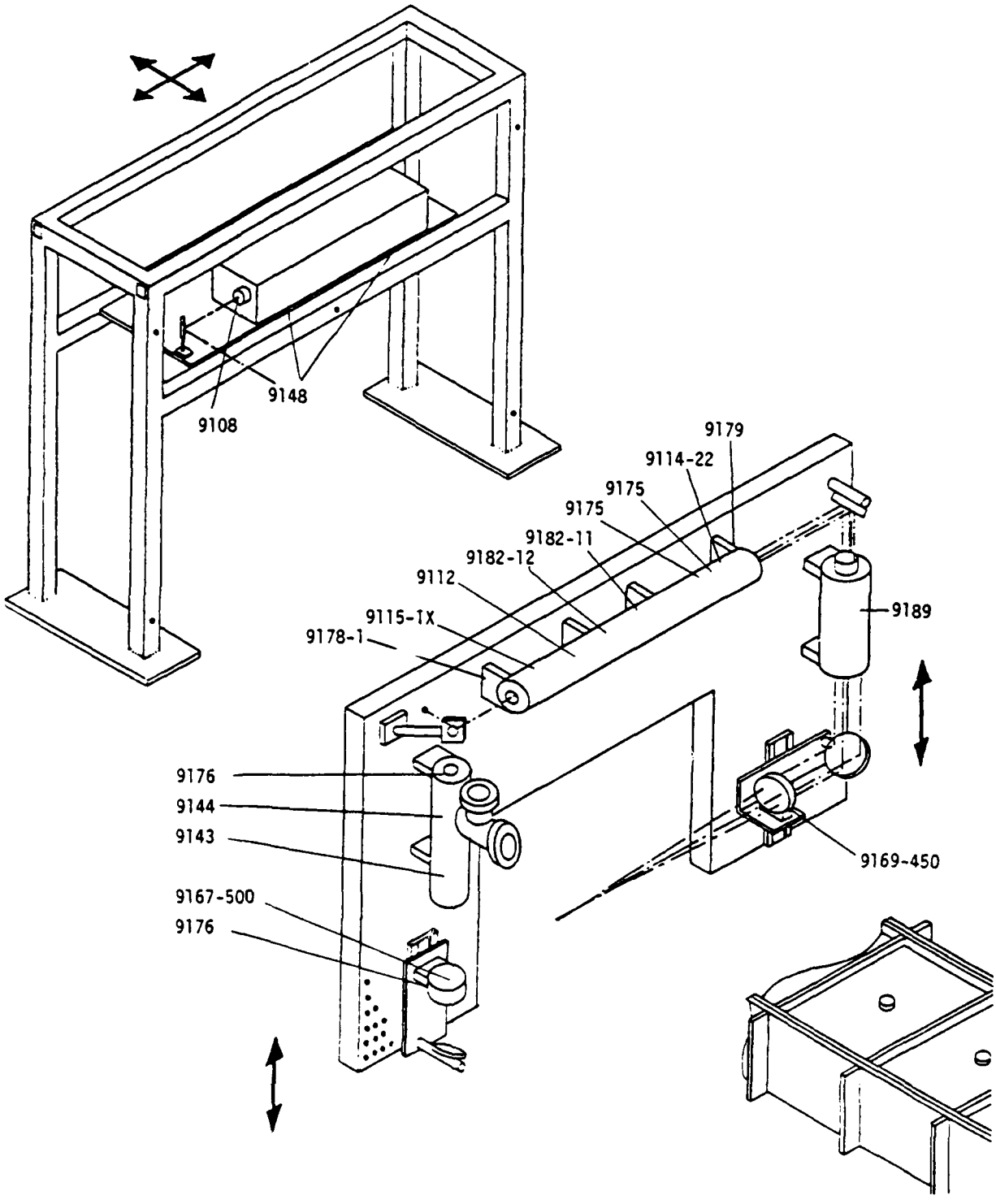

Figure 3.5 Measurement system.

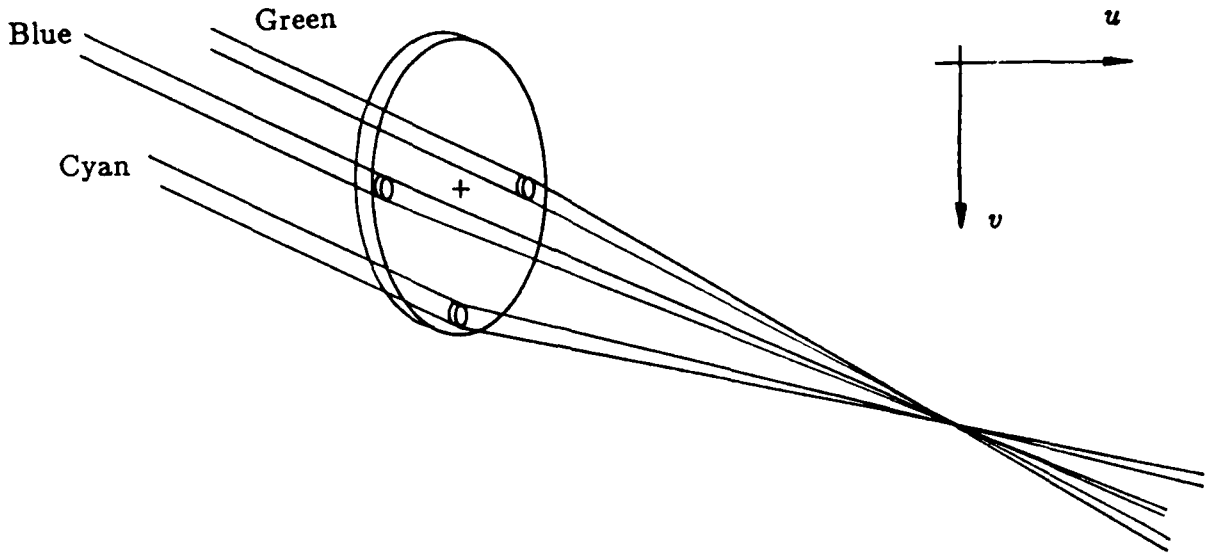

Figure 3.6 Three-beam system for measurement of $(u+v)/\sqrt{2}$ and $(u-v)/\sqrt{2}$.

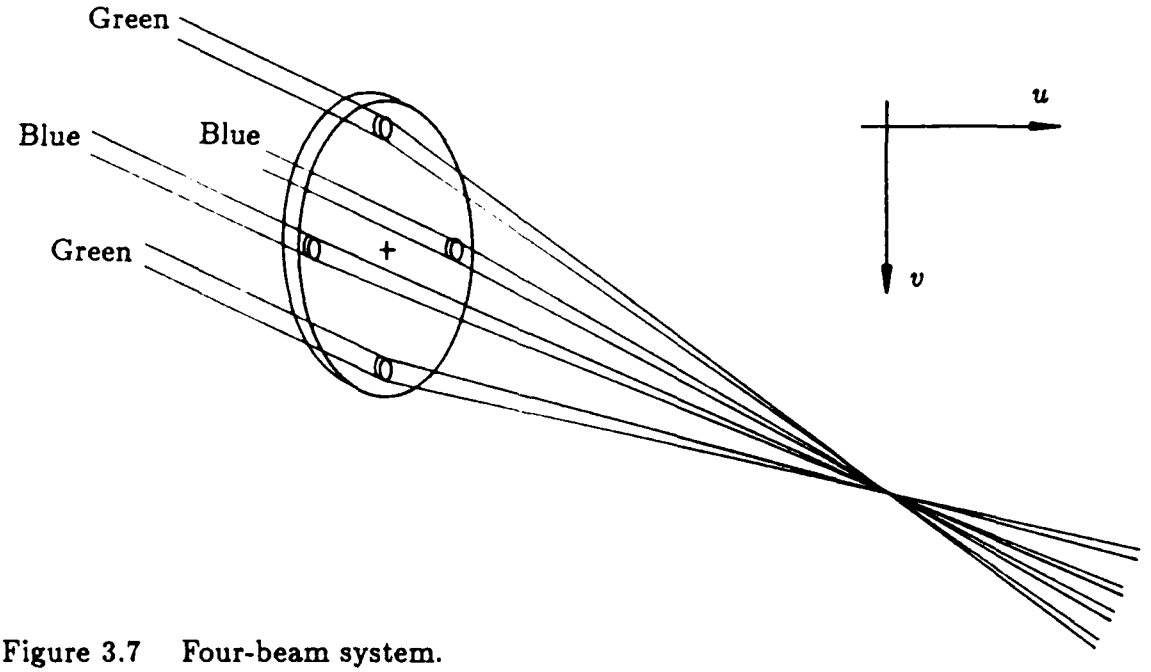

Figure 3.7 Four-beam system.

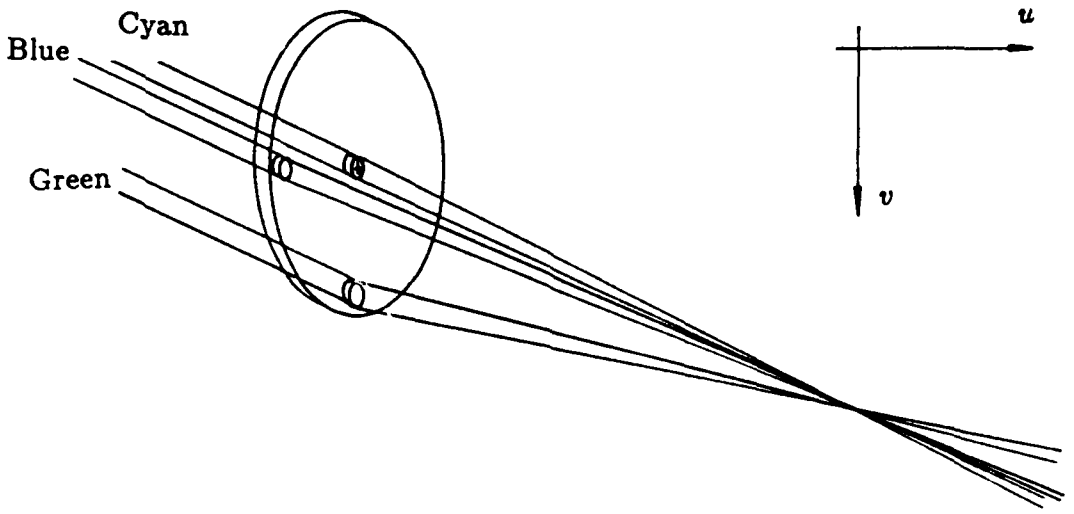

Figure 3.8 Three-beam system for measurement of u and v.

4. Qualification of the Facility and its Instrumentation

To make meaningful measurements of velocities in unsteady flows, one must be confident that the experiment reproduces the prescribed conditions accurately and that the measurement system has the necessary speed and resolution to capture all the features of interest. This confidence was gained through the performance of qualification exercises on the facility and the measurement equipment.

4.1 Measurement-System Qualification

The spatial resolution and the required sampling frequency of the measurement system were tested through evaluation of the correlation coefficient, $-\overline{u'v'}/(u'v')$, in a steady, flat-plate, turbulent boundary layer. According to Barlow & Johnston (1985), this quantity was especially sensitive to the spatial resolution of the laser-Doppler anemometer — inadequate resolution resulted in values of the coefficient which were substantially lower than expected.

It was desirable to make qualification measurements at the locations at which data would subsequently be taken — in the test section of the apparatus. The gate valve was therefore fixed in position so that there was no flow through the porous bottom wall of the test section, and a steady, zero-pressure-gradient, turbulent boundary layer was formed on the top wall of the tunnel. At this stage of the qualification, that the boundary layer was a true flat-plate one was not of prime importance, since a correlation coefficient of about 0.4 would be expected in any case (Tennekes & Lumley, §2.3).

As a preliminary exercise, a profile of the mean, streamwise component of velocity was taken, from which the local friction velocity of the boundary layer, u_τ, was deduced. This friction velocity was used to scale the results of reference-data sets, taken in the near-wall region of turbulent boundary layers, so that local estimates of the Kolmogoroff length and frequency scales could be made for the qualification

flow (Appendix A). These estimates were then used to choose the initial size of pinhole for the receiving optics and the sampling frequency necessary for correct deduction of $-\overline{u'v'}/(u'v')$.

The velocity profile shown in Figure 4.1 was taken about two thirds of the way along the test section. It was used for the calculations of Appendix A, which indicated that the orders of magnitude of the Kolmogoroff length and frequency scales would be 0.1 mm and 100 hertz respectively. If these estimates were to prove realistic, the lowest rate at which data could be sampled would be 200 hertz (Bracewell, §10). Now the spatial resolution was determined by the system's limiting aperture, a pinhole placed in the field-stop system immediately in front of the fixed receiving-optics train. When projected along the optical path to the probe volume, the aperture's size was magnified by a factor of around five, a result calculated from considerations of geometric optics. Collection of scattered light 15° off the optical axis further lengthened the measuring volume by the cosecant of this angle, an additional factor of about four. Resolution to the estimated order of the Kolmogoroff length scale would then require a pinhole of about 5 microns in diameter.

The values of correlation coefficent measured with this level of resolution are shown in Figure 4.2. Over the major part of the boundary layer, thev just exceeded 0.4 with a peak value of 0.42, in agreement with the expected results. No decrease in the correlation coefficient was noted when pinholes as large as 25 microns were used although still coarser resolution did produce values which were clearly too low, as noted by Barlow & Johnston (1985). If this pinhole size is translated back to multiples of η, the estimated Kolmogoroff length scale, it corresponds to a value of 11η.

By increasing the pinhole size from 5 to 25 microns, the data were validated by the trackers at rates between 2000 and 4000 hertz. These rates were an order of magnitude greater than the sampling frequency and so data acquired at these rates could be considered continuous. The addition of a little seeding (silicon carbide particles) had a slightly beneficial effect upon the data rates, but the strongest

influence was the power of the laser. Through careful tuning, the output of the laser (with an etalon installed) could be made to reach 200 milliwatts, the operating condition at which the highest data rates were reached for this optical system.

The frequency trackers used for these experiments validated a signal when it had been tracked for ten successive Doppler cycles. For example, an ideal sinusoidal signal, the downmix frequency of 200 kilohertz, was tracked at a validated-data rate of 20 kilohertz. This explanation of the validated-data rate is given so that meaningful comparisons may be made with data rates measured with other kinds of frequency-analysis equipment, which employ different validation techniques.

Eulerian time spectra of the "energy" content of the u, v and uv velocity measures were also taken in the steady, turbulent boundary layer. These "power" spectra are presented in Figure 4.3; they are the results of Fourier-transformed records of 32,768 point data sets, sampled at 400 hertz. The Eulerian time spectrum describes the temporal changes seen from a fixed point, with respect to the frame of reference in which the mean velocity at that point is zero. Consequently, this kind of spectrum measures the frequency of eddies *advected* past the observation point by other eddies (Tennekes & Lumley, §8.5) and may differ from a "true" wave-number spectrum. However, the shapes of the Eulerian time spectra at high frequencies did indicate an absence of noise- and ambiguity-broadening effects, since no significant flattening of the tails of the spectra is observed. Therefore the signal-to-noise ratios of data taken with this measurement system were considered satisfactory. Their shapes were similar to those reported by Barlow & Johnston (1985) in their experiments in parallel-channel flow. The lack of definition at low frequencies was attributed to the size of the data record; it was not considered sufficiently large to resolve the spectrum accurately *at the lowest frequencies*.

The performance of the measurement system, under unsteady conditions, was tested through Eulerian time spectra taken in the unsteady, turbulent boundary layer. The gate valve was driven at an oscillation frequency of 0.2 hertz and data were sampled at the same rate and for the same duration as for steady flow. The

data-validation rates were unchanged from their steady-flow values and the trackers showed no tendency to lose track of the unsteady velocity signal at this frequency, nor at frequencies as high as 2 hertz. The spectra taken in unsteady flow, together with the steady-flow spectra discussed above, are displayed in Figures 4.4 – 4.6. Although these spectra contained several interesting features, for the purposes of qualification, the region of importance was the high-frequency end. The slopes of the steady spectra and the unsteady spectra at high frequencies (much higher than the frequency of perturbation of the flow) were almost identical. Since isotropic behavior in this range of the spectrum was to be expected (Tennekes & Lumley, §8.3), the excellent agreement between the slopes of the steady and unsteady spectra implied that the resolution needs for steady-flow measurements were adequate for measurements in unsteady flow. The absence of significant flattening of the tails of the spectra indicated that ambiguity effects were again negligible.

4.2 Facility Qualification for Steady Flow

Qualification of steady flow in the facility was carried out through the measurement of velocity profiles in the steady, zero-pressure-gradient, turbulent boundary layer which developed on the top wall of the tunnel. The gate valve was set so that constant pressure conditions prevailed in the test section, as well as along the development section. By taking measurements far downstream in the test section, the risk that these data might suffer from effects of low Reynolds numbers would be minimized. Moreover, these measures could be taken in the knowledge that the spatial resolution of the laser-Doppler anemometer had already been refined, the required sampling frequency had been deduced and the signal-to-noise ratio of the system was adequate.

Profiles of U, V, $\overline{u'u'}$, $\overline{v'v'}$ and $-\overline{u'v'}$ were taken, with measurements at some thirty points in the boundary layer; at each point, 100,000 instantaneous values of u and v were measured at a sampling rate of 400 hertz, while the frequency trackers

validated data at rates between 2000 and 4000 hertz. A profile of mean, streamwise velocity is shown in Figure 4.1. A least-squares fit of Coles' mean velocity function was made to this profile — the parameters u_τ and δ were varied to achieve the best fit within the region limited by $y^+ > 50$ and $y/\delta < 0.8$ (Coles 1968). The profile, normalized according to this fitted function, is shown in Figure 4.7 — good agreement with the expected result is evident, even where $y^+ = 2$, the nearest point to wall at which data were taken.

Deduction of the friction velocity, u_τ, from Coles' mean velocity function, enabled the near-wall measures of u', v' and $-\overline{u'v'}$ to be plotted in a normalized form, which allowed comparison with reference-data sets. In Figures 4.8 – 4.10, reduced measures of u', v' and $-\overline{u'v'}$ are shown for values of y^+ from 2 to 50. The measures of u'/u_τ and $-\overline{u'v'}/u_\tau^2$ appeared to match those of Laufer (1954); the values of v'/u_τ were noticeably higher than those of Laufer, but in good agreement with the more recent measurements of Barlow & Johnston (1985). The asymptotic behavior of v', as the wall was approached, was evidently incorrect. The flattening of the profile might be attributed to wall vibration in the vertical plane. It might also be a consequence of the measuring volume interfering with the wall and causing light scattered at this surface to reach the receiving optics.

The profile of V, the wall-normal component of mean velocity, is shown in Figure 4.11; it was several orders of magnitude smaller than U throughout the boundary layer. Although no reference data could be found for the purposes of comparison, the tendency towards negative values as the wall was approached, rather than zero, might be attributed to slight curvature in the plexiglass walls of the apparatus. Curvature which varied in the wall-normal direction would cause minor misalignments of the measuring volume; the shape of the profile might then be due to contamination of V measurements by fractional proportions of U, of sign and magnitude which varied according to the local curvature.

The premise that the flow was two-dimensional could be tested by making measurements across the span of the tunnel, at fixed distances below the top wall. The

variation in mean streamwise velocity across the central 40% of the tunnel was limited to a small percentage of its average value, as shown in Figure 4.12. Spanwise variations in V, $\overline{u'u'}$, $\overline{v'v'}$ and $-\overline{u'v'}$ are displayed in Figures 4.13 – 4.16; in general, they too were within a small percentage of their mean values and flat at the center. There was no evidence of dramatic non-uniformity in the spanwise direction, the presence of which might indicate strong, local, streamwise vorticity.

4.3 Facility Qualification for Unsteady Flow

The facility was designed so that a turbulent boundary layer, which had developed under essentially steady, constant-pressure conditions, would be subjected to well-defined, free-stream unsteadiness in the test section. Here, the locally unsteady mainstream was to be characterized by:

(*i*) a linear decrease in time-mean, free-stream velocity in the streamwise direction,

(*ii*) a linear increase in the amplitude of its deterministic velocity component, in the streamwise direction,

(*iii*) a linear, streamwise variation in free-stream velocity at each discrete phase in the unsteady cycle.

Measurements were made by Jayaraman *et al.* (1982) to test how well these requirements were met. For the most part, excellent agreement was reached between the prescribed and measured behavior. At low frequencies of gate-valve oscillation, however, the streamwise gradient of the time-mean decrease in free-stream velocity was not as steep its high-frequency counterpart. Phase-averaged measurements indicated that there was also a slight departure from the third of the above criteria; at phases corresponding to the constant-pressure condition in the test section (around 0°), the streamwise variation in mainstream velocity was not quite linear. These imperfections were thought to have little effect upon the unsteady, turbulent

boundary layer. As no changes had been made to the oscillation scheme used by Jayaraman *et al.* (1982), these qualification measurements were not retaken.

An important aspect of this experiment is the nominally steady development of the flow, upstream of the test section. That this requirement was met could be verified by making measurements in the development section, while unsteady conditions prevailed in the test section. By measuring the velocities, u and v, at each discrete phase associated with the downstream oscillation, their phase-averaged values, $\langle u \rangle$ and $\langle v \rangle$, could be deduced. The root-mean-square deviations of $\langle u \rangle$ and $\langle v \rangle$ from their mean values during the unsteady cycle then indicated the size of the upstream disturbance. Normalized plots of this organized disturbance are shown in Figures 4.17 and 4.18; it was always less than two percent of the mean free-stream velocity and reached its largest value near the wall, as the frequency of oscillation increased. Moreover, the peak r.m.s. value of upstream disturbance was an order of magnitude smaller than its downstream counterpart, which reached 17% of the mean free-stream velocity in the mainstream in the test section and still larger values within the unsteady boundary layer there.

The two-dimensionality of the unsteady flow was tested by making measurements across the span of the tunnel, while unsteady conditions prevailed. Measures of the time-averaged quantities, U, V, $\overline{u'u'}$, $\overline{v'v'}$ and $-\overline{u'v'}$ were taken in the test section, over the range of frequencies for which profiles of unsteady velocities were to be taken. The spanwise variation of U, normalized by the free-stream velocity in the development section, is shown in Figure 4.19; it was a small percentage of its mean value across the central 40% of the tunnel and very flat at the center. Results are only presented for the case of gate-valve oscillation at 1.0 hertz, although they were representative of data taken at other frequencies. The spanwise measures of V, $\overline{u'u'}$, $\overline{v'v'}$ and $-\overline{u'v'}$ are shown in Figures 4.20 – 4.23; they too exhibited a welcome flatness at the center of the tunnel, with non-uniformities restricted to a small percentage of their mean values. Since neither the steady nor the unsteady

flow appeared to suffer from significant spanwise variation in any of the measured quantities, the two-dimensionality of the flow was considered satisfactory.

Phase-averaged measures of the instantaneous free-stream velocity, taken two thirds of the way along the test section, are shown in Figure 4.24; these measures were averaged over 400 ensembles. As a check upon the accuracy with which the gate-valve oscillation translated to a sinusoidal variation in the mainstream, the data set was decomposed into its Fourier components — the ratio of the "energy" at the fundamental frequency to the total "energy" in the phase-averaged flow (not including the mean flow) was greater than 99.5% for all frequencies shown. For comparison, the free-stream variation at the beginning of the test section is shown in Figure 4.25. Ideally, it should not vary with phase angle; however, in actuality, there was some harmonic content but it was clearly minimal compared to that in the test section (Figure 4.24).

Thus the qualification procedures described in this chapter indicated that the measurement system performed adequately and that both steady and unsteady flow in the facility matched their prescribed forms. The response of the turbulent boundary layer to forced free-stream unsteadiness could then be investigated according to the experimental plan of §3.4, in the knowledge that the results should be trustworthy.

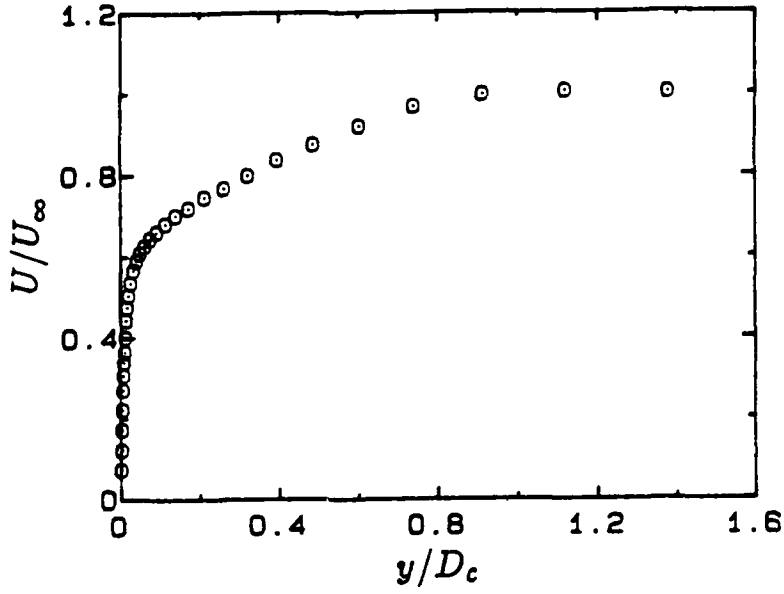

Figure 4.1 Profile of U under steady, constant-pressure conditions, $Re_{\delta_2} = 3115$. D_c is the boundary-layer thickness, deduced from a fit of Coles' mean velocity function.

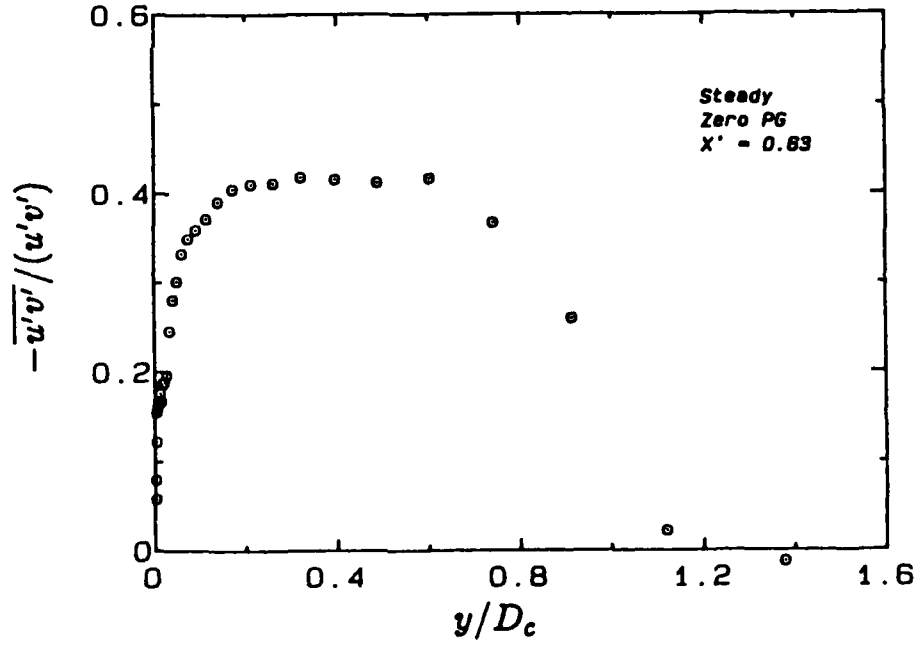

Figure 4.2 Profile of the correlation coefficient, $-\overline{u'v'}/(u'v')$, under steady conditions.

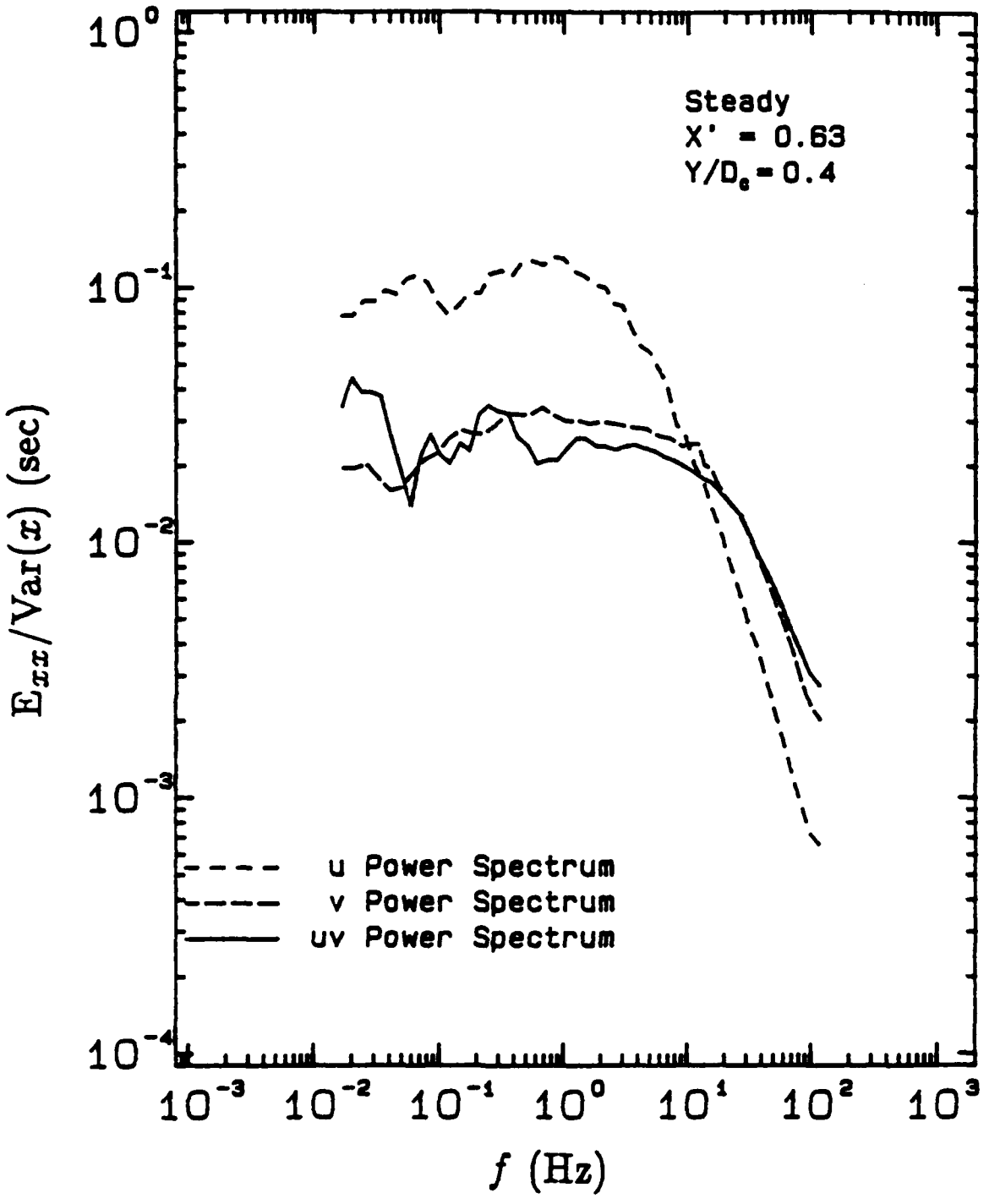

Figure 4.3 Power spectra in the steady, constant-pressure boundary layer.

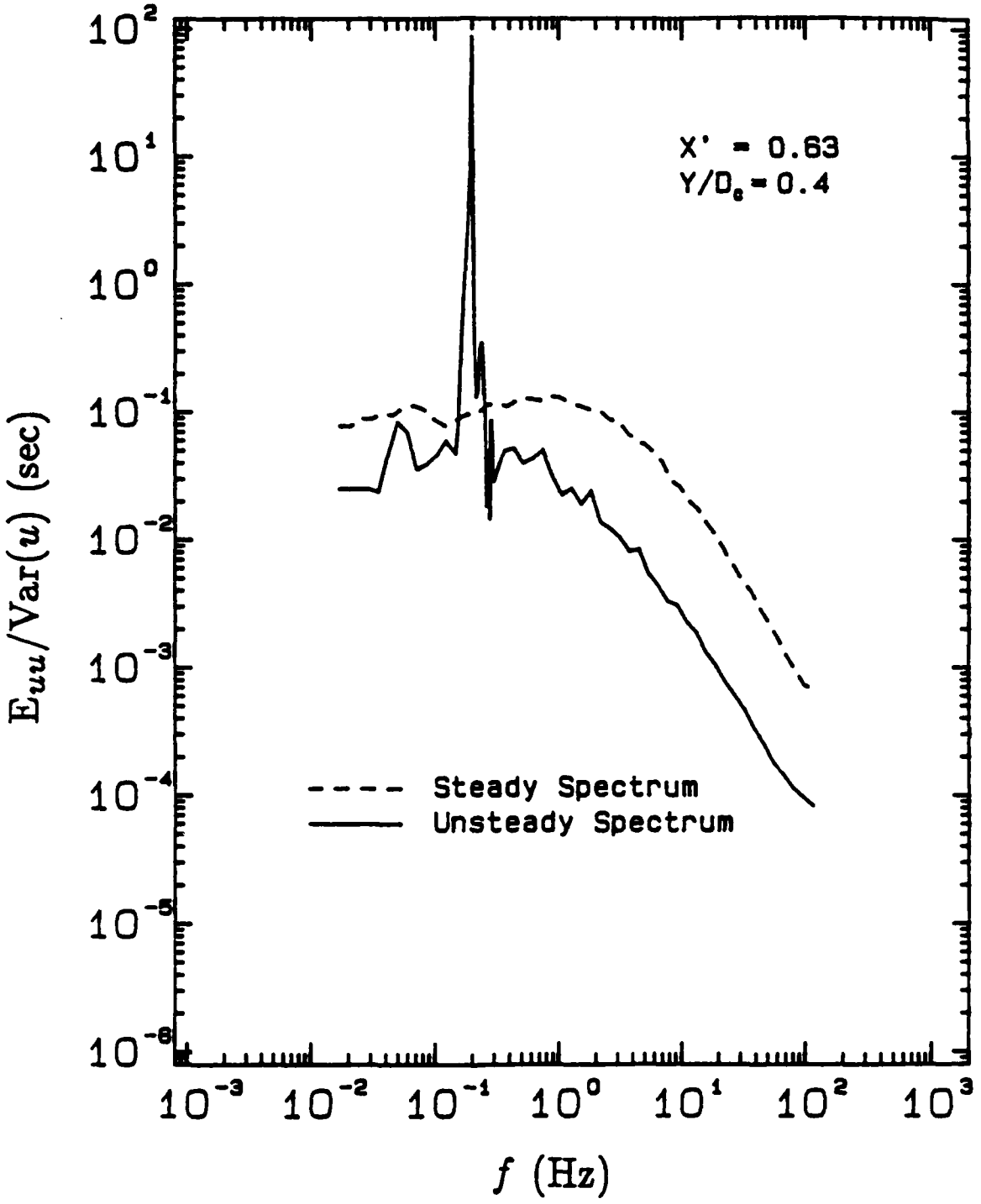

Figure 4.4 Power spectra of uu in the turbulent boundary layer under steady and unsteady conditions.

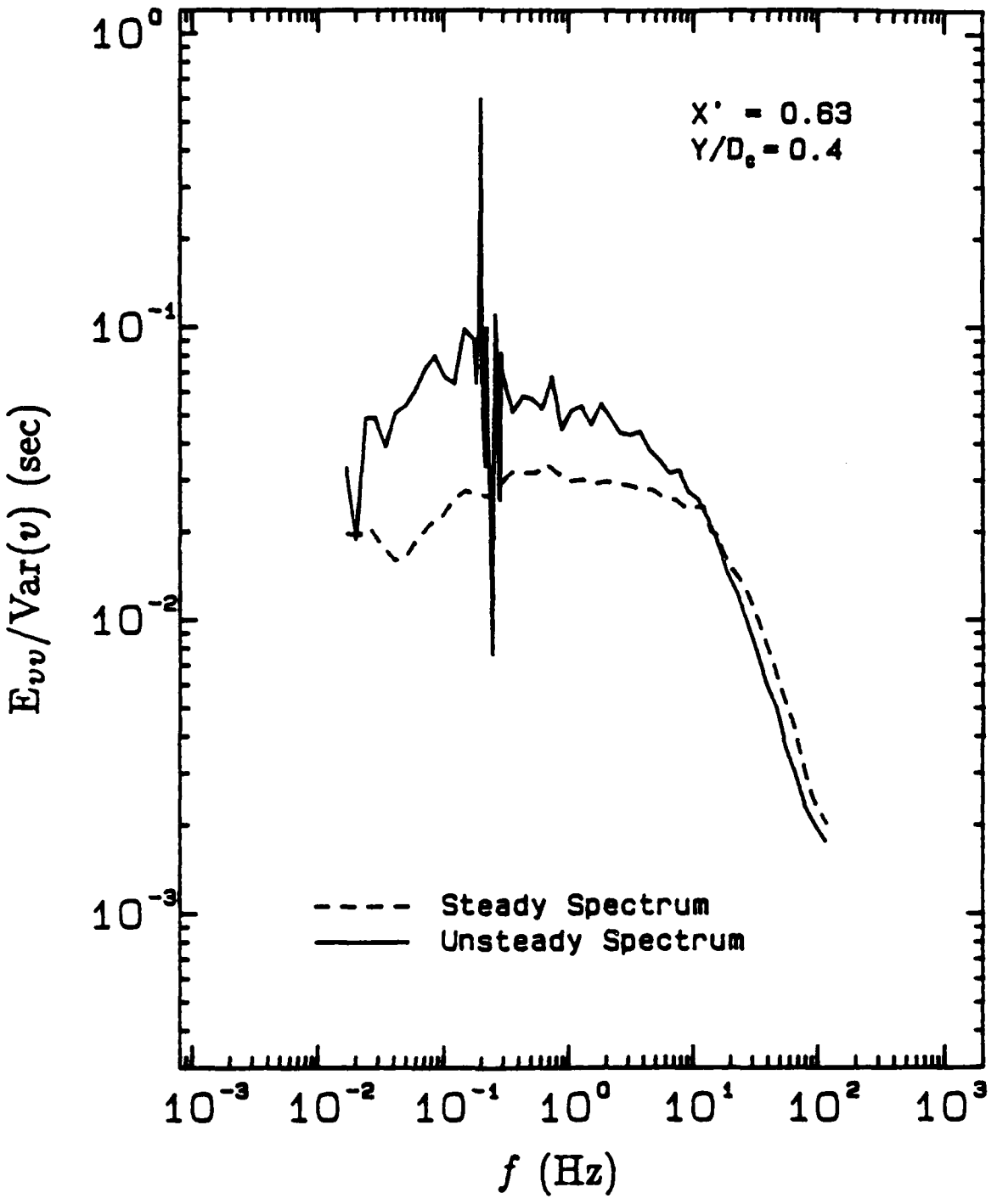

Figure 4.5 Power spectra of vv in the turbulent boundary layer under steady and unsteady conditions.

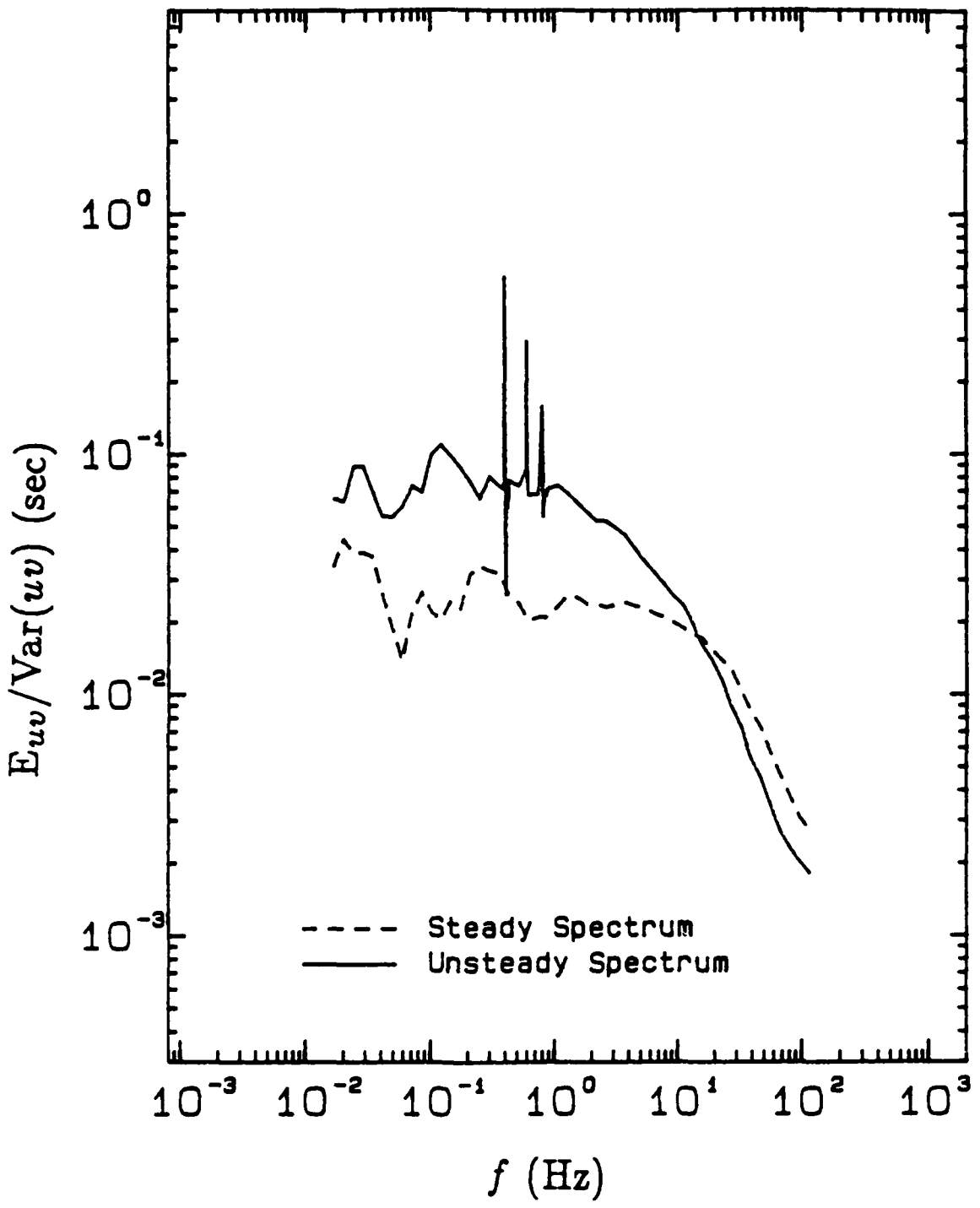

Figure 4.6 Power spectra of uv in the turbulent boundary layer under steady and unsteady conditions.

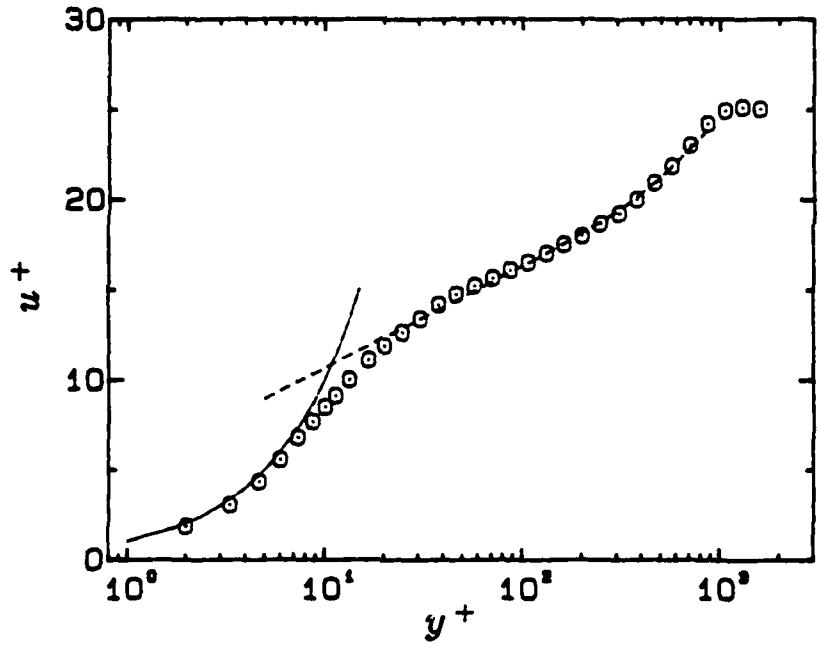

Figure 4.7 Profile of U, normalized according to Coles' mean velocity function, under steady, constant-pressure conditions.

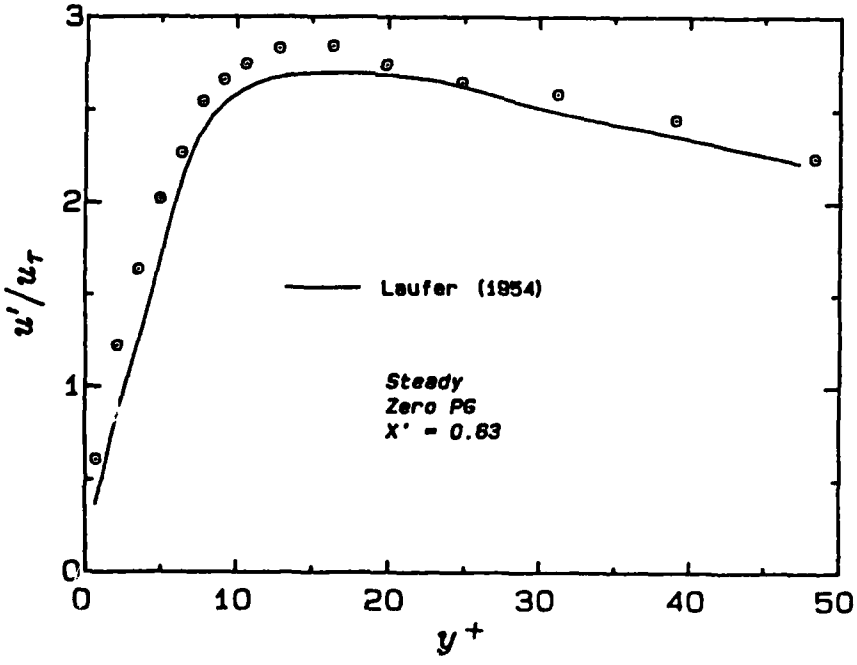

Figure 4.8 Normalized near-wall values of u' under steady, constant-pressure conditions.

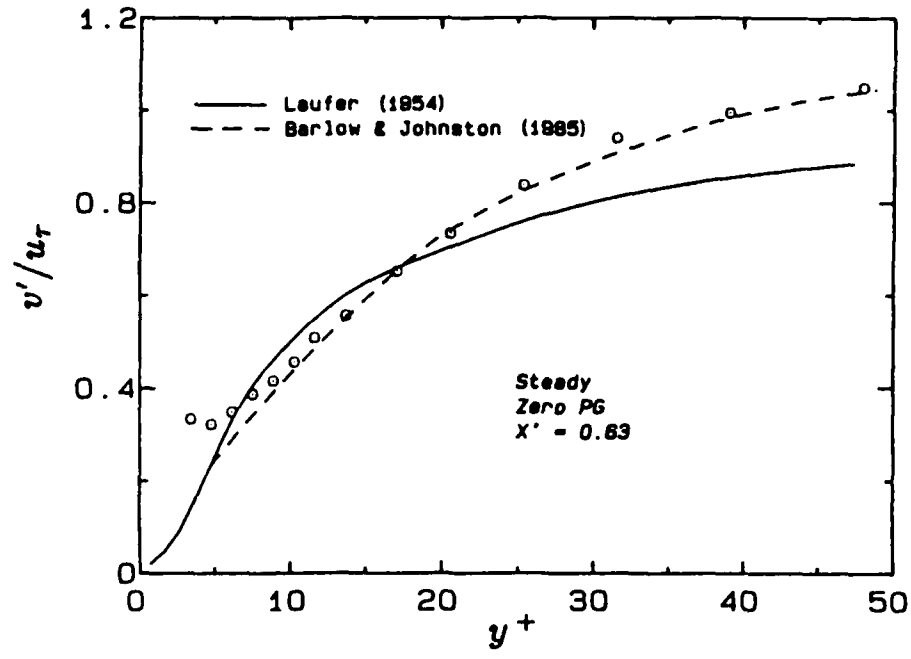

Figure 4.9 Normalized near-wall values of v' under steady, constant-pressure conditions.

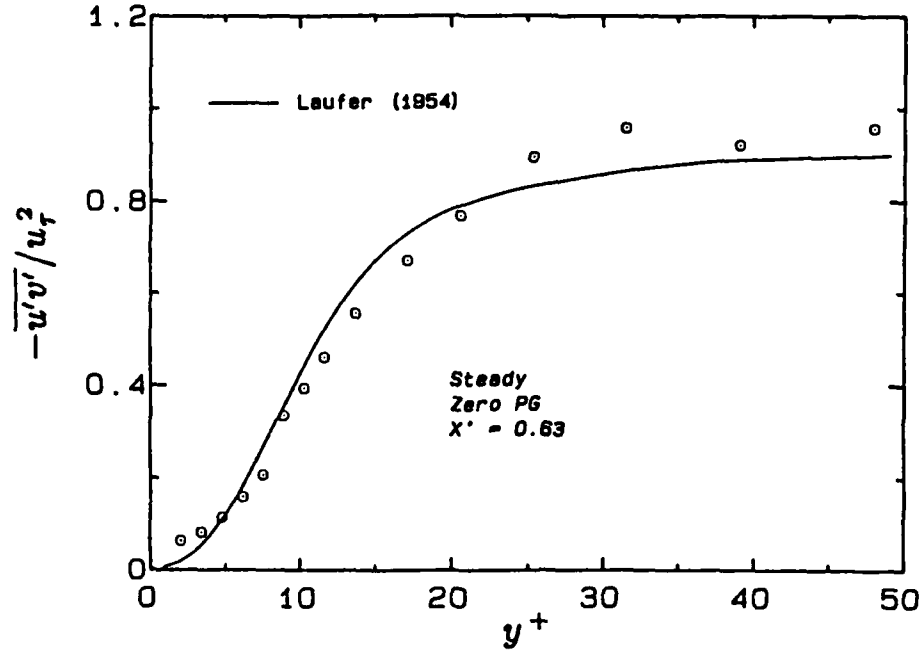

Figure 4.10 Normalized near-wall values of $-\overline{u'v'}$ under steady, constant-pressure conditions.

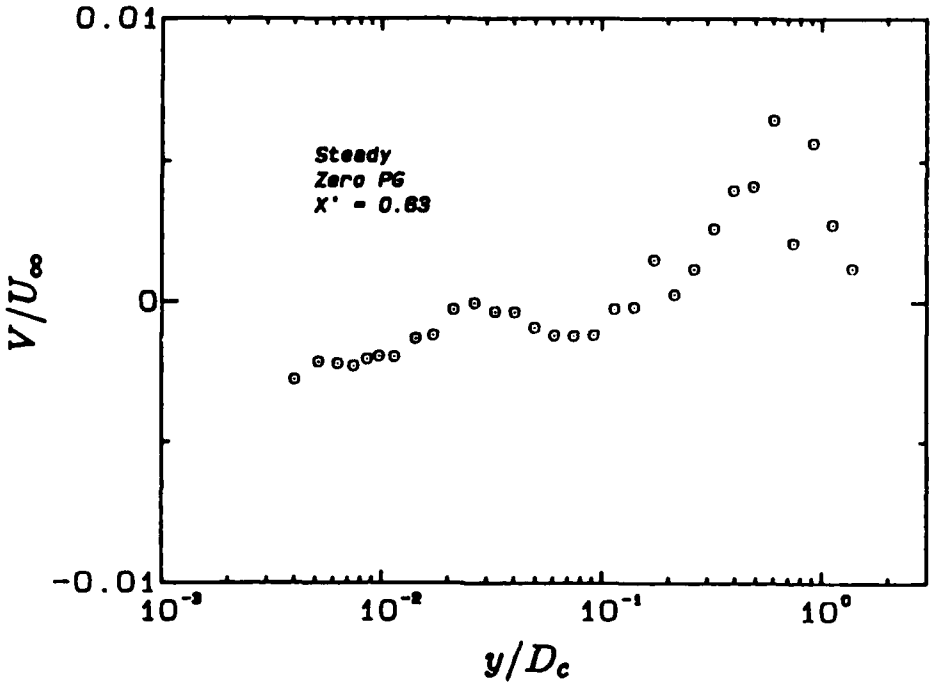

Figure 4.11 Profile of V under steady, constant-pressure conditions.

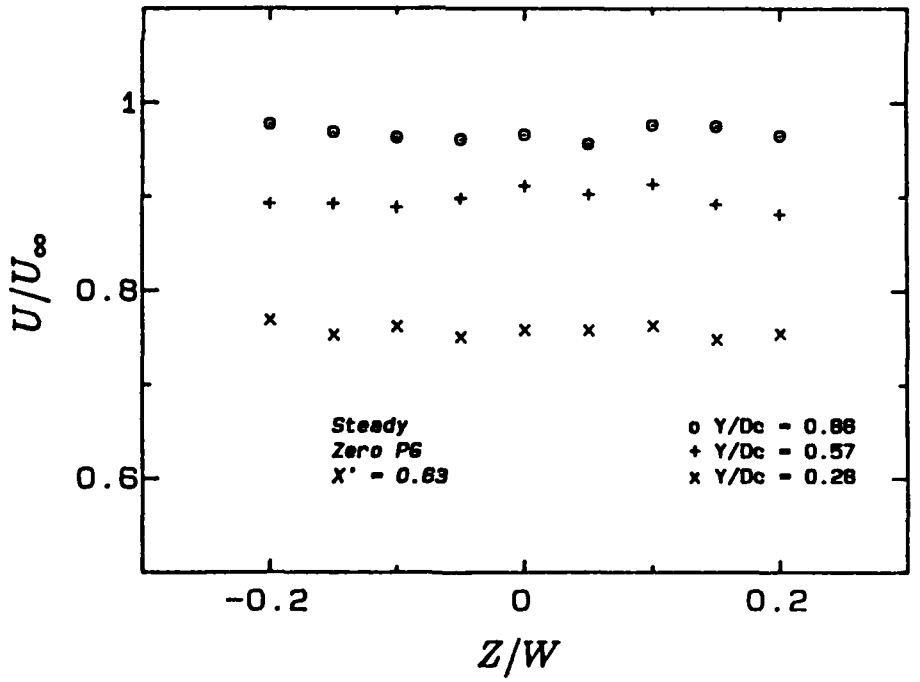

Figure 4.12 Spanwise variation of U under steady, constant-pressure conditions.

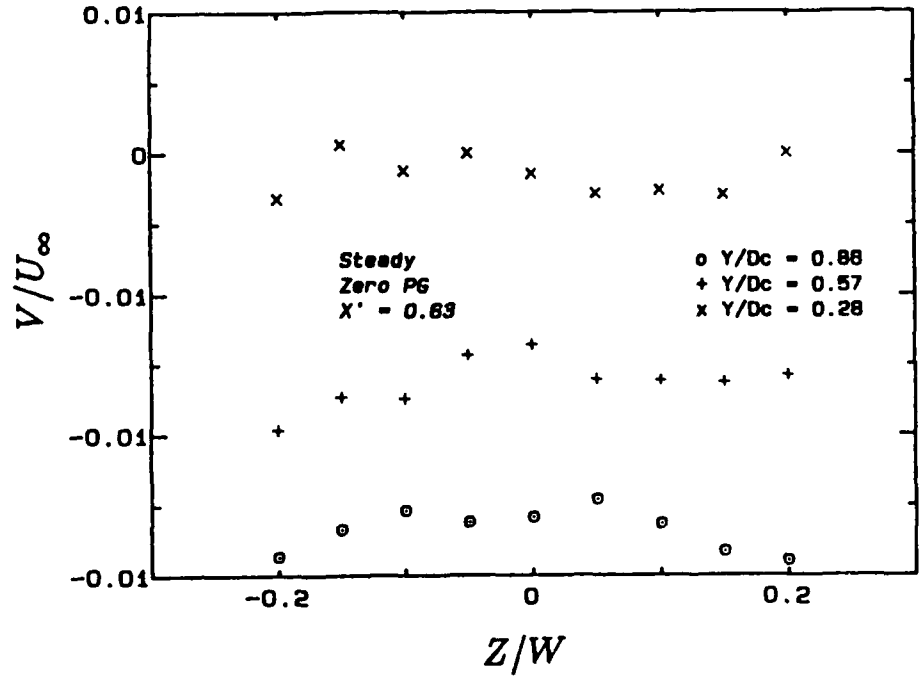

Figure 4.13 Spanwise variation of V under steady, constant-pressure conditions.

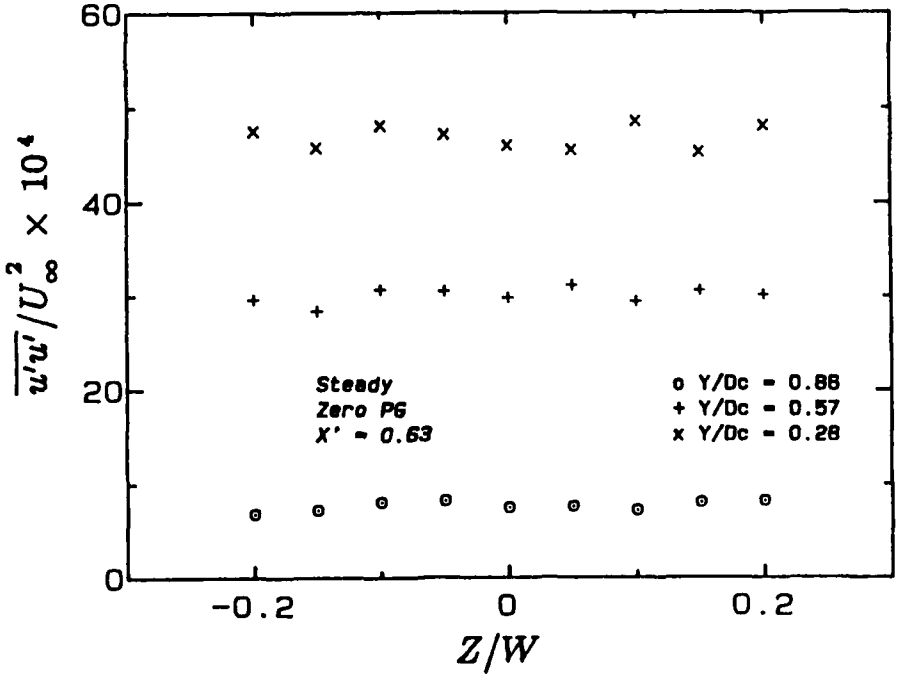

Figure 4.14 Spanwise variation of $\overline{u'u'}$ under steady, constant-pressure conditions.

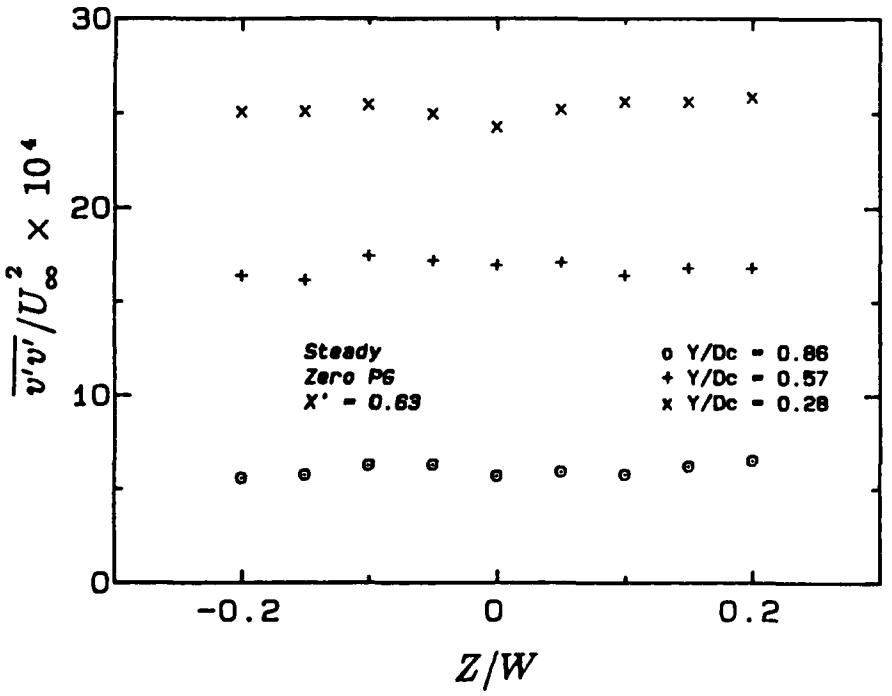

Figure 4.15 Spanwise variation of $\overline{v'v'}$ under steady, constant-pressure conditions.

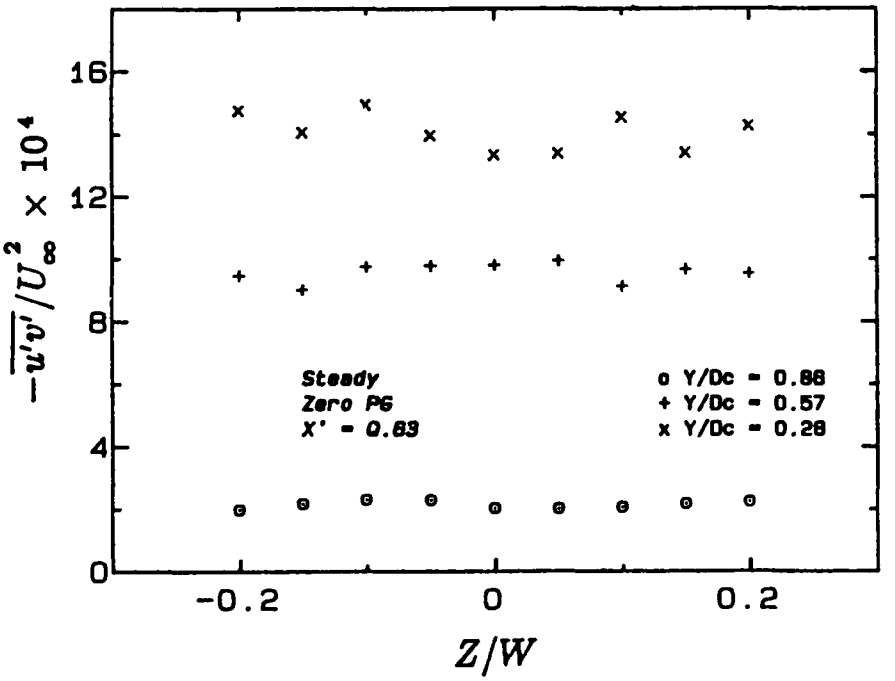

Figure 4.16 Spanwise variation of $-\overline{u'v'}$ under steady, constant-pressure conditions.

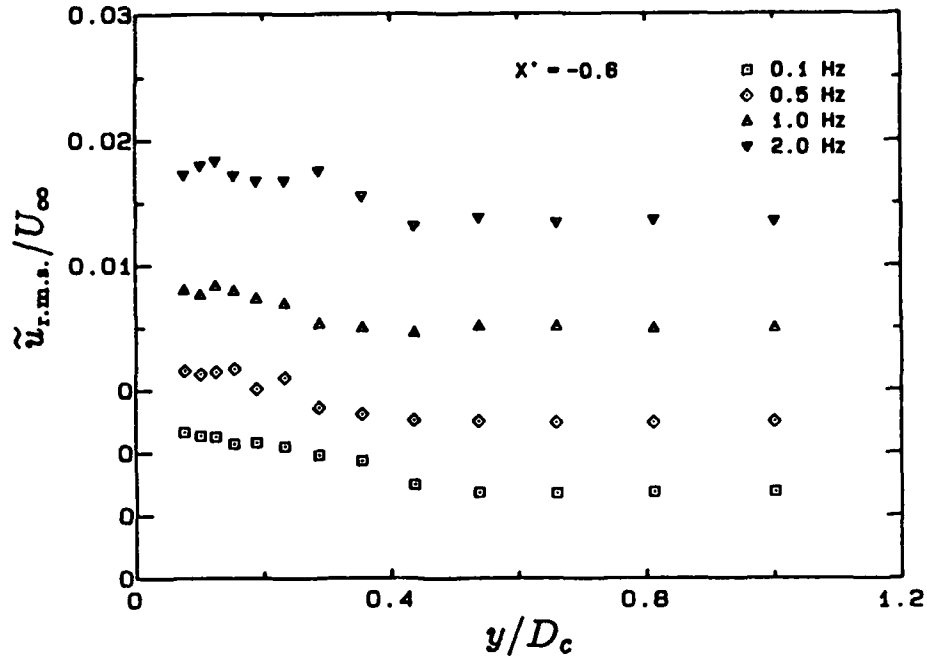

Figure 4.17 R.m.s. upstream disturbance in $\langle u \rangle$.

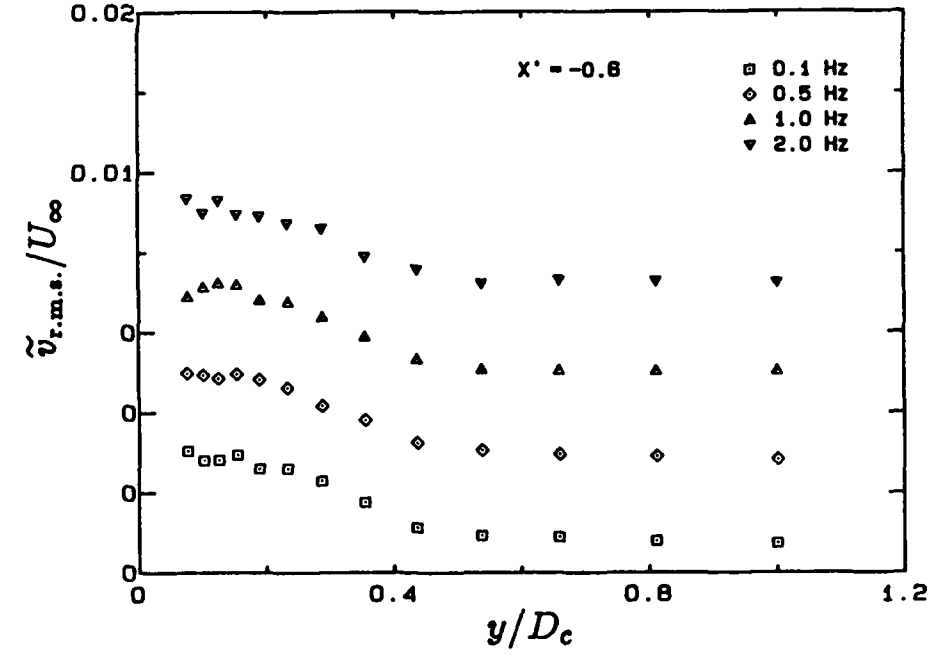

Figure 4.18 R.m.s. upstream disturbance in $\langle v \rangle$.

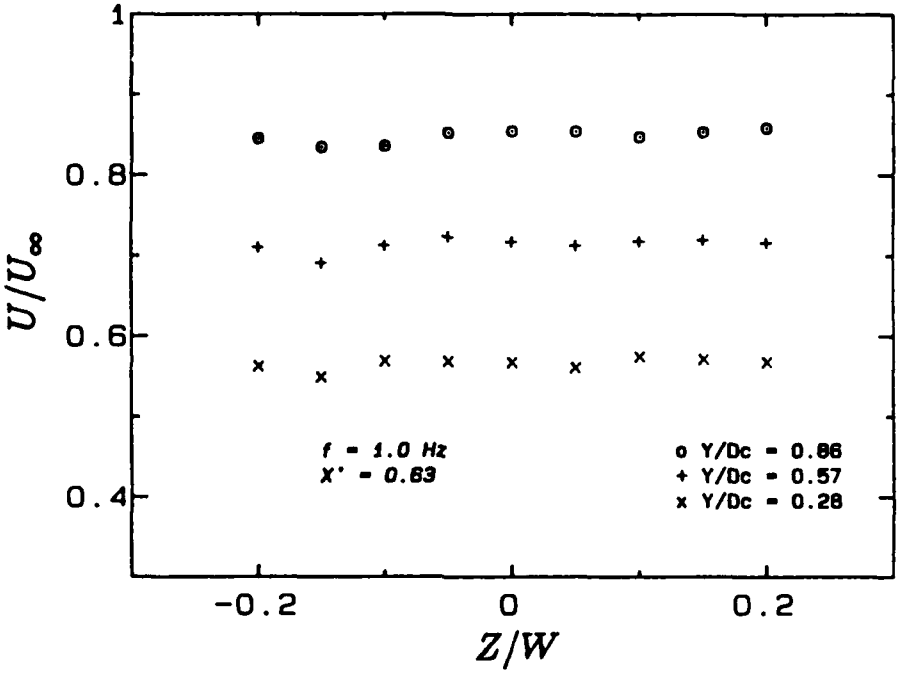

Figure 4.19 Spanwise variation of U under unsteady conditions.

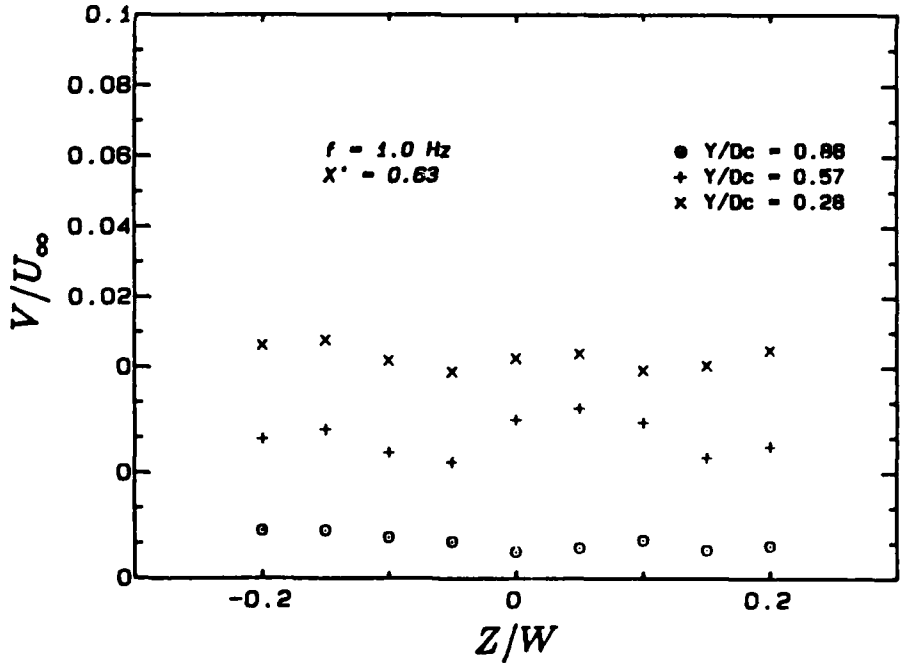

Figure 4.20 Spanwise variation of V under unsteady conditions.

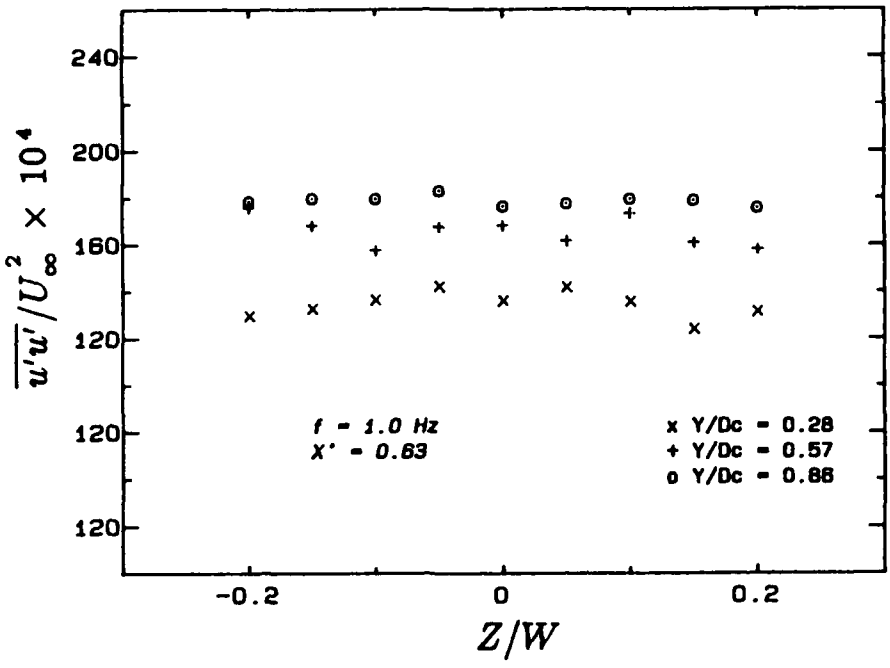

Figure 4.21 Spanwise variation of $\overline{u'u'}$ under unsteady conditions.

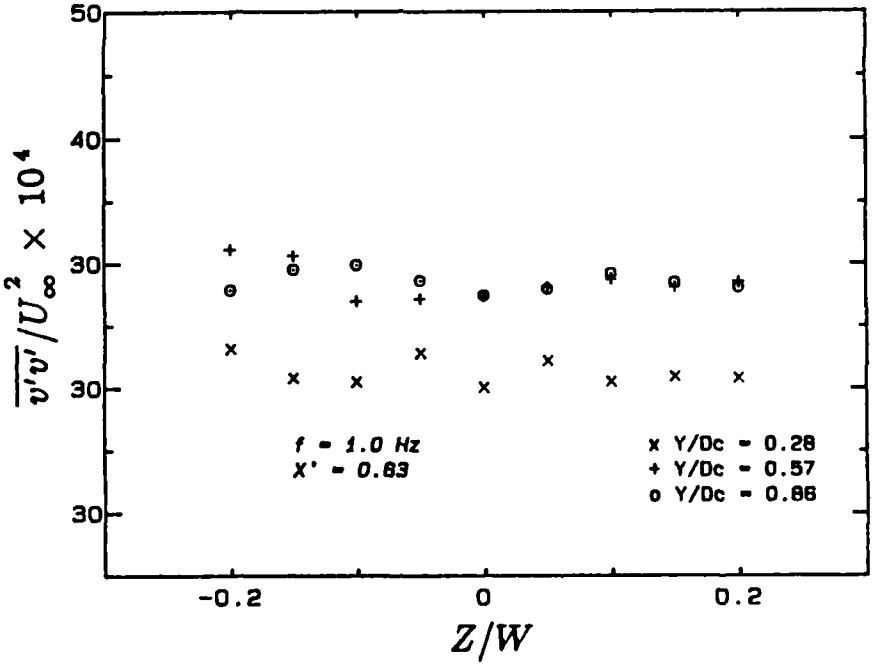

Figure 4.22 Spanwise variation of $\overline{v'v'}$ under unsteady conditions.

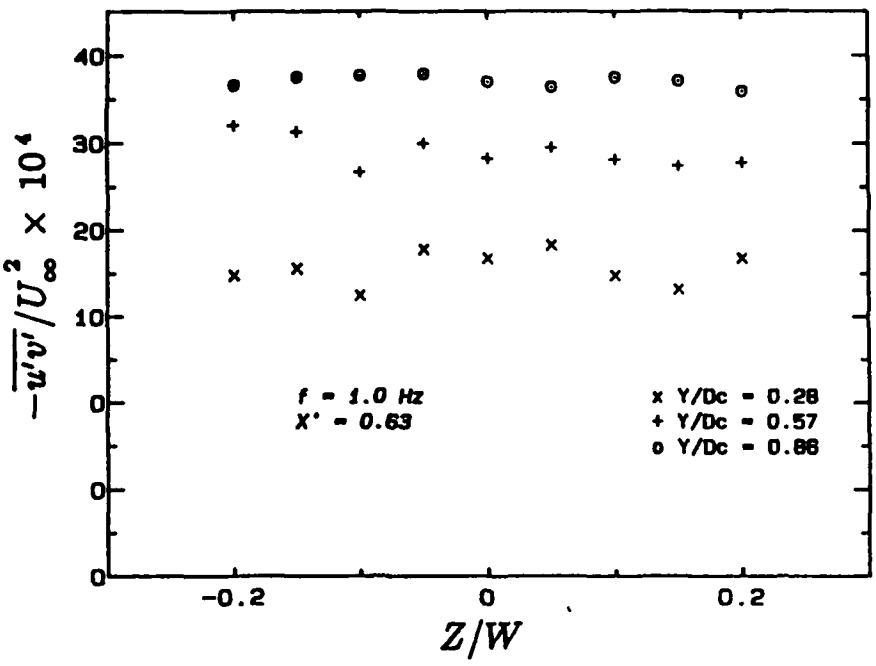

Figure 4.23 Spanwise variation of $-\overline{u'v'}$ under unsteady conditions.

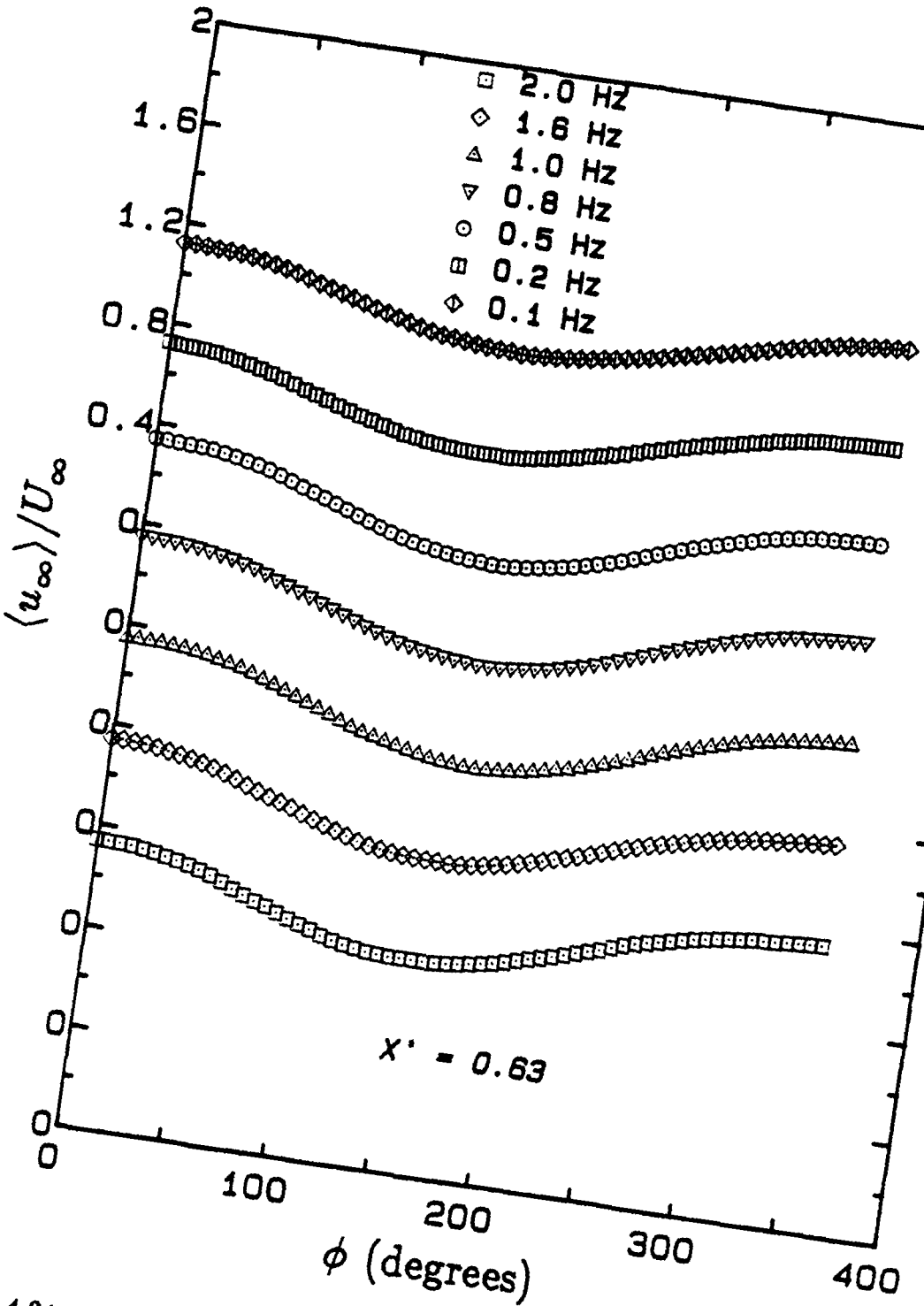

Figure 4.24 Variation of $\langle u_\infty \rangle$ with phase angle. $X' = 0.63$

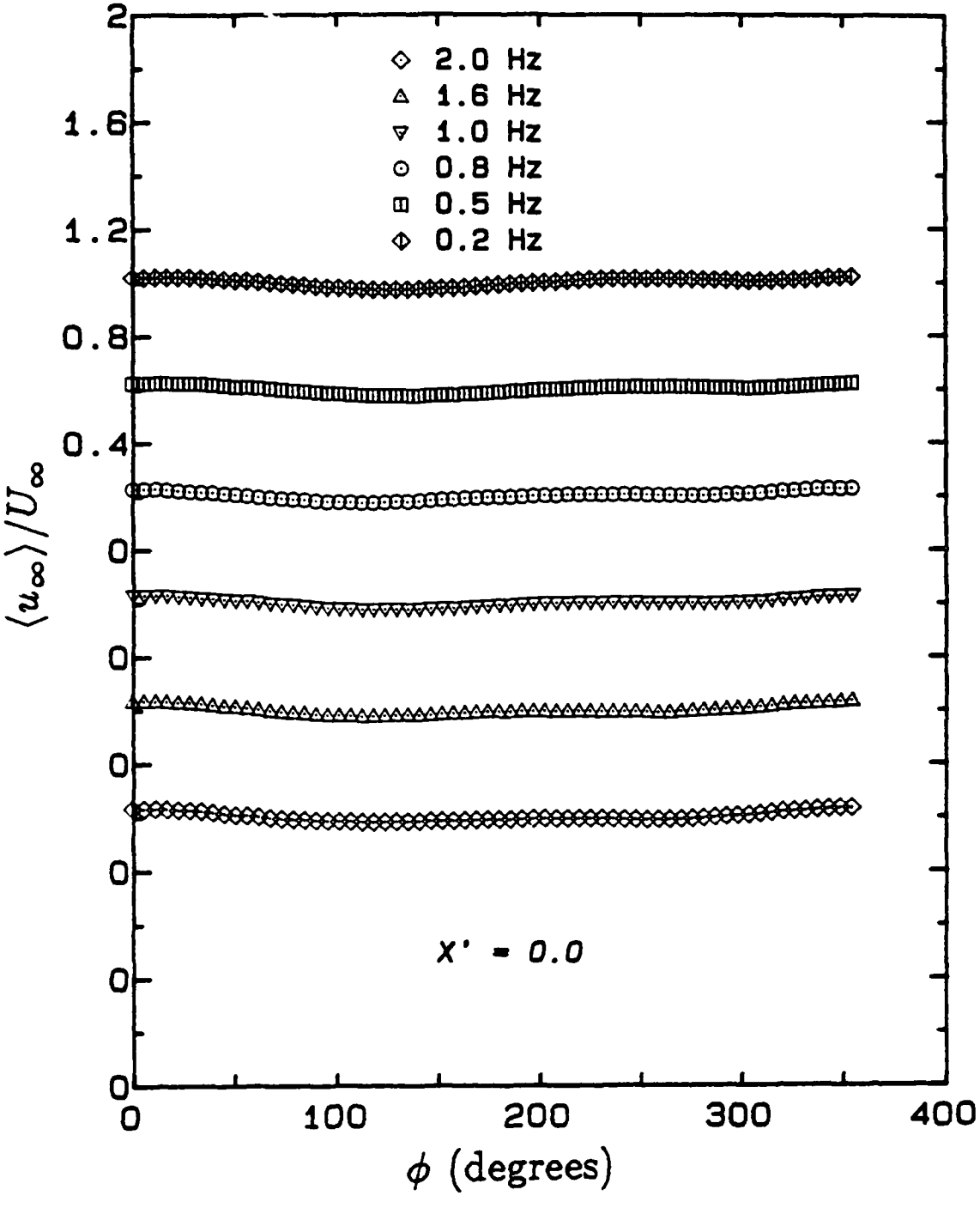

Figure 4.25 Variation of $\langle u_\infty \rangle$ with phase angle. $X' = 0.0$

5. Time-Averaged Unsteady Flow

Measurements describing the mean or time-averaged behavior of the organized, unsteady flow are now presented. Important results are given extra emphasis; brief summaries of these findings are preceded by a bullet and written in indented italicized text, a format chosen to aid the reader in identifying the key points in chapters in which experimental results are discussed. The invariance of time-averaged measures to different frequencies of imposed unsteadiness is examined, together with the contention that transport of fluid in the mean, unsteady field does not differ from steady flow at an equivalent mean condition.

The momentum equation for the time-averaged transport of a fluid under unsteady conditions (2.2.10) takes the form:

$$\frac{\partial}{\partial x_k}(U_k U_i) = -\frac{1}{\rho}\frac{\partial P}{\partial x_i} - \frac{\partial}{\partial x_k}(\overline{u_k' u_i'} + \overline{\tilde{u}_k \tilde{u}_i}) + \nu \frac{\partial^2 U_i}{\partial x_k \partial x_k} .$$

Variation of the time-averaged flow with frequency of imposed unsteadiness is possible through frequency dependence in:

(i) the time-averaged velocity fields, U_i ,

(ii) the pressure gradients, $\partial P/\partial x_i$,

(iii) the divergence of time-averaged measures of turbulence, $\partial(\overline{u_k' u_i'})/\partial x_k$ and

(iv) the divergence of time-averaged products of deterministic components of velocity, $\partial(\overline{\tilde{u}_k \tilde{u}_i})/\partial x_k$.

While the mean, streamwise gradient in pressure was prescribed as invariant with frequency at each x station and qualified through surveys of U_∞ and $\tilde{u}_\infty$ (§4.3), the behavior of the other velocity terms could be deduced from measurements and these are examined in the following sections.

5.1 Measures of Mean Velocity

Profiles of U, normalized by their free-stream values, are shown in Figures 5.1 – 5.3 ; they were measured at $X' = 0.0$, $X' = 0.45$ and $X' = 0.63$ respectively. In each graph, the abscissa is the distance from the wall, y , divided by D_c ; this latter quantity is the boundary-layer thickness, found by fitting Coles' mean velocity function to the profile (Coles 1968). The fitting procedure minimized the squares of deviations between the data and the prescribed function through variation of the function's parameters, u_τ and D_c , over part of the profile. This scheme appeared to give good fits for turbulent boundary layers in constant-pressure and adverse-pressure-gradient flows. Although a near-wall velocity scale, u_τ, was evaluated from this procedure, there is no evidence that it is related to the wall shear in the same way, or through constants (κ and C) of the same value, as in steady flow (though comparisons of such a velocity scale with measures of the near-wall velocity gradient in the time-averaged unsteady flow might clarify this issue). Consequently, in time-averaged unsteady flows, this fitting scheme was used only as a tool for consistent evaluation of a boundary-layer thickness which did not require inordinate numbers of measurements to be made in the outermost parts of the boundary layer.

- *Time-averaged measures of U were invariant with frequency of forced free-stream unsteadiness throughout the boundary layer.*

The profiles of U in Figures 5.1 – 5.3 show no obvious variation with the frequency of imposed unsteadiness. A pronounced log-linear region was evident at each x location. At $X' = 0.45$, the near-wall variation was of similar form to the $u^+ \sim y^+$ relationship observed in steady flow. This effect was more difficult to detect in measurements at $X' = 0.63$ — the addition of an extra profile and the enlarged wake regions, associated with the mean-adverse gradient in pressure, tended to compress the variation of U near the wall in this graph. The wakes at $X' = 0.45$ were a smaller proportion of the profiles than at $X' = 0.63$, as one would expect with the distribution of mean, free-stream velocity: $U_\infty = U_0(1 - AX')$. At

$X' = 0.0$, the wakes were still smaller and the unsteady profiles appeared almost identical to the one taken at this location under steady conditions, also shown in Figure 5.1; only minor discrepancies were evident in the curvature of the profile near the wall.

- *Profiles of U appeared comparable to their steady-flow counterparts and the familiar linear, log-linear and wake regions could be identified clearly.*

Profiles of V were also measured; they are shown in Figure 5.4, at $X' = 0.63$, and did not appear to exhibit any frequency dependence. The profiles seemed to contain two almost-linear regions — one represented by the four outermost points, where the free-stream gradient appeared to prevail, and the other covering the wake of the boundary layer, descending more steeply towards the boundary condition at the wall of no normal velocity. Criticism of these observations, through comparison with measurements in other related experiments, was not possible due to the lack of any relevant unsteady V data.

- *Time-averaged measures of V were invariant with frequency of forced free-stream unsteadiness throughout the boundary layer.*

As measurements of V are difficult to make with any appreciable degree of certainty, these results must be treated with caution. The near-wall behavior in Figure 5.4 did not appear to approach a wall value of zero — possibly an indication that, through slight misalignments of the measurement system, the true values of V in this region were buried under fractional measures of U. Measurements of V in the outer boundary layer seemed less likely to be erroneous. If a consistent misalignment problem, resulting in the interpretation of fractional contributions of U as values of V, were significant here, then profiles of V would appear as scaled versions of their U counterparts rather than taking the shapes of Figure 5.4. Moreover, the normal gradient of V in the free stream could be tested against the expected

AD-A184 856 EXPERIMENTAL STUDY OF THE FLUID MECHANICS OF UNSTEADY TURBULENT BOUNDARY LAYERS(U) STANFORD UNIV CA THERMOSCIENCES DIV G J BRERETON ET AL MAY 87 TF-29 2/3

UNCLASSIFIED ARO-19976 4-EG DAAG29-83-K-0056 F/G 20/4 NL

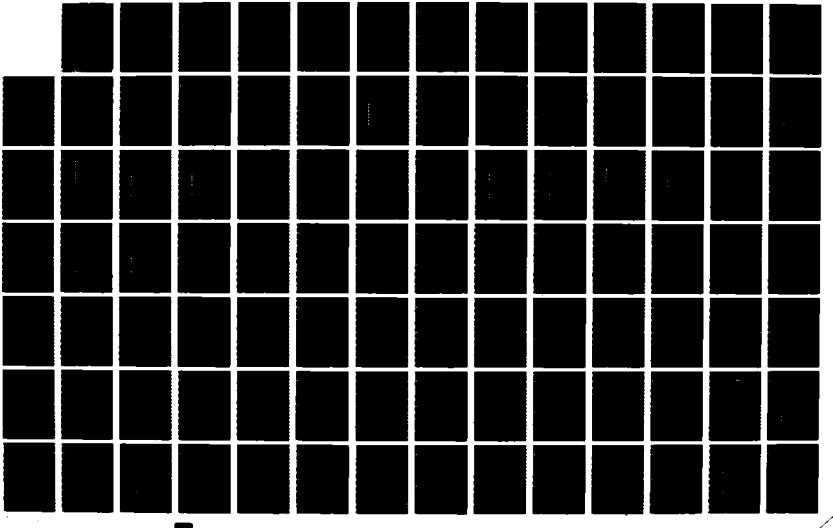

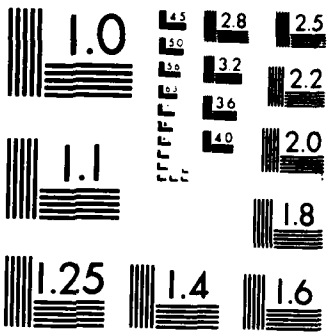

MICROCOPY RESOLUTION TEST CHART
NATIONAL BUREAU OF STANDARDS-1963-A

value obtained via the continuity equation (2.2.4) and the prescribed mean conditions for U_∞ (3.4.1). This free-stream gradient (when normalized by U_∞/D_c) should then be around 0.025, a value which matched the normal variation of the four outermost data points reasonably well. Consequently the outer measures of V were considered more trustworthy than the near-wall ones. A treatment of the estimated uncertainties in these data is given in Appendix F.

5.2 Turbulence Measurements

That profiles of U appeared to be independent of the frequency of unsteadiness is not an indication that time-averaged turbulence measures would necessarily do so too, despite their dependence through (2.2.10). Values of U were typically so much larger than those of the turbulent quantities, $\overline{u'u'}$ and $-\overline{u'v'}$, that any frequency dependence in the turbulence measures might not be noticeable in U profiles. Consequently, direct measurement was necessary for reliable evaluation of the frequency dependence of turbulence measures.

Profiles of mean, unsteady values of $\overline{u'u'}$ are shown in Figures 5.5 and 5.6, at $X' = 0.63$ and $X' = 0.0$ respectively; there was no obvious variation with frequency in either figure. At $X' = 0.63$, the profiles appeared typical of steady, adverse-pressure-gradient ones — the plateau-like appearance, with peaks at its inner and outer bounds, was comparable in shape and in magnitude to the profile measured under steady conditions similar to the time-averaged, unsteady ones (*i.e.* Andersen 1972). Measurements at $X' = 0.0$ likewise showed no dependence upon frequency. However, when compared with the steady profile at this location (Figure 5.6), it was evident that, in both the inner and outer parts of the boundary layer, the mean, unsteady profiles rose and descended more smoothly than their steady counterpart.

The particular function of $\overline{u'u'}$ which appears in the x-momentum equation, (2.2.10) with $i = 1$, is its gradient in the streamwise direction. If this variation is smooth and can be approximated by the difference between its values in Figures 5.5

and 5.6, divided by their spatial separation, then it is clearly of negligible magnitude when compared to inertial terms on the left-hand side of the x-momentum equation.

The other time-averaged turbulence term in the x-momentum equation is the wall-normal gradient of Reynolds stress, $-\partial(\overline{u'v'})/\partial y$. Profiles of the time-averaged Reynolds stress are shown in Figure 5.7, at $X' = 0.63$; no significant variation in $-\overline{u'v'}$ was apparent over the range of frequencies of unsteadiness which was investigated. The profiles appeared to be very similar in size and shape to those taken under comparable steady conditions (*e.g.* Andersen 1972). Mean, unsteady data taken at $X' = 0.0$ are displayed in Figure 5.8. Although these profiles appeared to be invariant with frequency, they differed markedly from the profile taken under steady conditions at this x location (also shown in Figure 5.8); the inner growth and outer decline in the steady profile were much steeper than in its unsteady counterparts — possibly an indication of the extreme sensitivity of $-\overline{u'v'}$ to unsteady, upstream disturbances or to small deviations from the nominally steady conditions at $X' = 0.0$.

- *In measurements of $-\overline{u'v'}$ at the inlet to the test section, differences between the steady and time-averaged unsteady profiles were observed — an indication that, in computational predictions of these data, initial conditions based on time-averaged unsteady measures would be more appropriate than steady ones.*

The streamwise gradient of $-\overline{u'v'}$ contributes to the right-hand side of the y-momentum equation, (2.2.10) with $i = 2$. It is likely to be of the same magnitude as $\partial(\overline{u'u'})/\partial x$ and much less significant than the other mean turbulence term of this equation, $\partial(\overline{v'v'})/\partial y$. Profiles of $\overline{v'v'}$ are shown in Figure 5.9 at $X' = 0.63$. Although the flatness at the wall was suspect, the rest of the profile was as expected in flow under comparable steady conditions and no variation with frequency was evident. At $X' = 0.0$, steady and unsteady profiles could be compared and they are

both shown in Figure 5.10. Agreement between them was reasonably good and the differences observed in $-\overline{u'v'}$ measurements were not reproduced in the $\overline{v'v'}$ data.

- *Profiles of $\overline{u'u'}$, $\overline{v'v'}$ and $-\overline{u'v'}$ were invariant with frequency and were similar in appearance to their steady-flow counterparts.*

5.3 Products of Periodic Velocities

Just as the mean momentum equations describing steady, turbulent flow (2.2.10) differ from their laminar counterparts through the inclusion of the "stress" tensor, $\partial(\overline{u_k' u_i'})/\partial x_k$, the time-averaged momentum equations of unsteady, turbulent flow are distinct from the equivalent steady-flow equations because of the additional tensor of products of periodic velocities, $\partial(\overline{\tilde{u}_k \tilde{u}_i})/\partial x_k$. While $\partial(\overline{u_k' u_i'})/\partial x_k$ is known to reach significant values near the wall, which result in the well-known differences in shape between laminar and turbulent boundary-layer profiles, the effects of $\partial(\overline{\tilde{u}_k \tilde{u}_i})/\partial x_k$ have not been a subject of serious study. At a stationary wall with no transpiration, the tensor is obviously zero. In the free stream, its contribution to the x-momentum equation may be simplified to $\partial(\overline{\tilde{u}_\infty \tilde{u}_\infty}/2)/\partial x$. Within the boundary layer, however, the behavior of this term cannot be deduced readily and so measurements of the pertinent quantities of this tensor are considered next.

In the x-momentum equation, this tensor expands to form the terms $\partial(\overline{\tilde{u}\,\tilde{u}}\,)/\partial x$ and $\partial(\overline{\tilde{u}\,\tilde{v}})/\partial y$. The quantity $\overline{\tilde{u}\,\tilde{u}}$ is shown in Figure 5.11, deduced from data taken at $X' = 0.63$. Its values at $X' = 0.0$ were a small percentage of those at $X' = 0.63$, over the entire boundary layer. It is significant that only near the wall did $\overline{\tilde{u}\,\tilde{u}}$ fall below its free-stream value for all frequencies of imposed unsteadiness. Values of $\overline{\tilde{u}\,\tilde{v}}$ are displayed in Figure 5.12 at the same x location, over the range of frequencies of unsteadiness. That $\overline{\tilde{u}\,\tilde{v}}$ was zero at the wall and flat was prescribed through the boundary conditions at the wall; its gradient in the free stream (displayed with a linear y axis in Figure 5.13) was also anticipated through the deterministic equation

of continuity (2.2.4) and closely matched the prescribed value of $-\partial(\overline{\tilde{u}_\infty \tilde{u}_\infty}/2)/\partial x$. What is not known *a priori* is its distribution between these bounding conditions — that it would take the form plotted in Figures 5.12 and 5.13.

At the higher frequencies of imposed unsteadiness (0.8 → 2.0 hertz), measures of $\overline{\tilde{u}\,\tilde{u}}$ did not vary from their asymptotic free-stream value except very near the wall; this behavior is predicted by the analytic solution to the Stokes equation, the simplified version of the deterministic momentum equation, (2.2.11) with $i = 1$, which applies to high-frequency, organized unsteady flows (Appendix E). That it was followed at these frequencies is demonstrated in the following chapter. When this asymptotic, high-frequency behavior in $\overline{\tilde{u}\,\tilde{u}}$ was observed, the normal gradient of $\overline{\tilde{u}\,\tilde{v}}$, imposed by the free-stream conditions, persisted within the boundary layer at an almost constant value over a region which corresponded to the entire wake in profiles of U. This behavior may also be explained in terms of asymptotic, high-frequency (Stokes) flow, in which the outer part of the flow acts as a slug.

Now, $$\frac{\partial}{\partial y}(\overline{\tilde{u}\,\tilde{v}}) = \overline{\tilde{u}\frac{\partial \tilde{v}}{\partial y}} + \overline{\tilde{v}\frac{\partial \tilde{u}}{\partial y}} = -\overline{\tilde{u}\frac{\partial \tilde{u}}{\partial x}} + \overline{\tilde{v}\frac{\partial \tilde{u}}{\partial y}}\,.$$

In the outer flow, $$\frac{\partial \tilde{u}}{\partial y} = 0 \quad \text{and} \quad \tilde{u} = \tilde{u}_\infty\,.$$

Consequently, $$\frac{\partial}{\partial y}(\overline{\tilde{u}\,\tilde{v}}) = -\overline{\tilde{u}_\infty \frac{\partial \tilde{u}_\infty}{\partial x}} = -\frac{\partial}{\partial x}\left(\frac{\overline{\tilde{u}_\infty \tilde{u}_\infty}}{2}\right)$$

everywhere except in a thin Stokes layer near the wall, as observed in Figure 5.13 for the higher frequencies of imposed unsteadiness.

- *The periodic, wall-normal component of velocity, $\tilde{v}$, made an important contribution to the $\partial(\overline{\tilde{u}_k \tilde{u}_i})/\partial x_k$ tensor.*

At lower frequencies, where measures of $\widetilde{u}\,\widetilde{u}$ within the boundary layer "overshot" their free-stream values, the normal gradient of $\widetilde{u}\,\widetilde{v}$ was considerably steeper than its free-stream value over almost all the outer boundary layer. The term $-\widetilde{u}\,\partial\widetilde{u}/\partial x$ clearly exceeded its free-stream value within the boundary layer and contributed to the steeper, normal gradient of $\widetilde{u}\,\widetilde{v}$. The role of $\widetilde{v}\,\partial\widetilde{u}/\partial y$ is not obvious from theory nor was it calculated explicitly in this study.

- *The term $\partial(\widetilde{u}_k\widetilde{u}_i)/\partial x_k$ played a significant role in the mean x-momentum equation and its magnitude was dependent on the frequency of forced free-stream unsteadiness.*

In the y-momentum equation, the tensor of mean correlations of periodic velocity products comprises the quantities, $\partial(\widetilde{u}\,\widetilde{v}\,)/\partial x$ and $\partial(\widetilde{v}\,\widetilde{v}\,)/\partial y$, which may be expressed as $\partial(\widetilde{v}\,\widetilde{v}/2)/\partial y + \widetilde{u}\,(\partial\widetilde{v}/\partial x)$. Profiles of $\widetilde{v}\,\widetilde{v}$ are shown in Figure 5.14 at $X' = 0.63$, at the frequencies of unsteadiness for which this study was conducted. To assess the importance of this quantity, its magnitude was compared to that of the dominant turbulence measure of the y-momentum equation, $\partial(\overline{v'v'})/\partial y$. Profiles of $\overline{v'v'}$ are shown, with a linear y axis, in Figure 5.15. It is clear from these figures that the normal gradient of $\overline{v'v'}$ was much larger than that of $\widetilde{v}\,\widetilde{v}$. Unless the tensor's streamwise derivative was significantly greater than $\partial(\overline{v'v'})/\partial y$, periodic measures would be unlikely to play a dominant role in the time-averaged y-momentum equation.

As the frequency dependence of the mean of products of periodic velocity has been established, its significance in the x-momentum equation may now be assessed through comparison with the streamwise gradient in pressure. First, the x-momentum equation, (2.2.10) with $i = 1$, for the free stream is written as:

$$\frac{1}{\rho}\frac{\partial P}{\partial x} = -\frac{\partial}{\partial x}(U_\infty U_\infty) - \frac{\partial}{\partial y}(U_\infty V_\infty) - \frac{\partial}{\partial x}(\overline{\widetilde{u}_\infty\widetilde{u}_\infty}) - \frac{\partial}{\partial y}(\overline{\widetilde{u}_\infty\widetilde{v}_\infty}) \ ,$$

or
$$\frac{1}{\rho}\frac{\partial P}{\partial x} = -\frac{\partial}{\partial x}\left(\frac{U_\infty U_\infty}{2}\right) - \frac{\partial}{\partial x}\left(\frac{\overline{\tilde{u}_\infty \tilde{u}_\infty}}{2}\right),$$

where $\partial(\overline{\tilde{u}_\infty \tilde{u}_\infty}/2)/\partial x$ is the contribution of the periodic components of velocity. In this flow, $U_\infty = U_0(1 - AX')$ and $\tilde{u}_\infty = U_0 AX' \cos\omega t$. It follows that:

$$\frac{1}{\rho}\frac{\partial P}{\partial x} = -\frac{U_0^2 A}{2L}(2AX' - 2) - \frac{U_0^2 A}{2L}(AX').$$

The proportion of the total pressure gradient attributed to the time-averaged correlation of periodic velocities is therefore $(-AX')/(2 - 3AX')$. At $X' = 0.63$, for $A = 0.24$, this contribution amounts to 10% of the pressure gradient in the free stream.

From order-of-magnitude analyses of the mean momentum equations, the normal gradient in pressure in the mean, unsteady, turbulent boundary layer was estimated as zero (Jayaraman *et al.*, 1982); therefore $\partial P/\partial x \simeq \partial P_\infty/\partial x$. At the higher frequencies of imposed unsteadiness (0.8 → 2.0 hertz), where slug flow was expected, the proportion of the pressure gradient due to the periodic velocities, $\partial(\overline{\tilde{u}\,\tilde{u}}/2)/\partial x$, remained at its free-stream value (~ 10% at $X' = 0.63$) over the whole boundary layer except the thin, near-wall Stokes layer. At lower frequencies, values of $\overline{\tilde{u}\,\tilde{u}}$ within the boundary layer were generally comparable to or greater than high-frequency ones (Figure 5.11) and so the contribution of $\partial(\overline{\tilde{u}\,\tilde{u}}/2)/\partial x$ was likely to be at least a similar proportion of the streamwise pressure gradient.

Given the significance of the mean products of periodic velocities, where, in this flow, $\tilde{u}_\infty = \tilde{u}_\infty(x)$, it is doubtful that the mean, unsteady flow could be represented adequately by steady flow at an equivalent mean condition — the additional periodic terms, which oppose the prevailing adverse-pressure gradient and reduce its effective value in the free stream and within the boundary layer (by about 10% at $X' = 0.63$),

were too large to be inconsequential. If the mean, unsteady flow is to be represented by an equivalent steady flow, then the effects of the periodic terms (which obviously do not exist in steady flow) might be accommodated by a modified or "effective" pressure gradient. This term would be almost constant across the boundary layer to satisfy the y-momentum equation. If it is chosen to match the unsteady, free-stream conditions, it would be 10% too small at the wall where there are no periodic effects. Conversely, if the periodic terms are ignored so that the pressure gradient at the wall is properly represented, then the entire outer flow would be inadequately described by a pressure gradient which was 10% too large.

These conclusions about the importance of deterministic terms in the mean x-momentum equation have implications concerning the use of information about steady flows to infer quantities which, at present, cannot be measured reliably in unsteady flows. The tensor, $\partial(\overline{\widetilde{u}_k\widetilde{u}_i})/\partial x_k$, was zero at the wall and significant in the boundary layer and in the free stream in this flow. In many unsteady flows, its behavior within the boundary layer is completely unknown. The notion that mean values of surface friction in the unsteady flow can be deduced by indirect means, such as fitting against reference functions for steady flow or using steady-flow correlations based on values of integral parameters, therefore seems to be an unqualified one unless the $\partial(\overline{\widetilde{u}_k\widetilde{u}_i})/\partial x_k$ tensor is either known to be zero or measured and shown to play no role of significance anywhere in the flow.

- *Computational schemes aimed at the accurate prediction of unsteady flows in mean, adverse-pressure gradients should make provision for modeling, or preferably direct calculation, of the* $\partial(\overline{\widetilde{u}_k\widetilde{u}_i})/\partial x_k$ *tensor.*

- *In this adverse-pressure-gradient flow, neglect of the* $\partial(\overline{\widetilde{u}_k\widetilde{u}_i})/\partial x_k$ *tensor would lead to inadequate characterization of the boundary layer.*

5.4 Kinetic-Energy Transfer

The apparent invariance of mean velocities and mean turbulence measures to the frequency of imposed, organized unsteadiness may also be examined through the time-averaged exchange of kinetic energy between the mean, deterministic and turbulent fields. In §2.3, the time-averaged energy equations were derived and three production tensors were revealed. Their dominant terms were selected and measured throughout the boundary layer, over the range of frequencies from 0.1 to 2.0 hertz.

The quantity $\overline{u'_k u'_\alpha}(\partial U_\alpha/\partial x_k)$ serves to transfer kinetic energy from the mean $(U_\alpha U_\alpha)$ field to the turbulent $(\overline{u'_\alpha u'_\alpha})$ field when negative, just as in the corresponding steady flow. If the "energy" contents of only the streamwise components of velocity are considered (UU and $\overline{u'u'}$), order-of-magnitude estimates imply that the dominant term of the production tensor is $\overline{u'v'}(\partial U/\partial y)$; it is shown in Figure 5.16 , deduced from measurements made at $X' = 0.63$ — the normal gradient of U was found by a piecewise-cubic spline fit. As time-averaged profiles of U and $-\overline{u'v'}$ showed no obvious frequency dependence, it is no surprise that this production term appeared insensitive to the frequency of imposed, organized unsteadiness. Time-averaged energy transfer was from the mean field to the turbulent field and its magnitude (when normalized by U_∞^3/D_c) reached a peak of about 1% very close to the wall (in the vicinity of $y/D_c \simeq 0.007$). The general shape of this production term was similar to that reported by Klebanoff for a typical (steady) turbulent boundary layer (in Kline *et al.* 1967). Its role in transferring energy between the velocity fields is illustrated in Figure 5.17.

- *The important production term, which accounted for transfer of turbulent kinetic energy between the mean and turbulent fields, in a time-averaged sense, was invariant with frequency — its profile was comparable in shape to that of the equivalent steady-flow measure.*

In unsteady turbulent flow, the mean ($U_\alpha U_\alpha$) field transfers kinetic energy to both the turbulent ($\overline{u'_\alpha u'_\alpha}$) and deterministic ($\overline{\tilde{u}_\alpha \tilde{u}_\alpha}$) velocity fields; energy transfer to the latter field is described by the tensor $\overline{\tilde{u}_k \tilde{u}_\alpha}(\partial U_\alpha / \partial x_k)$. Considering only the streamwise component of the velocity field, the significant term of the production tensor measured in this study was $\overline{\tilde{u}\,\tilde{v}}(\partial U/\partial y)$; measurements of this quantity are displayed in Figure 5.18 for four frequencies from the range for which data were taken at $X' = 0.63$. Frequency dependence was evident at low frequencies of unsteadiness, where the periodic velocity ($\tilde{u}$) overshot its amplitude in the free stream — this effect was reflected in small transfers of energy (not exceeding 0.5 %) between the mean and deterministic fields in the wake of the boundary layer. Peak energy transfer appeared to take place very near the wall and was comparable in magnitude to the energy transferred from the mean to the turbulent field near the wall ($\sim 1\%$).

The turbulent field, $\overline{u'u'}$, receives energy not only from the mean UU field (for which measurements of the significant production term are plotted in Figure 5.16) but also from the deterministic field, $\overline{\tilde{u}\,\tilde{u}}$. The significant production term measured in this study is $\overline{u'v'(\partial \tilde{u}/\partial y)}$ and it is shown in Figure 5.19. The time-averaged correlation between phase-conditioned values of $-u'v'$ and the deterministic, normal gradient in streamwise velocity was clearly dependent upon frequency near the wall. Although the magnitude of mean energy transfer from the organized, unsteady field to the turbulent one was small in comparison to energy transfer from the mean field, the decrease in its peak value at the wall, with increasing frequency of unsteadiness, was notable — presumably $\partial \tilde{u}/\partial y$ and $-u'v'$ were only well correlated, in a time-averaged sense, at low (quasi-steady) frequencies of imposed, organized unsteadiness.

- *Frequency dependence was noted in a small, time-averaged production term.*

Deduction of $\partial\tilde{u}/\partial y$ was carried out through a piecewise-cubic spline fit to the phase-conditioned data. Attempts to fit standard steady-flow functions (such as Coles' mean velocity profile) to the phase-averaged velocity profiles were not successful; in fact, forcing the data to fit a log-linear function resulted in a reversal of the sign of this production term (when compared to the value inferred using the spline fit) for all but the lowest frequencies of imposed, organized unsteadiness — a result in agreement with the conclusion of Blondeaux & Colombini (1985) that logarithmic laws would not apply instantaneously to the unsteady flow.

- *Log-linear descriptions of the instantaneous, phase-averaged profiles of streamwise velocity were not appropriate for unsteady, turbulent boundary layers.*

From the low-frequency profiles of Figure 5.18, peak production of $\overline{u'u'}$ in the unsteady, turbulent boundary layer took place in the vicinity of $y/D_c \simeq 0.007$. When profiles of the other production terms for $\overline{u'u'}$ were plotted against a logarithmic abscissa, they peaked around this value too. Now, from the observations of Binder & Kueny (1981), Cousteix & Houdeville (1983) proposed that when unsteady effects are confined to a sufficiently thin region near the wall, they cannot affect the turbulent production process. This proposal may be examined for the case of production of $\overline{u'u'}$, via the quantity $\overline{-u'v'(\partial\tilde{u}/\partial y)}$, where the necessary information relating frequency, a measure of the thickness the Stokes layer and D_c (at $X' = 0.63$) is presented in Table 5.1. From this table, it is clear that the significant, low-frequency measures of $\overline{-u'v'(\partial\tilde{u}/\partial y)}$ (in Figure 5.18) correspond to values of $\sqrt{2\nu/\omega}/D_c$ which were considerably greater than 0.007. Moreover, at high frequencies, as $\sqrt{2\nu/\omega}/D_c$ approached 0.007, the production term became negligible, in agreement with this proposal.

Unsteady effects, however, manifest themselves in phase-dependent ways which obviously cannot be accounted for in comparisons of a time-averaged production term with an order-of-magnitude estimate of a dynamic length scale. Thus, what

TABLE 5.1

Thickness Scales of the Unsteady Boundary Layer

f	$\sqrt{2\nu/\omega}$	D_c	$\sqrt{2\nu/\omega}/D_c$
sec^{-1}	mm	mm	
0.1	1.876	62.0	0.0303
0.2	1.326	61.3	0.0216
0.5	0.839	58.9	0.0143
0.8	0.663	58.0	0.0114
1.0	0.593	58.2	0.0102
1.6	0.469	58.6	0.0080
2.0	0.419	58.6	0.0072

is not clear is whether the decrease of this particular production term with growing frequencies (and decreasing values of $\sqrt{2\nu/\omega}/D_c$) is due to the confinement of unsteady effects *per se* to increasingly small regions of influence at the wall, or whether, at high frequencies of mainstream disturbance, the unsteady effects on production are important but behave in a manner which merely renders $-\widetilde{u'v'}$ and $\partial\widetilde{u}/\partial y$ poorly correlated, in a time-averaged sense.

If the peak values of these energy-production terms were representative of the magnitudes of transfer of kinetic energy between velocity fields, then the mean (UU) field transferred comparable amounts of energy to the deterministic $(\widetilde{u}\,\widetilde{u})$ and turbulent $(u'u')$ fields. Near-wall transfer of energy to the turbulent field in steady flow is associated with the "bursting" event; that time-averaged, unsteady flow was dominated by the corresponding production term, $\overline{u'v'}(\partial U/\partial y)$, which was insensitive to the frequency of imposed unsteadiness is in agreement with the observations of Cousteix & Houdeville (1983) that unsteadiness appears to have no influence on the qualitative description of the bursting process. Although the near-wall transfer of energy from the mean to the deterministic field appeared to be of comparable importance (at least quantitatively), it is not thought to be associated with an organized, structural phenomenon which might play an equivalent role to the bursting event.

5.5 Turbulence Structure

Mean turbulence structure in the organized, unsteady flow may be described in terms of time-averaged turbulence measurements. As these measurements were restricted in complexity to the squares and cross product of u' and v', the scope of the structural parameters considered for this study was limited to $-\overline{u'v'}/(\overline{u'u'}+\overline{v'v'})$ and the coefficient of correlation between u' and v', $-\overline{u'v'}/(u'v')$. Since the data sets were saved, other parameters, of this complexity or less, may be computed in the future if desired. To examine the relationship between Reynolds stress and normal gradient in streamwise velocity, time-averaged values of mixing length and eddy viscosity were also deduced for the unsteady flow.

In organized, unsteady flow, mean quantities which are composed of more than one fundamental measurement may be computed in two different ways. For example, the mean value of the quotient of two variables (say a/b) may be formed from the ratio of the time-averaged values of these quantities, $\overline{a}/\overline{b}$, or from the time average of their phase-conditioned ratio, $\overline{\langle a/b \rangle}$ or $(\overline{a}/\overline{b})\overline{\langle(1+\widetilde{a}/\overline{a})/(1+\widetilde{b}/\overline{b})\rangle}$. Differences in the results of the two averaging processes would be expected when the deterministic components were significant proportions of their means and produced strong negative correlations when time averaged.

The parameter $-\overline{u'v'}/(\overline{u'u'}+\overline{v'v'})$, is a two-dimensional equivalent to Townsend's structural parameter, $-\overline{u'v'}/\overline{q^2}$, which is often presumed to be constant in turbulent shear flows (the assumption of structural similarity). The two kinds of time-averaged structural parameters, $-\overline{u'v'}/(\overline{u'u'}+\overline{v'v'})$ and $\overline{\langle -u'v'/(u'u'+v'v')\rangle}$, measured in this study are displayed in Figures 5.20 and 5.21 respectively; profiles at each of the frequencies of imposed unsteadiness are presented, deduced from measurements at $X' = 0.63$. No frequency dependence was apparent nor was any significant difference between the results of the two time-averaging processes evident — an indication that the deterministic Reynolds stress did not form a strong negative correlation with the deterministic component of this two-dimensional measure

of the turbulent kinetic energy. The values of this structural parameter (~ 0.16 over most of the outer boundary layer) were similar to those measured by Cutler & Johnston (1984) under steady, adverse-pressure-gradient conditions.

- *The structural parameters,* $-\overline{u'v'}/(\overline{u'u'}+\overline{v'v'})$ *and* $\overline{\langle -u'v'/(u'u'+v'v')\rangle}$ *, were indistinguishable in value and invariant with frequency.*

The coefficient of correlation between u' and v', $-\overline{u'v'}/(u'v')$, is useful in most practical calculation methods involving transport equations and is typically about 0.4 in turbulent shear flows (Tennekes & Lumley, §2.3). Profiles of the time-averaged measures of this correlation coefficient, $-\overline{u'v'}/(u'v')$ and $\overline{\langle -u'v'/(u')(v')\rangle}$, are shown in Figures 5.22 and 5.23 for the range of frequencies of organized unsteadiness over which data were taken at $X' = 0.63$. Time-averaged values of the correlation coefficient showed no dependence upon frequency of unsteadiness nor did the results of the two time-averaging procedures exhibit any noticeable differences. Presumably there was no significant negative correlation between the deterministic Reynolds stress and the deterministic component of the phase-conditioned product of u' and v'. The time-averaged, unsteady value of the correlation coefficient reached a peak of around 0.36 and exceeded 0.3 over most of the outer boundary layer; this value was significantly lower than that measured in the constant pressure boundary layer, though its proportional reduction was comparable with that of the structural parameter, $-\overline{u'v'}/(\overline{u'u'}+\overline{v'v'})$, which was in good agreement with steady, adverse-pressure-gradient measurements.

- *The correlation coefficients,* $-\overline{u'v'}/(u'v')$ *and* $\overline{\langle -u'v'/(u')(v')\rangle}$ *, were indistinguishable in value and invariant with frequency.*

Now in preliminary measurements in the steady, flat-plate, boundary layer, low values of this correlation coefficient were synonymous with inadequate spatial resolution, insufficient data rates or imperfect alignment of the optical system. However, measurements made under steady, zero-pressure-gradient conditions, both prior to

and immediately after the unsteady experiments, yielded correlation coefficients of around 0.4 over most of the boundary layer with no changes having been made to the measurement system. Since the spectra for steady and unsteady flow, discussed in §4.1, indicated that resolution requirements were similar, the "low" measures of correlation coefficient in unsteady flow were not attributed to inadequacies in the measurement system. Nor was any minor vibration associated with the generation of the forced unsteadiness thought to be problematic — it would be surprising if the same reduction in this coefficient resulted from vibration forced over a range of different frequencies. Consequently, these measurements of correlation coefficient were not considered untrustworthy. That they were significantly smaller than the measurements of Cousteix & Houdeville (1983) (which were about 0.45), in their measurements of low-amplitude unsteadiness under zero-pressure-gradient conditions, might result from the difference in pressure gradients or from a combination of the effects of pressure gradients and forced unsteadiness. The equivalent measurements at $X' = 0.0$ (where both the amplitude of the forced unsteadiness and the pressure gradient were nominally zero) resulted in correlation coefficients, the peak values of which barely approached 0.4 (Figure 5.24). This profile of the mean, unsteady correlation coefficient was dissimilar to both the steady, zero-pressure-gradient one (Figure 4.2) and the unsteady, adverse-pressure gradient one (Figure 5.22). Therefore the cause of the "low" values of correlation coefficient, observed at $X' = 0.63$, was not identified conclusively — it might be due to either the mean adverse-pressure gradient or the combination of forced unsteadiness and mean, adverse-pressure-gradient conditions.

The relationship between Reynolds stress and the normal gradient in streamwise velocity forms the basis of simple turbulence models such as the "Boussinesq" or eddy-viscosity model and Prandtl's mixing-length model. Although more sophisticated schemes surpass them in performance, they are still useful, practical, engineering tools whose possible applications in mean, unsteady flow warrants careful attention. The mixing length, ℓ, is defined as $\ell^2 = -\overline{u'v'}/(|\partial U/\partial y|\,\partial U/\partial y)$ and

represents a dispersion length scale for turbulent transport of momentum. Alternatively, the mixing-length relationship may be viewed as a relationship which makes good dimensional sense in a turbulent shear flow dominated by a single turbulent-velocity scale, in an environment of scale ℓ (Tennekes & Lumley, §2.3). This latter description, which implies neither that a fluid element undergoing turbulent motions conserves its momentum nor that the mechanism which produces the "stress", $-\overline{u'v'}$, be necessarily local, is perhaps more useful for this study and avoids some criticisms commonly leveled at the former, more classical, explanation of the role of ℓ.

Mixing-length profiles are shown in Figures 5.25 and 5.26 for seven frequencies of imposed, organized unsteadiness at $X' = 0.63$. In view of the frequency independence of mean measures of $-\overline{u'v'}$ and U, it is no surprise that ℓ is also invariant with frequency. There is no discernible difference between the mean evaluation of ℓ by either of the two time-averaging procedures. In the inner boundary layer, the relation used in steady flow, $\ell/y = 0.41$, appears to describe the unsteady flow reasonably well, with the exception of very-near-wall region where curvature is evident.

Profiles of the eddy viscosity, $\nu_t = -\overline{u'v'}/(\partial U/\partial y)$, were deduced from measurements at $X' = 0.63$. Its time-averaged values are displayed in Figures 5.27 and 5.28 and a welcome invariance to different frequencies of unsteadiness is observed. There was no evidence of strong negative correlation between deterministic values of Reynolds stress and velocity gradient at any frequency.

- *The mixing lengths, $\overline{\ell}$ and $\overline{\langle \ell \rangle}$, and the eddy viscosities, $\overline{\nu_t}$ and $\overline{\langle \nu_t \rangle}$, were indistinguishable in value and invariant with frequency.*

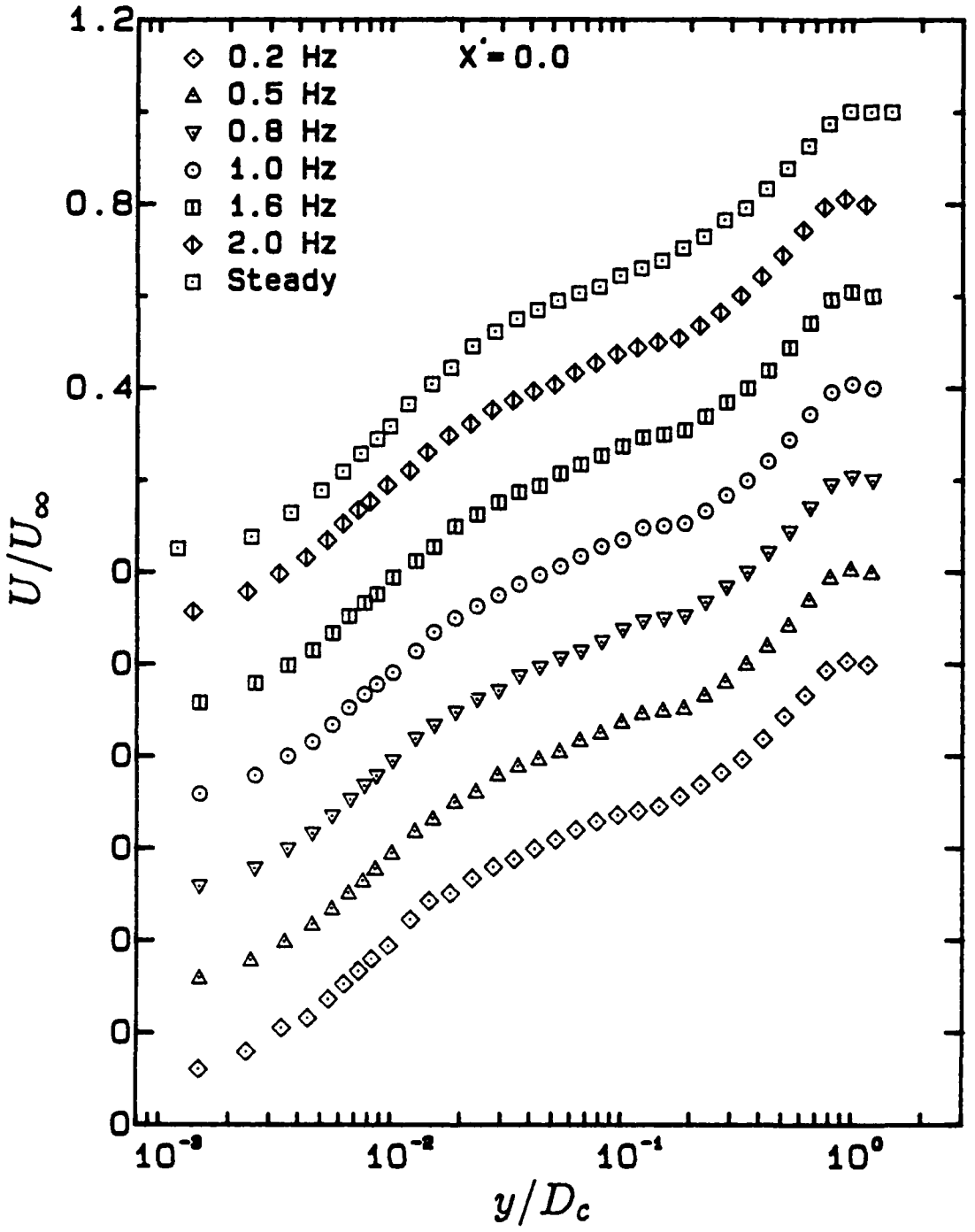

Figure 5.1 Time-averaged profiles of U/U_∞ under steady and unsteady conditions. $X' = 0.0$

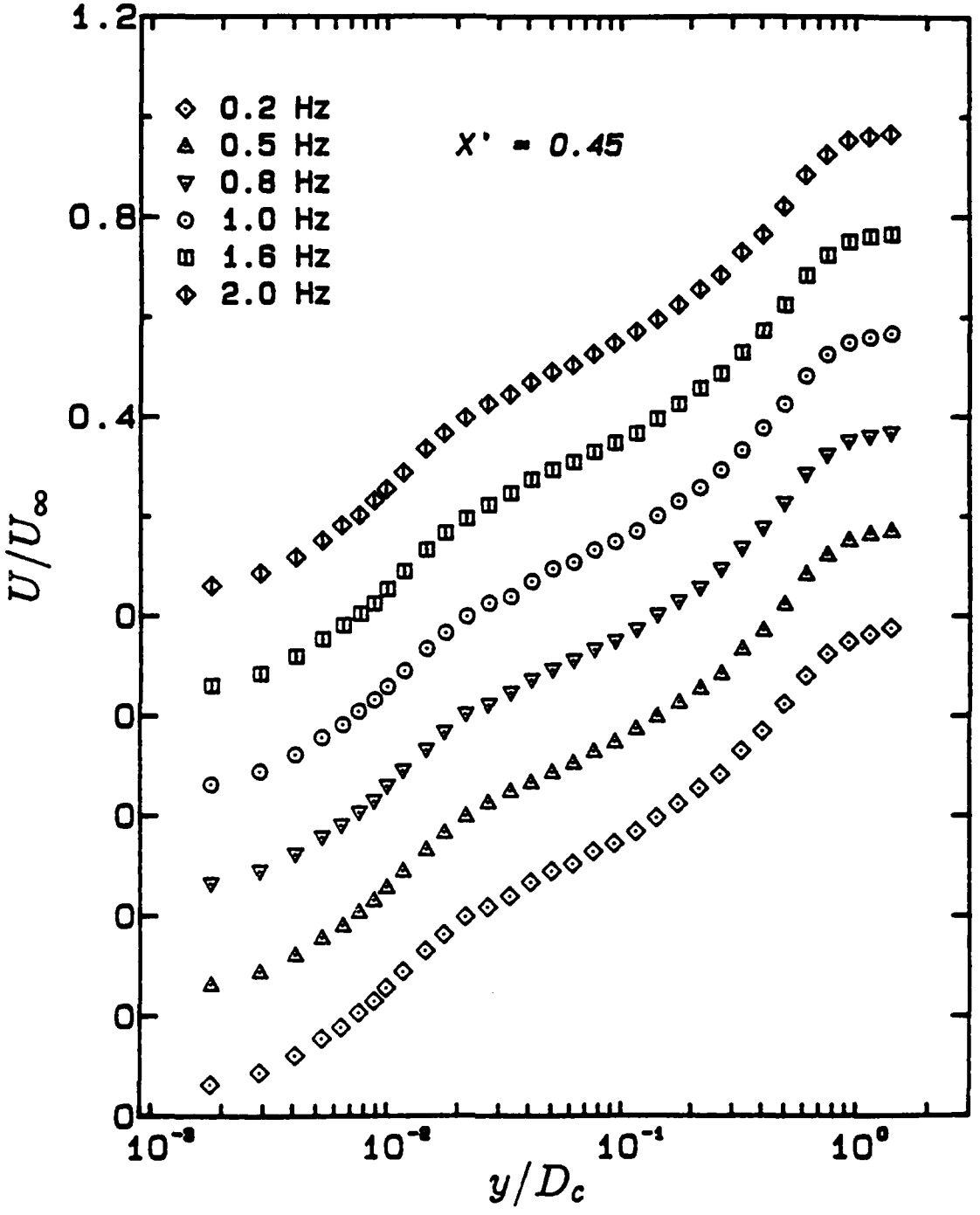

Figure 5.2 Time-averaged profiles of U/U_∞ under unsteady conditions. $X' = 0.45$

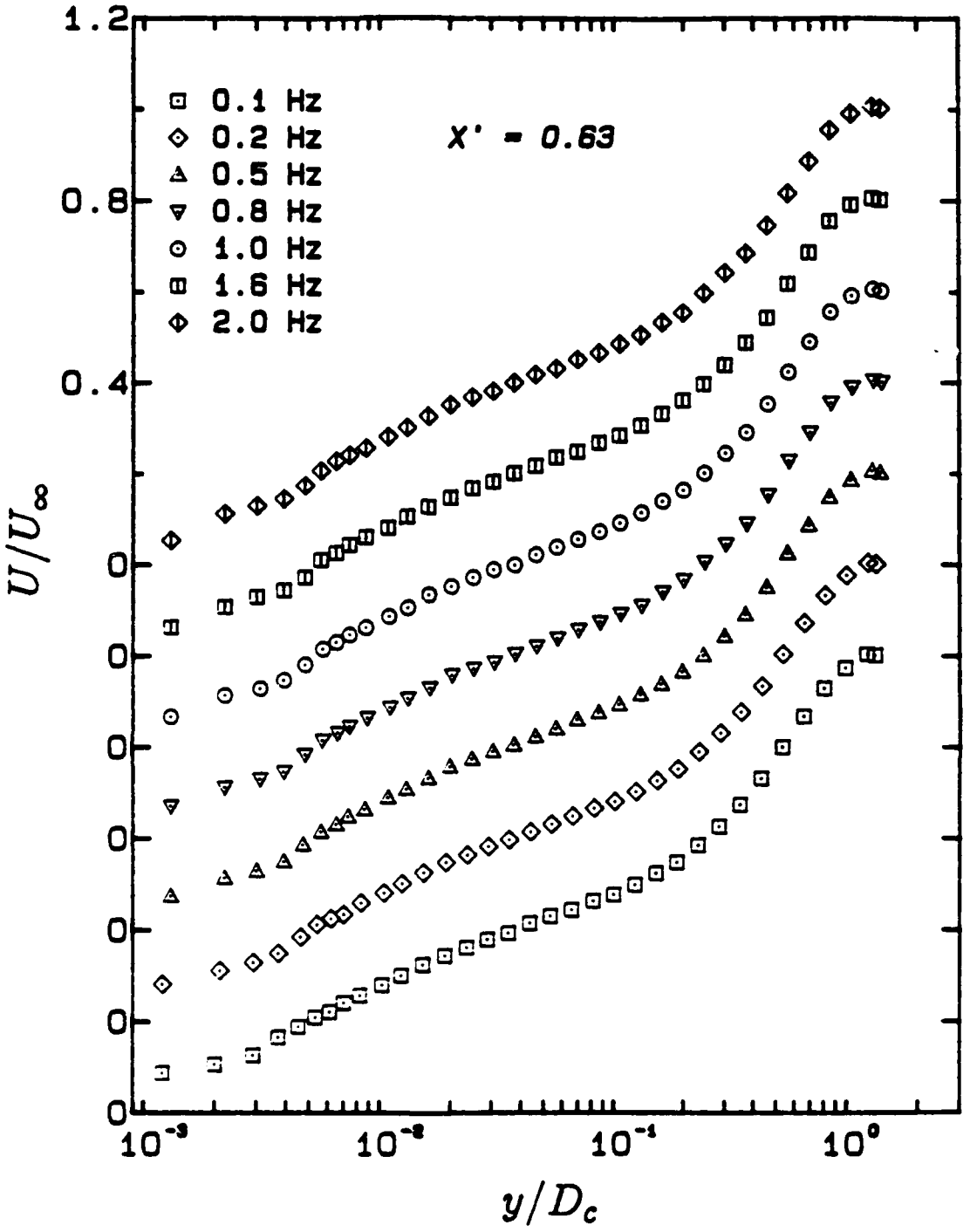

Figure 5.3 Time-averaged profiles of U/U_∞ under unsteady conditions. $X' = 0.63$

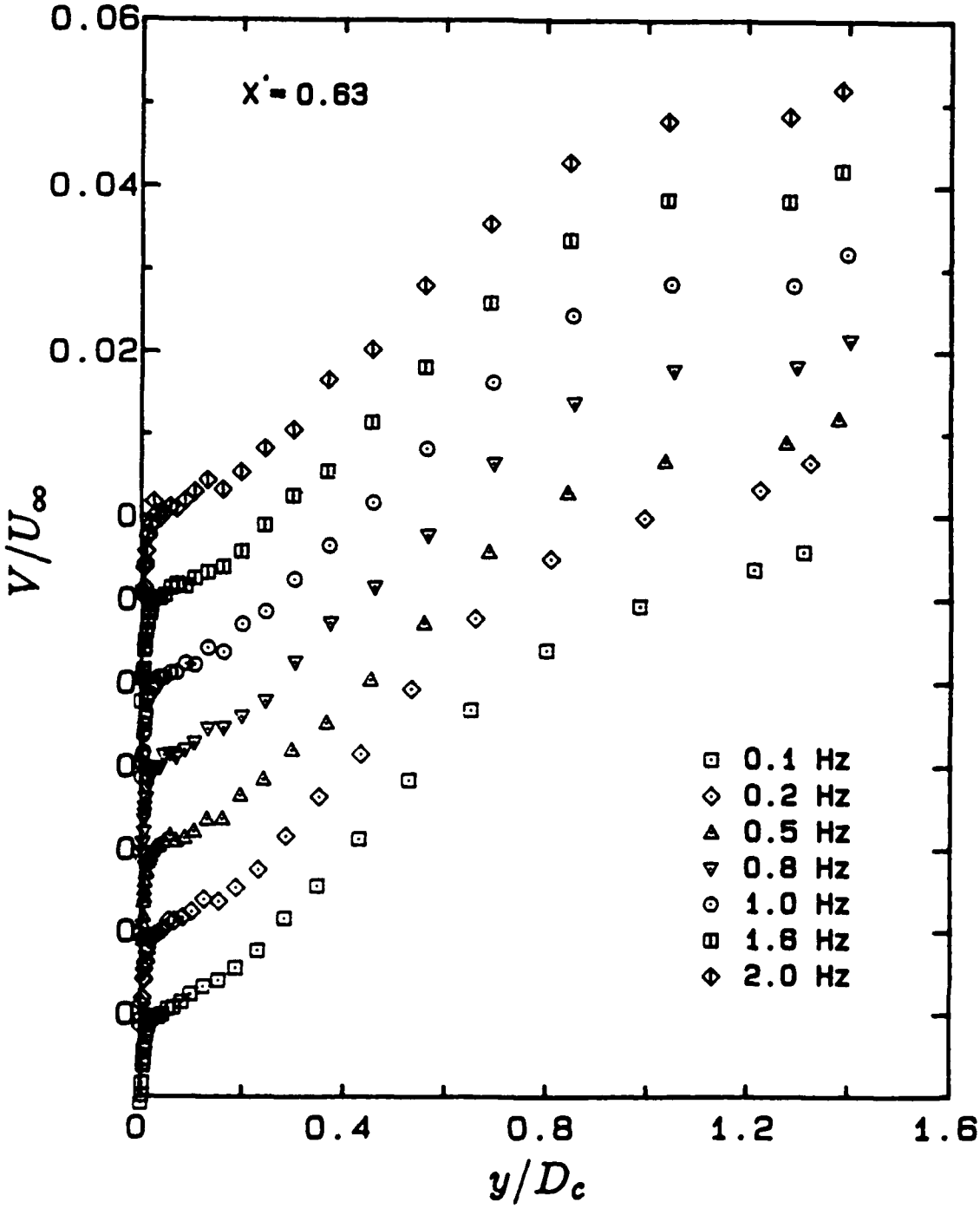

Figure 5.4 Profile of V/U_∞ under unsteady conditions. $X' = 0.63$

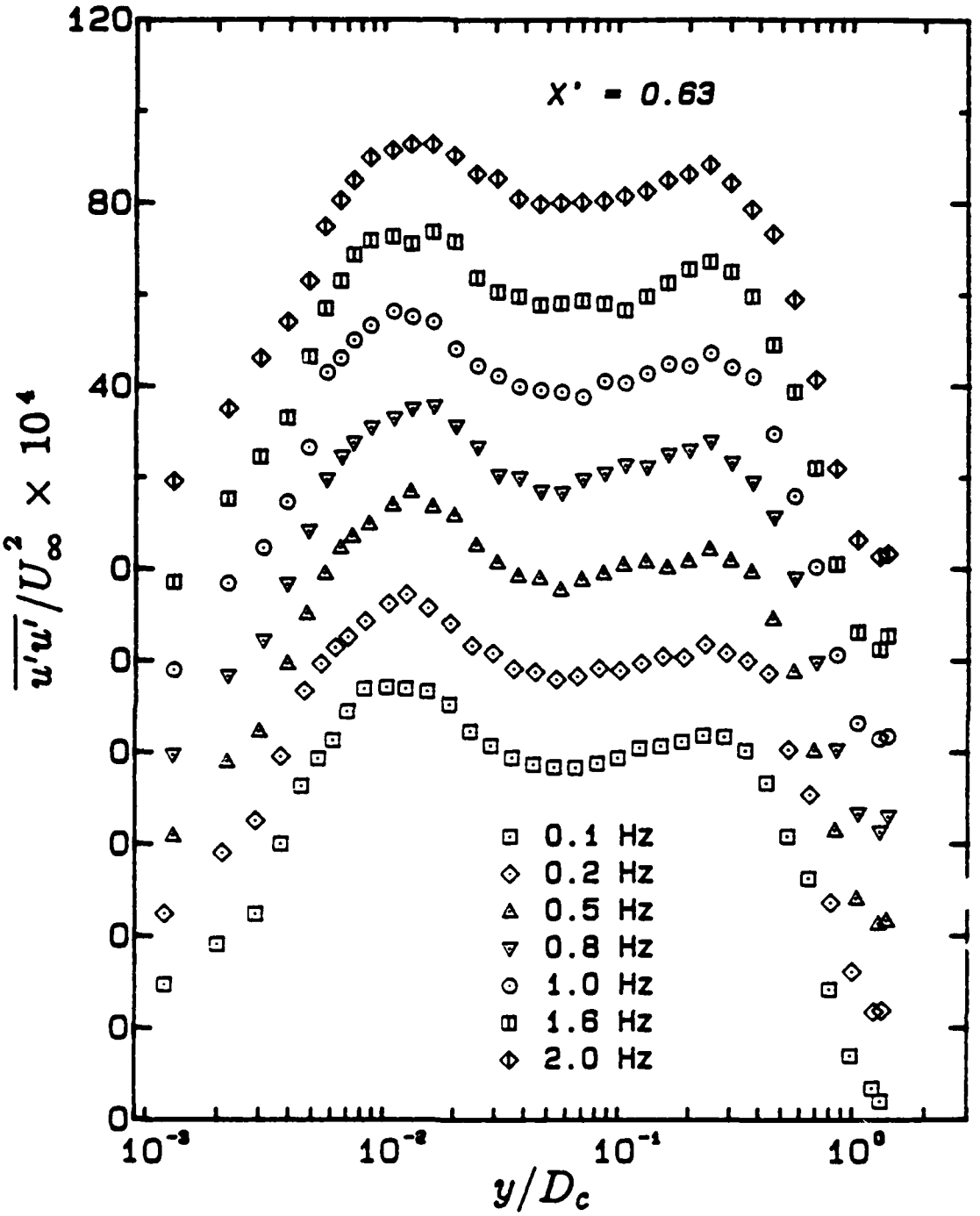

Figure 5.5 Time-averaged profiles of $\overline{u'u'}/U_\infty^2$ under unsteady conditions. $X' = 0.63$

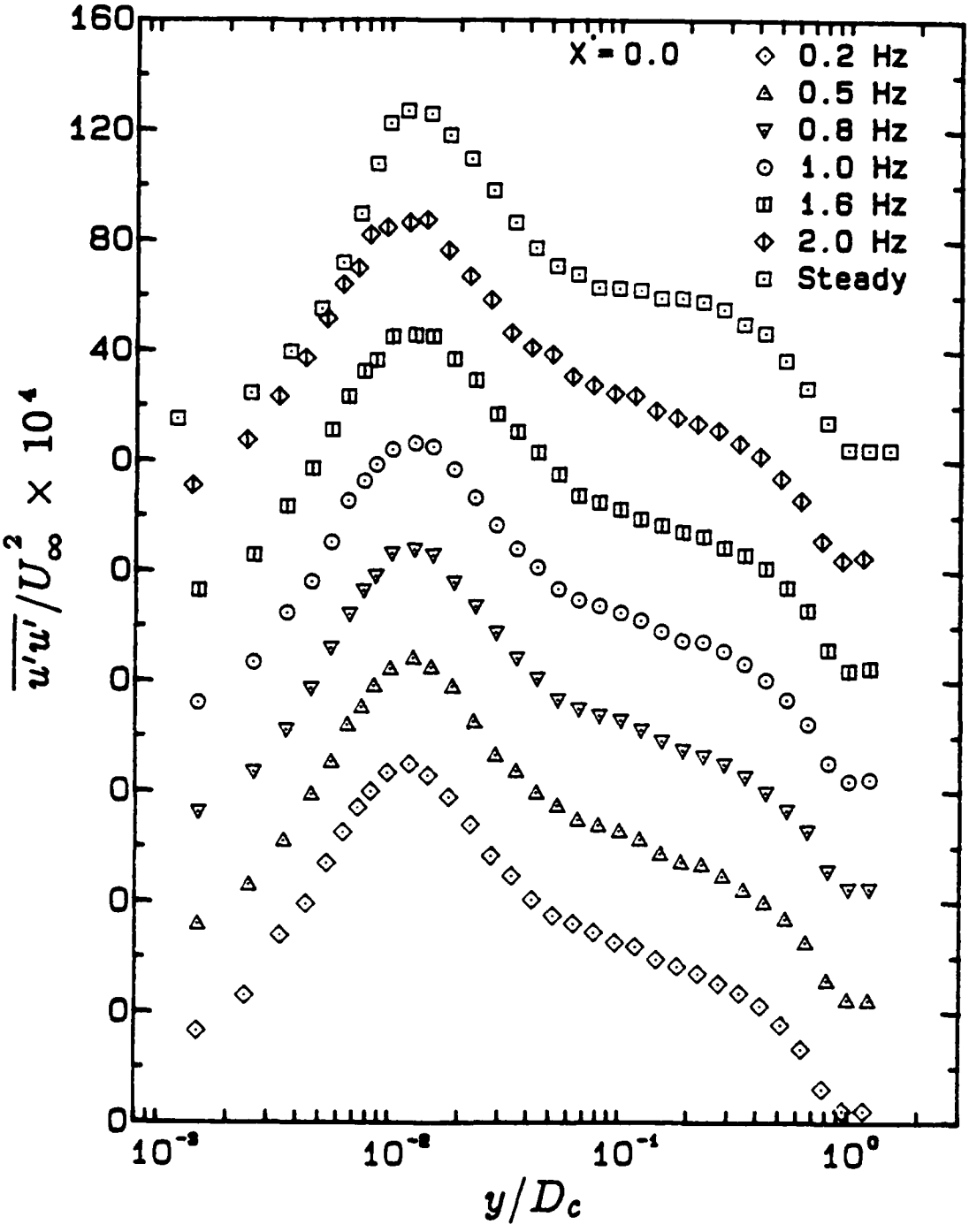

Figure 5.6 Time-averaged profiles of $\overline{u'u'}/U_\infty^2$ under steady and unsteady conditions. $X' = 0.0$

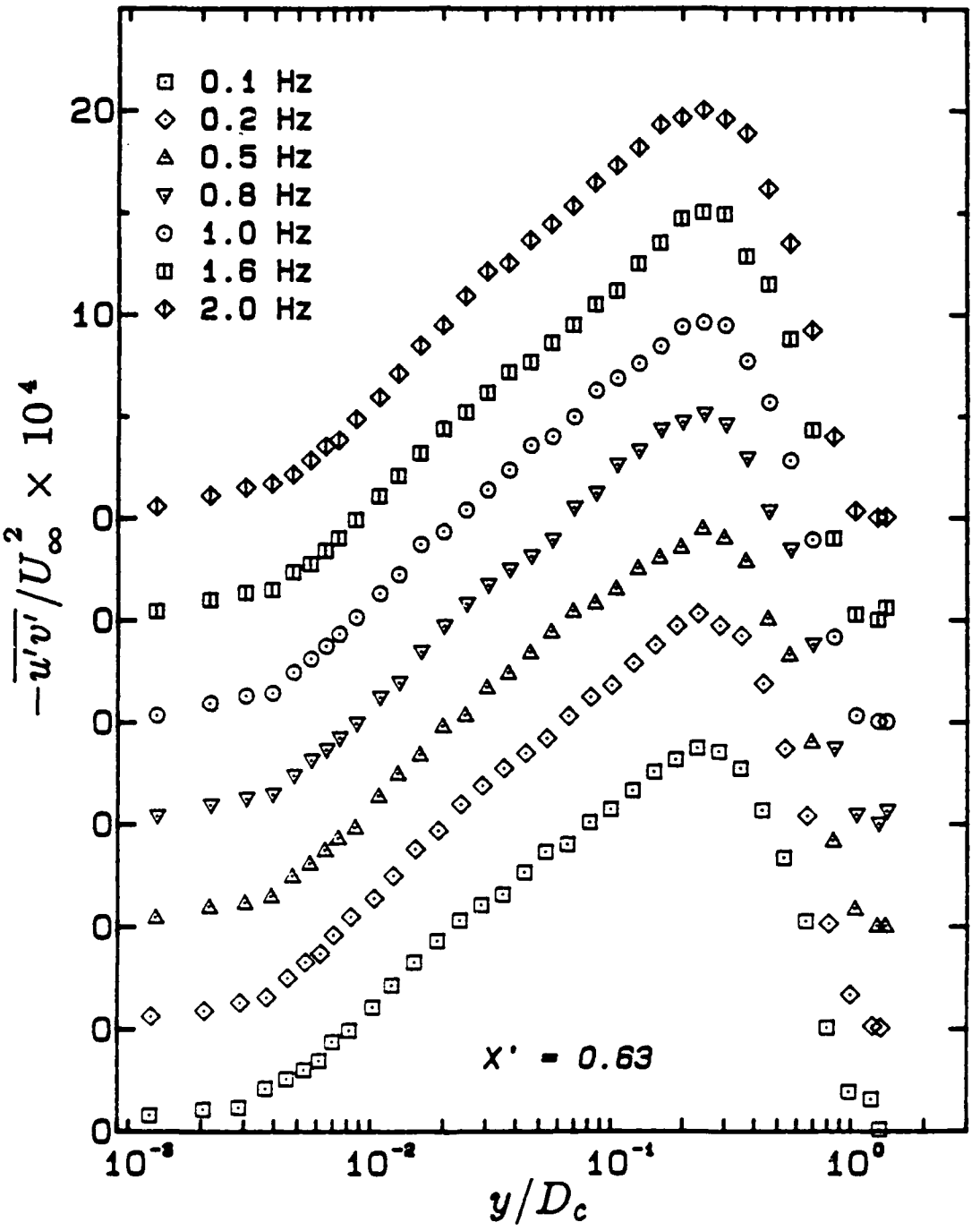

Figure 5.7 Time-averaged profiles of $-\overline{u'v'}/U_\infty^2$ under unsteady conditions. $X' = 0.63$

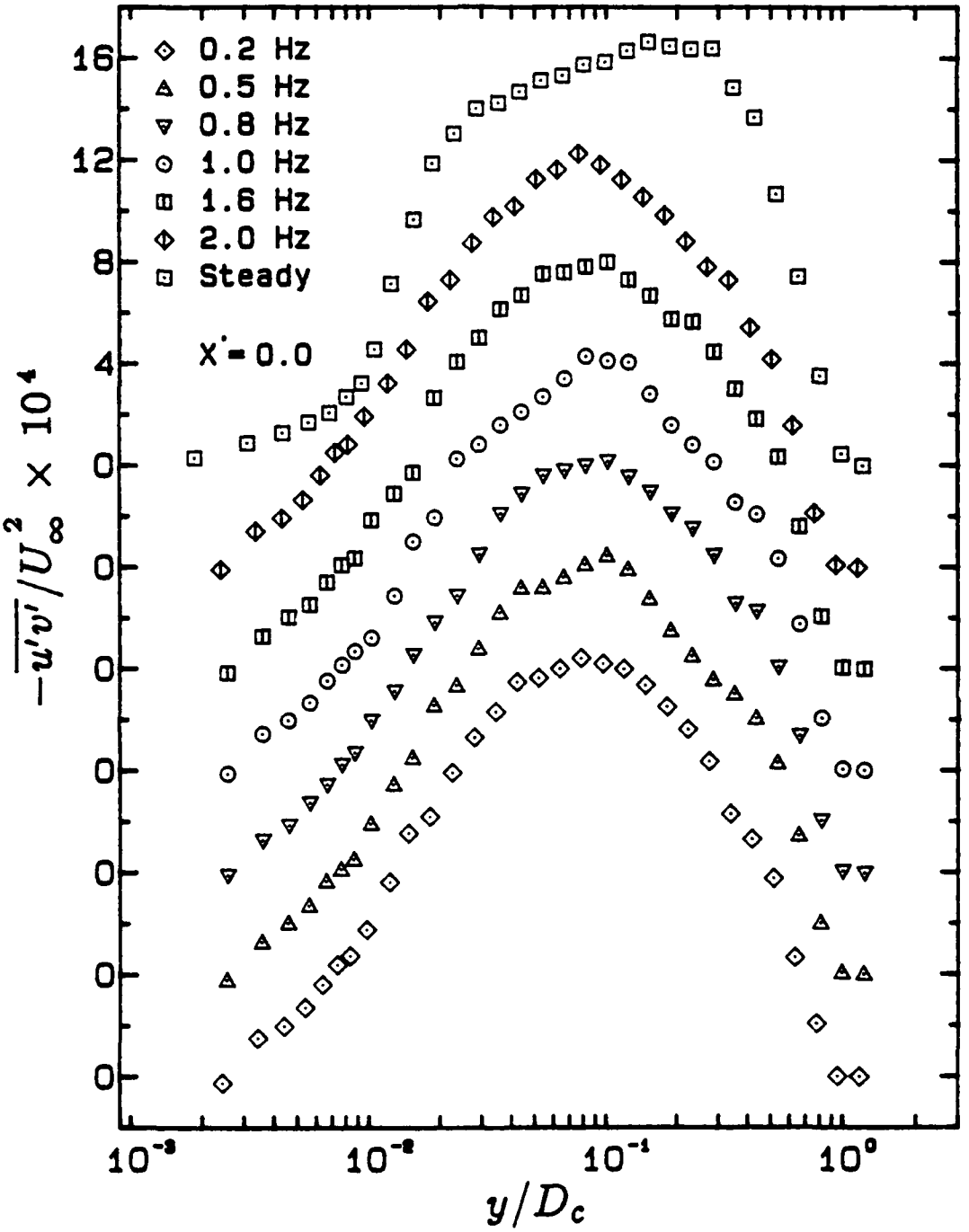

Figure 5.8 Time-averaged profiles of $-\overline{u'v'}/U_\infty^2$ under steady and unsteady conditions. $X' = 0.0$

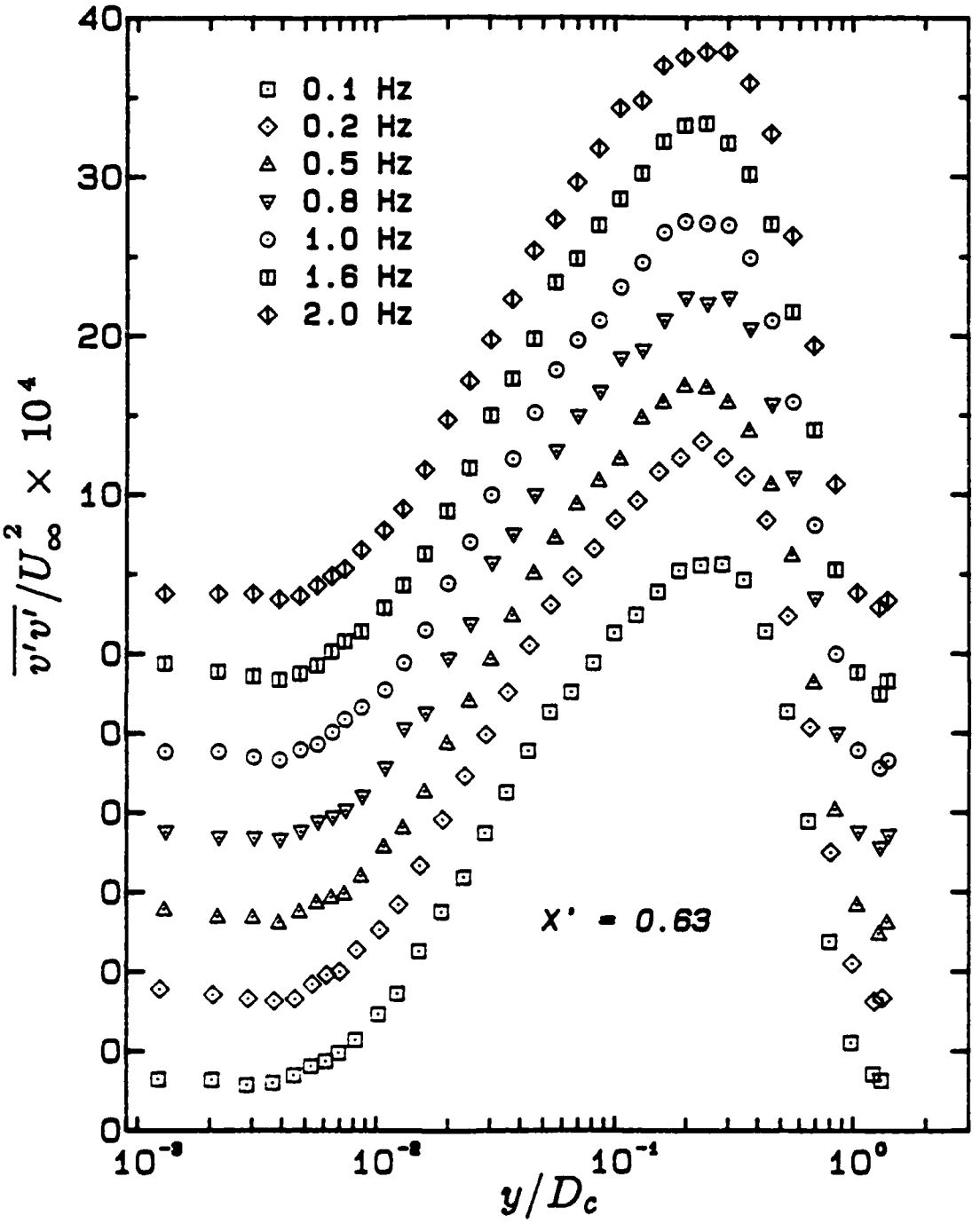

Figure 5.9 Time-averaged profiles of $\overline{v'v'}/U_\infty^2$ under unsteady conditions. $X' = 0.63$

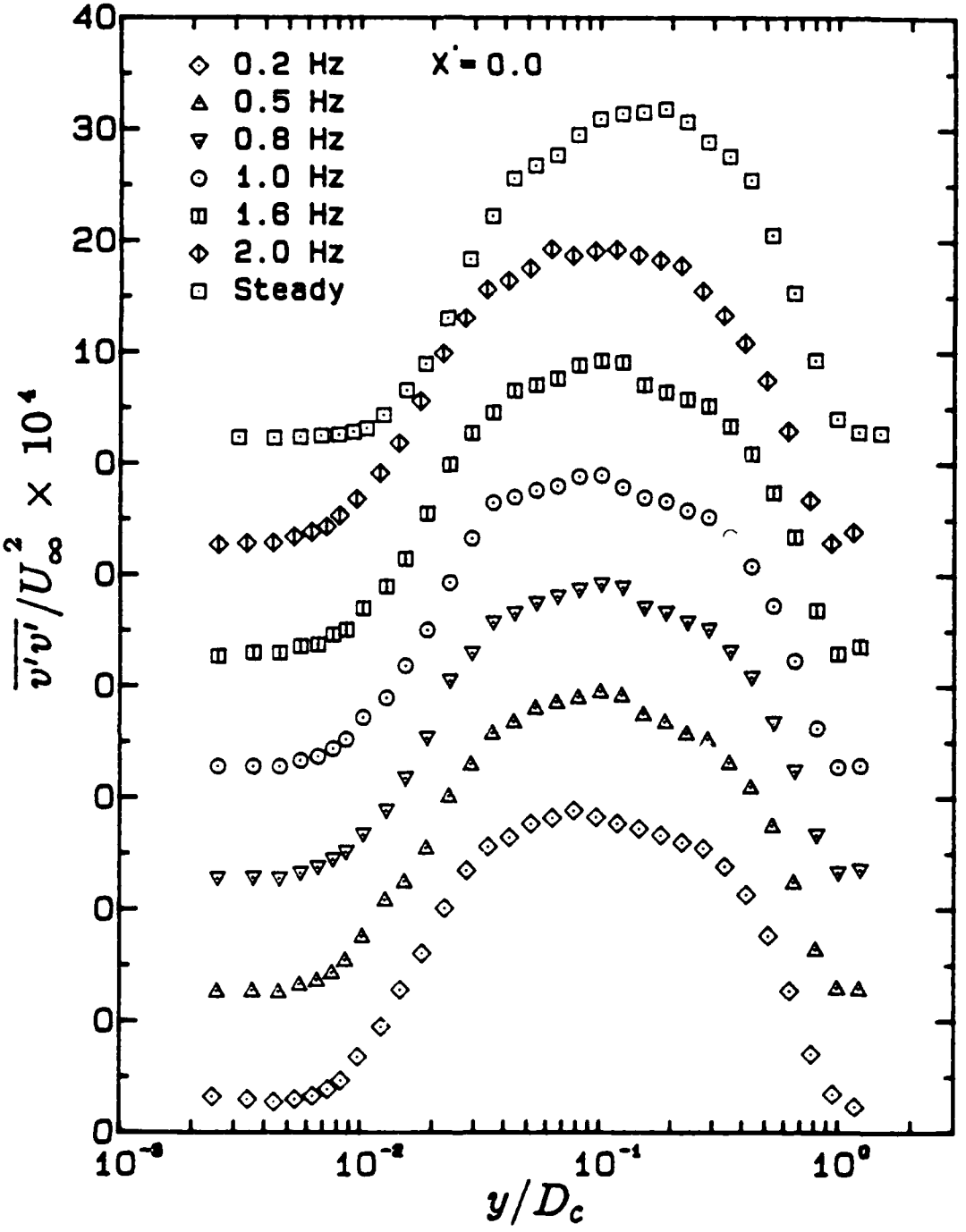

Figure 5.10 Time-averaged profiles of $\overline{v'v'}/U_\infty^2$ under steady and unsteady conditions. $X' = 0.0$

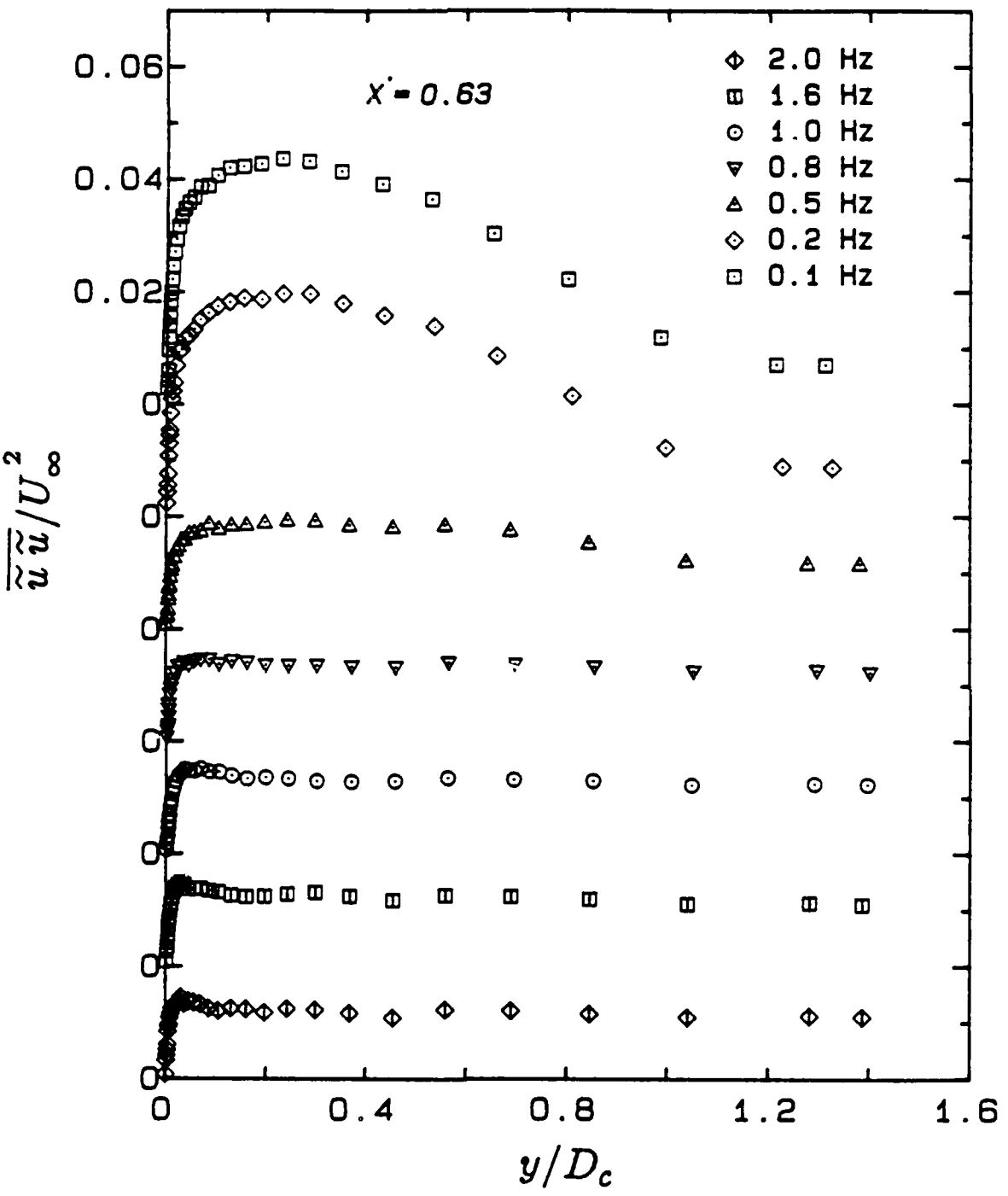

Figure 5.11 Time-averaged profiles of $\overline{\tilde{u}\,\tilde{u}}/U_\infty^2$ under unsteady conditions. $X' = 0.63$

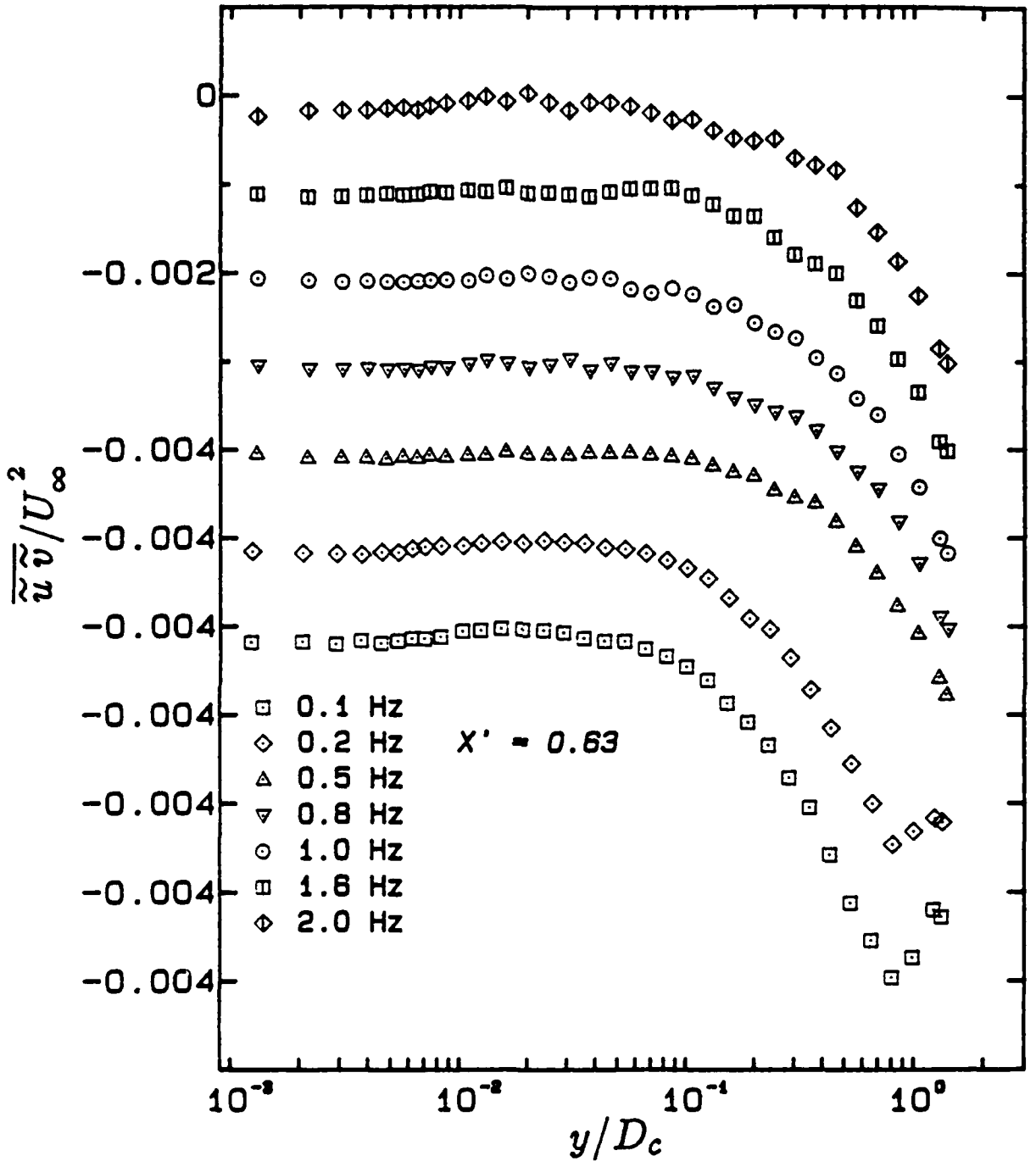

Figure 5.12 Time-averaged profiles of $\widetilde{\overline{u}}\widetilde{\overline{v}}/U_\infty^2$ under unsteady conditions. $X' = 0.63$

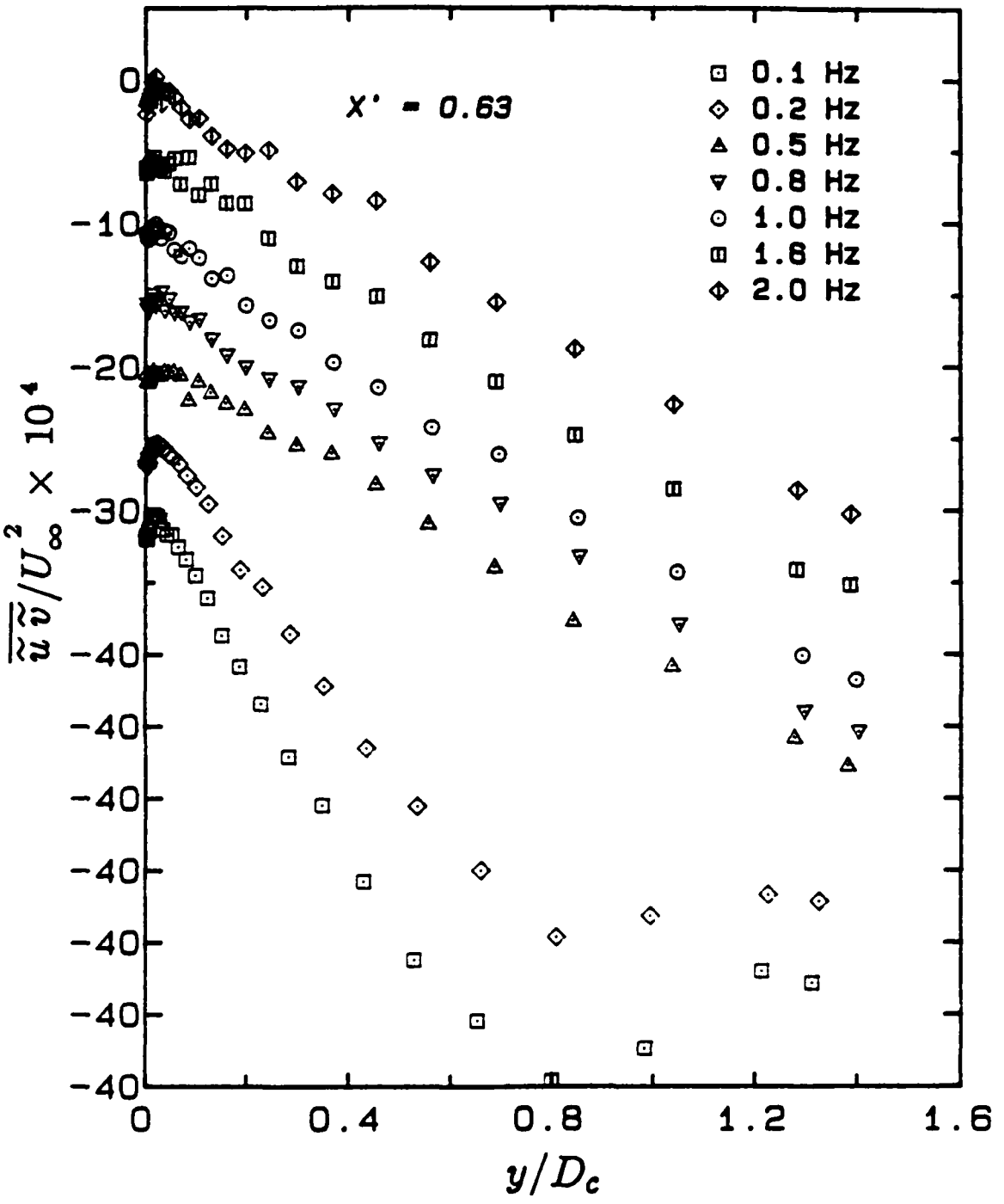

Figure 5.13 Time-averaged profiles of $\widetilde{\overline{u}}\widetilde{\overline{v}}/U_\infty^2$ under unsteady conditions. $X' = 0.63$

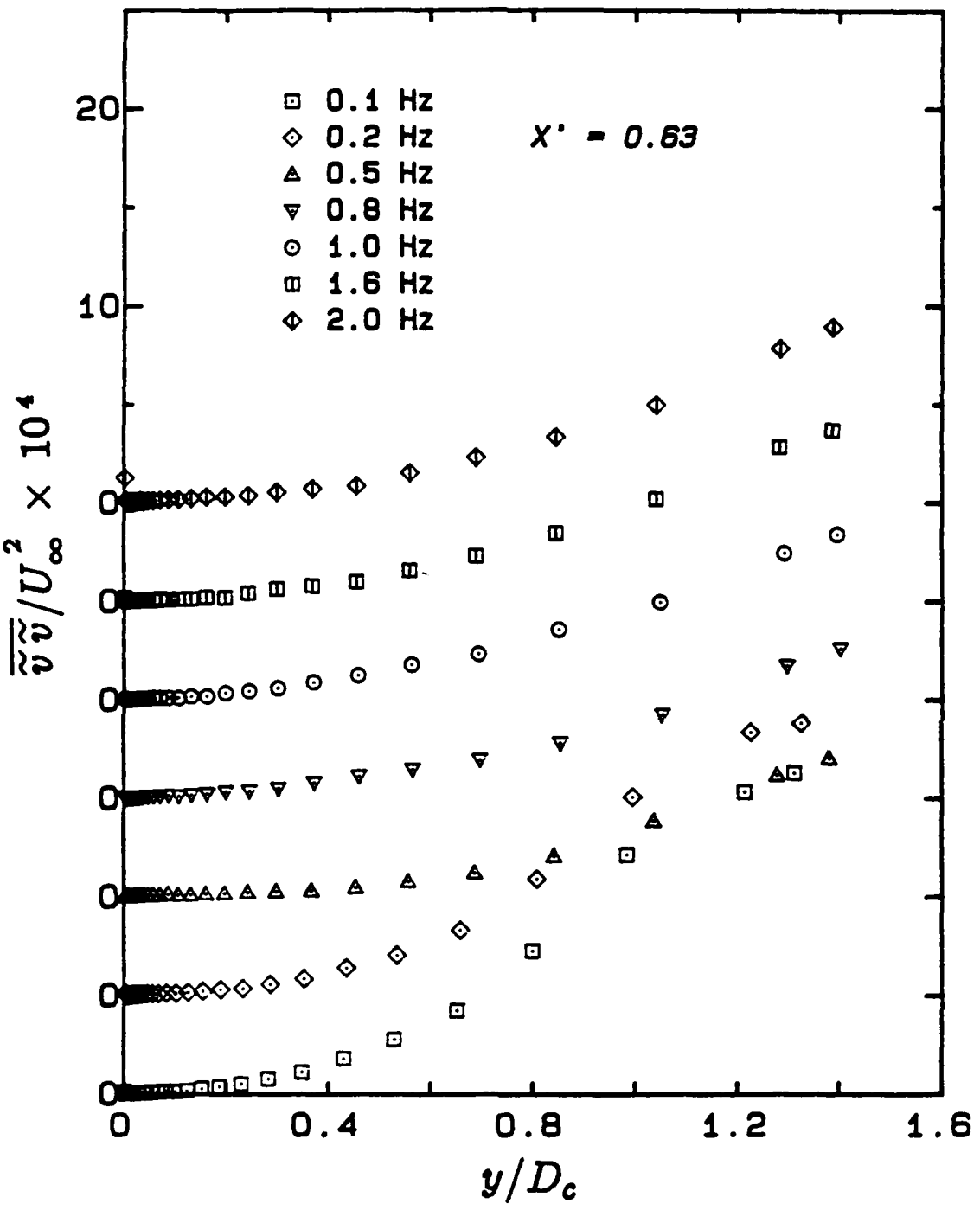

Figure 5.14 Time-averaged profiles of $\widetilde{v}\widetilde{v}/U_\infty^2$ under unsteady conditions.
$X' = 0.63$

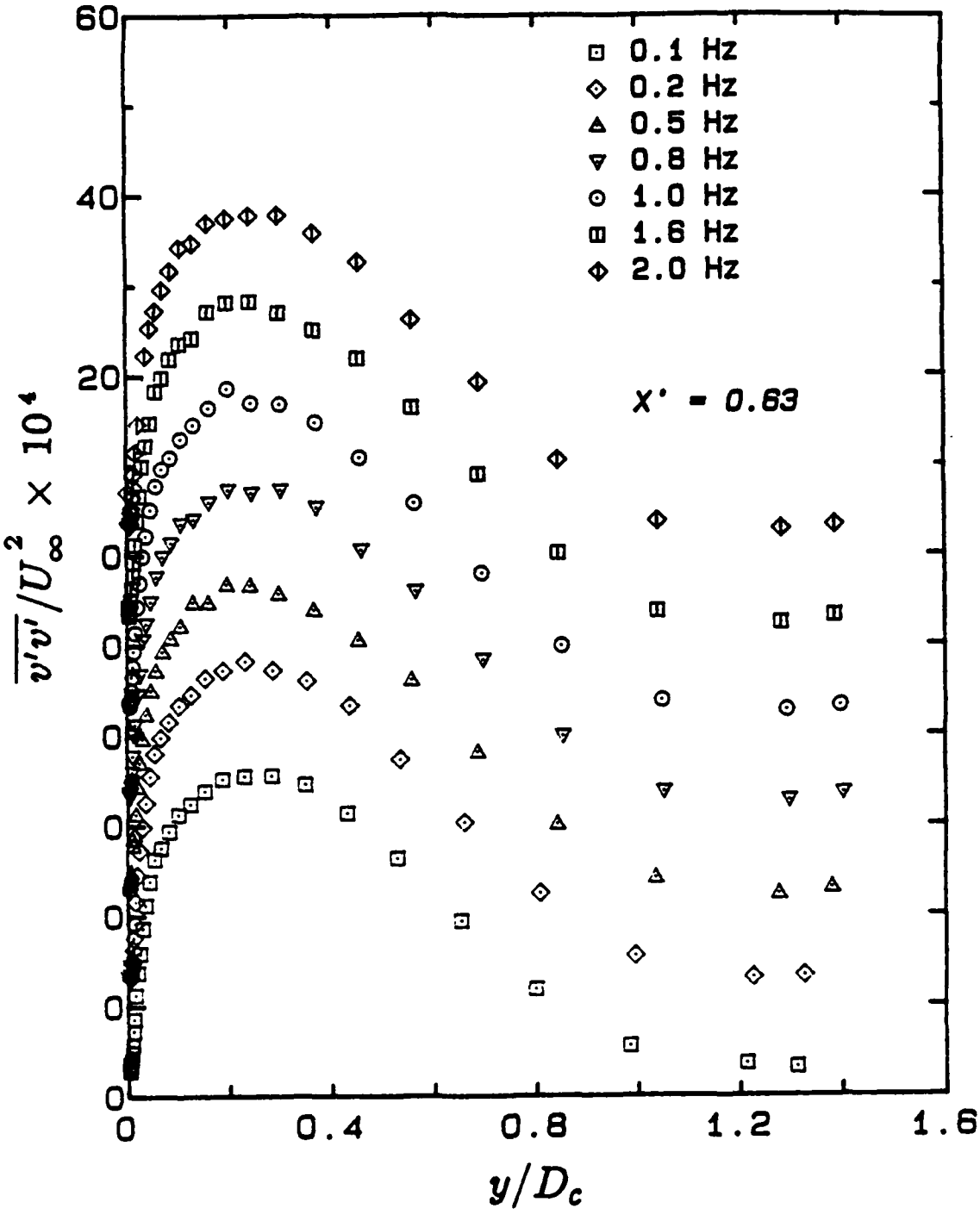

Figure 5.15 Time-averaged profiles of $\overline{v'v'}/U_\infty^2$ under unsteady conditions. $X' = 0.63$

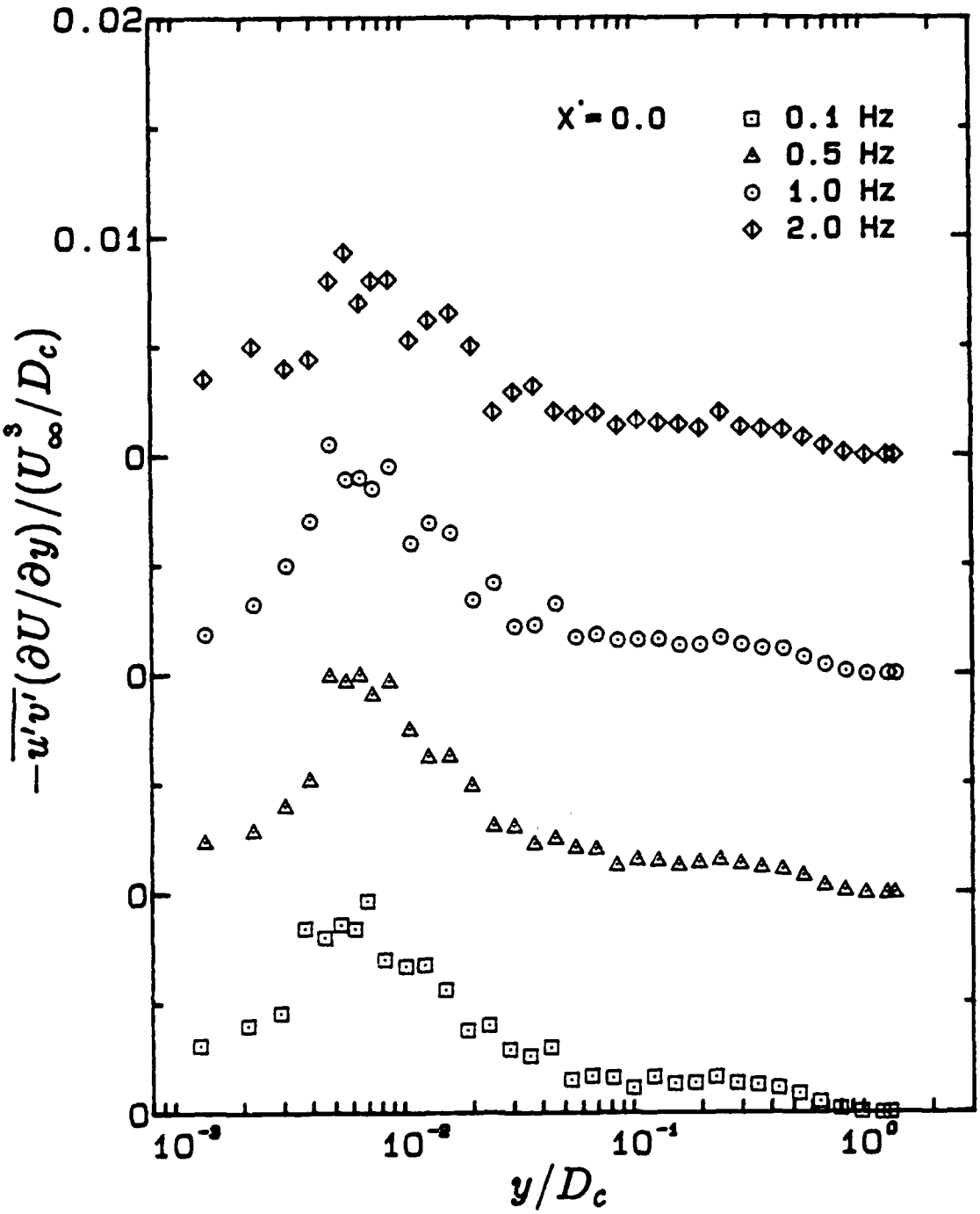

Figure 5.16 Time-averaged, normalized profiles of $-\overline{u'v'}(\partial U/\partial y)$ under unsteady conditions. $X' = 0.63$

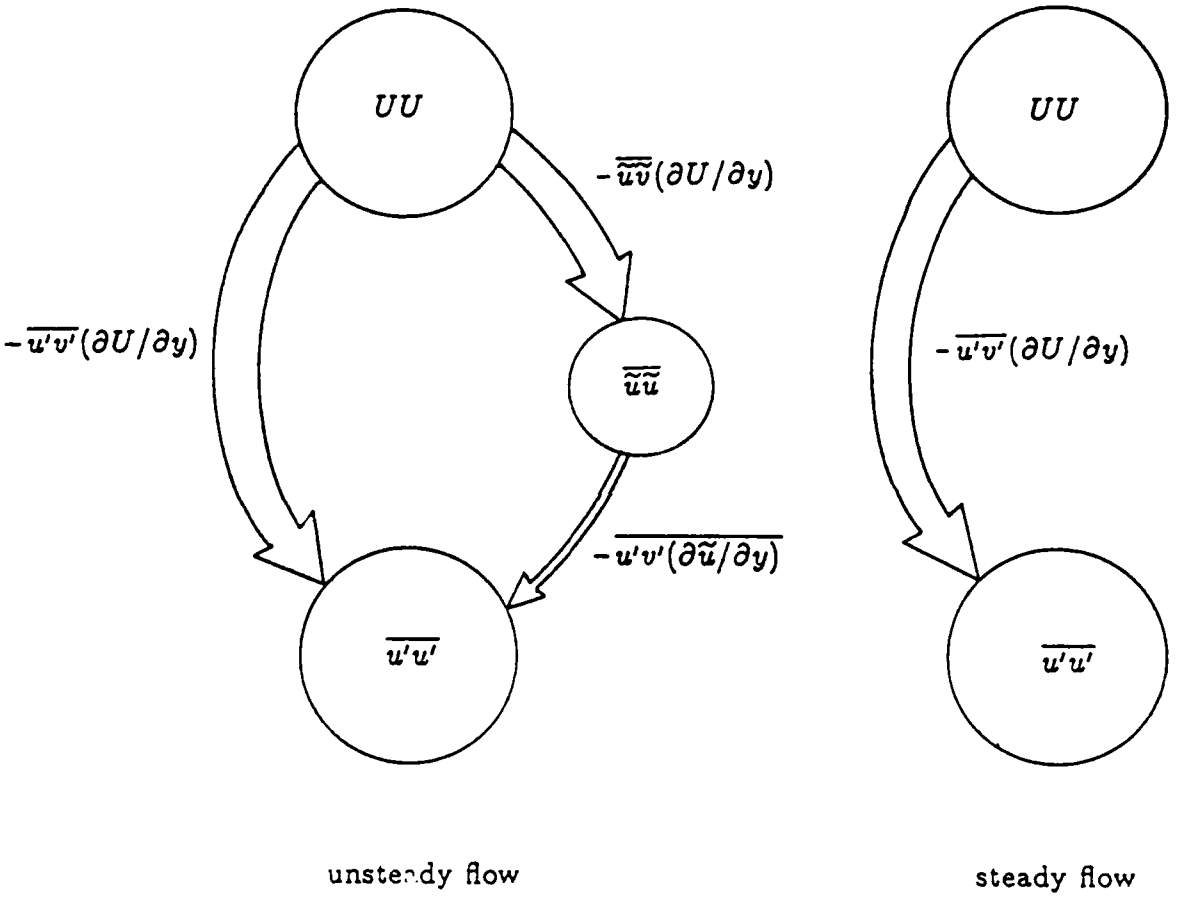

Figure 5.17 Transfer of kinetic energy between velocity fields near the wall (the thickness of each arrow represents the relative size of the energy-transfer term).

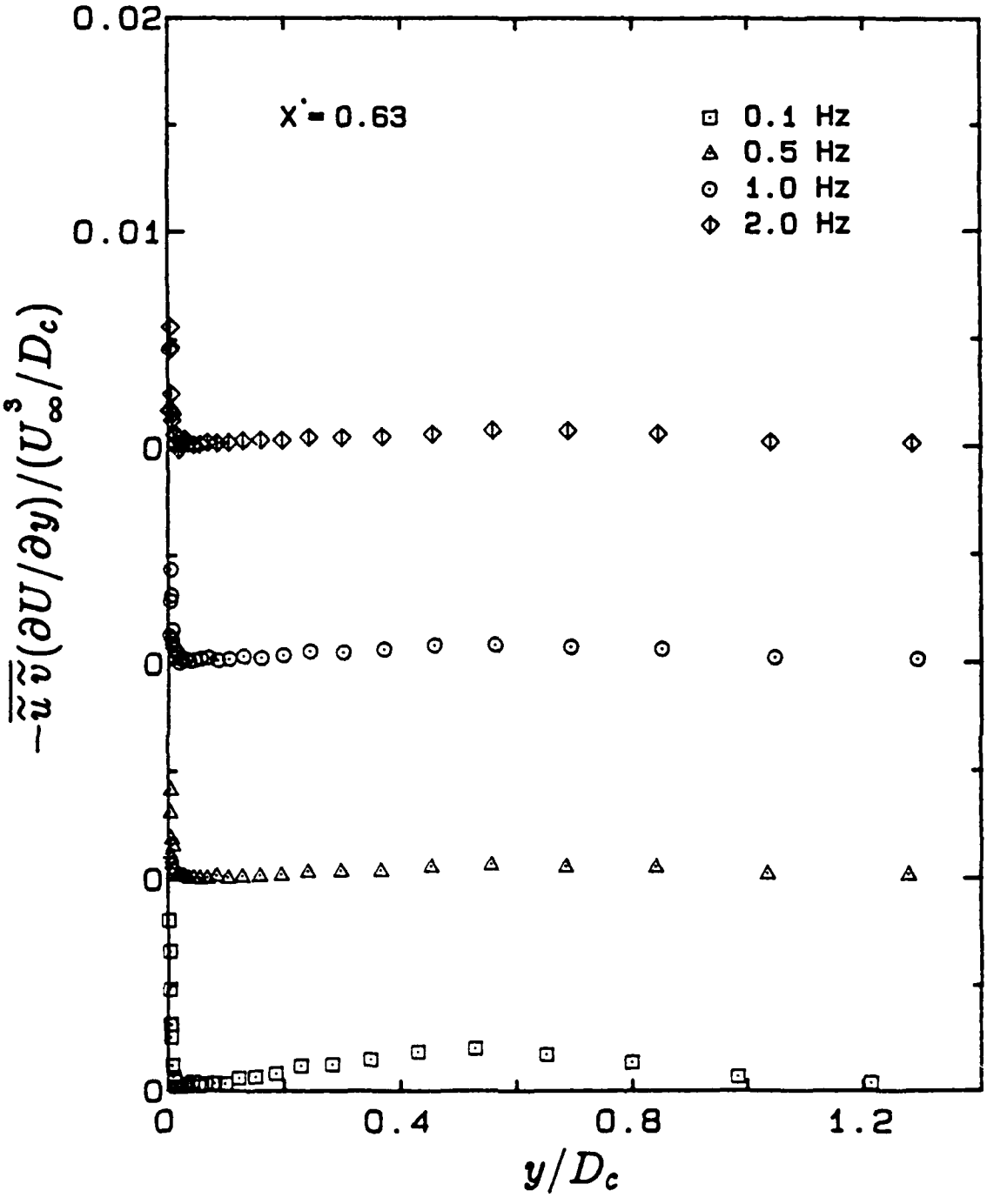

Figure 5.18 Time-averaged, normalized profiles of $-\widetilde{\widetilde{u}}\,\widetilde{\widetilde{v}}(\partial U/\partial y)$ under unsteady conditions. $X' = 0.63$

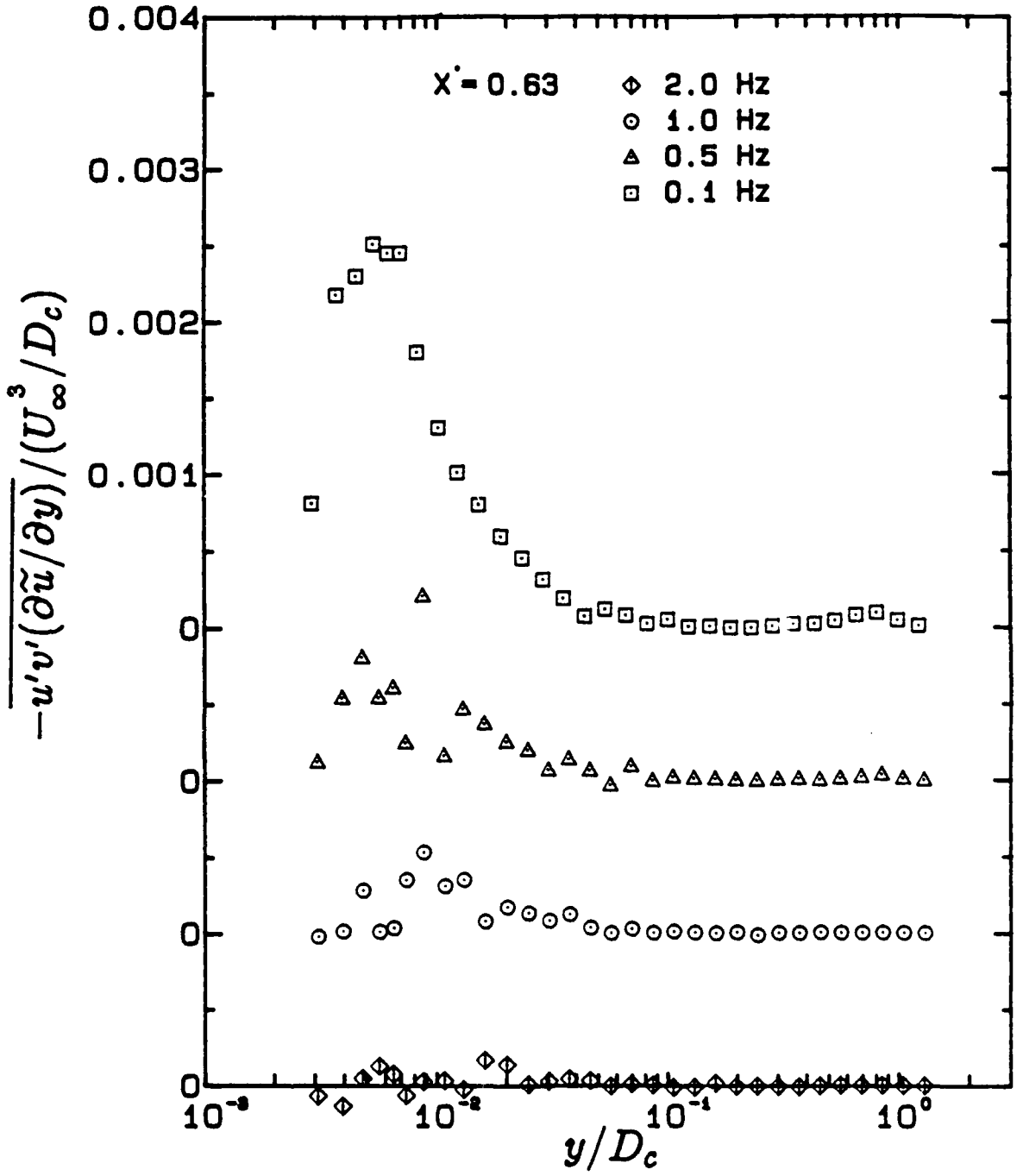

Figure 5.19 Time-averaged, normalized profiles of $-\overline{u'v'(\partial\tilde{u}/\partial y)}$ under unsteady conditions. $X' = 0.63$

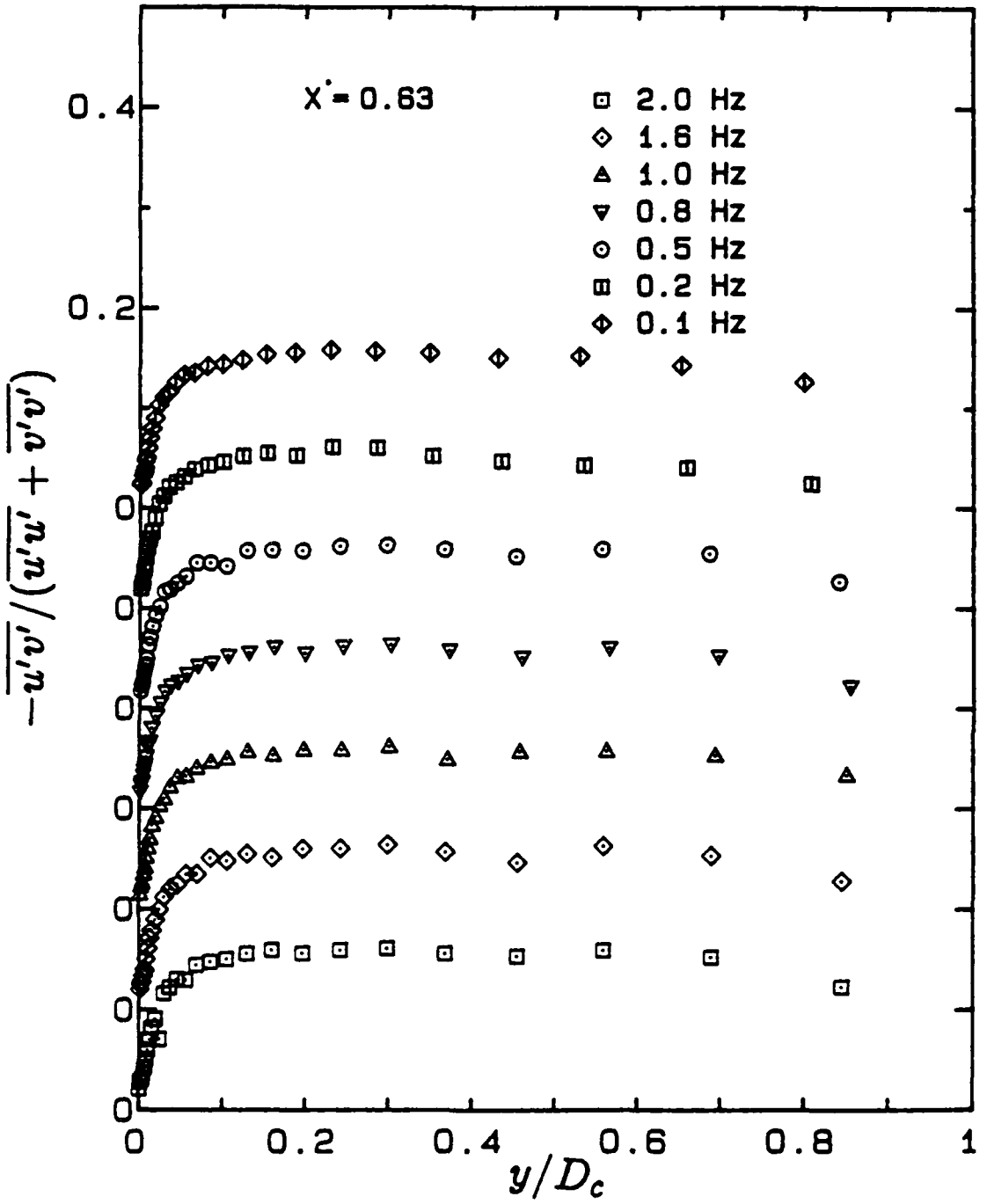

Figure 5.20 Time-averaged profiles of $-\overline{u'v'}/(\overline{u'u'}+\overline{v'v'})$ under unsteady conditions. $X' = 0.63$

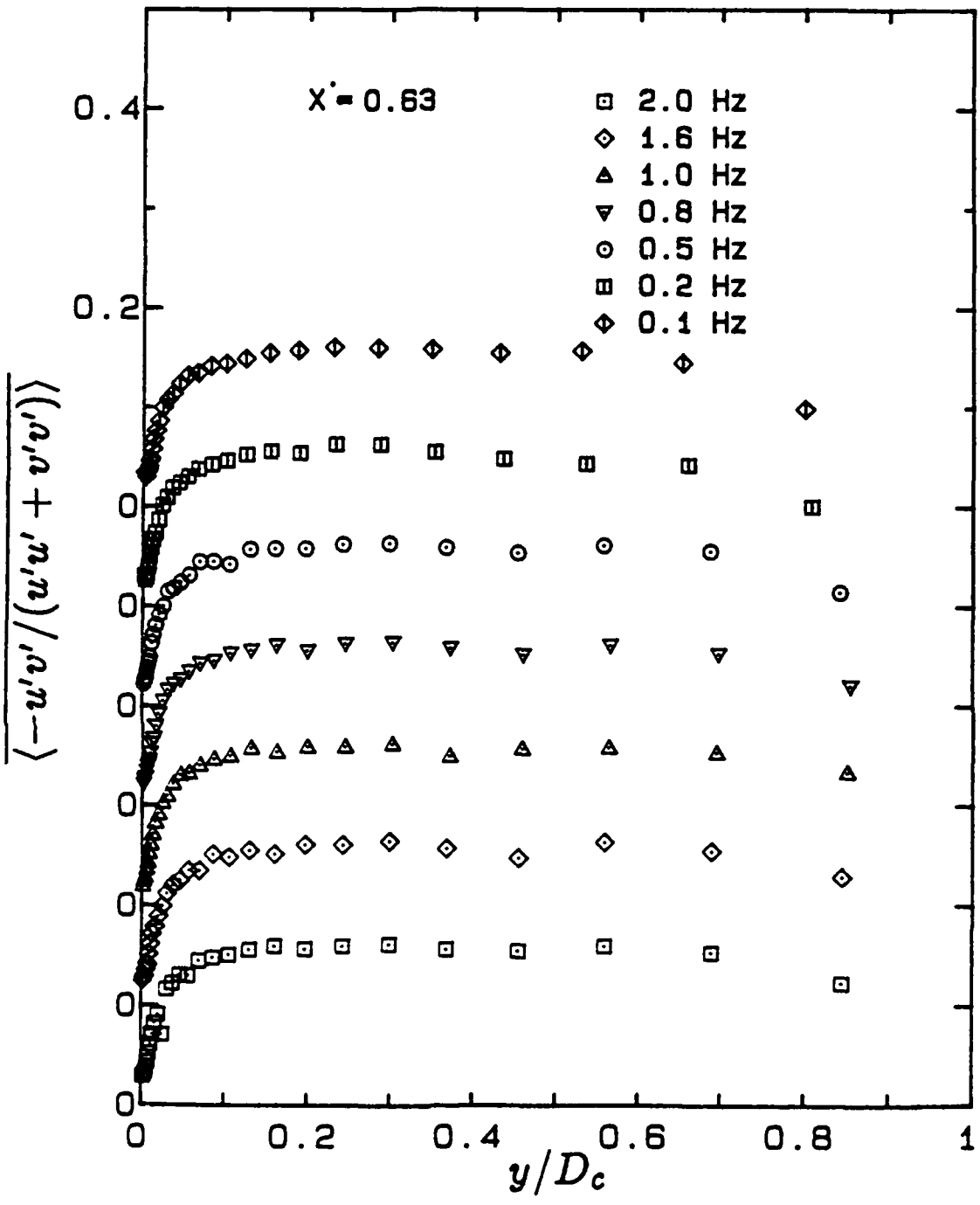

Figure 5.21 Time-averaged profiles of $\overline{\langle -u'v'/(u'u'+v'v')\rangle}$ under unsteady conditions. $X' = 0.63$

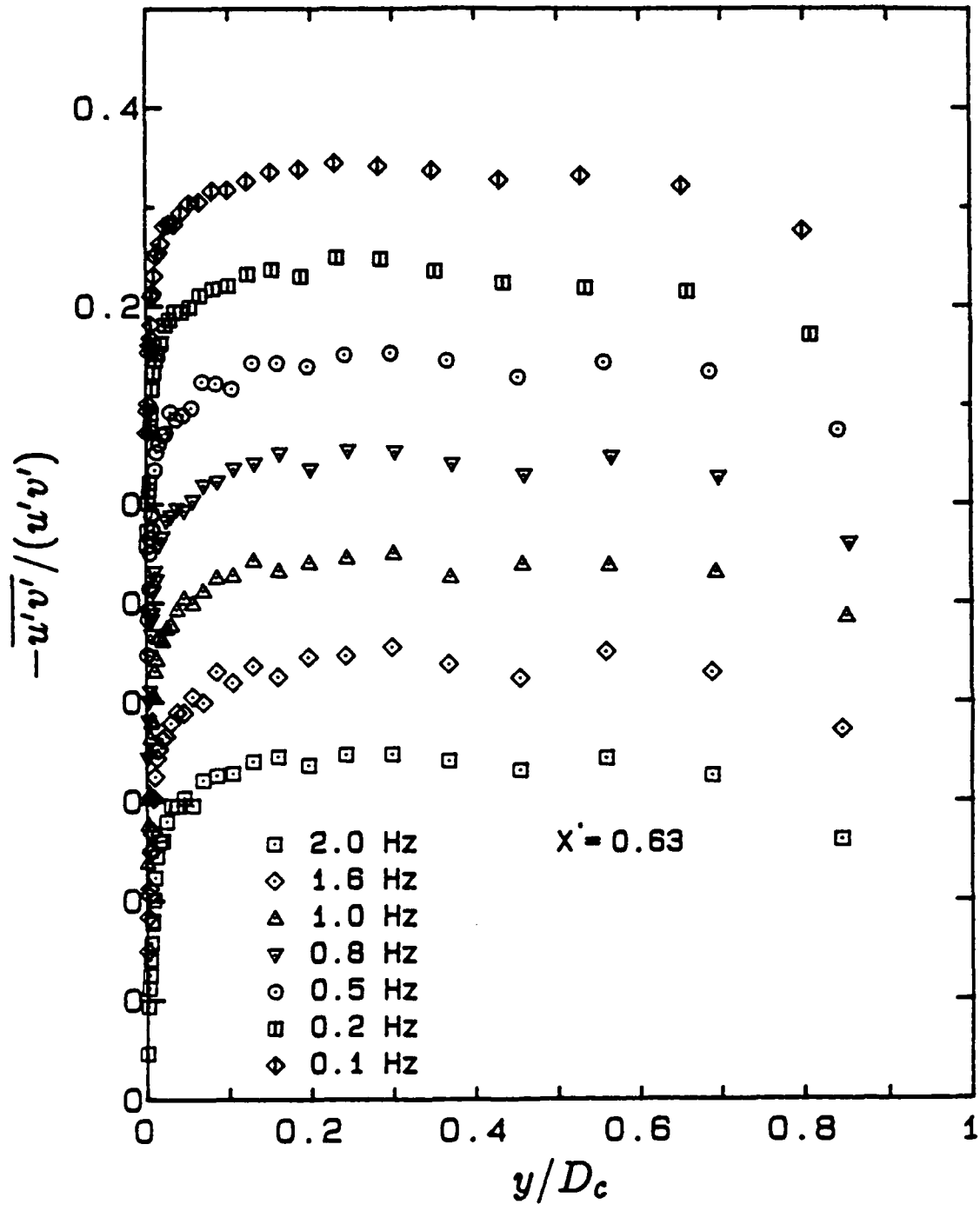

Figure 5.22 Time-averaged profiles of $-\overline{u'v'}/(u'v')$ under unsteady conditions. $X' = 0.63$

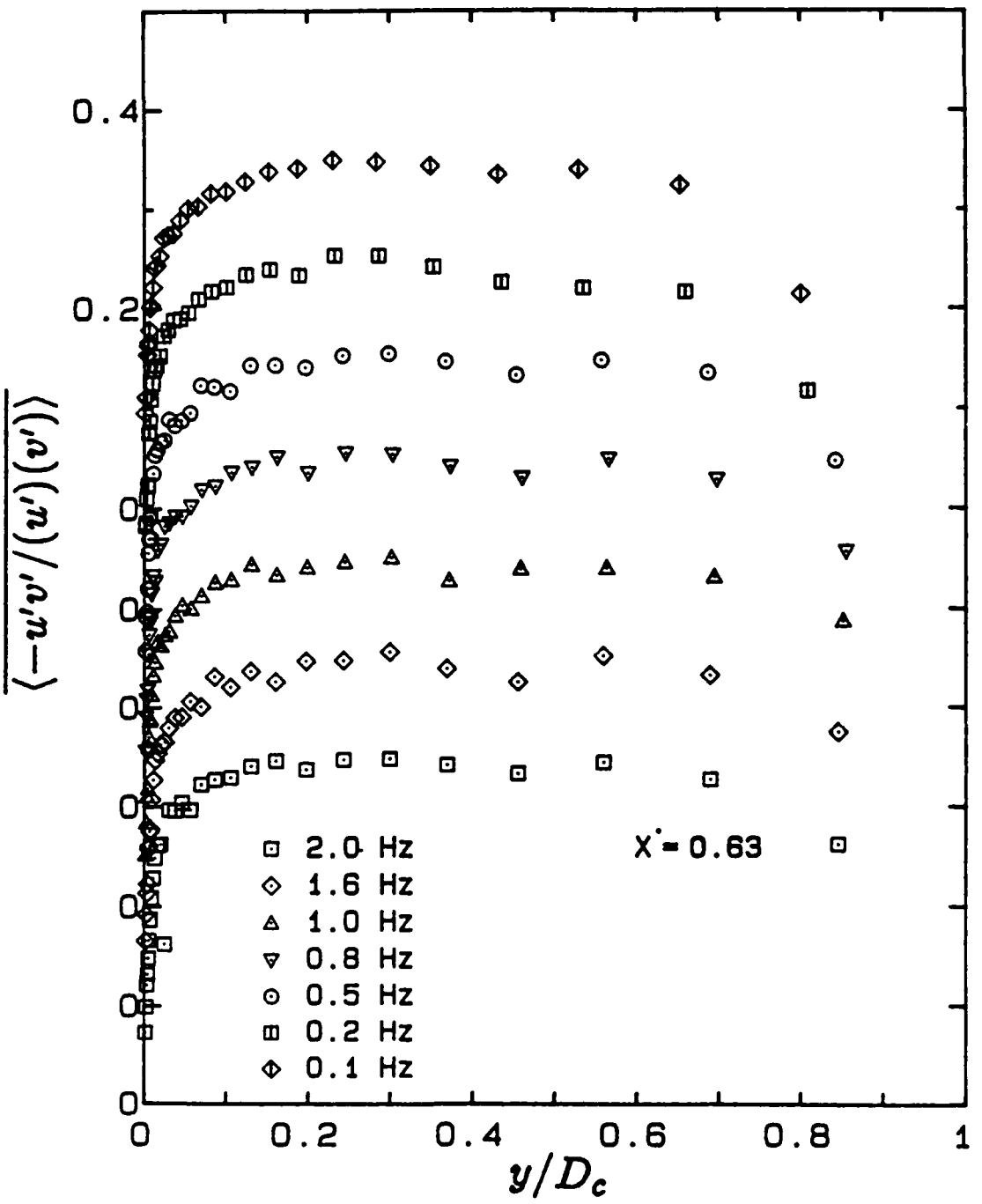

Figure 5.23 Time-averaged profiles of $\overline{\langle -u'v'/(u')(v')\rangle}$ under unsteady conditions. $X' = 0.63$

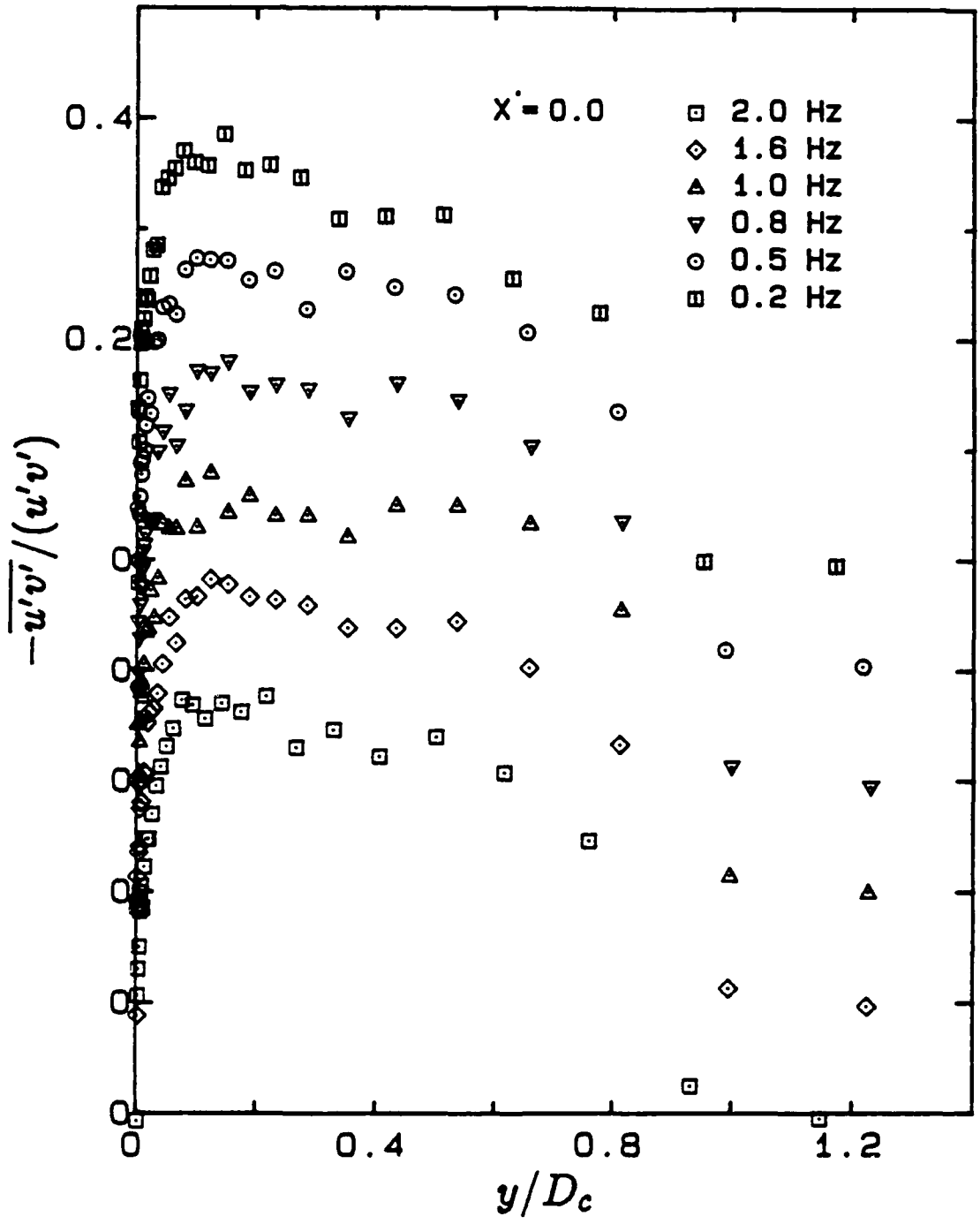

Figure 5.24 Time-averaged profiles of $-\overline{u'v'}/(u'v')$ under unsteady conditions. $X' = 0.0$

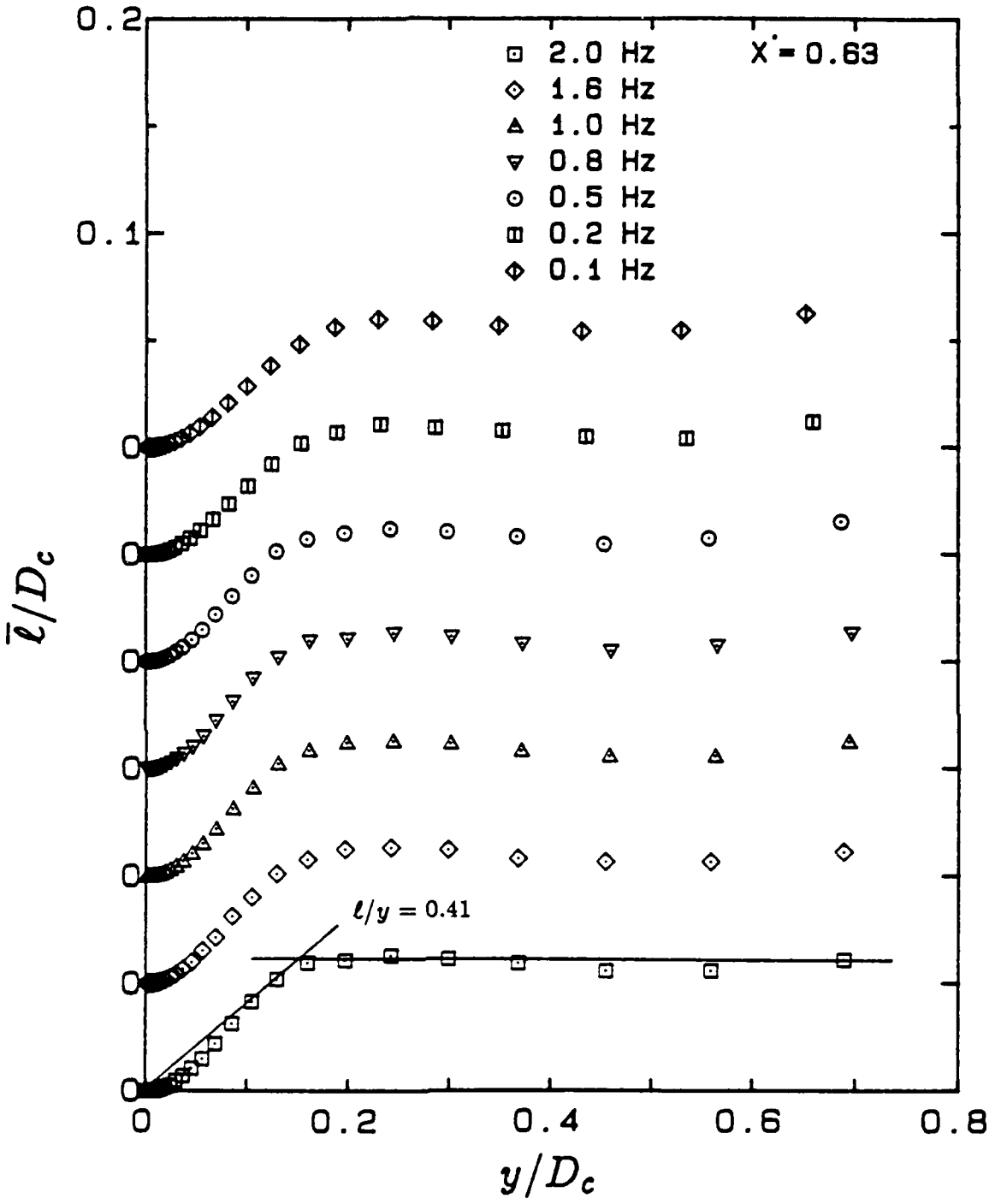

Figure 5.25 Time-averaged profiles of mixing length, $\bar{\ell}$, under unsteady conditions. $X' = 0.63$

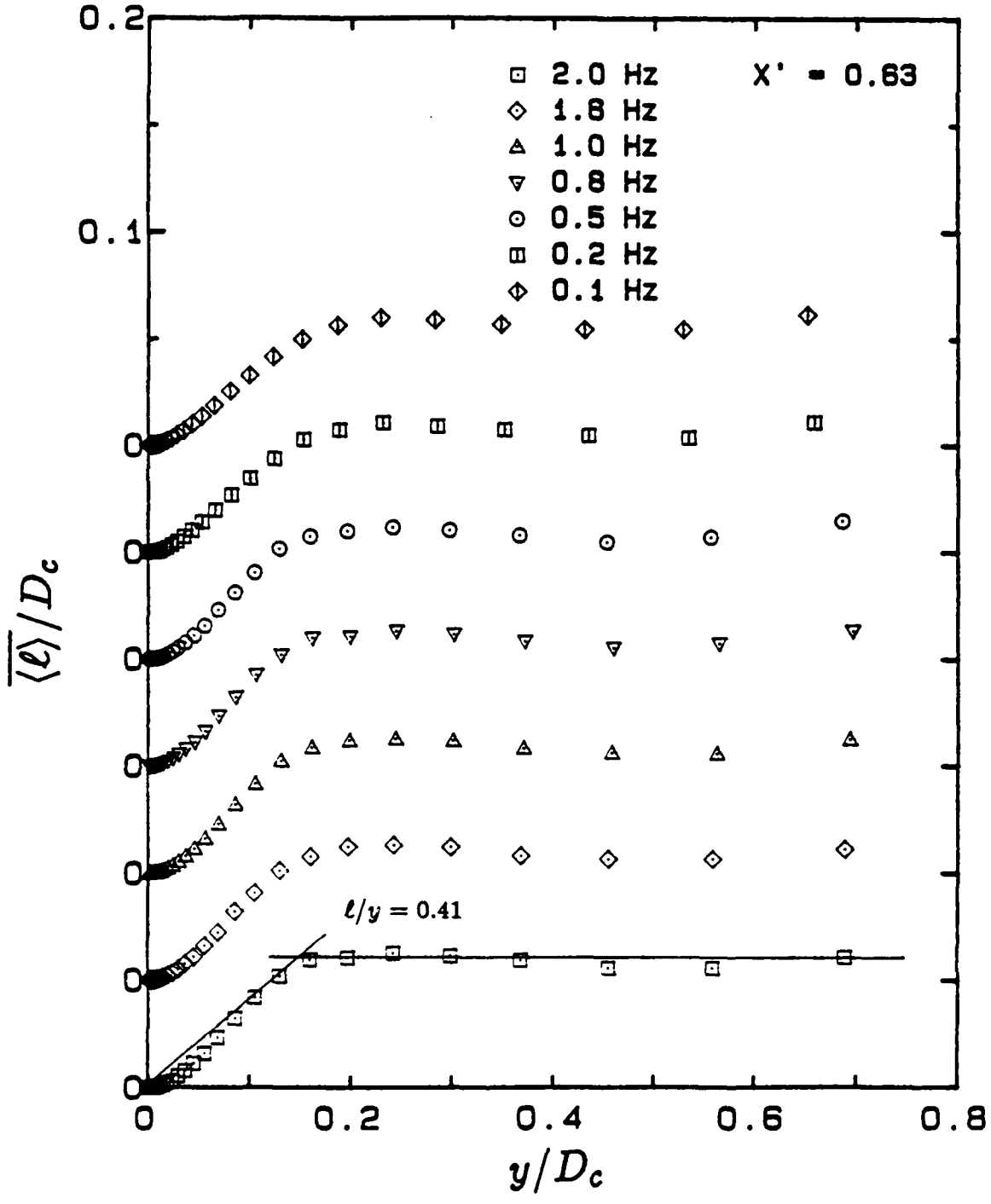

Figure 5.26 Time-averaged profiles of mixing length, $\overline{\langle \ell \rangle}$, under unsteady conditions. $X' = 0.63$

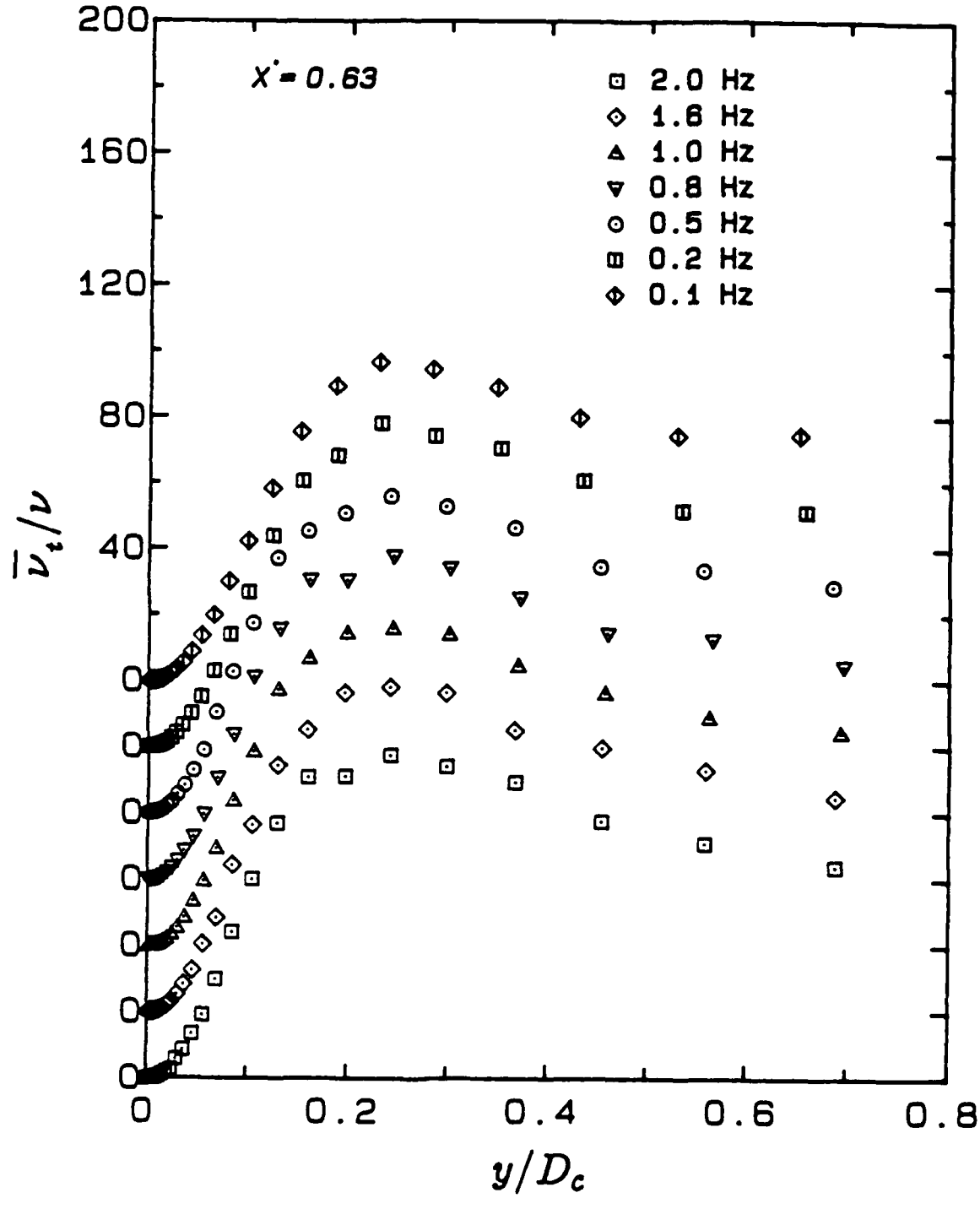

Figure 5.27 Time-averaged profiles of eddy viscosity, $\bar{\nu}_t$, under unsteady conditions. $X' = 0.63$

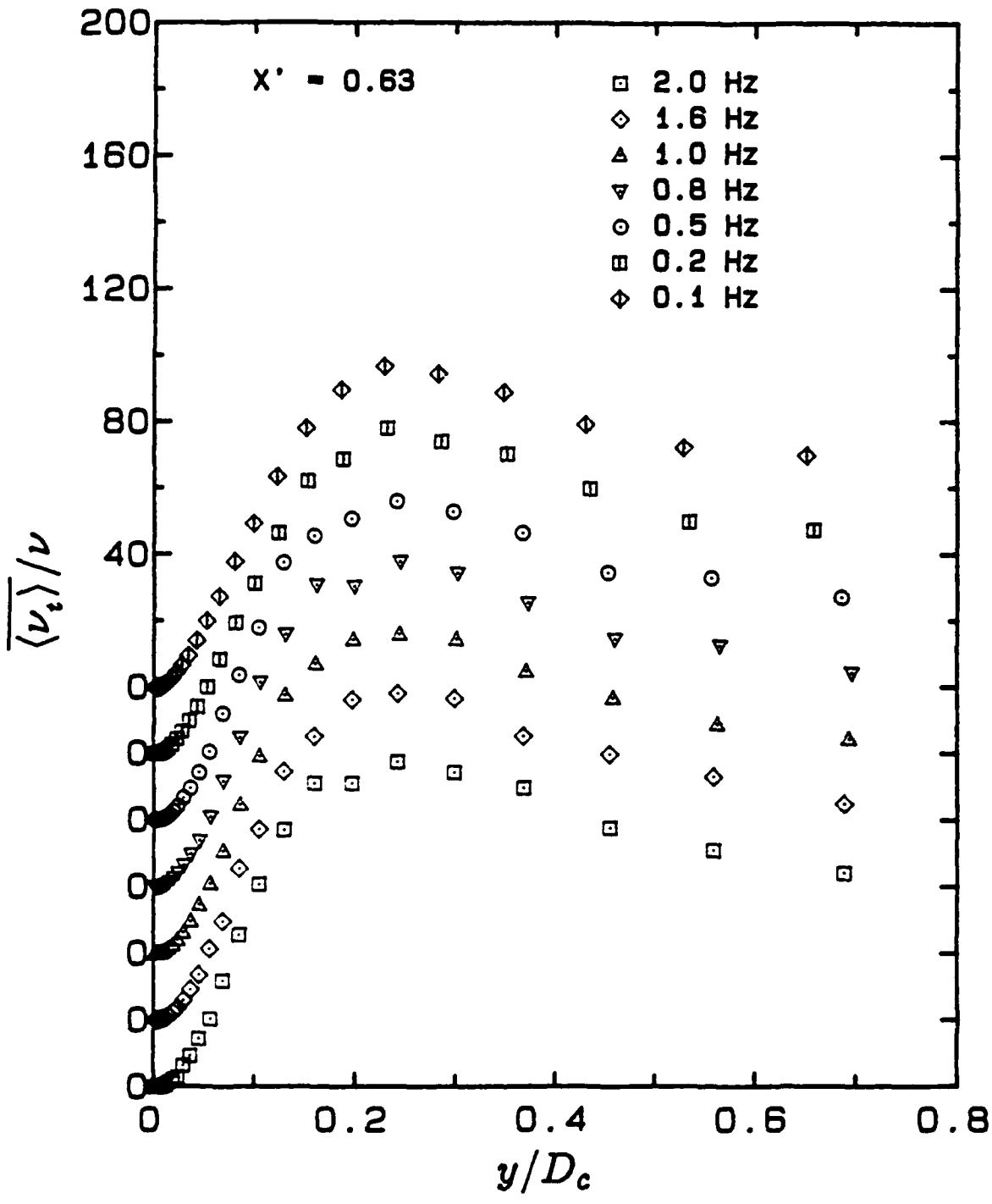

Figure 5.28 Time-averaged profiles of eddy viscosity, $\overline{\langle \nu_t \rangle}$, under unsteady conditions. $X' = 0.63$

6. Phase-Conditioned Unsteady Flow

The phase-conditioned or organized, unsteady behavior of the flow is considered in this chapter. Measurements of the response of the turbulent boundary layer to different frequencies of imposed free-stream unsteadiness are examined and, when appropriate, compared with the two asymptotic, unsteady modes of behavior:

(*i*) low-frequency, quasi-steady flow,

(*ii*) high-frequency flow, for which the streamwise velocity may be described by the analytic solution to the unsteady momentum equation.

The measurements are then used to develop some insight into the structure of the unsteady turbulence field.

6.1 Asymptotic Behavior

The deterministic momentum equation describing transport of a fluid under unsteady conditions (2.2.11) is:

$$\frac{\partial \tilde{u}_i}{\partial t} + \frac{\partial}{\partial x_k}(U_k \tilde{u}_i + \tilde{u}_k U_i) = -\frac{1}{\rho}\frac{\partial \tilde{p}}{\partial x_i} - \frac{\partial}{\partial x_k}(\widetilde{u'_k u'_i} + \widetilde{\tilde{u}_k \tilde{u}_i}) + \nu \frac{\partial^2 \tilde{u}_i}{\partial x_k \partial x_k} \ .$$

Its asymptotic, low-frequency form is simply the above equation without the leading unsteady term:

$$\frac{\partial}{\partial x_k}(U_k \tilde{u}_i + \tilde{u}_k U_i) = -\frac{1}{\rho}\frac{\partial \tilde{p}}{\partial x_i} - \frac{\partial}{\partial x_k}(\widetilde{u'_k u'_i} + \widetilde{\tilde{u}_k \tilde{u}_i}) + \nu \frac{\partial^2 \tilde{u}_i}{\partial x_k \partial x_k} \ , \qquad (6.1.1)$$

a form which admits only spatial derivatives of these unsteady terms. Now the forcing free-stream perturbation oscillated almost purely at its fundamental frequency,

as shown in §4.3. If the harmonic content of each of the other dependent variables of this equation is assumed to comprise only the contribution at the fundamental frequency of unsteadiness, *i.e.*

$$\widetilde{u} = |\widetilde{u}|\cos(\omega t + \phi_u) \ , \quad \widetilde{u'u'} = |\widetilde{u'u'}|\cos(\omega t + \phi_{u'u'}) \ , \ etc.,$$

and the magnitudes of products of deterministic velocities, $\widetilde{\widetilde{u}_k\widetilde{u}_i}$, (second harmonics) are negligible, then all significant terms of this equation would oscillate at the fundamental frequency. For the case of asymptotically slow, quasi-steady perturbation, all dependent variables have infinite time to respond to the forcing free-stream velocity, $\widetilde{u}_\infty$, and so phase variations should tend to zero. Therefore all dependent variables which increase as $\widetilde{u}_\infty$ grows should do so in phase with $\widetilde{u}_\infty$; those which decay as $\widetilde{u}_\infty$ increases should respond 180° out of phase with $\widetilde{u}_\infty$. This behavior characterizes the expected quasi-steady response of measures of velocities and turbulent quantities to the unsteady free stream.

The asymptotic, high-frequency form of the x-momentum equation is often called the Stokes equation:

$$\frac{\partial \widetilde{u}}{\partial t} = -\frac{1}{\rho}\frac{\partial \widetilde{p}}{\partial x} + \nu \frac{\partial^2 \widetilde{u}}{\partial y \partial y} \ . \tag{6.1.2}$$

The formulation of this equation and its analytic solution for the boundary conditions of this flow are described in Appendix E. This solution requires that:

(*i*) the outer flow reacts as a slug, in response to free-stream-velocity perturbations,

(*ii*) unsteady, streamwise velocities of magnitudes which differ from the unsteady, free-stream ones are accommodated within a thin layer next to the wall (the Stokes layer),

(*iii*) within the Stokes layer, the streamwise velocity leads the perturbing free-stream velocity in phase, the phase advance reaching its maximum value of 45° at the wall.

If the premises upon which the Stokes solution is based are met adequately, the response of the flow to high-frequency perturbations in free-stream velocity should embody these features.

6.2 Measures of Organized Unsteady Velocity

The response of the velocity fields to the unsteady, free-stream disturbance was analyzed through Fourier decomposition of ensemble-averaged velocity data, recorded at 512 discrete, evenly spaced times during each cycle of the disturbance. This decomposition enabled the response to be characterized in terms of amplitudes and phases corresponding to each of the 256 discernible harmonics. Since the harmonic content at the fundamental frequency exceeded 97% of the total harmonic content of $\tilde{u}$, throughout the boundary layer at all frequencies at which unsteadiness was imposed, $\hat{u}_1$ and $\phi_{1,u}$ (which represented the first harmonic of $\tilde{u}$) could be presumed to characterize the response of $\tilde{u}$ to free-stream unsteadiness.

Profiles of $\hat{u}_1$, the amplitude of the first harmonic of the deterministic, streamwise velocity, are shown in Figure 6.1 ; they were measured at $X' = 0.63$ at seven frequencies of unsteadiness between 0.1 and 2.0 hertz. The ordinate normalization is by the magnitude of the first harmonic of the local free-stream disturbance, $\hat{u}_{1,\infty}$, and the abscissa is the distance from the wall, y, divided by D_c (defined in §5.1). The corresponding phase information is displayed in Figure 6.2 ; it is expressed as the phase lead of the first harmonic, $\phi_{1,u}$, relative to the phase of the free-stream disturbance, ϕ_{1,u_∞}.

- *The response of the deterministic streamwise velocity, $\tilde{u}$, to forced free-stream unsteadiness was strongly dependent on frequency.*

For the lowest frequency of imposed unsteadiness at which measurements were made (0.1 hertz), the phase of the first harmonic of $\tilde{u}$ appeared to be almost constant throughout the boundary layer; only in the outermost part of the wake was any phase variation evident (in Figure 6.2). This slight variation in phase constituted a small lag in the response of the boundary layer to the free-stream oscillations, of around 10°, which might be attributed to viscous, inertial effects. With the exception of the phase variation in the outer wake, this phase profile matched the quasi-steady description of the response of $\tilde{u}$ to the forced unsteadiness.

At an imposed unsteadiness of 0.2 hertz, the phase remained constant over the bulk of the boundary layer. However, the wake layer accommodating phase variations penetrated further within the boundary layer and the response of the bulk of the boundary layer lagged further behind the free stream — an effect explained by the viscous, inertial character of the boundary layer. At higher frequencies of unsteadiness, phase variation was observed throughout the boundary layer as departure from the quasi-steady asymptote became complete.

The corresponding profiles of amplitudes of $\tilde{u}$ at low frequencies could not be compared readily with quasi-steady measures. As explained in §3.4, under truly quasi-steady conditions the boundary layer separated at the most adverse pressure gradients in the cycle, whereas, at frequencies of unsteadiness as low as 0.1 hertz, it remained attached. However it would seem, from Figure 6.1, that the approach towards the quasi-steady asymptote might correspond to boundary-layer values of $\hat{u}_1$ overshooting their free-stream values by increasingly greater margins. That this pronounced overshoot is consistent with the approach to a quasi-steady asymptote is illustrated by the instantaneous and time-averaged velocity profiles of Figure 6.3. The profiles in this figure at phase angles of 0° and 180°, and at the mean condition of the flow are comparable to steady velocity profiles in boundary layers at constant pressure, under strongly adverse pressure gradients and under moderately adverse pressure gradients respectively (with the exception of the measurements nearest the wall). Since the profiles at 0° and 180° represent the maxima and minima

of $\langle u \rangle$, their deviations from the mean condition correspond to the amplitude of oscillation, $\hat{u}_1$, which overshoots its free-stream value by factors approaching three, at $y/D_c \simeq 0.2$. Hence the quasi-steady asymptote does appear to be characterized by a pronounced overshoot of $\hat{u}_1$ within the boundary layer. The results displayed in Figure 6.1 indicated that the magnitude of the overshoot grew with decreasing frequency, as this asymptote was approached.

The profiles of $\hat{u}_1$, in Figure 6.1, seemed to take the form anticipated for asymptotic, high-frequency behavior at frequencies of 0.8 hertz and higher — $\hat{u}_1$ prevailed at its free-stream value over all the boundary layer except in a thin layer at the wall, which accomodated amplitudes of changing magnitude as the wall was approached (shown in Figure E.2). Also, the thickness of this wall layer appeared to decrease with increasing frequency, an observation which is consistent with the analysis of Appendix E. If coupled with constant phase in the outer boundary layer, this variation in $\tilde{u}$ would indicate that the bulk of the flow responded as a slug to the imposed unsteadiness. As no other development of the shape of the profile was evident as the frequency of imposed unsteadiness increases above 0.8 hertz, the asymptotic, high-frequency behavior of $\hat{u}_1$ appeared to have been reached at this frequency.

In contrast to the approach of $\hat{u}_1$ to its high-frequency asymptote at 0.8 hertz, the corresponding phase profile of $\phi_{1,u}$ continued to develop with increasing frequency. At 2.0 hertz, the highest frequency at which this study was conducted, the phase profile beyond the Stokes layer was not quite constant — a lag of up to 8° was evident. Within the Stokes layer, the phase advance approached 30° at the point closest to the wall at which measurements were made. How well this phase profile compared with the Stokes solution may be judged from Figure 6.4. As the phase data of Jayaraman *et al.* (1982), taken at the same frequency but at greater amplitudes of local unsteadiness, were in very good agreement with the Stokes solution, the assumptions on which the Stokes solution is based (in Appendix E) may not have been met adequately at a frequency of 2.0 hertz, at $X' = 0.63$.

- *The response of the deterministic streamwise velocity, $\widetilde{u}$, to forced free-stream unsteadiness could be described in terms of variation between:*

(i) an asymptotic low-frequency form, which corresponded to the quasi-steady condition of constant phase across the boundary layer,

(ii) an asymptotic high-frequency form which matched the analytic solution to the quasi-laminar Stokes equation.

A criterion for determining when agreement with the Stokes solution was to be expected was deduced in Appendix E. The requirement that the magnitude of the unsteady term greatly exceed that of the convective terms, in the deterministic x-momentum equation (2.2.11), translated to the provision that the Strouhal number, $\omega X/U_0$, would greatly exceed one for the boundary conditions of this flow. Here ω is the imposed unsteadiness expressed as an angular velocity, X is the distance along the test section and U_0 is the free-stream velocity at the entrance to the test section. Plots of $\widehat{u}_1/\widehat{u}_{1,\infty}$ and $\phi_{1,u} - \phi_{1,u_\infty}$ for flow at different values of this Strouhal number are displayed in Figures 6.5 and 6.6. The Strouhal numbers correspond to the four highest frequencies for which experiments were conducted at $X' = 0.45$ and $X' = 0.63$. In each graph, the abscissa is $y/\sqrt{2\nu/\omega}$, the dimensionless, independent variable of the Stokes solution. While good agreement with the asymptotic amplitude variation is observed for flow at all Strouhal numbers for which profiles are plotted (in Figure 6.5), the phase data of Figure 6.6 are much more poorly grouped. Although better agreement is observed with increasing Strouhal number, the highest values are too low to reproduce the desired asymptotic advance in phase near the wall. From the data of Jayaraman *et al.* (1982), it would appear that the desired asymptotic behavior was observed only if this Strouhal number exceeded ten.

Now high-frequency flow can be considered to have reached its asymptotic condition only if both the phase and amplitude are in good agreement with the asymptotic form. From the results of this study it would seem that when the amplitude

matches the asymptotic form it should not be taken as an indication that the phase necessarily would do so too.

- *As the high-frequency condition was approached, the asymptotic amplitude was matched at lower frequencies than were necessary to satisfy the corresponding phase requirement.*

The response of the wall-normal component of velocity, $\tilde{v}$, to forced variation in $\tilde{u}$ may also be expressed in terms of its phase and amplitude at different frequencies of imposed, free-stream unsteadiness. As the first harmonic of $\tilde{v}$ was always the most energetic, typically accounting for between 70% and 99% of the total harmonic content, profiles of $\hat{v}_1$ and $\phi_{1,v}$ were considered characteristic of $\tilde{v}$ and are shown in Figures 6.7 and 6.8 respectively; $\hat{v}_1$ is normalized by the local forcing term, $\hat{u}_{1,\infty}$, and $\phi_{1,v}$ is plotted relative to the phase of the perturbation, ϕ_{1,u_∞} . In the interests of consistency with the $\tilde{u}$ measures discussed earlier, the data shown in these figures were deduced from measurements made at $X' = 0.63$, although the equivalent results at $X' = 0.45$ were qualitatively very similar.

A linear abscissa was preferred for graphs of measures of $\tilde{v}$ because of the emphasis this scaling lent to the behavior of the outer flow. Such emphasis was desirable as the uncertainty of near-wall measures of $\langle v \rangle$ was considerably larger than that of outer values. Now the boundary condition of no transpiration at the wall required that $\tilde{v}$ was zero there. As measures of $\langle v \rangle$ generally remained small near the wall, compared to $\langle u \rangle$, slight misalignments in the optical system may have introduced significant uncertainties which might have exceeded the detectable measures of $\langle v \rangle$ in this region. While amplitudes remained small (as illustrated by the $\hat{v}_1$ measures, plotted against a logarithmic abscissa in Figure 6.9), phases of negligibly small quantities, buried in noise, were typified by large, erratic variations which should be attributed to the unsuitability of Fourier decomposition for data of such uncertainty in this near-wall region. Hence this abscissa scaling was chosen to focus on the regions of greater certainty in the data.

At the lowest frequencies of forced unsteadiness, the response of $\widetilde{v}$ led the forcing perturbation by about 170° over the major part of the boundary layer (Figure 6.8). This response might be interpreted more clearly as variation in the opposite sense to $\widetilde{u}$, with a lag of around 10°. The flatness of the phase profile was consistent with the description of quasi-steady flow and no departure from the free-stream value was observed until the near-wall region was approached (where the phase data became untrustworthy). The sense of the $\widetilde{v}$ data ($\sim 180°$ out of phase with $\widetilde{u}$) is consistent with a quasi-steady model of the flow — as the instantaneous pressure gradient becomes more adverse and $\langle u \rangle$ decreases, $\langle v \rangle$ increases throughout the boundary layer. This behavior appears to be followed by the profiles of $\langle v \rangle$ taken at the lowest frequency of forced unsteadiness, displayed in Figure 6.10. Unfortunately, it was not possible to criticize or compare the data of Figure 6.10 with values obtained by other researchers because of the acute shortage of V data in boundary layers under different pressure gradients, and the apparent absence of any other measurements of $\widetilde{v}$.

The sense of the $\widetilde{v}$ measures might also be anticipated from the deterministic continuity equation: $\partial\widetilde{v}/\partial y = -\partial\widetilde{u}/\partial x$. In the quasi-steady limit, the phase and sense of $\partial\widetilde{u}/\partial x$ within the boundary layer are the same as in the free stream. Since the free-stream velocity took the form: $\widetilde{u}_\infty = U_0 A X' \cos\omega t$, it follows that $\partial\widetilde{v}/\partial y$ should take the phase and sense of $-\cos\omega t$ or $\cos(\omega t + \pi)$.

At low frequencies of forced unsteadiness, the normal gradient of $\widehat{v}_1$ appeared to persist at its free-stream value throughout the boundary layer, at approximately the value prescribed there by the deterministic continuity equation (Figure 6.8). Furthermore, from Figure 6.9, the magnitude of $\widehat{v}_1$ would appear to exceed a small percentage of the forcing amplitude, $\widehat{u}_{1,\infty}$, only in the outer 90% of the boundary layer, a region which coincided with the one over which $\partial(\widetilde{u}\,\widetilde{v})/\partial y$ was shown to be significant in the mean x-momentum equation (in §5.3). This observation emphasizes the importance of inclusion of $\widetilde{v}$ information in prediction schemes aimed at accurate representation of the mean field of this flow.

The uncertainties involved in trying to gauge the size of each term in the deterministic y-momentum equation, for a forced perturbation in the x direction, render the deduction of an asymptotic, high-frequency form an extremely difficult task. Therefore no analytic description is proposed, although the almost-linear variation of $\langle v \rangle$ with y implied that a simple form might exist. The asymptotic, high-frequency condition which could be devised readily is found from the deterministic equation of continuity. At high frequencies of imposed unsteadiness, the slug-like response of $\widehat{u}_1$ dictates that $\partial \widetilde{v}/\partial y = -\partial \widetilde{u}_\infty/\partial x$ over all the boundary layer but the Stokes layer (the $\widetilde{u}$ Stokes layer). In the outer flow, where phase information could be deduced clearly, the phase implications of this asymptotic behavior are no different from the quasi-steady ones. The corresponding implications about the magnitude of the normal gradient of $\widehat{v}_{1,\infty}$ also appear to have been met at all frequencies at which this study was conducted. To emphasize this point, profiles of $\langle v \rangle$ at a frequency of 1.6 hertz are shown in Figure 6.11; any differences between $\langle v \rangle$ at 0.1 and 1.6 hertz are obviously only slight ones. Therefore it was not possible to conclude whether $\widetilde{v}$ followed either a high- or low-frequency, or indeed any, asymptotic form in the range of frequencies at which forced, free-stream unsteadiness was imposed.

- *No asymptotic behavior could be identified in measures of $\widetilde{v}$, the wall-normal component of deterministic velocity.*

6.3 Unsteady Flow Characterization

The success in describing the response of the streamwise, deterministic, velocity field to free-stream unsteadiness in terms of variation between asymptotic modes of the deterministic x-momentum equation implies that the dominant terms of this equation should play an important role in the characterization of organized, unsteady flows. The apparent invariance of the mean flow to the imposition of organized unsteadiness (demonstrated in §5), in contrast to the strong dependence on

TABLE 6.1

Characterizations of the Unsteady Flow

f	$\sqrt{2\nu/\omega}$	$X' = 0.45$				$X' = 0.63$			
Hz	mm	S_X	S_δ	ℓ_s^+	ω^+	S_X	S_δ	ℓ_s^+	ω^+
0.1	1.88					0.363	0.059	32.44	.0019
0.2	1.33	0.514	.081	27.72	.0026	0.728	0.116	22.99	.0038
0.5	0.84	1.283	.202	17.64	.0064	1.829	0.280	14.76	.0092
0.8	0.66	2.052	.324	14.02	.0102	2.936	0.443	11.60	.0149
1.0	0.59	2.568	.404	12.50	.0128	3.672	0.556	10.35	.0187
1.6	0.47	4.126	.648	9.81	.0208	5.894	0.899	8.08	.0306
2.0	0.42	5.172	.819	8.73	.0262	7.386	1.126	7.19	.0387

frequency of the behavior of the deterministic velocity field, implies that no more than a very weak link can exist between the mean and unsteady fields of velocity. Hence the equations which describe them should be only weakly coupled and so mean measures *per se* should be of very little influence in the unsteady velocity field. Consequently, the influence of the deterministic velocity in organized unsteady flow might be characterized by this Strouhal number alone, which represents the ratio between the dominant unsteady and convective terms of the deterministic x-momentum equation.

- *The ratio of the leading unsteady and convective terms of the $\tilde{u}$ momentum equation was proposed as a parameter for characterizing the response of $\tilde{u}$ to forced free-stream unsteadiness.*

For the particular boundary conditions of this flow, the Strouhal number takes the form $S_X = \omega X/U_0$ when this ratio is estimated as its free-stream value (see Appendix E). While the ω dependence is general for any unsteady boundary conditions, the X dependence is a consequence of the design of this experiment. Similarly, the dependence on U_0 results from its role in the unsteady convective term,

$\partial(U\tilde{u})/\partial x$, which happens to be important for the particular boundary conditions of this experiment, rather than through a general dependence on the mean field.

Several other dimensionless parameters have been suggested for the characterization of unsteady flows; they include ω^+, ℓ_S^+ and S_δ. The latter quantity is of the same form as S_X, only the mean boundary-layer thickness and mainstream velocity are combined as a local time scale for the mean flow. The parameter ω^+ is defined as the angular velocity, ω, scaled by the kinematic viscosity, ν, and normalized by the square of the mean friction velocity, u_τ; ℓ_S^+ is the square root of twice the reciprocal of ω^+. These parameters were computed for each of the experiments conducted and their values, together with those of S_X, are shown in Table 6.1. The quantity u_τ was estimated by fitting Coles' mean velocity function to time-averaged profiles. Although there are inaccuracies inherent in the application of such a scheme to this unsteady flow, described in §5.3, it was considered adequate for rough estimates of this nature.

If the experiments are arranged according to increasing size of characteristic parameter, the same order results regardless of the parameter chosen. While, at first inspection, this invariance might appear to be a vindication of the equal importance of all these parameters, on closer examination it seems to be the result of a fortuitous similarity between the streamwise variations in the local mean and unsteady conditions, which, once again, appears to be no more than a consequence of the design of this particular experiment. The X dependence of S_X is imitated by S_δ $(\omega\delta/U_\infty)$ as the conditions of the mean flow happen to correspond to a pressure gradient which becomes increasingly adverse with downstream distance, and hence U_∞ decreases with X while δ increases. Similarly, ω^+ mimics the X dependence of the unsteady flow through the streamwise decrease of u_τ, which results from the streamwise deceleration of the mean flow. Had the experiment been designed with a different variation in its mean flow, more might have been revealed about the performance of these parameters in characterizing the influence of deterministic velocity in organized unsteady flow.

- *The performance of the proposed parameter was adequate but barely distinguishable from that of other parameters, the forms of which were based on different premises. This finding was thought to be due to the similarity in the streamwise variation in mean and deterministic velocities which resulted from the design of this particular experiment.*

6.4 Measurements of Periodic Turbulence

The response of turbulence measures to forced free-stream unsteadiness may also be examined in terms of the phase and amplitude of periodic quantities such as $\widetilde{u'u'}$, $\widetilde{v'v'}$ and $-\widetilde{u'v'}$. However, profiles of these turbulence terms are not monotonic since they are required to approach zero both at the wall and in the free stream. Consequently, forms more complicated than the smooth, continuous variations observed in phase and amplitude profiles of $\tilde{u}$ and $\tilde{v}$ are anticipated and additional references to phase-conditioned profiles of $\langle u'u' \rangle$, $\langle v'v' \rangle$, and $\langle -u'v' \rangle$ are helpful in clarifying the nature of the unsteady turbulence behavior. All data were deduced from measurements made at $X' = 0.63$ although the behavior of the boundary layer at $X' = 0.45$ was qualitatively no different.

The first harmonics of $\widetilde{u'u'}$, $\widetilde{v'v'}$ and $-\widetilde{u'v'}$ were the most energetic for all frequencies of imposed unsteadiness. While $\widehat{u'u'}_1$ characteristically accounted for between 40% and 95% of the total harmonic content of $\widetilde{u'u'}$, throughout the boundary layer at all frequencies of mainstream unsteadiness, the proportional harmonic contents of $\widehat{v'v'}_1$ and $-\widehat{u'v'}_1$ only reached these percentages at the lowest frequencies at which this study was conducted. As the frequency of perturbation increased, the fractions of the total harmonic contents due to $\widehat{v'v'}_1$ and $-\widehat{u'v'}_1$ decreased. When the free stream was perturbed at 2.0 hertz, $\widehat{v'v'}_1$ and $-\widehat{u'v'}_1$ typically contributed from 5% to 40% of the total harmonic content, but never more than 50%. That a large proportion of the harmonic content of $\widetilde{u'u'}$ and $-\widetilde{u'v'}$ is at the fundamental frequency, at the lowest frequencies of forced unsteadiness, supports the assumption of §6.1 that

these terms of the deterministic x-momentum equation would oscillate primarily at their first harmonic for the case of quasi-steady perturbation of the mainstream.

- *At low frequencies of forced unsteadiness, the deviation of measures of phase-conditioned turbulence from their mean value was similar to the expected quasi-steady response.*

Profiles of the phase-averaged measures, $\langle u'u' \rangle$, $\langle v'v' \rangle$ and $\langle -u'v' \rangle$, together with their mean values, are shown in Figures 6.12 – 6.14 at 0.1 hertz. It is evident that both the phase-averaged profiles, at 0° and 180°, intersect the mean profile at almost coincident points in each graph. Although there is appreciable scatter in these data, the shapes of the profiles are similar to those reported under comparable steady conditions by Andersen (1972). The equivalent profiles at 2.0 hertz are shown in Figures 6.15 – 6.17 and in each case the deviation of the two phase-averaged profiles from the mean is reduced considerably from its low-frequency values such that their deviations are barely perceptible from scatter.

- *Periodic turbulence measures were strongly dependent on frequency of forced unsteadiness.*

Profiles of the phase and amplitude of $\widehat{u'u'}_1$, $\widehat{v'v'}_1$ and $-\widehat{u'v'}_1$ are now examined. The amplitude variations, normalized by the square of the local perturbation velocity, $\widehat{u}_{1,\infty}$, are shown in Figures 6.18 – 6.20. The deviations of phase-averaged measures from their means (in Figures 6.12 – 6.14) are represented by the two pronounced peaks in the amplitude profiles at low frequencies (in Figures 6.18 – 6.20). Between these peaks, the amplitudes fall almost to zero at the point in the boundary layer corresponding to the intersection of mean and phase-conditioned measures. Since the phase-averaged profiles of $\langle u'u' \rangle$, $\langle v'v' \rangle$ and $\langle -u'v' \rangle$ at 0.1 hertz were comparable to quasi-steady ones, and there was little difference between the profiles of $\widehat{u'u'}_1$, $\widehat{v'v'}_1$ and $-\widehat{u'v'}_1$ at 0.1 and 0.2 hertz, these might be considered

the asymptotic, quasi-steady forms of the amplitudes of $u'u'$, $v'v'$ and $-u'v'$ for this flow.

- *High frequency behavior was characterized by greatly reduced amplitudes in the periodic measures:* $\widehat{u'u'}_1$, $\widehat{v'v'}_1$ *and* $-\widehat{u'v'}_1$.

As the frequency of perturbation in the mainstream increased, the deviations of $\langle u'u' \rangle$, $\langle v'v' \rangle$ and $\langle -u'v' \rangle$ from their mean values decreased, as did the corresponding amplitudes of the periodic quantities. For each measure, the outer peak appeared to recede more rapidly than the inner one. At 2.0 hertz, the shapes of the outer peaks seemed to have lost their definition; the low amplitudes of these deterministic turbulence measures might then correspond to an approach to the "frozen" condition reported by Ramaprian & Tu (1979) in their study of oscillatory pipe flow.

- *At the highest frequencies of forced unsteadiness, these amplitudes were negligible in the outer part of the boundary layer although still significant in the inner part.*

If periodic turbulence were considered purely as a shear-related quantity, which might be described adequately in Boussinesq terms alone, the near-wall peaks of the amplitudes of these measures would be expected to approach the wall with increasing frequency of perturbation — *i.e.* a collapse of amplitude data might be expected if an abscissa based on a measure of Stokes-layer thickness, such as $y/\sqrt{2\nu/\omega}$, were employed. From Figures 6.18 – 6.20, it is clear that the positions of the inner peaks in amplitude are independent of forcing frequency and so a Boussinesq model of deterministic turbulence is not implied by these measurements.

- *In contrast to the high-frequency behavior of* $\widetilde{u}$ *(for which an abscissa scaling on a frequency-dependent length scale was appropriate), an abscissa incorporating a mean length scale suited profiles of periodic turbulence measures.*

Phase profiles corresponding to $\widehat{u'u'}_1$, $\widehat{v'v'}_1$ and $-\widehat{u'v'}_1$ are shown in Figures 6.21 – 6.23, where the ordinate is the phase lead relative to the forcing function, *i.e.* $\phi_{1,u'u'} - \phi_{1,u_\infty}$. In each graph, phase information is presented at four of the seven frequencies — attempts to include data at more frequencies in each graph resulted in overlapping of data from adjacent shifted axes and a subsequent reduction in clarity. At the lowest frequency of imposed unsteadiness, each deterministic turbulence measure lagged the perturbing mainstream slightly; phase variation within the profile was limited to the outer part of the wake, as was observed in the response of $\tilde{u}$. The dramatic shift in phase, by 180°, corresponded to the point of intersection between the mean and phase-averaged measures of the turbulent quantities. Since this intersection need not occur at the same place, at each phase in the unsteady cycle, and since the neighboring region corresponds to small difference between mean and phase-conditioned quantities, a noisy appearance in the phase measures is to be expected there. At 0.2 hertz, the phase lag was a little larger. This observation is again consistent with the response of $\tilde{u}$ and appears to represent departure from the quasi-steady asymptote.

At higher frequencies of imposed unsteadiness, the behavior of the phases of $u'u'$, $v'v'$ and $-u'v'$ was more difficult to interpret. The variation in the outer boundary layer (beyond the intersection of mean and phase-conditioned measures) became erratic as deterministic measures became smaller and more poorly defined. Near the wall, however, $\phi_{1,u'u'}$, $\phi_{1,v'v'}$ and $\phi_{1,-u'v'}$ each varied in rather different fashions which are examined in more detail in §6.7.

6.5 Phase-Conditioned Products of Periodic Velocities

The equation describing unsteady transport of momentum in a fluid with constant properties (2.2.11) includes terms which represent the divergence of products of periodic velocities, *i.e.* $\partial(\widetilde{\tilde{u}_k\tilde{u}_i})/\partial x_k$. Since such terms are the products of two oscillating components of velocity, they are likely to be typified by a strong response

at the second harmonic of the forcing frequency in the organized unsteady flow. As the responses of other quantities of this momentum equation to forced mainstream unsteadiness were predominantly at the fundamental frequency (§6.2, §6.4), the role of the tensor, $\partial(\widetilde{\tilde{u}_k\tilde{u}_i})/\partial x_k$, might be presumed to be an uninfluential one in this flow. The validity of such an assumption is now tested through examination of measurements of the relevant quantities of this tensor.

In the phase-conditioned x-momentum equation,

$$\frac{\partial \tilde{u}}{\partial t} + \frac{\partial}{\partial x}(2\,U\,\tilde{u} + \widetilde{u'u'} + \widetilde{\tilde{u}\,\tilde{u}}) + \frac{\partial}{\partial y}(V\,\tilde{u} + \tilde{v}\,U + \widetilde{v'u'} + \widetilde{\tilde{v}\,\tilde{u}}) = -\frac{1}{\rho}\frac{\partial \tilde{p}}{\partial x} + \nu\frac{\partial^2 \tilde{u}}{\partial x_k \partial x_k}\ ,$$

the deterministic products of oscillating velocities are represented by the terms $\partial(\widetilde{\tilde{u}\,\tilde{u}})/\partial x$ and $\partial(\widetilde{\tilde{u}\,\tilde{v}})/\partial y$. The limiting values of these quantities, at the wall and in the mainstream, may be deduced through the boundary conditions of this flow. As the wall was stationary with no transpiration, $\widetilde{\tilde{u}\,\tilde{u}}$ was zero there as was its streamwise gradient. Likewise, $\widetilde{\tilde{u}\,\tilde{v}}$ and its normal gradient were zero at the wall too. In the free stream, the contribution of these terms to the deterministic momentum equation, as second harmonics, may be assessed by substitution of the prescribed boundary conditions of the experiment. When applied in the mainstream, the x-momentum equation may be written in the form:

$$\begin{aligned} -\frac{1}{\rho}\frac{\partial \tilde{p}}{\partial x} &= \frac{\partial \tilde{u}_\infty}{\partial t} + \frac{\partial}{\partial x}(2\,U_\infty \tilde{u}_\infty + \widetilde{\tilde{u}_\infty \tilde{u}_\infty}) + \frac{\partial}{\partial y}(V_\infty \tilde{u}_\infty + \tilde{v}_\infty U_\infty + \widetilde{\tilde{v}_\infty \tilde{u}_\infty}) \\ &= \frac{\partial \tilde{u}_\infty}{\partial t} + \frac{\partial}{\partial x}(U_\infty \tilde{u}_\infty) + \frac{\partial}{\partial x}\Big(\frac{\widetilde{\tilde{u}_\infty \tilde{u}_\infty}}{2}\Big)\ . \end{aligned} \qquad (6.5.1)$$

In this formulation, $\partial(\widetilde{\tilde{u}_\infty \tilde{u}_\infty}/2)/\partial x$ is the portion of the phase-conditioned pressure gradient oscillating at the second harmonic of the disturbance. The conditions at the free-stream boundary of this flow were:

$$U_\infty = U_0(1 - AX') \qquad \text{and} \qquad \tilde{u}_\infty = U_0 AX' \cos\omega t \ .$$

Substitution of these conditions into (6.5.1) yields:

$$-\frac{1}{\rho}\frac{\partial \tilde{p}}{\partial x} = -\omega U_0 AX' \sin\omega t + \frac{U_0^2 A}{L}(1 - 2AX')\cos\omega t + \frac{U_0^2 A^2 X'}{2L}\cos 2\omega t \ . \quad (6.5.2)$$

The significance of the products of periodic velocities to the x-momentum equation may now be assessed by considering the ratio of amplitudes of the free-stream pressure gradient, at its first and second harmonics. This ratio is:

$$\frac{\left|\frac{\partial \hat{p}}{\partial x}\right|_2}{\left|\frac{\partial \hat{p}}{\partial x}\right|_1} = \frac{AX'}{2\sqrt{(1 - 2AX')^2 + S_X^2}} \ , \qquad (6.5.3)$$

from which it may be inferred that second harmonics are most important for the case of quasi-steady perturbation. For $A = 0.24$ and $X' = 0.45$ and 0.63, the ratio of amplitudes of first and second harmonics of pressure gradient takes the values 0.05 and 0.08 respectively. Since this ratio decreases in magnitude at higher frequencies of imposed unsteadiness (with increasing S_X), second harmonics are unlikely to play an important role within the unsteady boundary layer unless $\partial(\widetilde{\tilde{u}\,\tilde{u}})/\partial x$ and $\partial(\widetilde{\tilde{u}\,\tilde{v}})/\partial y$ exceed their free-stream values by appreciable margins at the lowest frequencies of imposed unsteadiness.

As the significance of second harmonics in the mainstream has been estimated, for quasi-steady disturbances, the relative importance of $\partial(\widetilde{\tilde{u}\,\tilde{u}})/\partial x$ within the boundary layer may be gauged conveniently from the ratio of $\widehat{\tilde{u}\,\tilde{u}}_2/\hat{u}_{1,\infty}^2$ to $\hat{u}_1/\hat{u}_{1,\infty}$. If streamwise gradients of $\widetilde{\tilde{u}\,\tilde{u}}$ do not vary dramatically across the boundary layer,

the peak values of $\partial(\widetilde{\widetilde{u}\,\widetilde{u}})/\partial x$ can be considered proportional to the maxima of $\widetilde{\widetilde{u}\,\widetilde{u}}$, which may be deduced from the profiles of $\widehat{u}_1$, shown in Figure 6.1. Since almost all the harmonic content was concentrated at the fundamental frequency, $\widetilde{u}$ could be assumed to take the form $\widetilde{u} = \widehat{u}_1 \cos(\omega t + \phi_{1,u})$, from which it follows that $\widehat{\widetilde{u}\,\widetilde{u}}_2 = \widehat{u}_1 \widehat{u}_1/2$. Now the largest values of $\widehat{u}_1$, when normalized by $\widehat{u}_{1,\infty}$, attained about 2.5 (in Figure 6.1, at 0.1 hertz). Consequently, the corresponding normalized value of $\widehat{\widetilde{u}\,\widetilde{u}}_2$ would reach around three. Since this boundary-layer ratio of second harmonics to first harmonics barely exceeded one, as opposed to one half in the free stream, it corresponded to little more than a local doubling in importance of second harmonics within the boundary layer, relative to their significance in the mainstream.

The magnitude of the normal gradient of $\widetilde{\widetilde{u}\,\widetilde{v}}$, relative to its free-stream value, may be deduced from Figure 6.24, in which the ordinate is $\widehat{\widetilde{u}\,\widetilde{v}}_2$ normalized by the square of the mainstream perturbation. A linear abscissa was employed for ease of estimation of normal gradients of $\widehat{\widetilde{u}\,\widetilde{v}}_2$. At high frequencies of imposed unsteadiness, the normal gradient within the boundary layer seemed to prevail at its free-stream value. At low frequencies, however, it appeared to reach from two to three times its free-stream value over a large portion of the boundary layer. Consequently, while the significance of second-harmonic terms of the deterministic x-momentum equation seemed to be somewhat greater within the boundary layer than in the free-stream, it was not dramatically so — this observation is consistent with the findings of §6.2 and §6.4 that, at low frequencies of forced unsteadiness, periodic measures oscillated almost entirely at the fundamental frequency. Hence, effects at the second harmonic of the forcing frequency did not appear to play a crucial role in the x-momentum equation.

The phase-conditioned y-momentum equation may be written as:

$$\frac{\partial \widetilde{v}}{\partial t} + \frac{\partial}{\partial x}(U\,\widetilde{v} + \widetilde{u}\,V + \widetilde{u'v'} + \widetilde{\widetilde{u}\,\widetilde{v}}) + \frac{\partial}{\partial y}(2\,V\,\widetilde{v} + \widetilde{v'v'} + \widetilde{\widetilde{v}\,\widetilde{v}}) = -\frac{1}{\rho}\frac{\partial \widetilde{p}}{\partial y} + \nu\frac{\partial^2 \widetilde{v}}{\partial x_k \partial x_k}\ ,$$

where the deterministic products of oscillating velocities are the terms $\partial(\widetilde{\widetilde{u}\,\widetilde{v}})/\partial x$ and $\partial(\widetilde{\widetilde{v}\,\widetilde{v}})/\partial y$; these quantities may also be expressed as $\partial(\widetilde{\widetilde{v}\,\widetilde{v}}/2)/\partial y + \widetilde{\widetilde{u}\,(\partial\widetilde{v}/\partial x)}$. Since $\widetilde{u}$ and $\widetilde{v}$ oscillated predominantly at the fundamental frequency, $\widetilde{\widetilde{u}\,\widetilde{v}}$ and $\widetilde{\widetilde{v}\,\widetilde{v}}$ would be most energetic at the second harmonic of the forcing frequency. The influence of these terms could then be assessed through comparisons of their magnitudes with quantities of the y-momentum equation which were characterized by a strong first-harmonic response.

The importance of the quantity, $\partial(\widetilde{\widetilde{v}\,\widetilde{v}}/2)/\partial y$, may be judged from comparisons with another term of the deterministic y-momentum equation which could be measured readily, $\partial(\widetilde{v'v'})/\partial y$. Now just as $\widehat{\widetilde{u}\,\widetilde{u}}_2$ could be estimated as $(\widehat{u}_1\widehat{u}_1)/2$, the magnitude of $\widehat{\widetilde{v}\,\widetilde{v}}_2$ may be evaluated as $(\widehat{v}_1\widehat{v}_1)/2$. Therefore, from the profiles of $\widehat{v}_1$ shown in Figure 6.7, it is implied that $\widehat{\widetilde{v}\,\widetilde{v}}_2$ would vary smoothly between values of 0 and 0.02 across the boundary layer, when normalized by the square of $\widehat{u}_{1,\infty}$. The normal gradients of $\widehat{v'v'}_2$ may be deduced from Figure 6.19. For the case of low-frequency disturbance, values of $\partial(\widehat{v'v'}_1)/\partial y$ were much larger than measures of $\partial(\widehat{\widetilde{v}\,\widetilde{v}}_2)/\partial y$. However, at high frequencies of imposed unsteadiness, they were of similar magnitudes. Therefore, unless the streamwise derivative, $\widetilde{u(\partial\widetilde{v}/\partial x)}$, reached values comparable to measures of $\partial(\widetilde{v'v'})/\partial y$ within the boundary layer, products of oscillating components of velocity might only attain the significance of turbulence measures in the deterministic y-momentum equation for mainstream disturbance at high frequencies.

Although the contributions of products of periodic velocities could not always be eliminated from consideration on the grounds of their magnitudes, there was no

substantial evidence that they played a role of any great significance in this flow. Therefore it is no surprise that the dominant harmonic of all other velocity measures is the fundamental frequency of perturbation, as illustrated in §6.2 and §6.4. Consequently the role of second-harmonic quantities in the deterministic momentum equations would seem to be restricted to the characterization of products of first harmonics.

- *The role of second-harmonic quantities in the deterministic momentum equations seemed to be restricted to the characterization of products of first harmonics. No other measures in this study exhibited any appreciable response at this harmonic frequency.*

6.6 Unsteady Kinetic-Energy Transfer

The phase-conditioned response of turbulence measures to imposed unsteadiness may be examined through the turbulent kinetic-energy equation. This equation, which was devised in its phase-conditioned form in §2.4, describes the unsteady transport of components of turbulent kinetic energy and is written as:

$$\frac{\partial}{\partial t}\left(\overline{\frac{u'_\alpha u'_\alpha}{2}}\right) + \frac{\partial}{\partial x_k}\left(U_k \overline{\frac{u'_\alpha u'_\alpha}{2}}\right) + \frac{\partial}{\partial x_k}\left(\overline{\widetilde{u}_k \frac{u'_\alpha u'_\alpha}{2}}\right) + \frac{\partial}{\partial x_k}\left(\overline{u'_k \frac{u'_\alpha u'_\alpha}{2}}\right) = -\overline{\frac{u'_i}{\rho}\frac{\partial p'}{\partial x_i}}$$

$$+ \nu \frac{\partial}{\partial x_k}\left(\overline{u'_\alpha \frac{\partial u'_\alpha}{\partial x_k}}\right) - \overline{u'_k u'_\alpha}\frac{\partial \widetilde{u}_\alpha}{\partial x_k} - \overline{u'_k u'_\alpha}\frac{\partial U_\alpha}{\partial x_k} - \nu \overline{\frac{\partial u'_\alpha}{\partial x_k}\frac{\partial u'_\alpha}{\partial x_k}} \ .$$

Comparison of this equation with its counterpart describing transport of $\overline{\widetilde{u}_\alpha \widetilde{u}_\alpha}$ (2.4.1) reveals the periodic production tensor, $-\overline{u'_k u'_\alpha (\partial \widetilde{u}_\alpha / \partial x_k)}$, which accounts

for transfer of kinetic energy back and forth between the turbulent and deterministic energy fields during an unsteady cycle. The above equation was derived in component form, rather than in summed form like a true energy equation, as only two of the three components of the turbulent kinetic energy could be measured in this study.

The equation describing phase-conditioned transport of $\widetilde{u'u'}$, (2.4.2) with $\alpha = 1$, contains the production terms $-\widetilde{u'u'(\partial\tilde{u}/\partial x)}$ and $-\widetilde{u'v'(\partial\tilde{u}/\partial y)}$, which appear with opposite sign in the corresponding equation for $\widetilde{\tilde{u}\,\tilde{u}}$. It also contains apparent- or pseudo-production terms — products of mean shear and oscillating turbulence measures which do not appear in the $\widetilde{\tilde{u}\,\tilde{u}}$ equation, *i.e.* $-\widetilde{u'u'}\,\partial U/\partial x$ and $-\widetilde{u'v'}\,\partial U/\partial y$. Of these quantities, $-\widetilde{u'v'(\partial\tilde{u}/\partial y)}$ and $-\widetilde{u'v'}\,\partial U/\partial y$ could be deduced from measurements made in this study. Furthermore, order-of-magnitude estimates indicated that, of these four terms, the measurable ones would be the most significant in this boundary-layer flow. The roles of these production terms are illustrated in Figure 6.25.

At all frequencies of imposed unsteadiness, the first harmonic of these production terms was the most energetic; near the wall it typically accounted for between 40% and 80% of the total harmonic content. No comparable concentrations of energy were found at other harmonics and so, for want of a better measure, $-\widetilde{u'v'(\partial\tilde{u}/\partial y)}$ and $-\widetilde{u'v'}\,\partial U/\partial y$ were represented by the amplitudes of their first harmonics, which are shown in Figures 6.26 and 6.27 respectively. These measures are plotted at four representative frequencies of unsteadiness in each figure. The ordinate normalization was chosen as U_∞^3/D_c for ease of comparison of these quantities with the mean production terms discussed in §5.4.

The amplitude of the oscillating production term, $-\widetilde{u'v'(\partial\tilde{u}/\partial y)}$, which transfers kinetic energy back and forth between the $\widetilde{u'u'}$ and $\widetilde{\tilde{u}\,\tilde{u}}$ fields, reached a maximum of about 0.6% near the wall, for all frequencies of imposed unsteadiness (Figure 6.26). The peak amplitude of this production term for $\widetilde{u'u'}$ was considerably greater than the magnitude of its mean counterpart, $-\overline{u'v'(\partial\tilde{u}/\partial y)}$, shown in Figure 5.18, and

about half that of the major term for time-averaged production of $\overline{u'u'}$, which was $-\overline{u'v'}\partial U/\partial y$ (in Figure 5.15). Therefore, while the phase-averaged measure $\langle -u'v'(\partial\widetilde{u}/\partial y)\rangle$ should, at times during an unsteady cycle, indicate net transfer of kinetic energy from the $\widetilde{u'u'}$ field to the $\widetilde{\widetilde{u}\,\widetilde{u}}$ field via this particular production term, the total production of $\langle u'u'\rangle$ would always be positive.

- *Transfer of the streamwise component of the turbulent kinetic energy was from the organized unsteady field ($\widetilde{\widetilde{u}\,\widetilde{u}}$) to the unorganized unsteady field ($\widetilde{u'u'}$) for all conditions under which these experiments were conducted.*

The frequency invariance of the amplitude of $-\widetilde{u'v'(\partial\widetilde{u}/\partial y)}$ implied that the unsteady correlation between the phase-conditioned shear stress, $\langle -u'v'\rangle$, and the periodic velocity gradient, $\partial\widetilde{u}/\partial y$, was unaffected by changes in the forcing frequency. In contrast, the pseudo-production term, $-\widetilde{u'v'}\,\partial U/\partial y$, clearly decreased in magnitude with increasing frequency (in Figure 6.27) such that, at 2.0 hertz, its peak value was less than one third of that of $-\widetilde{u'v'(\partial\widetilde{u}/\partial y)}$. This behavior was consistent with the expected frequency invariance of the mean shear (illustrated in §5.1) coupled with the decrease in amplitude of $-\widetilde{u'v'}$ with growing frequency, observed in §6.4.

The notion that unsteady effects cannot influence turbulence production, for the case of high-frequency perturbation (when such effects would be confined to thin layers at the wall), was examined in §5.4, where no conclusive evidence could be found for or against it. This idea may be re-examined in view of measurements of the periodic production terms for $\widetilde{u'u'}$, presented in this section. Profiles of $-\widetilde{u'v'(\partial\widetilde{u}/\partial y)}$ are shown in Figure 6.28; they are plotted against a logarithmic abscissa to accentuate the near-wall behavior. Although there was appreciable uncertainty in the data, as evidenced by the scatter, the profiles appeared to be invariant with frequency. Moreover, the peak of the amplitude of this production term for $\widetilde{u'u'}$ was found in the vicinity of $y/D_c \simeq 0.007$, precisely the position of

the maxima of $\widehat{u'u'}_1$ (in Figure 6.18) and the maxima of the production terms for $\overline{u'u'}$, reported in §5.4.

The invariance of the amplitude of $-\widetilde{u'v'(\partial\widetilde{u}/\partial y)}$ with increasing frequency, and the coincidence of its maxima with $y/D_c \simeq 0.007$ (which corresponded to the limit of Stokes layer at 2.0 Hz, when its thickness was approximated as $\sqrt{2\nu/\omega}$ in Table 5.1), seems to refute the idea that unsteady effects should not play a role in turbulence production when, at high frequencies of imposed unsteadiness, they would be confined to a thin layer at the wall. However, one should bear in mind that $\sqrt{2\nu/\omega}$ is no more than an order-of-magnitude estimate of a dynamic length scale and that extension of this study to much higher frequencies of imposed unsteadiness might be necessary to resolve this issue.

- *The notion that unsteady effects would not influence turbulence production at high frequencies of forced unsteadiness (which corresponded to thin Stokes layers) was examined but was not supported by the periodic-production measurements of this study.*

The spatial coincidence of the maxima of the mean and periodic production terms for $u'u'$ has some interesting implications about the possible similarities in mechanisms of turbulence production for $\overline{u'u'}$ and $\widetilde{u'u'}$. If periodic turbulence were strongly linked to mean turbulence, through similar production mechanisms which resulted in the coincident maxima of their measured production terms, this would help to explain why the normal variation of profiles of $\widehat{u'u'}_1$, $\widehat{v'v'}_1$ and $-\widehat{u'v'}_1$ scaled on an abscissa formed from mean quantities such as y/D_c, in stark contrast to the collapse of the deterministic velocity, $\widetilde{u}$, on an abscissa scaled according to a frequency-dependent parameter, $y/\sqrt{2\nu/\omega}$. However, investigation into mechanisms of unsteady turbulence production was beyond the scope of this study.

The production and pseudo-production terms for $\widetilde{v'v'}$ which could be evaluated from the measurements of this study are $-\widetilde{v'v'(\partial\widetilde{v}/\partial y)}$ and $-\widetilde{v'v'}\,\partial V/\partial y$; profiles of these measures are displayed in Figures 6.29 and 6.30 respectively. The ordinate

normalization and its scaling were selected to match those employed in graphs of the production terms for $\widetilde{u'u'}$ so that the magnitudes of production of $\widetilde{u'u'}$ and $\widetilde{v'v'}$ could be compared readily. From these figures, it would seem that the production of $\widetilde{v'v'}$ was negligible and that the periodic turbulence production was therefore strongly anisotropic.

- *Periodic production of turbulent kinetic energy was found to be strongly anisotropic — the energy transfer to $\widetilde{u'u'}$ greatly exceeded that to $\widetilde{v'v'}$.*

If production was not considered responsible for the presence of $\widetilde{v'v'}$ at significant amplitudes, the possibility arises that the net creation of $\widetilde{v'v'}$ was negligible and that its transport equation might be satisfied by setting the derivative following the organized motion of $\widetilde{v'v'}$ to zero, *i.e.*

$$\frac{\partial}{\partial t}\left(\widetilde{\frac{v'v'}{2}}\right) + \frac{\partial}{\partial x_k}\left(U_k\widetilde{\frac{v'v'}{2}}\right) + \frac{\partial}{\partial x_k}\left(\widetilde{u}_k\widetilde{\frac{v'v'}{2}}\right) \simeq 0 \,. \tag{6.6.1}$$

The plausibility of this idea could be tested through comparison of the estimated amplitudes of the terms comprising (6.6.1). However, the leading time derivative appeared to be much larger than either of the convective terms, rendering the idea of negligible creation of $\widetilde{v'v'}$ rather unlikely. Therefore additional terms, on the right-hand side of the $\widetilde{v'v'}$ equation, would be necessary to describe its behavior adequately.

Given the strong anisotropy in periodic production of turbulent kinetic energy and the appreciable magnitudes attained by measures of $\widehat{v'v'}_1$ (typically around 10% of $\widehat{u'u'}_1$, as may be seen in Figures 6.18 and 6.19), one might then speculate that the periodic energy content of $\widetilde{v'v'}$ is the result of inter-component transfer of turbulent kinetic energy from $\widetilde{u'u'}$. Were this the case, it would support the conclusions of Acharya & Reynolds (1975) that adequate representation of the periodic pressure-strain terms should be crucial to successful prediction of unsteady flows.

- *It was proposed that intercomponent transfer of turbulent kinetic energy was an important feature of periodic turbulence in the unsteady boundary layer.*

At high frequencies of imposed unsteadiness, the major production term for $\widetilde{u'u'}$ was $-\widetilde{u'v'(\partial\tilde{u}/\partial y)}$ (shown in Figure 6.26). As it reached significant values near the wall, its phase there could be discerned clearly through Fourier analysis. Profiles of the phase of this production term, relative to the phase of $\widetilde{u'u'}$, are shown in Figure 6.31. From this figure, it is clear that $\widetilde{u'u'}$ lagged further behind its major production term with increasing frequency. Alternatively, this trend may be viewed as the production term leading $\widetilde{u'u'}$ by increasing margins with growing frequency of mainstream perturbation. At 2.0 hertz, this advance in phase peaked at around 90°, precisely the phase advance (relative to $\widetilde{u'u'}$) of $\partial(\widetilde{u'u'})/\partial t$, the dominant term of the left-hand side of the $\widetilde{u'u'}$ transport equation.

The close agreement between $\phi_{1,\partial(u'u')/\partial t}$ and $\phi_{1,-u'v'\partial\tilde{u}/\partial y}$, at high frequencies of imposed unsteadiness, raised the possibility that the asymptotic, high-frequency transport equation for $\widetilde{u'u'}$ might take the approximate form:

$$\frac{\partial}{\partial t}\left(\frac{\widetilde{u'u'}}{2}\right) \simeq -\widetilde{u'v'}\frac{\partial\tilde{u}}{\partial y} \ . \tag{6.6.2}$$

The plausibility of this proposal could be tested through comparisons of the amplitudes of each term. To simplify comparisons, the profiles of $-\widetilde{u'v'(\partial\tilde{u}/\partial y)}$, which were displayed in normalized form in Figure 6.26, were re-normalized by $\hat{u}_{1,\infty}^3/D_c$ and shown in Figure 6.32 — near the wall this dimensionless production term peaked at a value slightly greater than one, for high frequencies of mainstream unsteadiness. The magnitude of the right-hand side of (6.6.2) is now estimated. Since $\widetilde{u'u'}$ could be approximated as $\widehat{u'u'}_1 \cos(\omega t + \phi_{1,u'u'})$, its amplitude could be represented by $\omega\ \widehat{u'u'}_1/2$. The near-wall magnitude of $\widehat{u'u'}_1/\hat{u}_{1,\infty}^2$ could be gauged from the

profiles of Figure 6.18, which, at high frequencies of unsteadiness, approached 0.1 near the wall. Multiplication of 0.1 by ω, by $\hat{u}_{1,\infty}/D_c$ (which took the value of 1.57 secs^{-1} at $X' = 0.63$) and division by two resulted in a dimensionless amplitude for $\partial(\widetilde{u'u'}/2)/\partial t$ of just under one — an indication that the magnitudes of the left- and right-hand sides of the proposed equation were indeed comparable.

The approximate agreement between the phases and amplitudes of the terms of (6.6.2) indicates that, at high frequencies of imposed unsteadiness, the transport equation for $\widetilde{u'u'}$ might take the form of (6.6.2) near the wall. That the partial derivative with respect to time of $\widetilde{u'u'}$ seems to be matched in phase and amplitude by the major production term does not indicate that other terms, such as inter-component, energy-transfer terms, are necessarily absent — just that they are probably small in comparison. It is interesting to note that dissipation does not appear to play a role in the proposed form of this deterministic equation — the absence of oscillating dissipation terms is consistent with the view of dissipation as a small-scale, high-wave-number phenomenon, in tune with a completely different part of the turbulence spectrum to the one at which unsteadiness was excited in these experiments.

- *A simplified high-frequency form of the transport equation for $\widetilde{u'u'}$, the largest of the periodic turbulence components, was proposed – its time derivative was balanced by its production at the highest frequencies of forced unsteadiness of this study.*

6.7 Structure of Periodic Turbulence

A description of phase-conditioned turbulence within the unsteady boundary layer is now developed using the themes examined in §5.5 for the turbulence structure of the mean flow as a starting point. In the time-averaged, unsteady boundary layer, profiles of mean velocities and of $u'u'$, $v'v'$ and $u'v'$ were invariant to different

frequencies of forced unsteadiness. Consequently, simple structural parameters such as correlation coefficients of u' and v', mixing lengths and eddy viscosities could be deduced and they were very similar to the equivalent measures for steady flow. Hence, the structure of turbulence in the mean field, according to these parameters, seemed to be unaffected by the presence of an oscillating unsteady field.

In turbulent flow, the strong correlation between u' and v' is thought to be maintained by the motions of eddies, the principal axes of which are roughly aligned with the direction of the mean rate of strain (Tennekes & Lumley, §2.3). Now if this correlation coefficient prevailed at its time-averaged value, at each instant in the unsteady cycle, it could imply an instantaneous response to the oscillating turbulence quantities of the mechanism which causes this strong correlation to be maintained. The phase-conditioned behavior of $\langle -\overline{u'v'}/(u')(v') \rangle$ could be examined in terms of deviations of its instantaneous values from the mean, $-\overline{u'v'}/(u')(v')$, which could be expressed conveniently as a root-mean-square deviation, *i.e.*

$$\langle -\overline{u'v'}/(u')(v') \rangle' = \sqrt{\langle -\overline{u'v'}/(u')(v') \rangle'^2} .$$

An r.m.s. representation was adopted, in preference to a Fourier one, as any harmonic content which the product of two oscillating quantities, divided by a third, might contain was not expected to be restricted to one dominant frequency.

Profiles of the mean correlation coefficient and its r.m.s. deviation are shown in Figures 6.33 and 6.34, at 0.1 and 2.0 hertz respectively. From these figures, it is clear that there is significant deviation from the mean value of the correlation coefficient during the unsteady cycle. the local ratio of $\langle -\overline{u'v'}/(u')(v') \rangle'$ to $-\overline{u'v'}/(u')(v')$ rarely fell below 15% throughout the boundary layer. These results are in good agreement with those of Cousteix & Houdeville (1983) which exhibited scatter of comparable magnitude about their mean value. Hence, the notion that the same mechanism which maintains the strong, time averaged correlation between u' and v' would apply instantaneously under unsteady conditions does not seem appropriate

this result might also have been anticipated from the strong differences in the phase profiles of $\widehat{u'u'}_1$, $\widehat{v'v'}_1$ and $-\widehat{u'v'}_1$, presented in §6.4.

- *Instantaneous correlations between u' and v' were not maintained at their time-averaged values under organized unsteady conditions.*

If correlations of instantaneous values of turbulence quantities provided an inadequate description of the turbulence field, then proposals that eddy viscosities or mixing lengths might relate instantaneous values of the Reynolds stress to the unsteady, local gradients of velocity would seem equally inappropriate. This point may be demonstrated by examination of the lag between $\phi_{1,-u'v'}$ and $\phi_{1,\partial\tilde{u}/\partial y}$, shown in Figure 6.35, in which this local phase difference is plotted over the inner 10% of the boundary layer (where $\phi_{1,\partial\tilde{u}/\partial y}$ could be discerned most clearly). While $\phi_{1,-u'v'}$ lagged further behind $\phi_{1,\partial\tilde{u}/\partial y}$ with increasing frequency of forced unsteadiness, it did not do so in a way which implied that a faithful representation of $\widetilde{u'v'}$ could be proposed in terms of the instantaneous velocity gradient, coupled with a simple phase-lag relationship. Therefore descriptions of the structure of turbulence, based on simple represention of the oscillating Reynolds stress in terms of other quantities of the deterministic momentum equation, appear to be inadequate in this unsteady boundary layer. Hence it is necessary to turn to the equations of the next-highest order — Reynolds-stress and kinetic-energy equations — to see if they allow a clearer interpretation of the structure of periodic turbulence.

- *The variation in phase between deterministic measures of streamwise velocity gradient and shear stress was not well organized — it did not imply any simple means of modeling periodic shear stress*

Examination of the component energy equations (2.4.2) revealed periodic production and pseudo-production terms which accounted for transfer of kinetic energy to and from the $\overline{u'u'}$ field, which were discussed in §6.6. For all frequencies of forced unsteadiness, the maxima of these periodic production terms occurred around

$y/D_c \simeq 0.007$, a position in the boundary layer coincident with the one at which the production terms for the *time-averaged*, unsteady turbulence measure, $\overline{u'u'}$, were greatest (discussed in §5.4 and shown in Figure 5.16). The spatial coincidence of these mean and phase-conditioned maxima implied that periodic production of turbulent kinetic energy could be the result of a modulation effect upon the mechanism of production of mean turbulent kinetic energy, at the frequency of forced unsteadiness. This idea is supported by the investigations of Kobashi & Hawakawi (1981) into the phase dependence of "bursts" in an unsteady, turbulent, boundary layer — their histograms of the number of detections of bursts at discrete times during an unsteady cycle indicated a roughly sinusoidal variation at the forcing frequency, superimposed on the mean detection level.

- *The maxima of periodic and time-averaged measures of production were coincidence in space — this finding raised the possibility that deterministic production might be a result of local modulation of the time-averaged process.*

If the phase-conditioned production of $u'u'$ is viewed as an effect of modulation of the mechanism for the mean production of turbulent kinetic energy, it is no surprise that the position in the boundary layer of the near-wall maxima of profiles of $\widehat{u'u'}_1$ scaled on a mean wall-normal measure, y/D_c (in Figure 6.18), regardless of the frequency of forced unsteadiness. That a mean scaling is appropriate for other periodic turbulent quantities, such as $\widehat{v'v'}_1$ and $-\widehat{u'v'}_1$, is evident from Figures 6.19 and 6.20. Since the behavior of the time-averaged field must be influenced by periodic effects, through their mutual dependence in the equations of fluid motion, the apparent coupling of unsteady turbulence production to its mean counterpart is a welcome reminder of that mutual dependence (in contrast to the absence of any obvious strong coupling between measures of U and $\widetilde{u}$). This coupling between time-averaged and periodic fields might then justify attempts to infer time-averaged

quantities such as y^+ for use in describing profiles of these periodic turbulence measures in unsteady flow.

Values of u_τ were then estimated from a fit of Coles' mean velocity function (Coles 1968) to the time-averaged velocity profiles of U (with careful consideration given to the uncertainty involved in employing this scheme for time-averaged unsteady flow, discussed in §5.3). This exercise matched the position corresponding to $y/D_c = 0.007$ in the time-averaged, unsteady boundary layer to one at which y^+ was estimated as $\simeq 8$, a value quite close to $y^+ \simeq 10$ at which Laufer (1954) reported maxima in turbulence-production measurements for steady pipe-flow experiments.

While the periodic production terms for $\widetilde{u'u'}$ were comparable in size to their mean counterparts, measurements of the production of $\widetilde{v'v'}$ were negligible. Yet the magnitude of $\widehat{v'v'}_1$ was typically around 10% of $\widehat{u'u'}_1$. This disparity in size of components of the phase-conditioned production tensor, coupled with the more equal distribution of turbulent kinetic energy, implied that the unsteady turbulence structure comprised a strongly anisotropic mechanism of production and a means of redistribution of turbulent kinetic energy towards a more isotropic state. One might then expect to find some evidence to support this notion in the phase-conditioned measurements of $u'u'$ and $v'v'$.

In Figure 6.36, profiles of the local difference in phase between the first-harmonic oscillations of $u'u'$ and $v'v'$ are plotted over the innermost 10% of the boundary layer, at all frequencies of forced unsteadiness for which this study was conducted. At low frequencies of imposed unsteadiness, there was negligible phase difference between the two unsteady turbulence measures. However, the local lag of $\widetilde{v'v'}$ behind $\widetilde{u'u'}$ became steadily greater with increasing frequency of forced unsteadiness, while the shapes of each profile seemed to differ from one another only by a scaling of the ordinate. Moreover, the maximum lead in phase of $\widetilde{u'u'}$ over $\widetilde{v'v'}$ roughly coincided with the position of peak production of $\widetilde{v'v'}$ in the unsteady boundary layer. These observations implied that inter-component transfer of turbulent kinetic energy between $\widetilde{u'u'}$ and $\widetilde{v'v'}$ might be the result of a redistribution process with a

local, characteristic, time scale which was invariant with frequency of unsteadiness. This proposal is supported by the good collapse of data in Figure 6.37; in this figure, the phase differences shown in Figure 6.36 were recast as time lags, through division by the forcing frequency. Now this collapse was appropriate for all but the two lowest frequencies of mainstream perturbation (which were characterized by somewhat larger time scales) — an indication that the local time scale for energy transfer was not completely invariant with frequency. However, the partial collapse of this data did raise the hope that a better characterization of $\phi_{1,u'u'} - \phi_{1,v'v'}$ might be revealed under further normalization by another local, unsteady quantity.

One might view this redistribution of turbulent kinetic energy towards a more isotropic state as a process associated with the dynamic behavior of eddies, where the time they take to re-orientate or "turn around" is characterized by the time scale found from Figure 6.37 (around 0.15 seconds at the position of peak turbulence production). The shape of these time-lag profiles is well defined and bears a strong resemblance to the profiles of $\widehat{u'u'}_1$ in the same part of the boundary layer (shown in Figure 6.18). Now since $\widehat{u'u'}_1$ was by far the largest of the measured terms in the deterministic Reynolds-stress tensor, and thus thought to be representative of the anisotropy of that tensor, it would seem that the local time for eddy re-orientation might scale on the local measure of Reynolds-stress anisotropy. This idea is supported by data shown in Figure 6.38, in which the time-lag measures of Figure 6.37, in the innermost 10% of the boundary layer do indeed collapse under normalization by the local value of $\widehat{u'u'}_1$, for all frequencies of imposed unsteadiness. If this finding was a general one which also applied to energy transfer between other components of the fluid's turbulent kinetic energy and other terms of the tensor of deterministic Reynolds-stress anisotropy, inter-component transfer of turbulent kinetic energy would seem to be well described in terms of eddies, which re-orientate themselves over characteristic times proportional to the local anisotropy of $\widehat{u'_i u'_j}$. This description corresponds to a periodic corollary to Rotta's well-known model

for the "slow" pressure-strain rate in steady turbulent flow (see, for example, Hinze 1975).

- *Since the well organized dependence of the phase lag amounted to a dynamic corollary to Rotta's model for the slow pressure-strain terms in the time-averaged field of flow, it would seem that the equivalent deterministic pressure-strain terms would be important in unsteady boundary-layer flow.*

It is also of interest to examine whether the characteristic time lags shown in Figure 6.37 are comparable to the equivalent time scales one might anticipate for the mean turbulent flow. Typically, the quotient k/ϵ is used to form a time scale for turbulent activity in modeling schemes for steady flows. In this experiment, at the position in the boundary layer which corresponded to peak production ($y/D_c \simeq 0.007$), k could be approximated as $\overline{u'u'}$ and ϵ could be assumed to be of the same order as $-\overline{u'v'}\partial U/\partial y$. Now from Figures 5.5 and 5.16, k could be taken as 0.01, when scaled by U_∞^2, and ϵ could be estimated as 0.01 multiplied by U_∞^3/D_c . Thus the turbulent time scale for the mean unsteady flow would roughly equate to the ratio of boundary-layer thickness to mainstream velocity — a turn-over time for a large eddy. This time scale took the value of ~ 0.1 seconds in these experiments. Considering the simplicity of the arguments used in its estimation, it was in remarkably good agreement with the time lag of $\widetilde{v'v'}$ behind $\widetilde{u'u'}$ of ~ 0.15 seconds, at $y/D_c \simeq 0.007$.

- *The lag in phase of $\widetilde{v'v'}$ behind $\widetilde{u'u'}$ was well organized it scaled on a local, turbulent time scale (of the same order as the local, turbulent time scale for the time-averaged flow) and a measure of the local, periodic anisotropy in the Reynolds stress.*

One might then speculate that the energy-redistribution process in oscillating, unsteady flow is simply a modulated form of the steady process, since they appear

to share the same characteristic time scale. This notion leads to the image of eddies rotating and deforming at a uniform rate to sustain the character of the time-averaged flow, and possibly those same eddies undertaking a superimposed, organized, unsteady role in accounting for the periodic behavior of the turbulent boundary layer.

Since redistribution of turbulent kinetic energy among its components is commonly attributed to the "slow" pressure-strain terms of the component energy equations, it is worth deducing the form of these terms to see if any further insight into inter-component transfer of energy is possible. Following Chou (1945), the turbulent component of the pressure may be deduced by taking the divergence of (2.2.9), yielding a Poisson equation for p'. After time and phase averaging, the deterministic "slow" pressure-strain terms may be expressed in the form used by Launder *et al.* (1975) for a position $\mathbf{x}$ in the flow:

$$\left.\overline{\frac{p'}{\rho}\frac{\partial u_i'}{\partial x_j}}\right|_{slow} = \frac{1}{4\pi}\int_{vol}\left\{\overline{\left(\frac{\partial^2 u_l' u_m'}{\partial x_l \partial x_m}\right)'\frac{\partial u_i'}{\partial x_j}}\right\}\left[\frac{1}{|\mathbf{x}-\mathbf{y}|}+\frac{1}{|\mathbf{x}-\mathbf{y}^*|}\right]d\text{vol}\ . \qquad (6.7.1)$$

In this expression, $\mathbf{y}^*$ is the image of the point $\mathbf{y}$ and integration is performed over $\mathbf{y}$ space in the semi-infinite domain in which $y_2 > 0$; the large prime denotes a quantity evaluated at $\mathbf{x}$. Now these terms take the form of a field effect, rather than a purely local one. However, unless the two-point correlation of the integrand in (6.7.1) maintains appreciable values at large separations, the factor $1/|\mathbf{x}-\mathbf{y}| + 1/|\mathbf{x}-\mathbf{y}^*|$ is likely to diminish the influence of field effects over any significant distances so that a predominantly local effect would not be an implausible result of this integration. Now if these pressure-strain terms are viewed as the agents of redistribution of turbulent kinetic energy, that their influence might be primarily a local one is consistent with the collapse of the time-lag data of Figure 6.37 under normalization

by $\widehat{u'u'}_1$ (in Figure 6.38). It is also consistent with the observations of §6.6 that profiles of the phase-averaged measure, $\langle v'v' \rangle$, intersected their mean profiles at the same position in the boundary layer at which profiles of $\langle u'u' \rangle$ and $\overline{u'u'}$ crossed.

If the findings of this section on the structure of unsteady turbulence are applicable at higher frequencies of imposed unsteadiness, one might speculate that the "frozen" turbulence condition, reported by Ramaprian & Tu (1979), would occur when the unsteadiness imposed on a turbulent boundary layer is of a periodicity much smaller than the time scales of inter-component energy transfer.

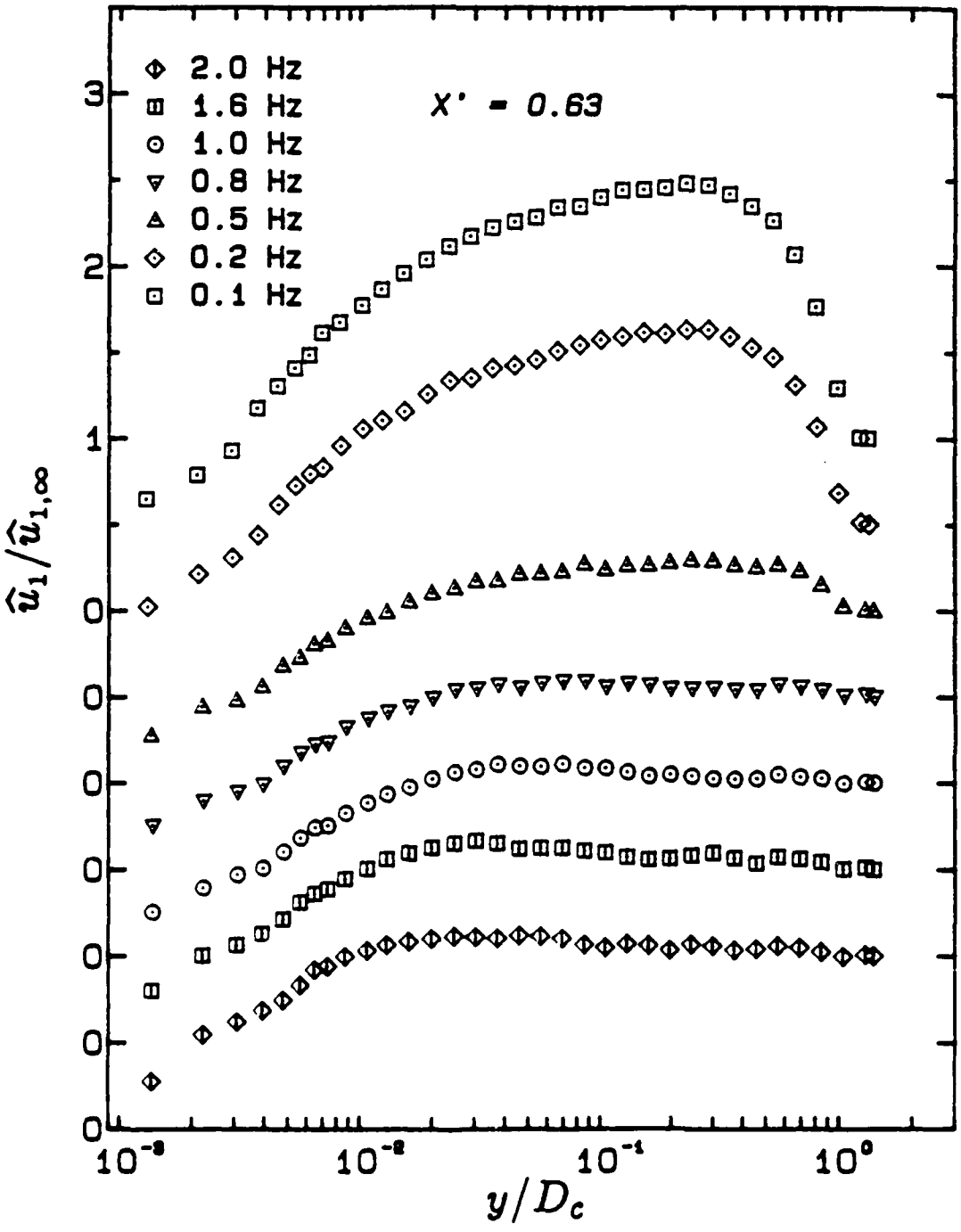

Figure 6.1 Profiles of $\hat{u}_1/\hat{u}_{1,\infty}$ under unsteady conditions.
$X' = 0.63$

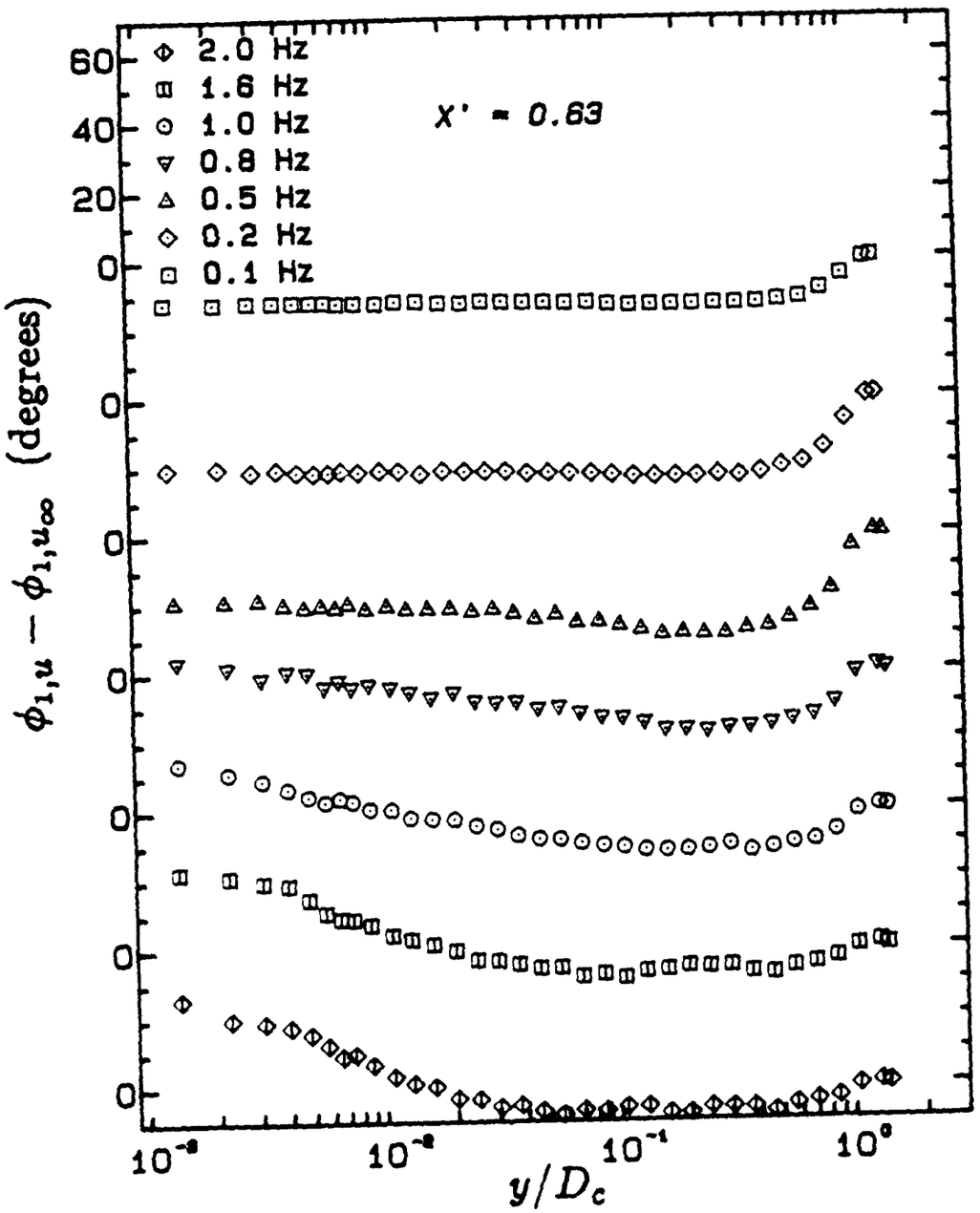

Figure 6.2 Profiles of $\phi_{1,u} - \phi_{1,u_\infty}$ under unsteady conditions.
$X' = 0.63$

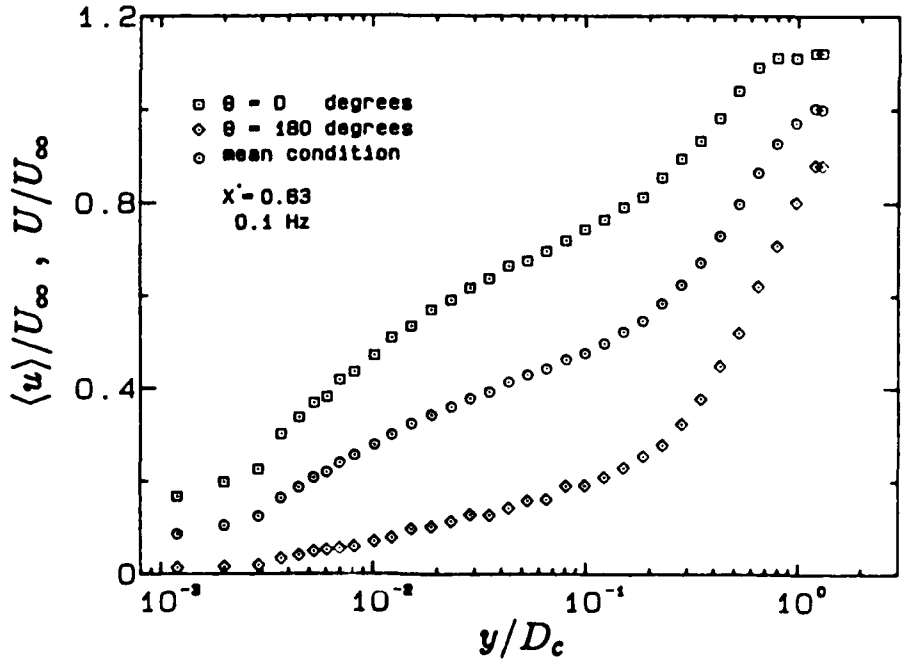

Figure 6.3 Profiles of U, $\langle u \rangle_{\phi=0^\circ}$ and $\langle u \rangle_{\phi=180^\circ}$ under unsteady conditions. $X' = 0.63$

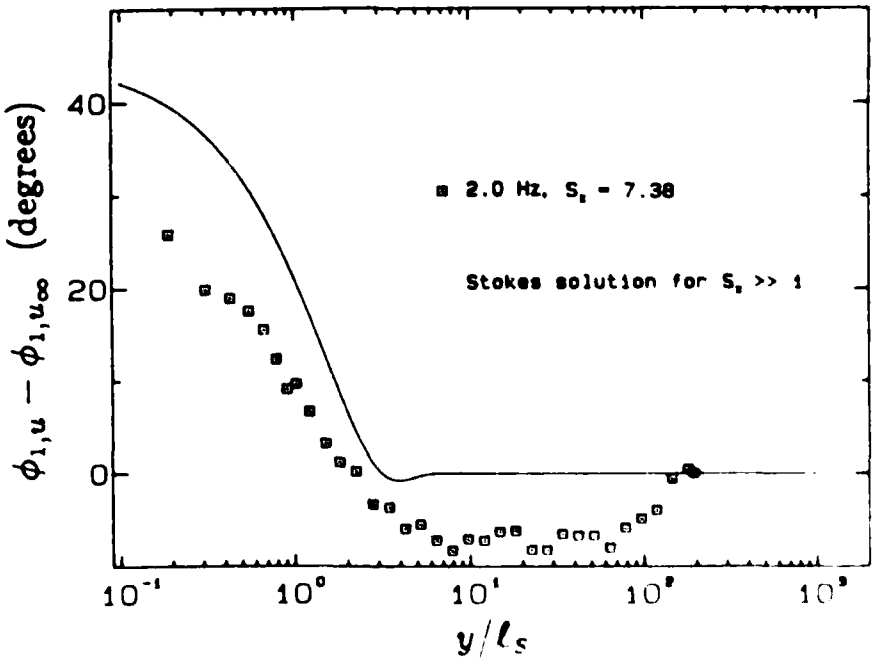

Figure 6.4 Profile of $\phi_{1,u} - \phi_{1,u_\infty}$ (at 2.0 hertz) and the Stokes solution. $X' = 0.63$

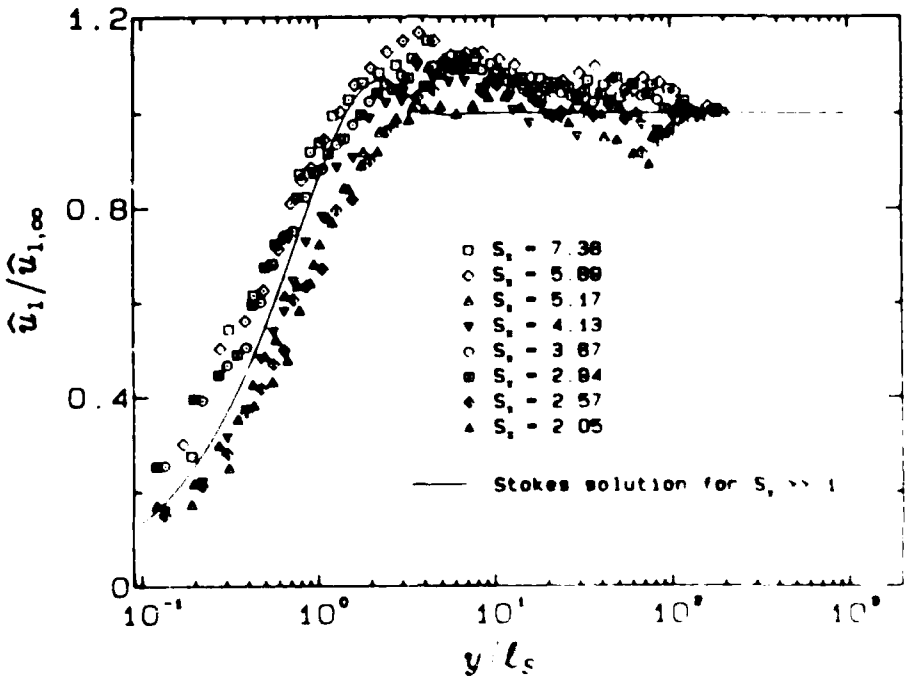

Figure 6.5 Profiles of $\hat{u}_1$, $\hat{u}_{1,\infty}$ at high Strouhal numbers

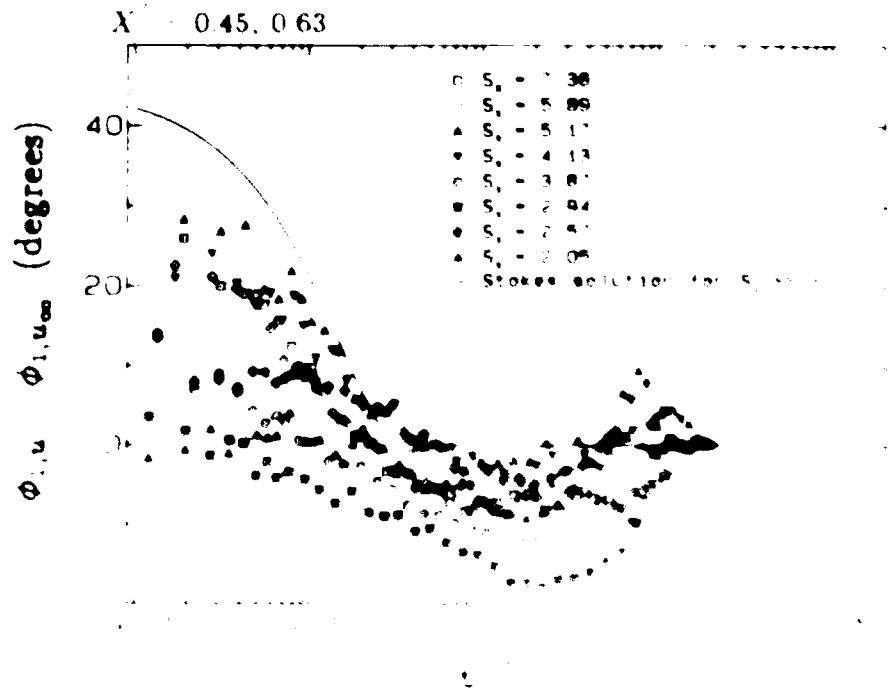

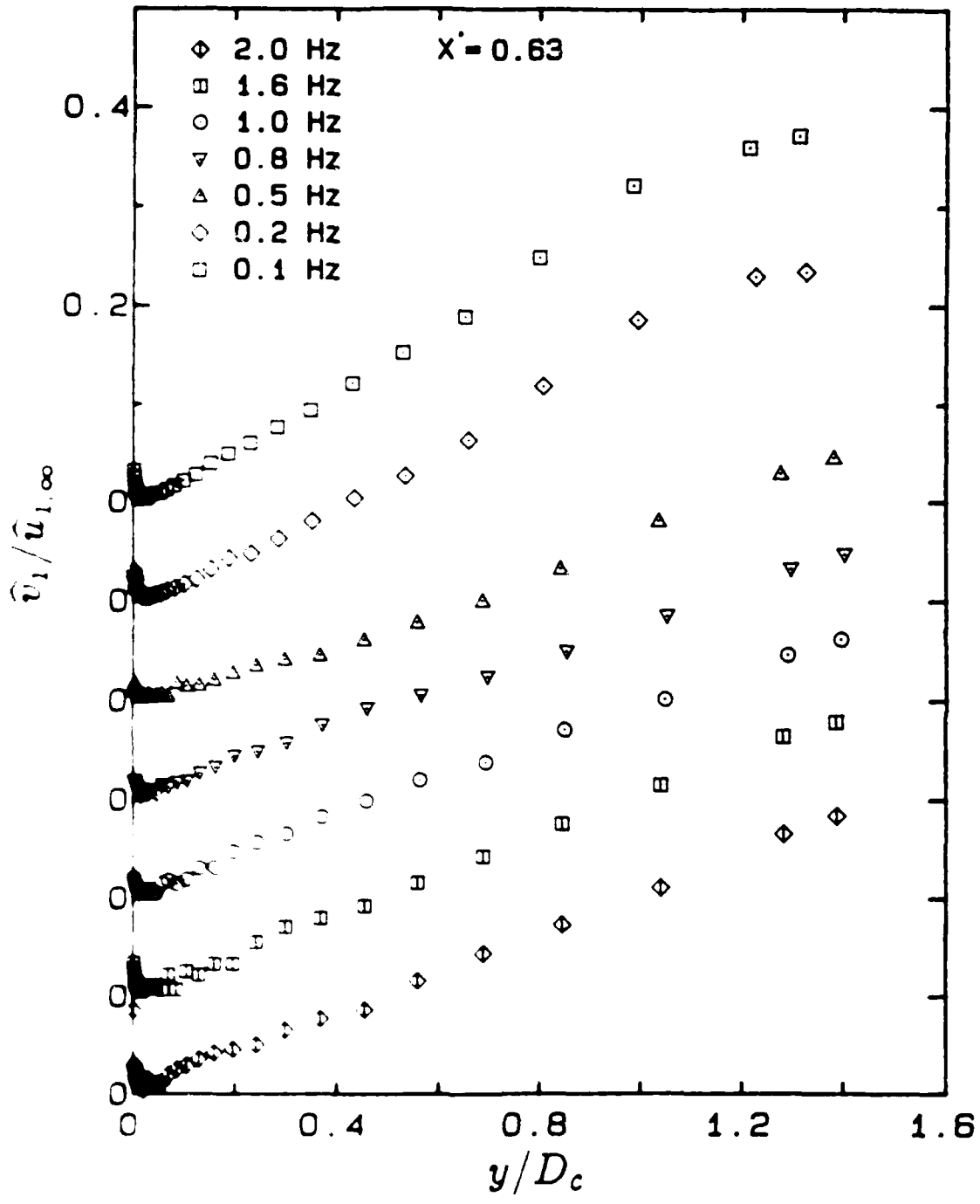

Profiles of $\hat{v}_1/\hat{u}_{1,s}$ under unsteady conditions.

$X' = 0.63$

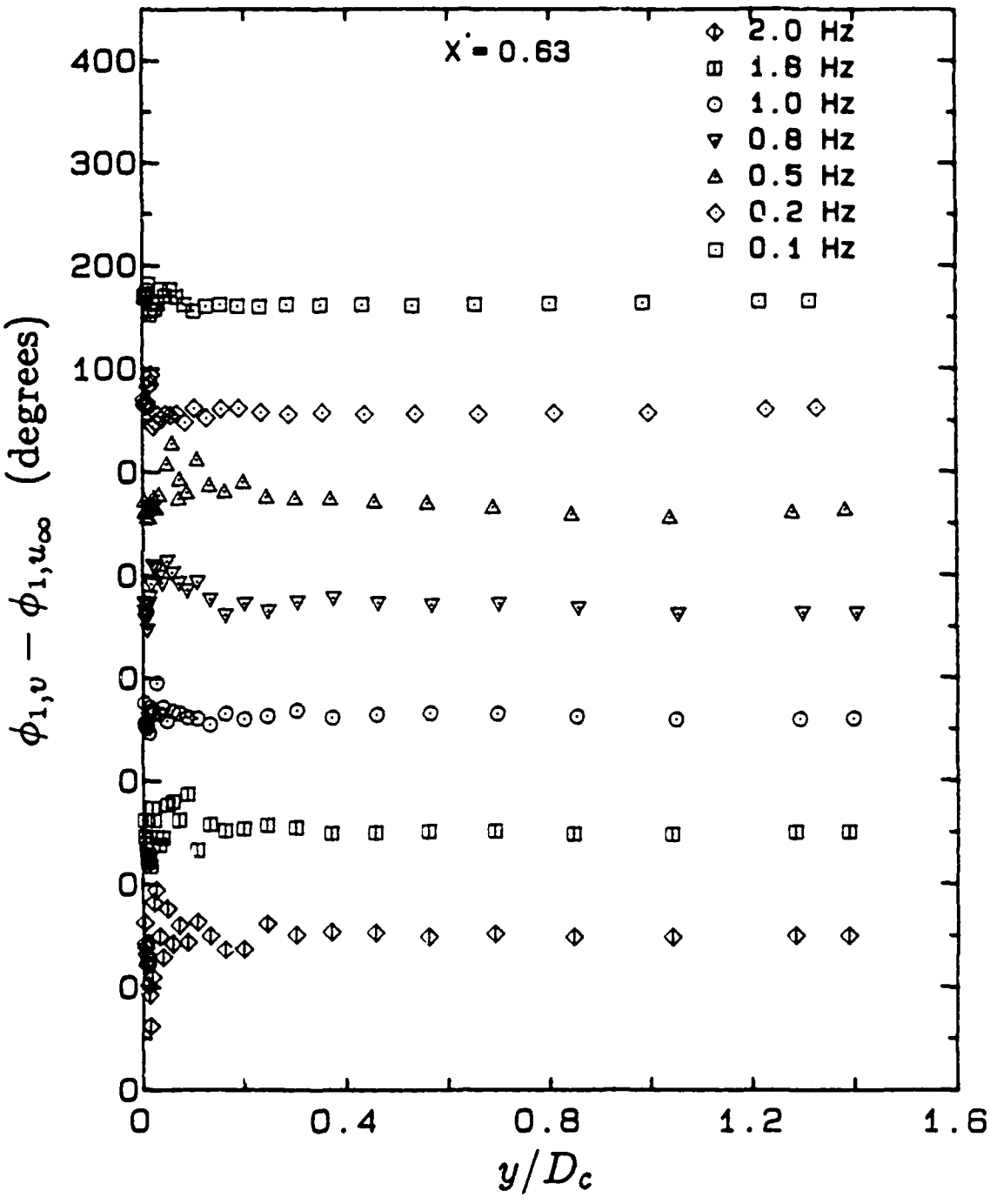

Figure 6.8 Profiles of $\phi_{1,v} - \phi_{1,u_\infty}$ under unsteady conditions. $X' = 0.63$

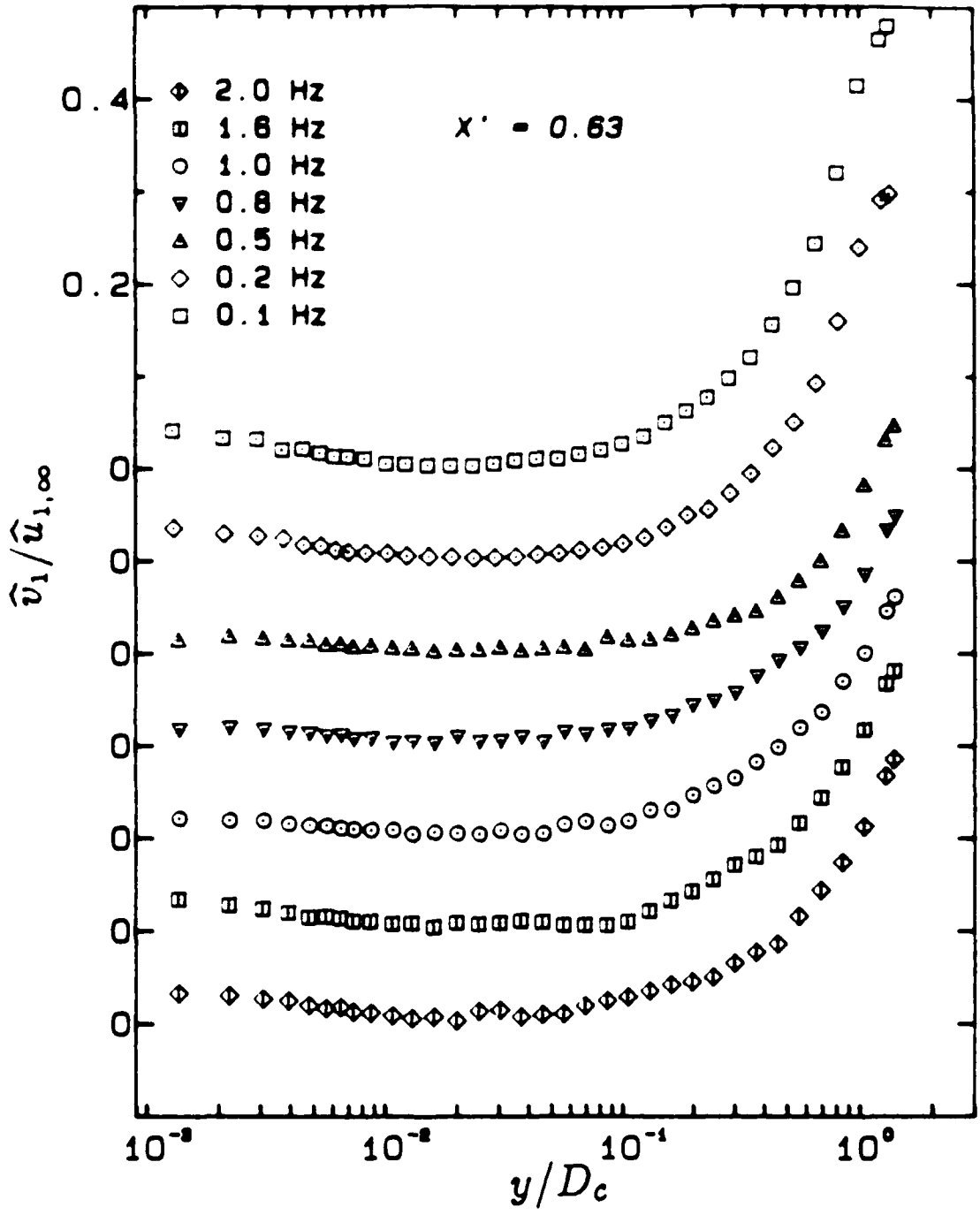

Figure 6.9 Profiles of $\hat{v}_1/\hat{u}_{1,\infty}$ under unsteady conditions.
$X' = 0.63$

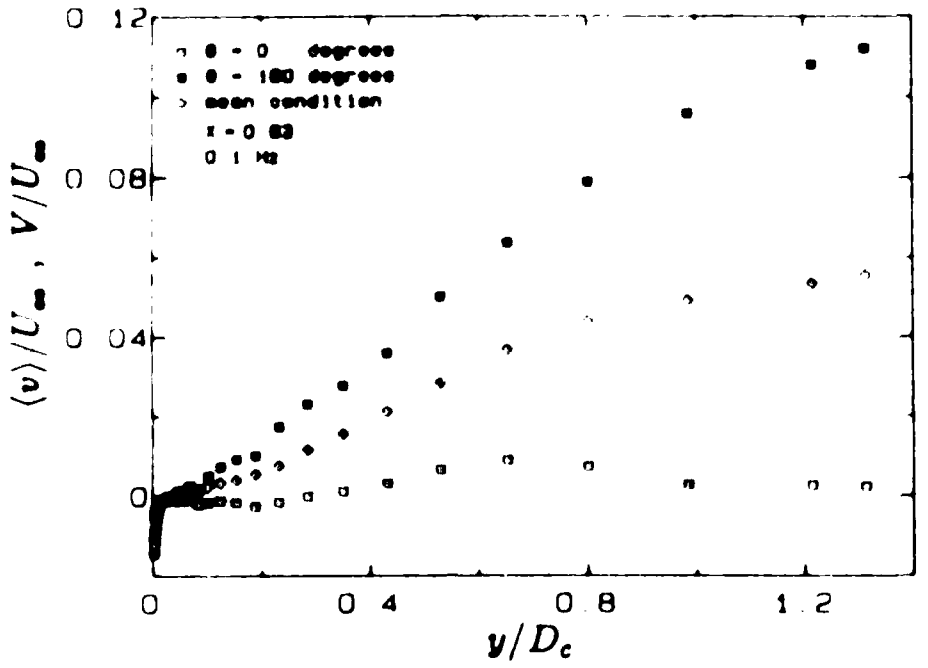

Figure 6.10 Profiles of V, $\langle v \rangle_{\phi=0^\circ}$ and $\langle v \rangle_{\phi=180^\circ}$ under unsteady conditions at 0.1 hertz

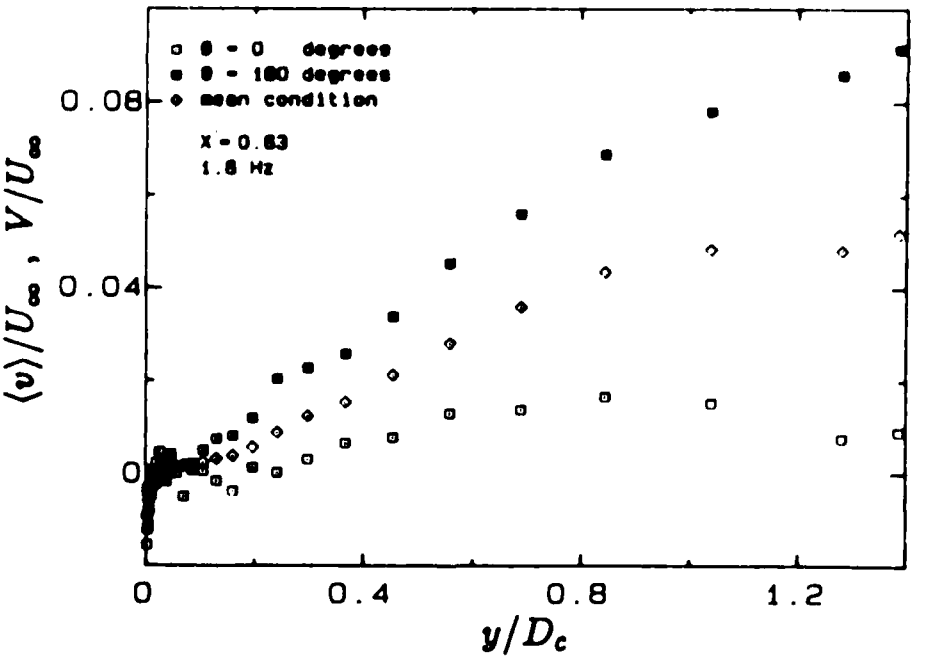

Figure 6.11 Profiles of V, $\langle v \rangle_{\phi=0^\circ}$ and $\langle v \rangle_{\phi=180^\circ}$ under unsteady conditions at 1.6 hertz

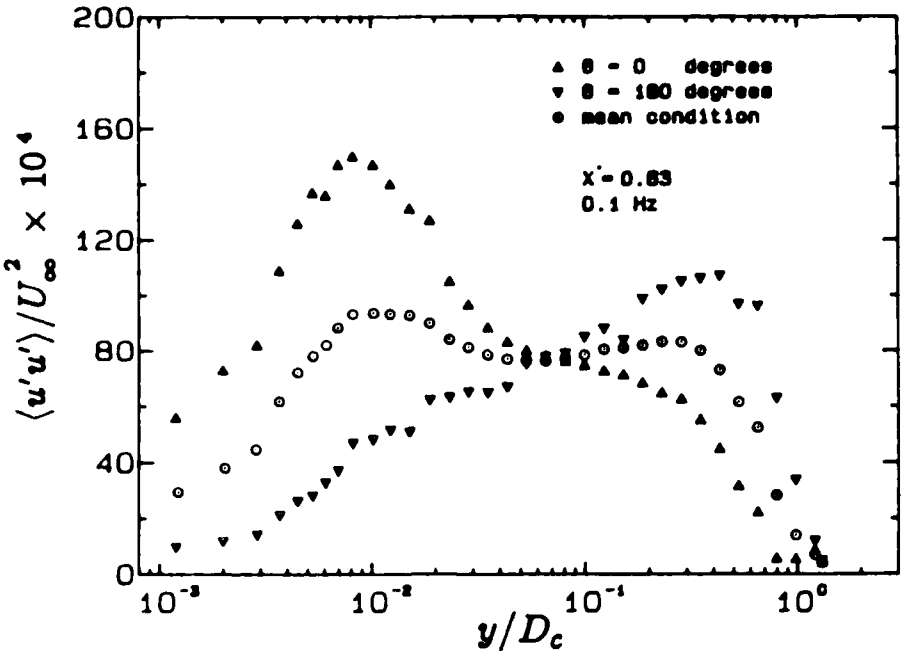

Figure 6.12 Profiles of $\overline{u'u'}$, $\langle u'u' \rangle_{\phi=0^\circ}$ and $\langle u'u' \rangle_{\phi=180^\circ}$ under unsteady conditions at 0.1 hertz

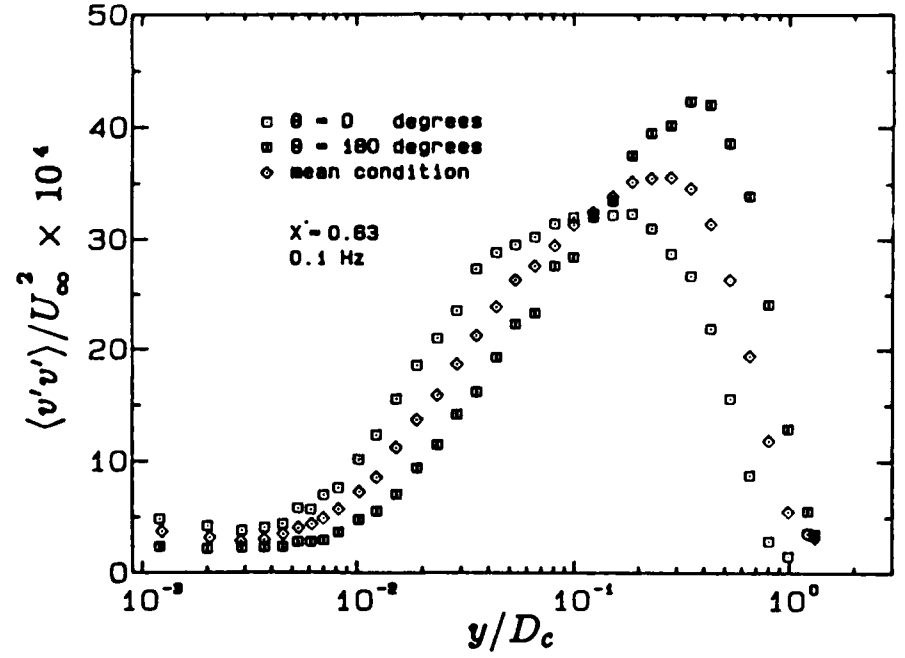

Figure 6.13 Profiles of $\overline{v'v'}$, $\langle v'v' \rangle_{\phi=0^\circ}$ and $\langle v'v' \rangle_{\phi=180^\circ}$ under unsteady conditions at 0.1 hertz

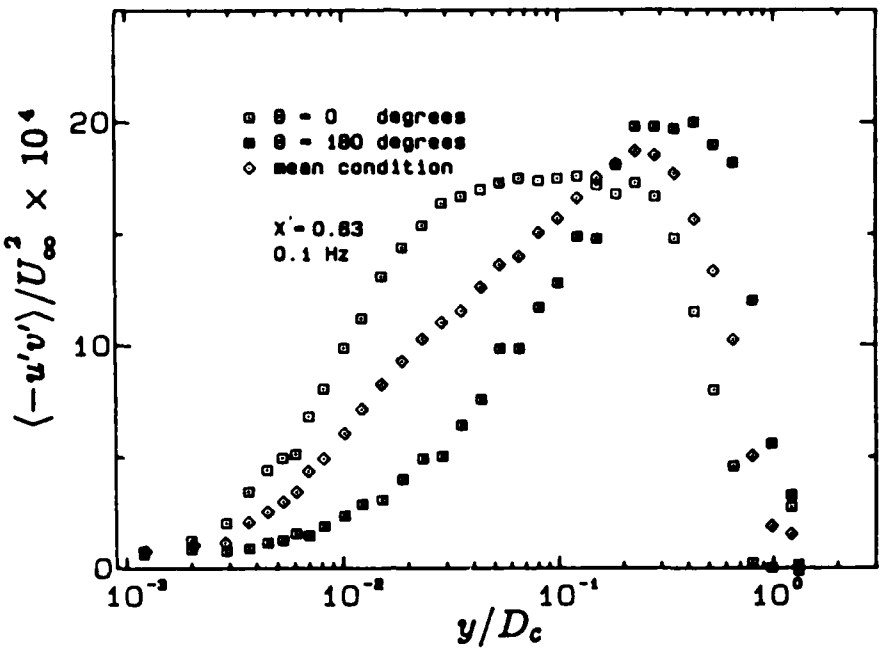

Figure 6.14 Profiles of $-\overline{u'v'}$, $\langle -u'v' \rangle_{\phi=0^\circ}$ and $\langle -u'v' \rangle_{\phi=180^\circ}$ under unsteady conditions at 0.1 hertz

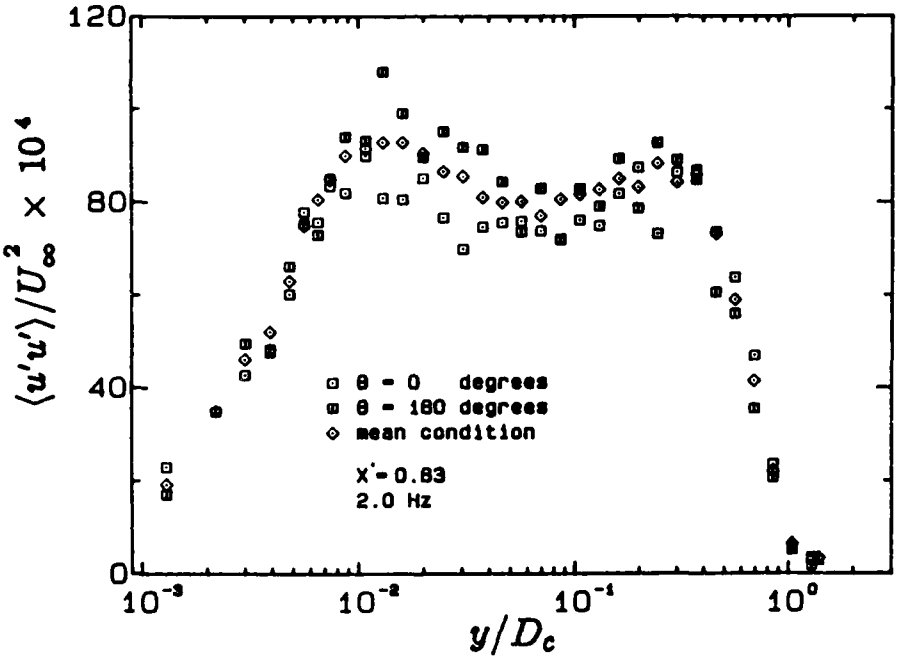

Figure 6.15 Profiles of $\overline{u'u'}$, $\langle u'u' \rangle_{\phi=0^\circ}$ and $\langle u'u' \rangle_{\phi=180^\circ}$ under unsteady conditions at 2.0 hertz

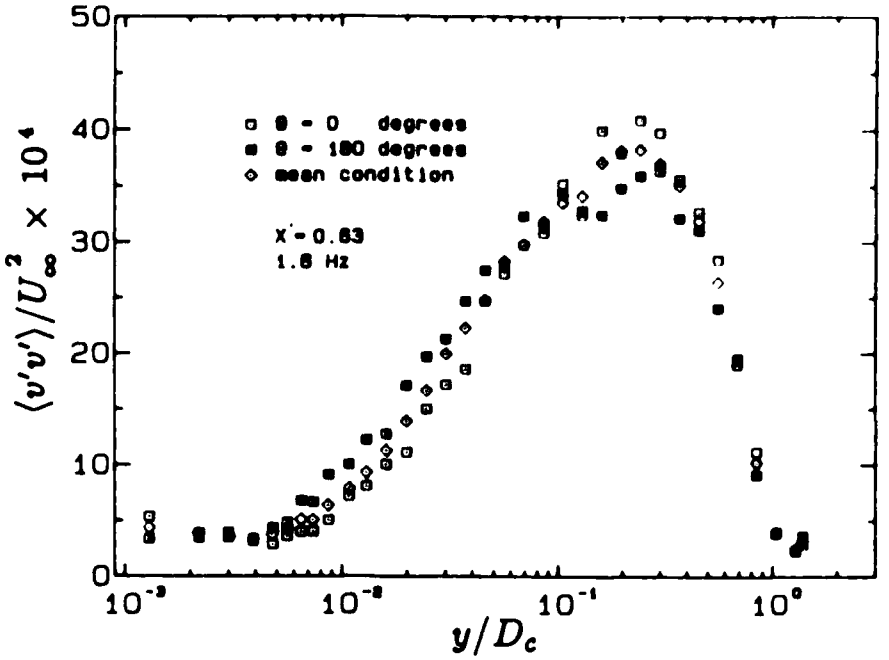

Figure 6.16 Profiles of $\overline{v'v'}$, $\langle v'v' \rangle_{\phi=0^\circ}$ and $\langle v'v' \rangle_{\phi=180^\circ}$ under unsteady conditions at 1.6 hertz

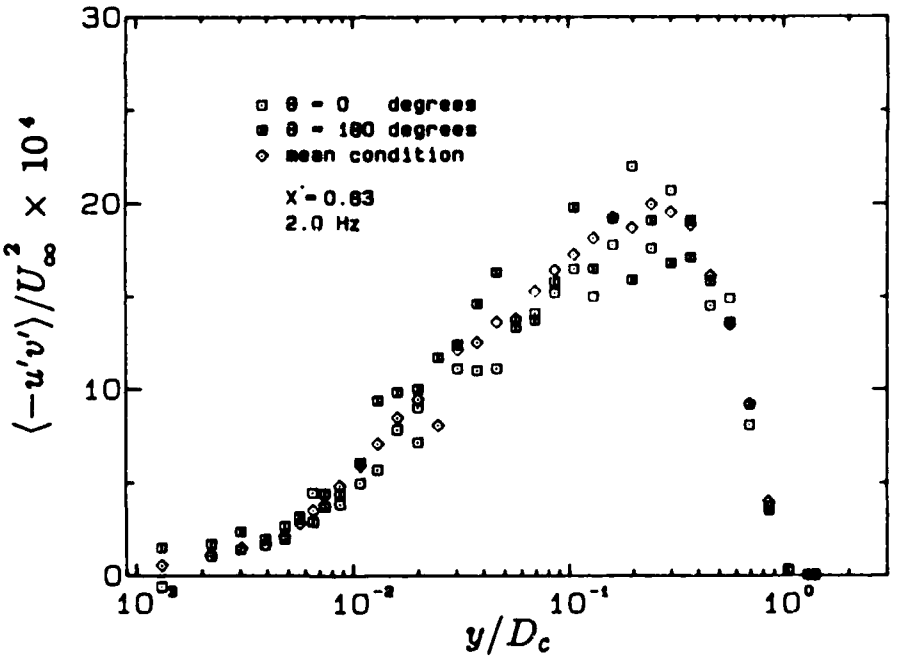

Figure 6.17 Profiles of $-\overline{u'v'}$, $\langle -u'v' \rangle_{\phi=0^\circ}$ and $\langle -u'v' \rangle_{\phi=180^\circ}$ under unsteady conditions at 2.0 hertz

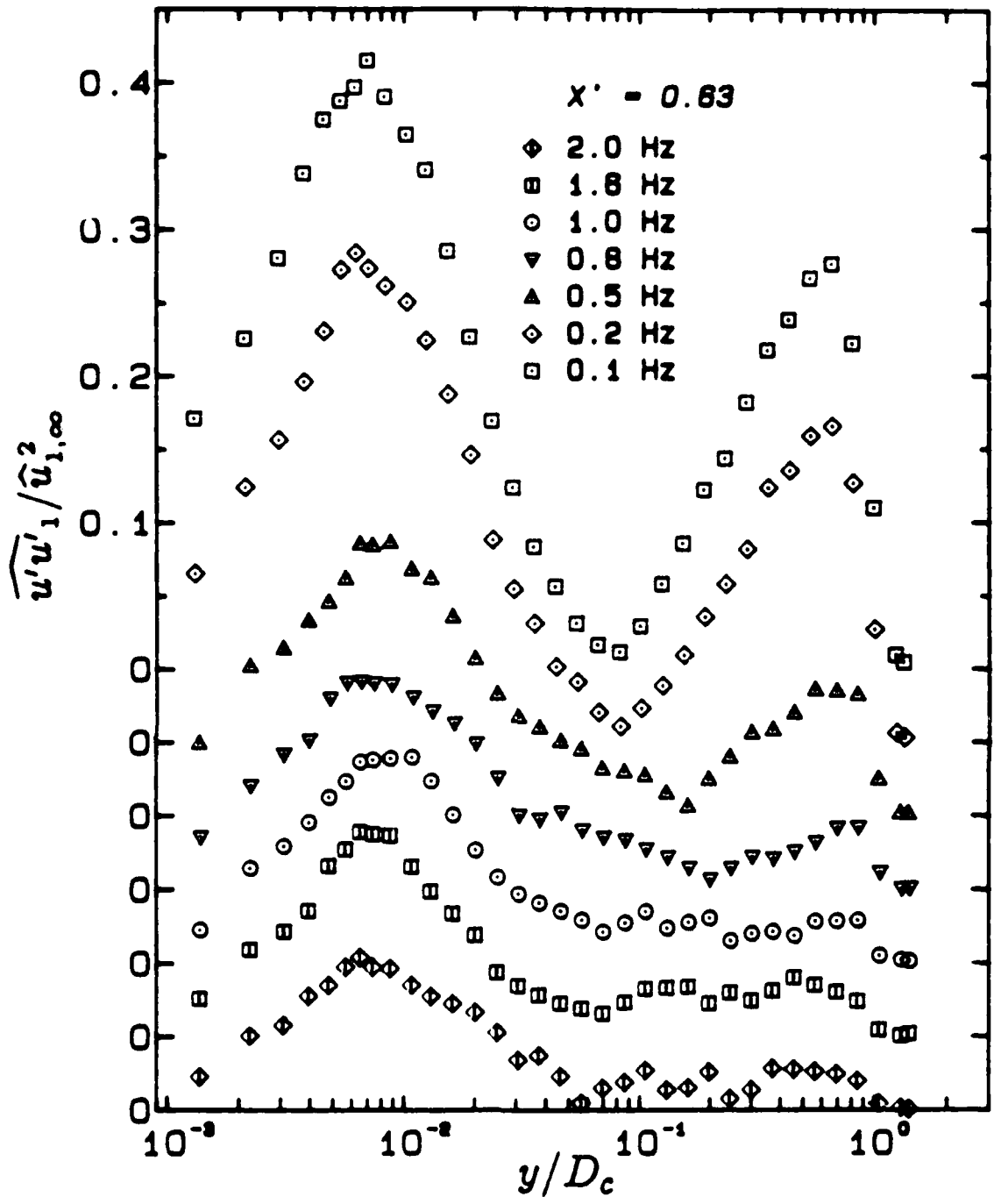

Figure 6.18 Profiles of $\widehat{u'u'}_1/\hat{u}^2_{1,\infty}$ under unsteady conditions.
$X' = 0.63$

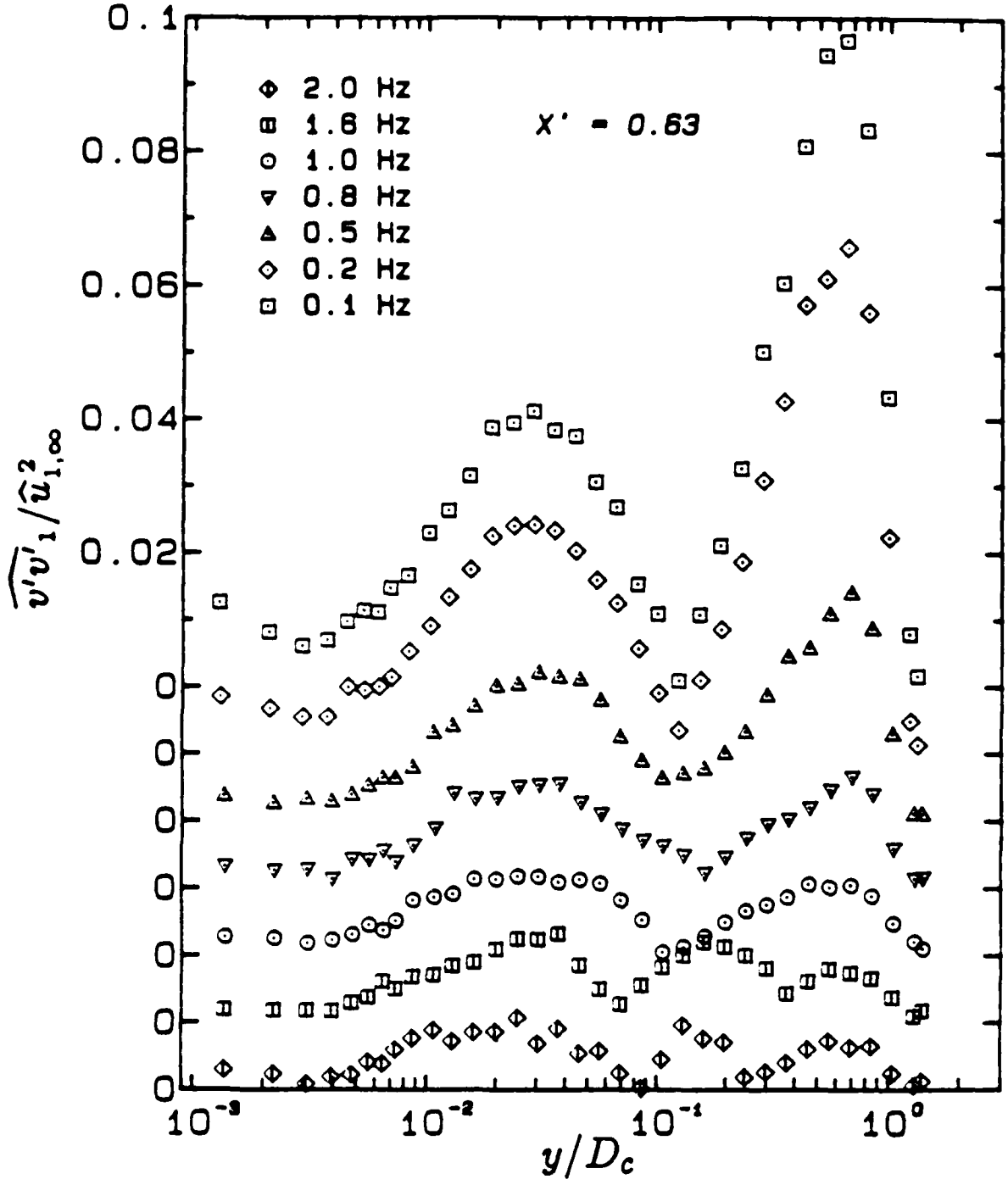

Figure 6.19 Profiles of $\widehat{v'v'}_1/\widehat{u}^2_{1,\infty}$ under unsteady conditions.
$X' = 0.63$

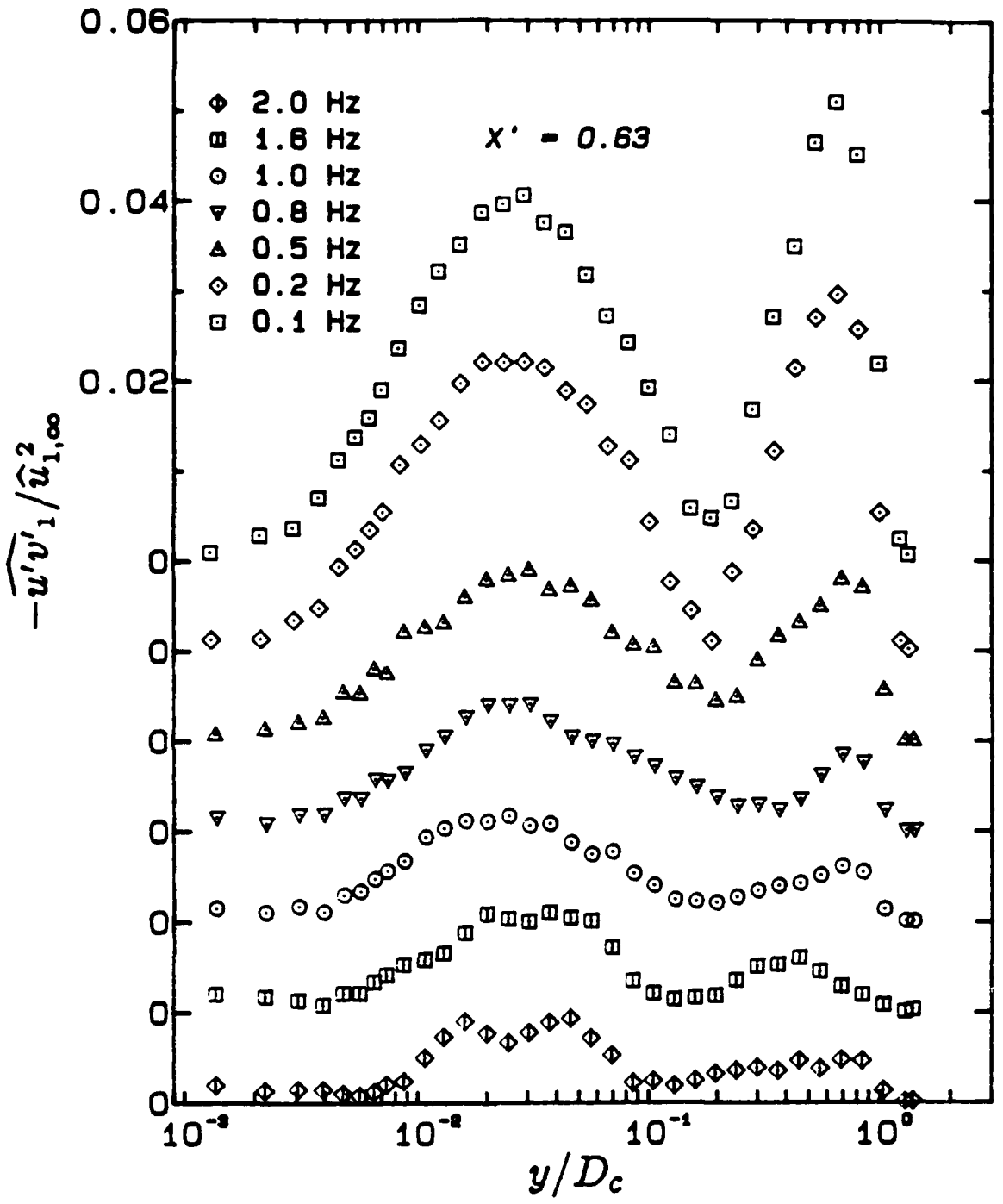

Figure 6.20 Profiles of $-\widehat{u'v'}_1/\widehat{u}^2_{1,\infty}$ under unsteady conditions.
$X' = 0.63$

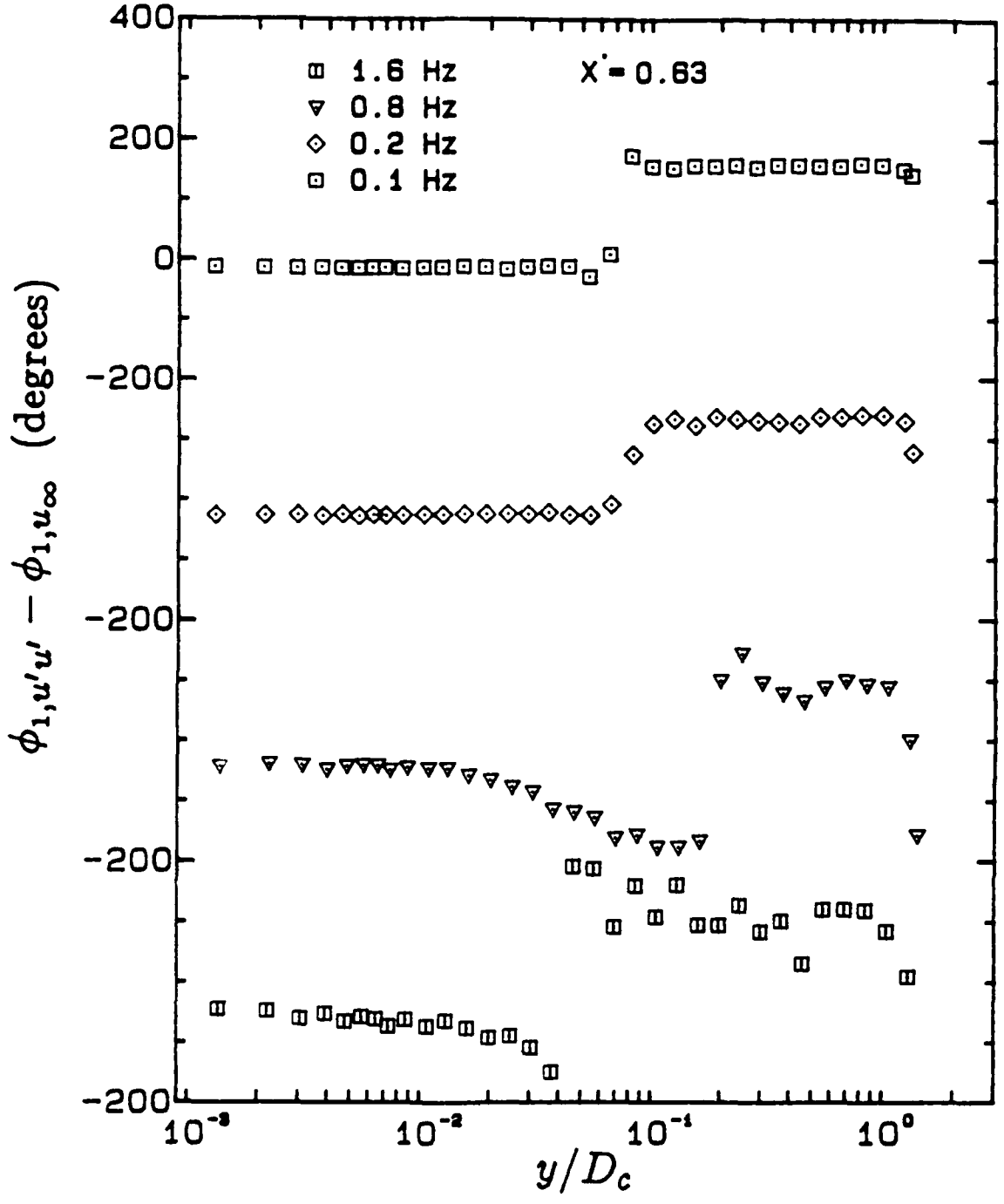

Figure 6.21 Profiles of $\phi_{1,u'u'} - \phi_{1,u_\infty}$ under unsteady conditions.
$X' = 0.63$

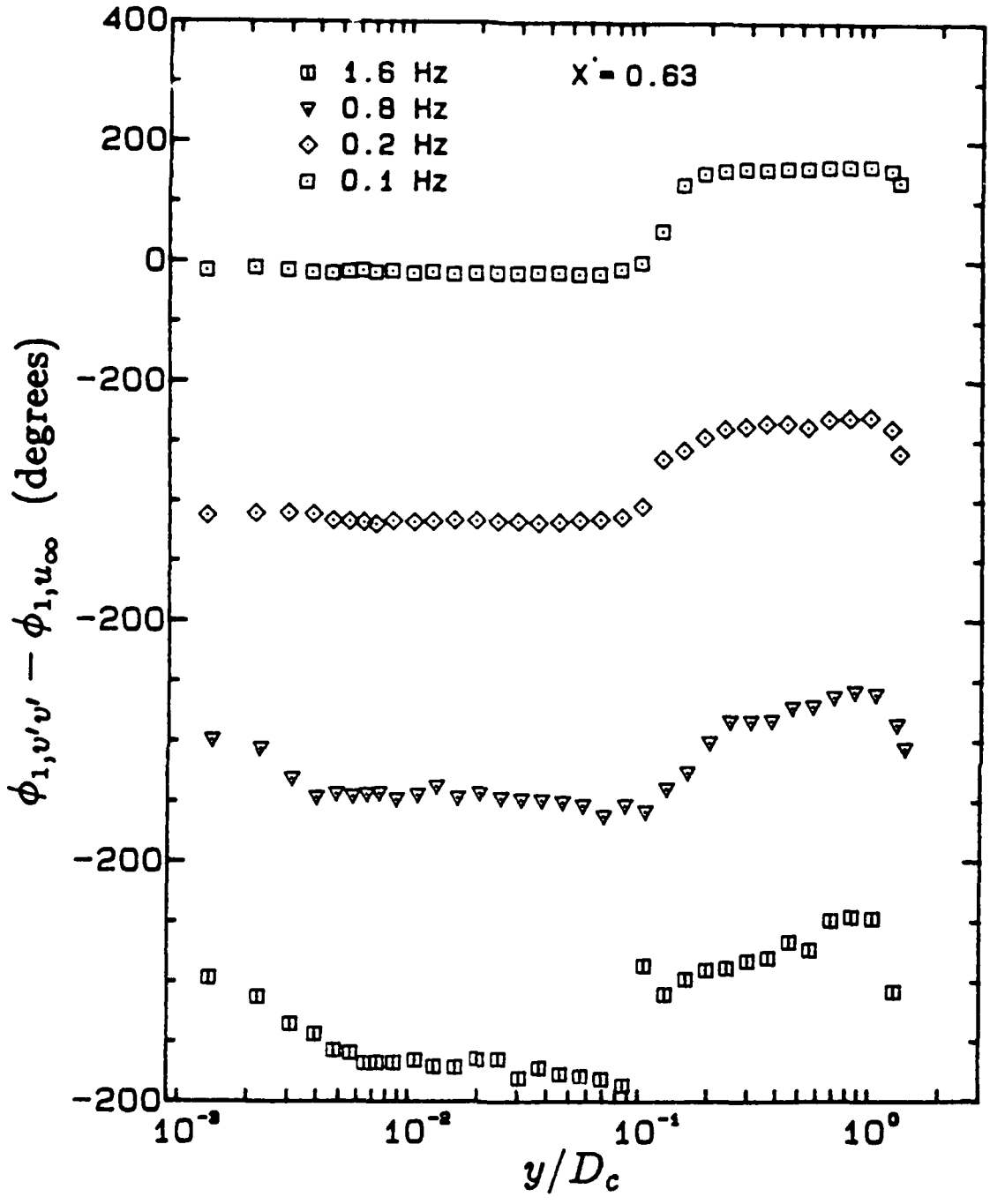

Figure 6.22 Profiles of $\phi_{1,v'v'} - \phi_{1,u_\infty}$ under unsteady conditions.
$X' = 0.63$

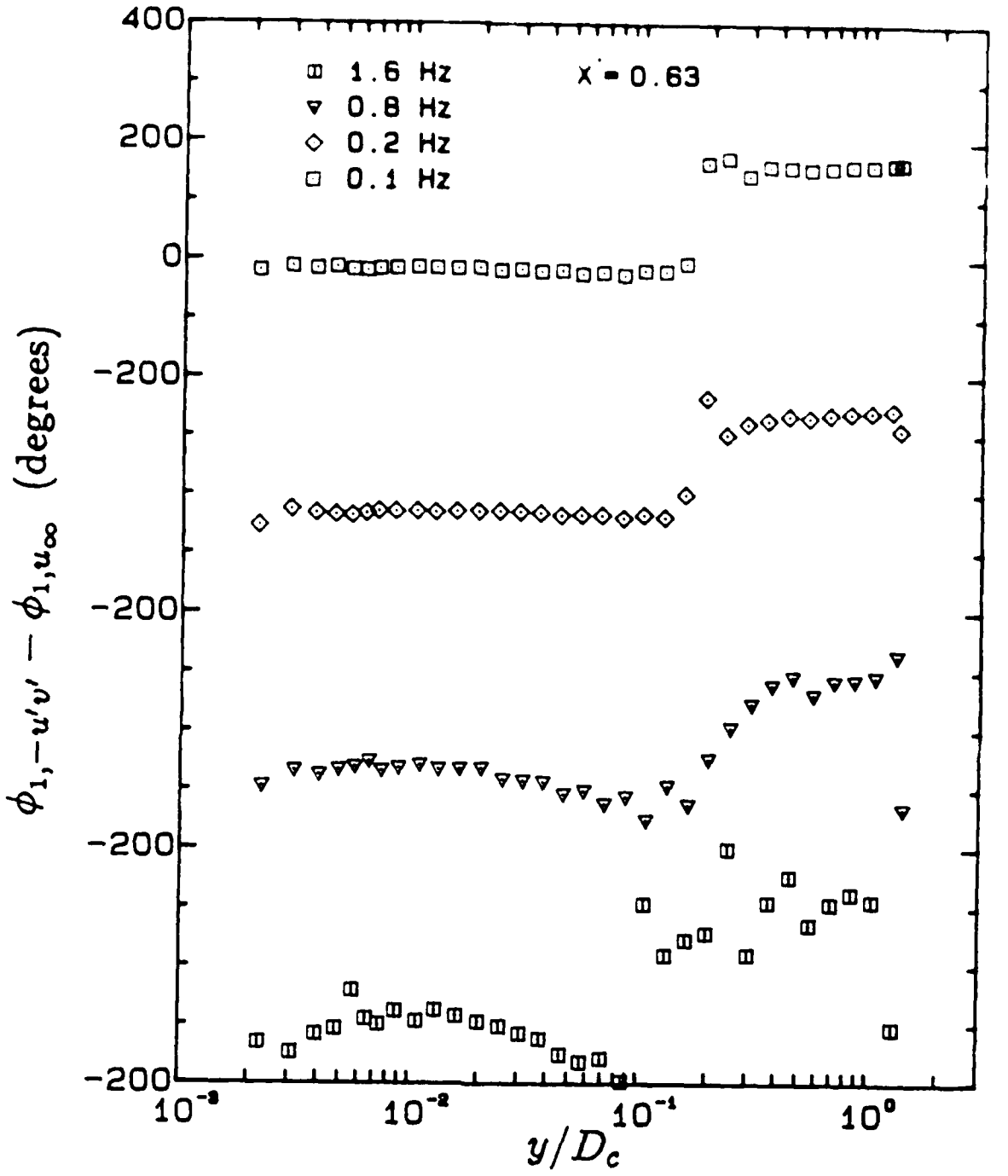

Figure 6.23 Profiles of $\phi_{1,-u'v'} - \phi_{1,u_\infty}$ under unsteady conditions.
$X' = 0.63$

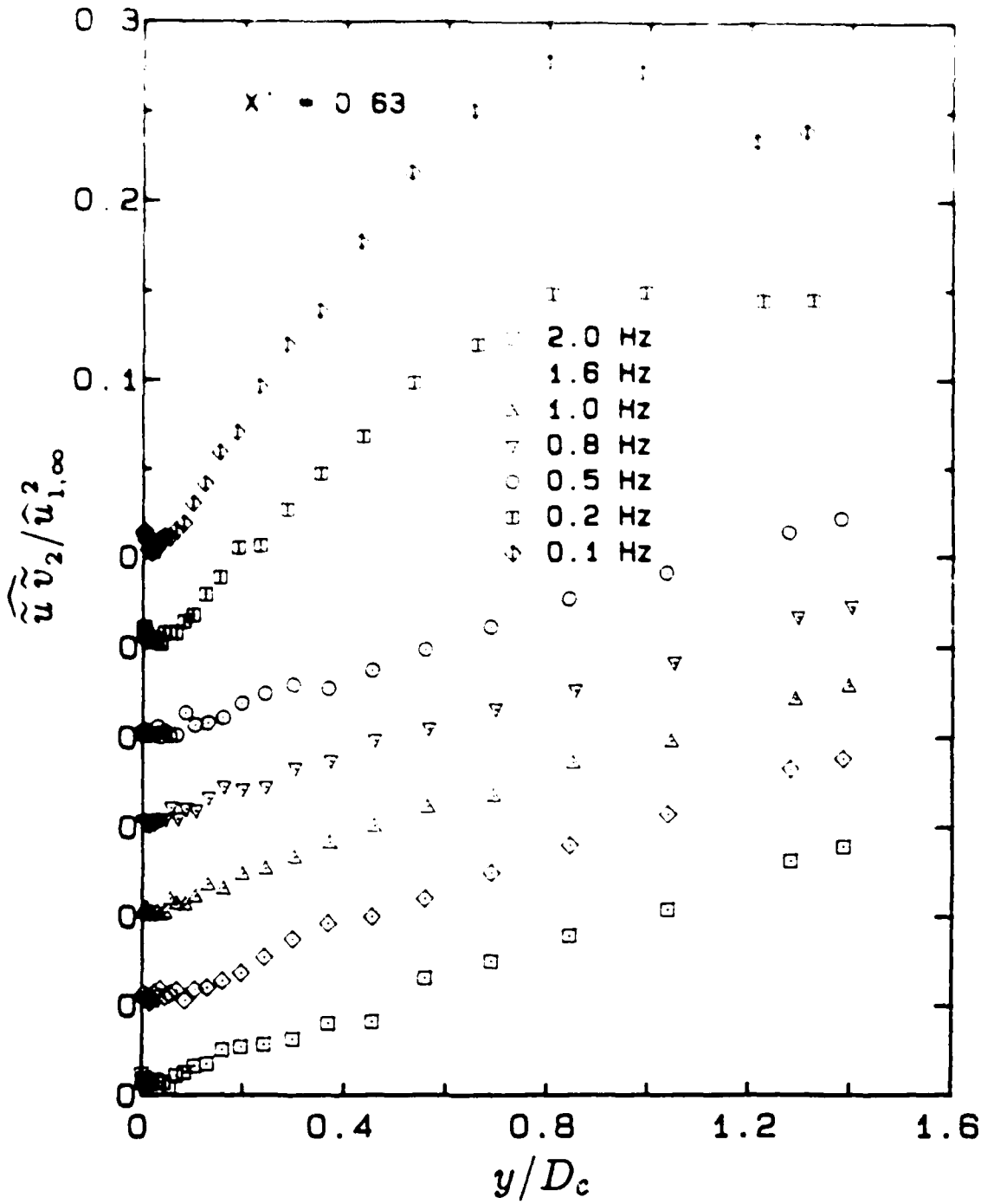

Figure 6.24 Profiles of $\widetilde{\widetilde{u}}\,\widetilde{\widetilde{v}}_2/\widehat{u}^2_{1,\infty}$ under unsteady conditions.
$X' = 0.63$

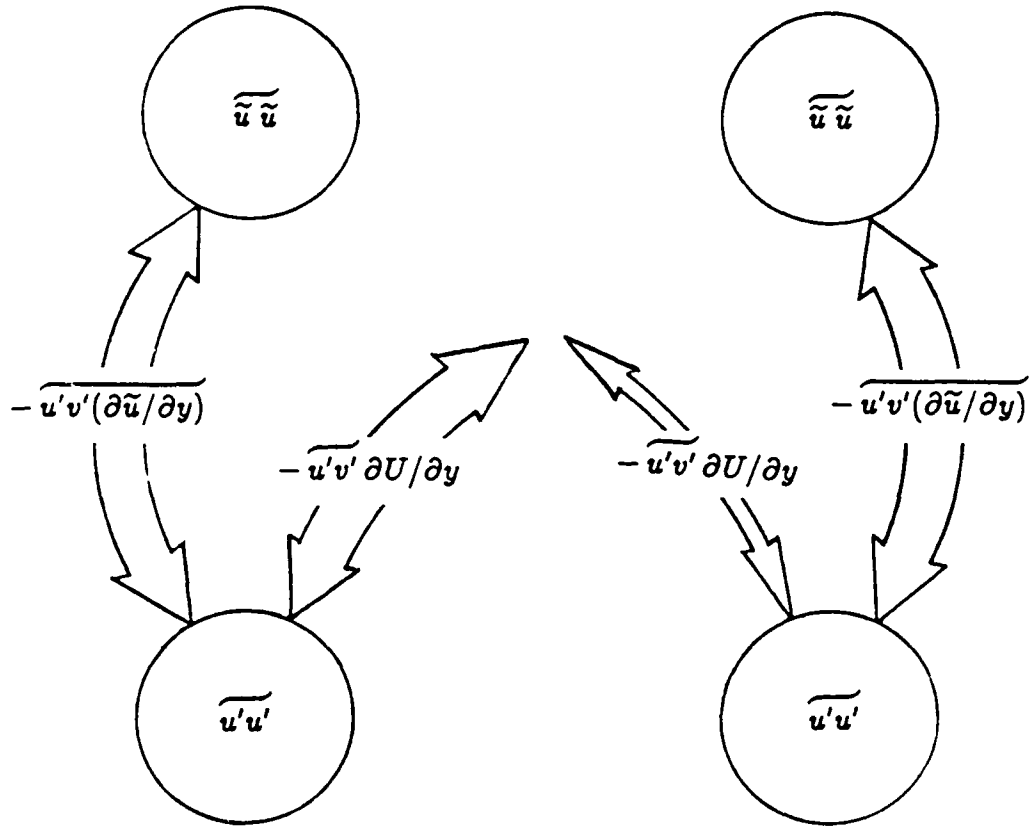

low-frequency flow

high-frequency flow

Figure 6.25 Unsteady transfer of kinetic energy between [illegible] wall (the thickness of each arrow represents [illegible] energy-transfer term).

AD-A184 856 EXPERIMENTAL STUDY OF THE FLUID MECHANICS OF UNSTEADY TURBULENT BOUNDARY LAYERS(U) STANFORD UNIV CA THERMOSCIENCES DIV G J BRERETON ET AL MAY 87 TF-29 3/3

UNCLASSIFIED ARO-19976 4-EG DAAG29-83-K-0056 F/G 20/4 NL

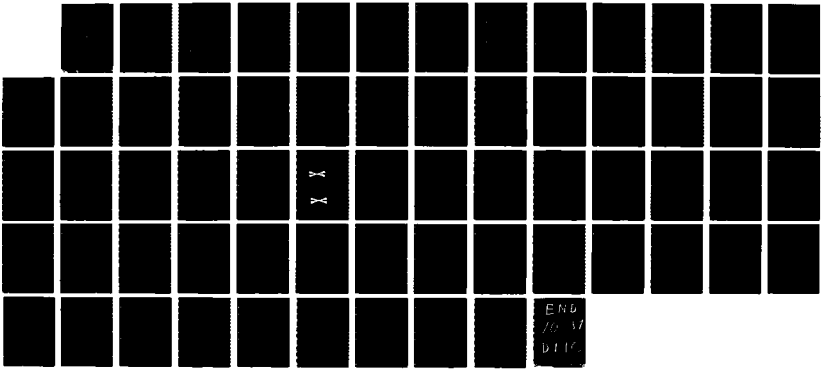

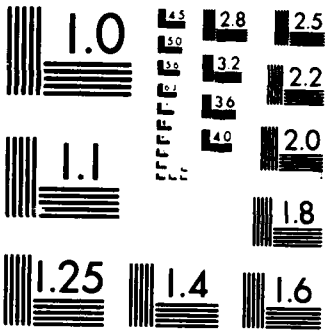

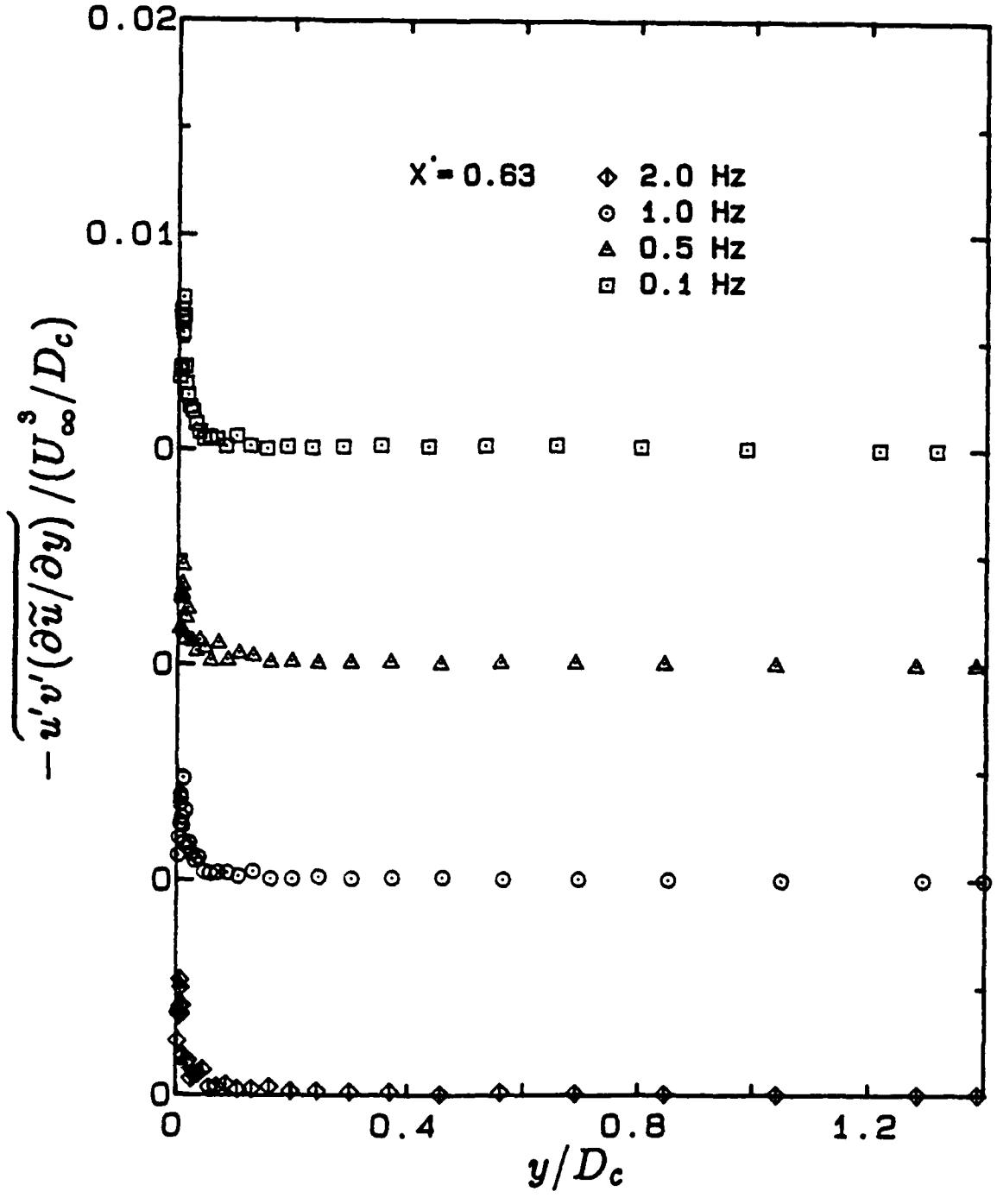

Figure 6.26 Normalized profiles of the amplitude of $-\overline{u'v'(\partial\tilde{u}/\partial y)}$, at its first harmonic, under unsteady conditions. $X' = 0.63$

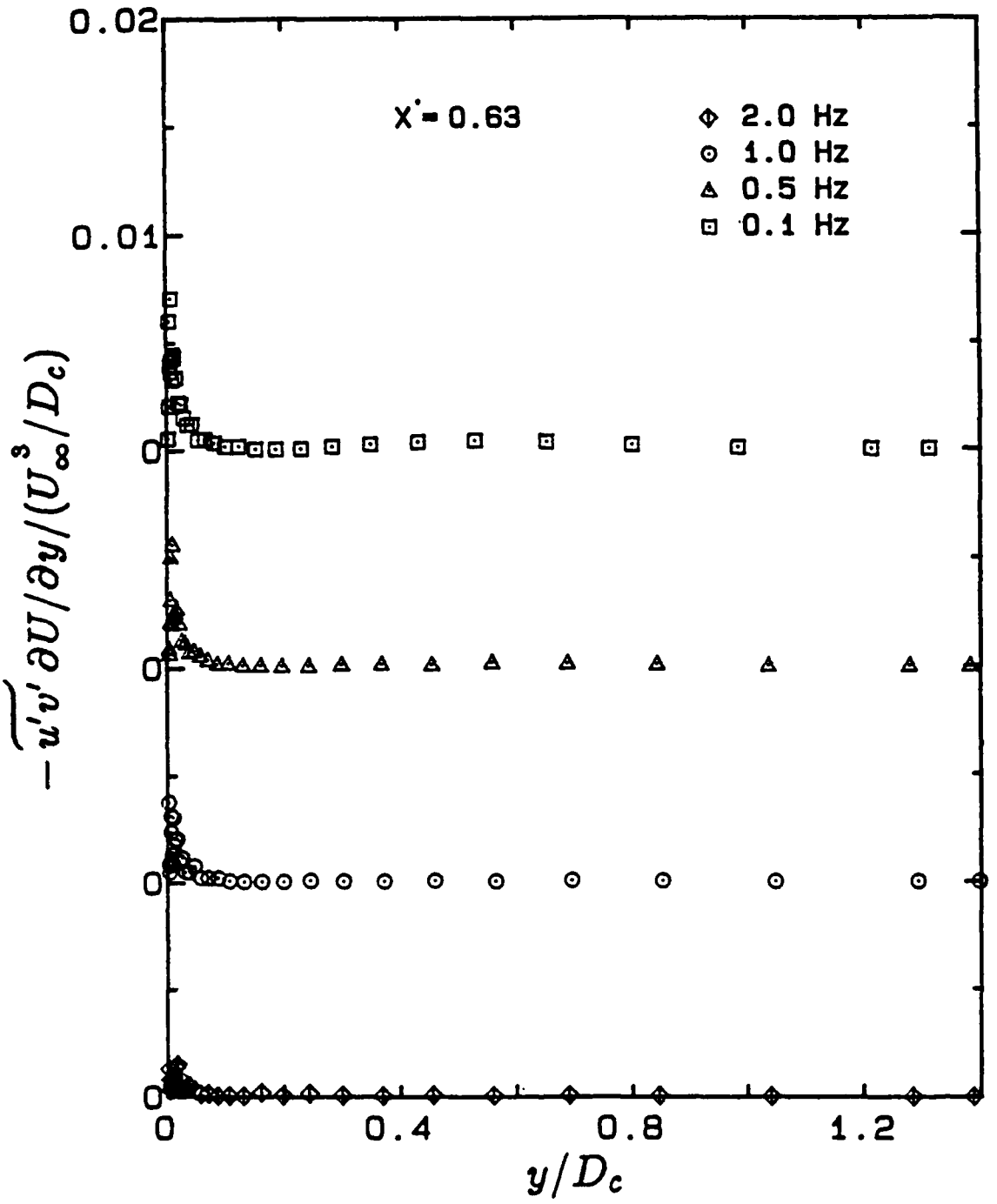

Figure 6.27 Normalized profiles of the amplitude of $-\widetilde{u'v'}\,\partial U/\partial y$, at its first harmonic, under unsteady conditions. $X' = 0.63$

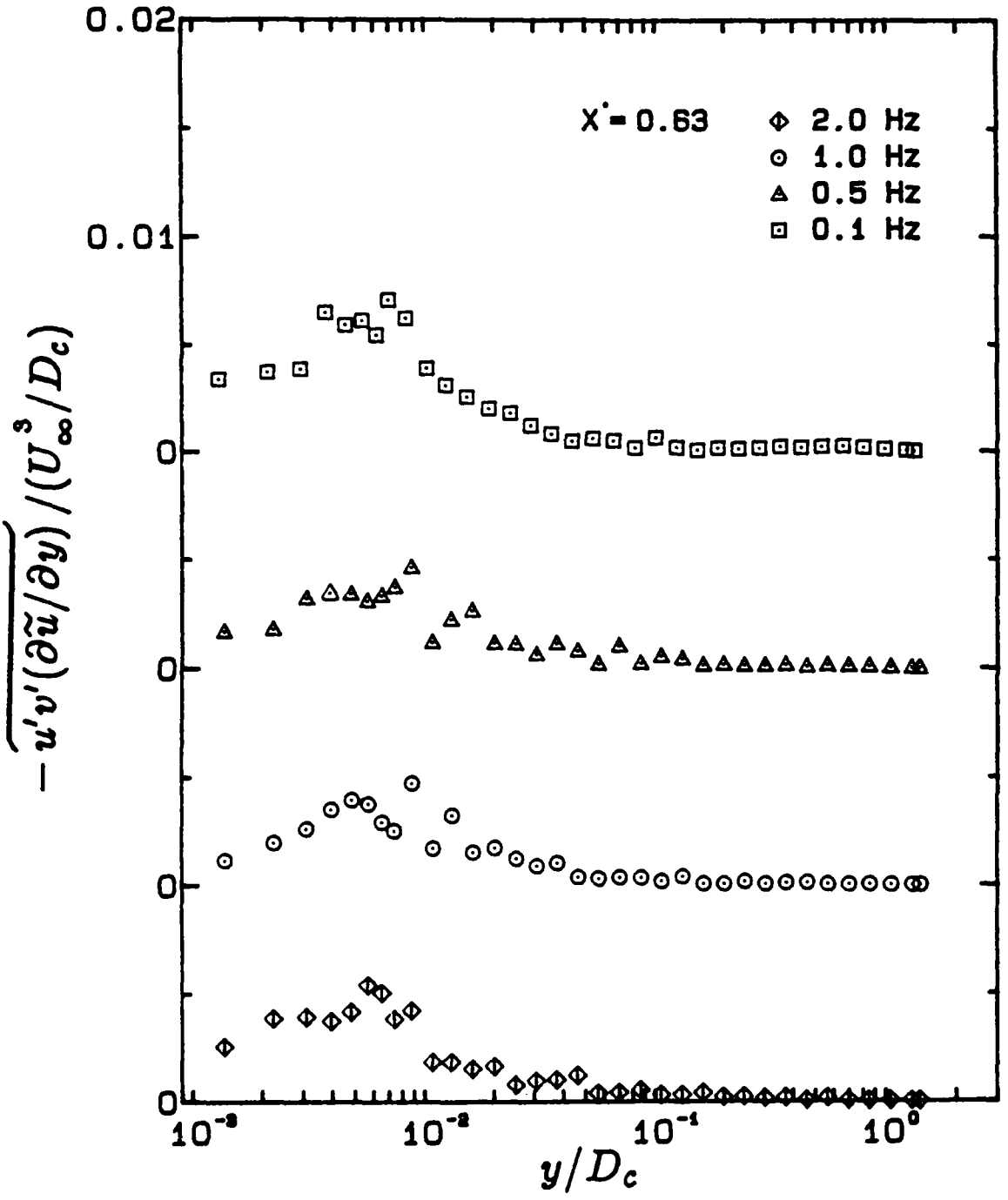

Figure 6.28 Normalized profiles of the amplitude of $-\widetilde{u'v'(\partial\tilde{u}/\partial y)}$, at its first harmonic, under unsteady conditions. $X' = 0.63$

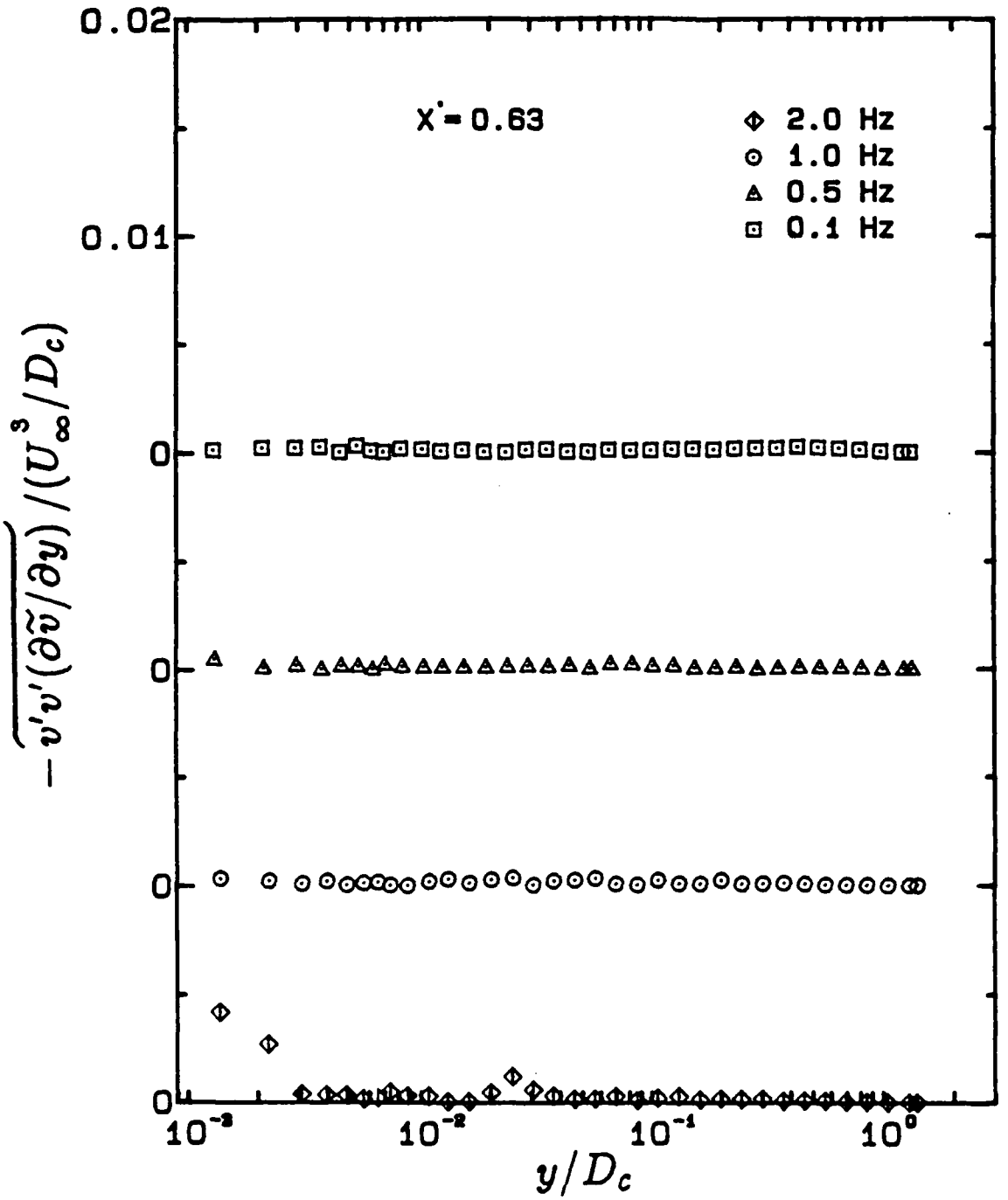

Figure 6.29 Normalized profiles of the amplitude of $-\overline{v'v'(\partial\tilde{v}/\partial y)}$, at its first harmonic, under unsteady conditions. $X' = 0.63$

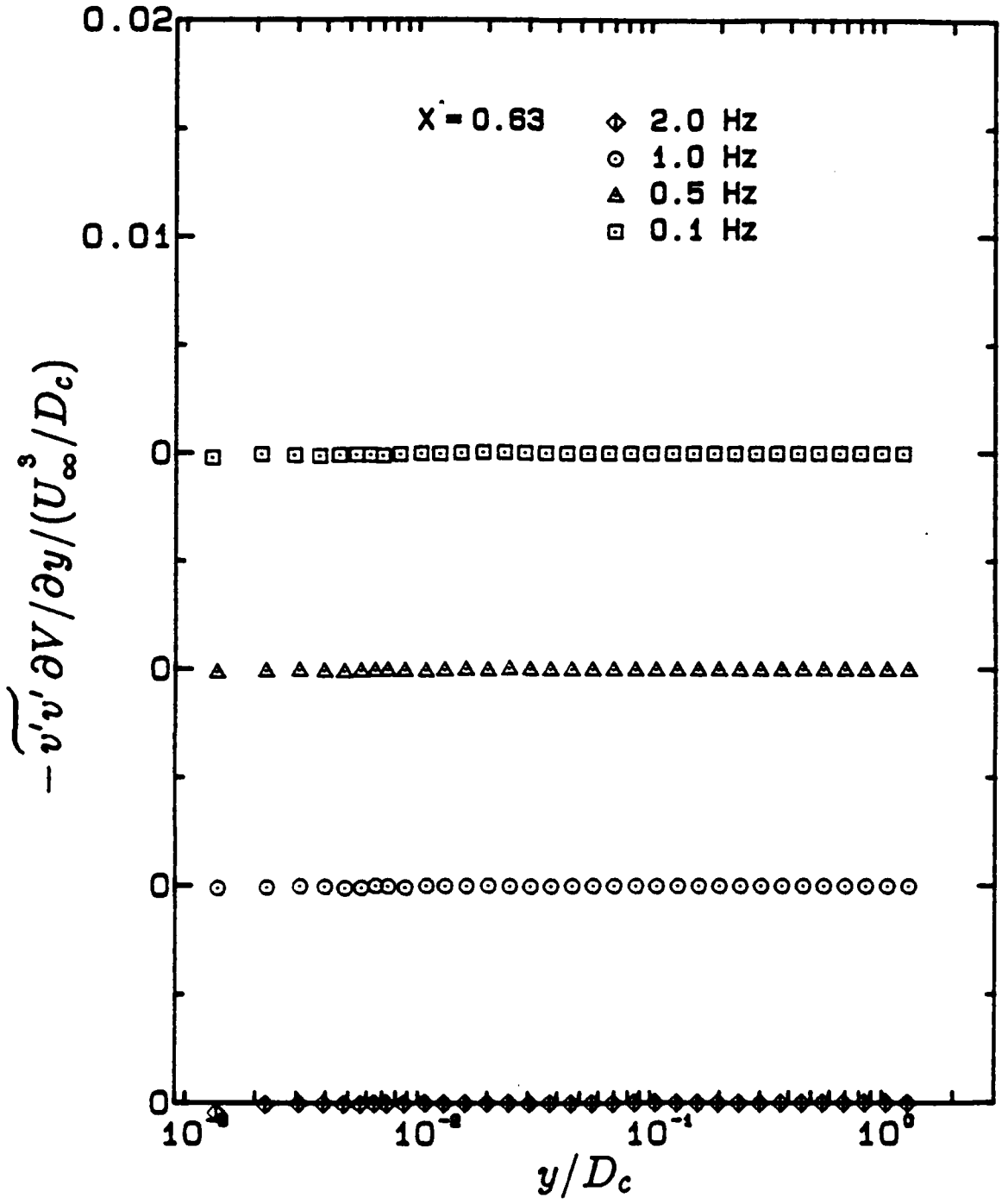

Figure 6.30 Normalized profiles of the amplitude of $-\widetilde{v'v'}\,\partial V/\partial y$, at its first harmonic, under unsteady conditions. $X' = 0.63$

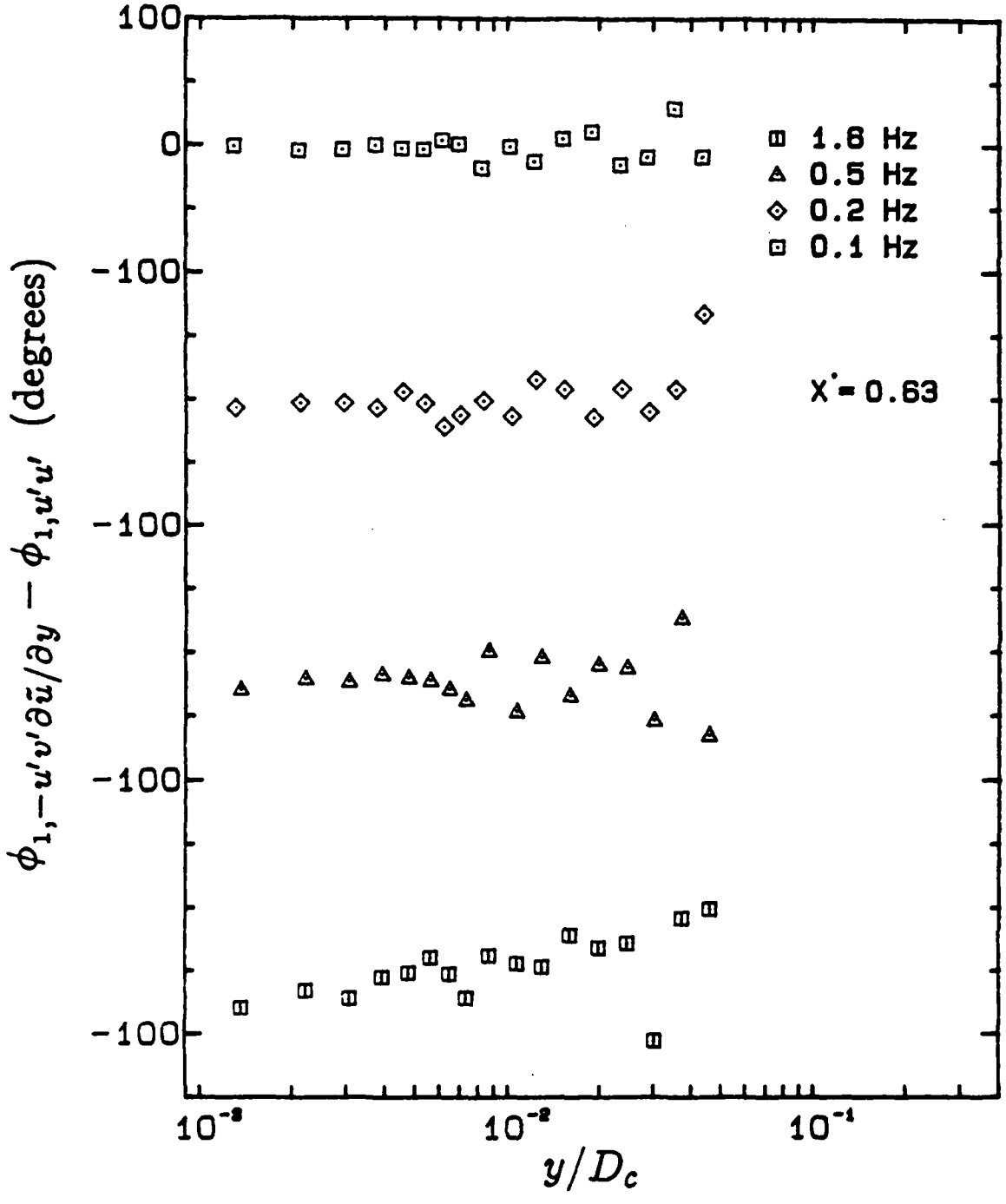

Figure 6.31 Profiles of $\phi_{1,-u'v'\partial\tilde{u}/\partial y} - \phi_{1,u'u'}$ under unsteady conditions. $X' = 0.63$

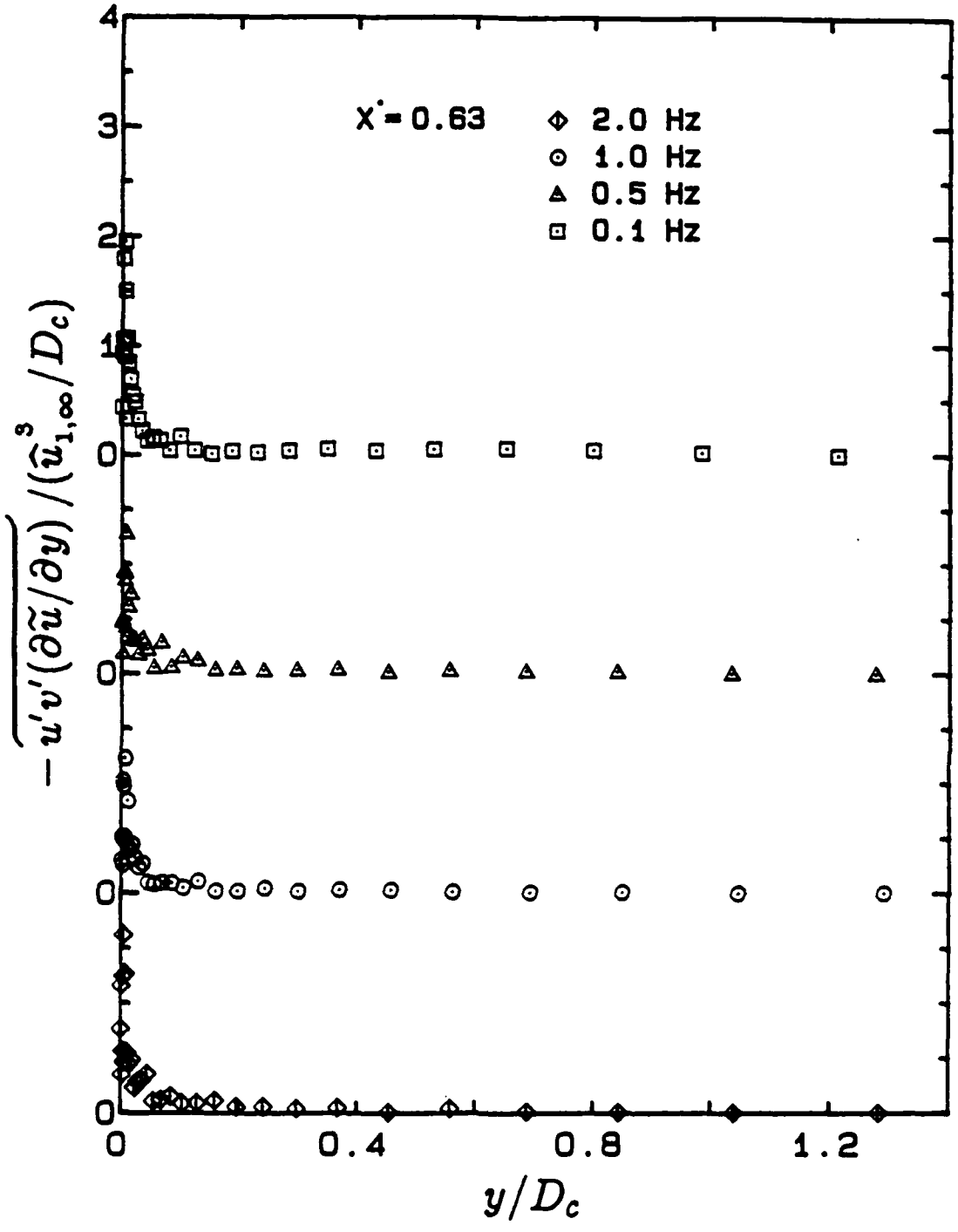

Figure 6.32 Normalized profiles of the amplitude of $-\overline{u'v'(\partial\tilde{u}/\partial y)}$, at its first harmonic, under unsteady conditions. $X' = 0.63$

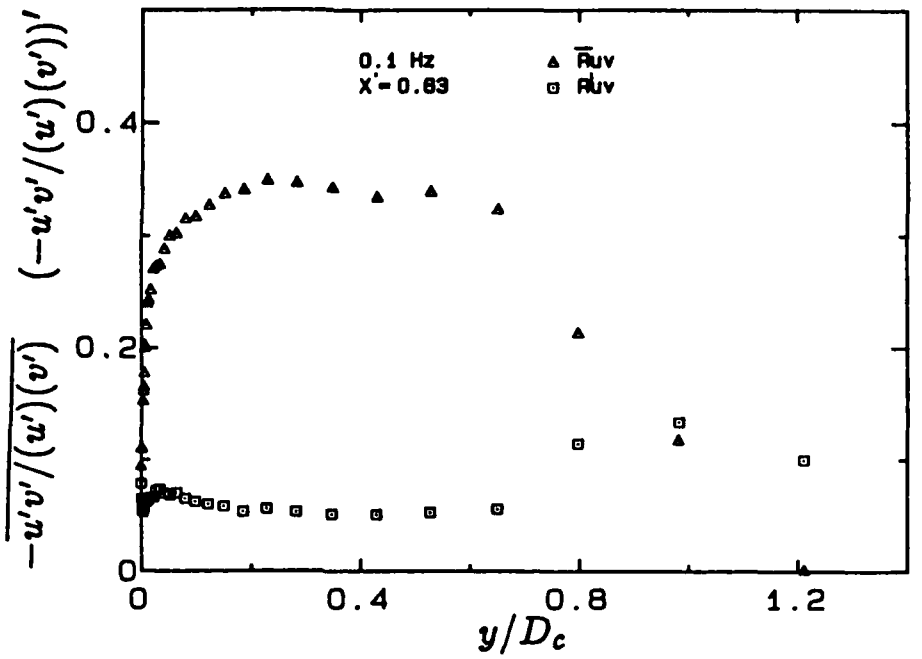

Figure 6.33 Profiles of $\overline{-u'v'/(u')(v')}$ and $(-u'v'/(u')(v'))'$ at 0.1 hertz. $X' = 0.63$

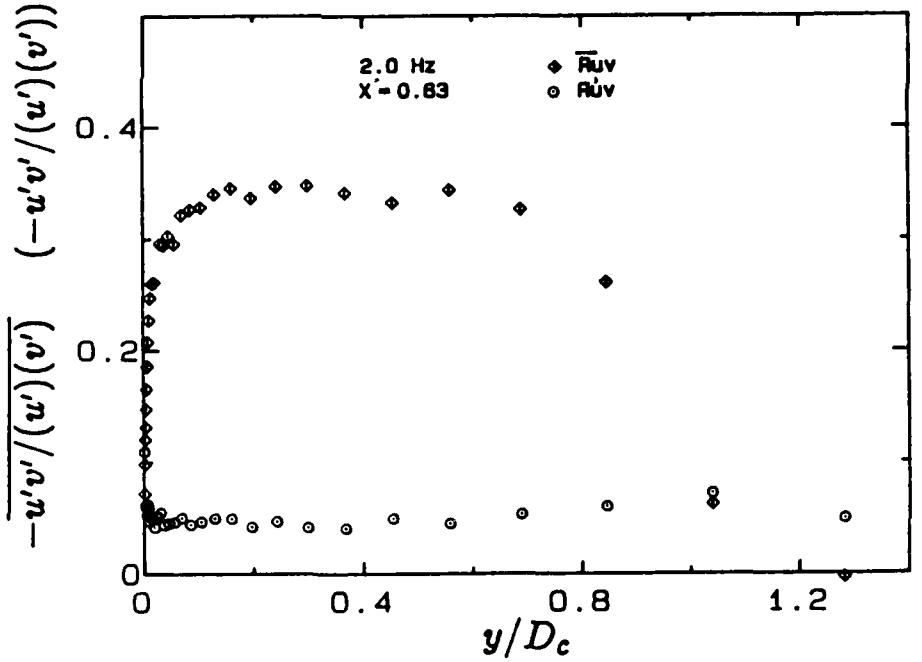

Figure 6.34 Profiles of $\overline{-u'v'/(u')(v')}$ and $(-u'v'/(u')(v'))'$ at 2.0 hertz. $X' = 0.63$

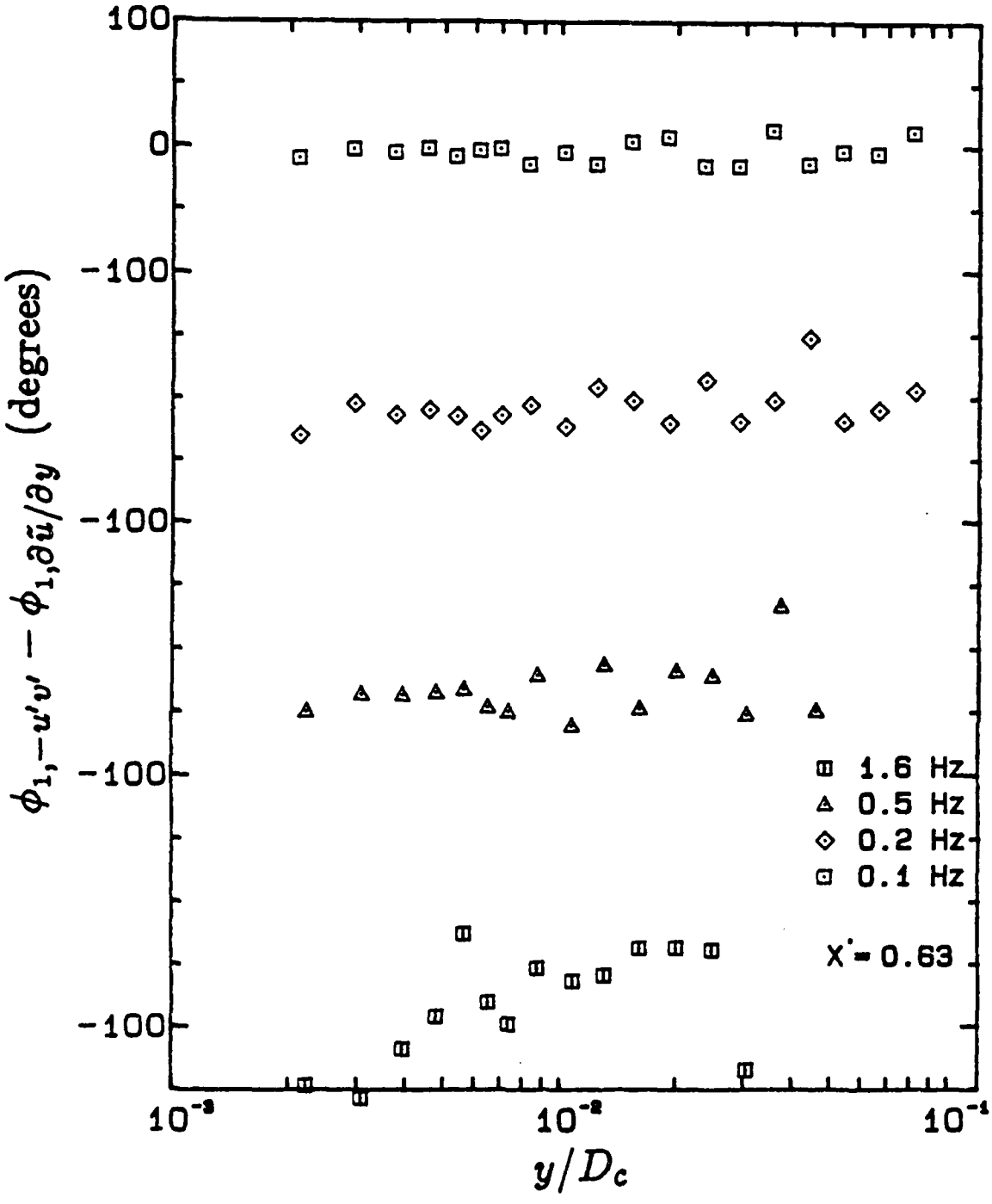

Figure 6.35 Profiles of $\phi_{1,-u'v'} - \phi_{1,\partial\tilde{u}/\partial y}$ under unsteady conditions. $X' = 0.63$

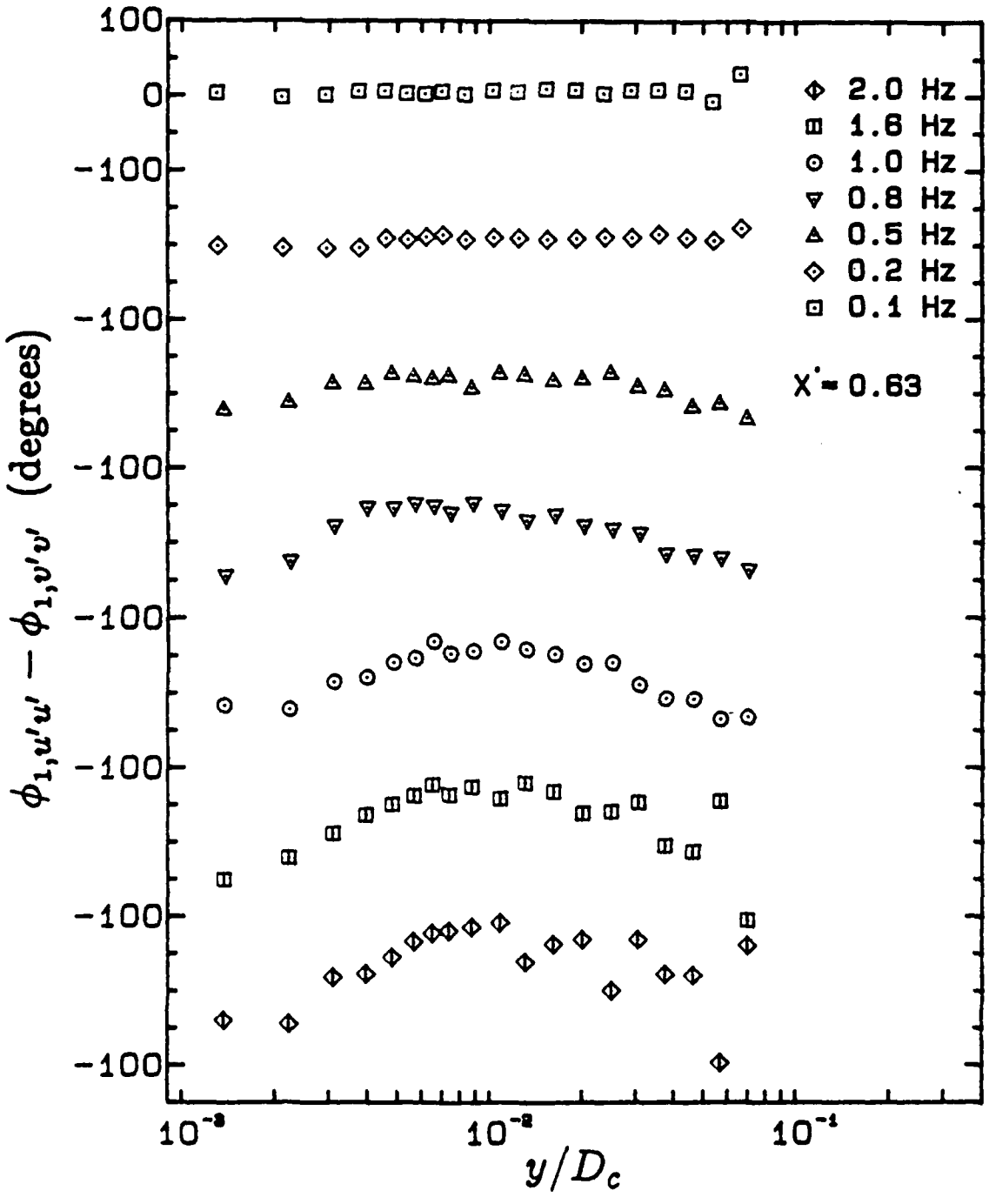

Figure 6.36 Profiles of $\phi_{1,u'u'} - \phi_{1,v'v'}$ under unsteady conditions.
$X' = 0.63$

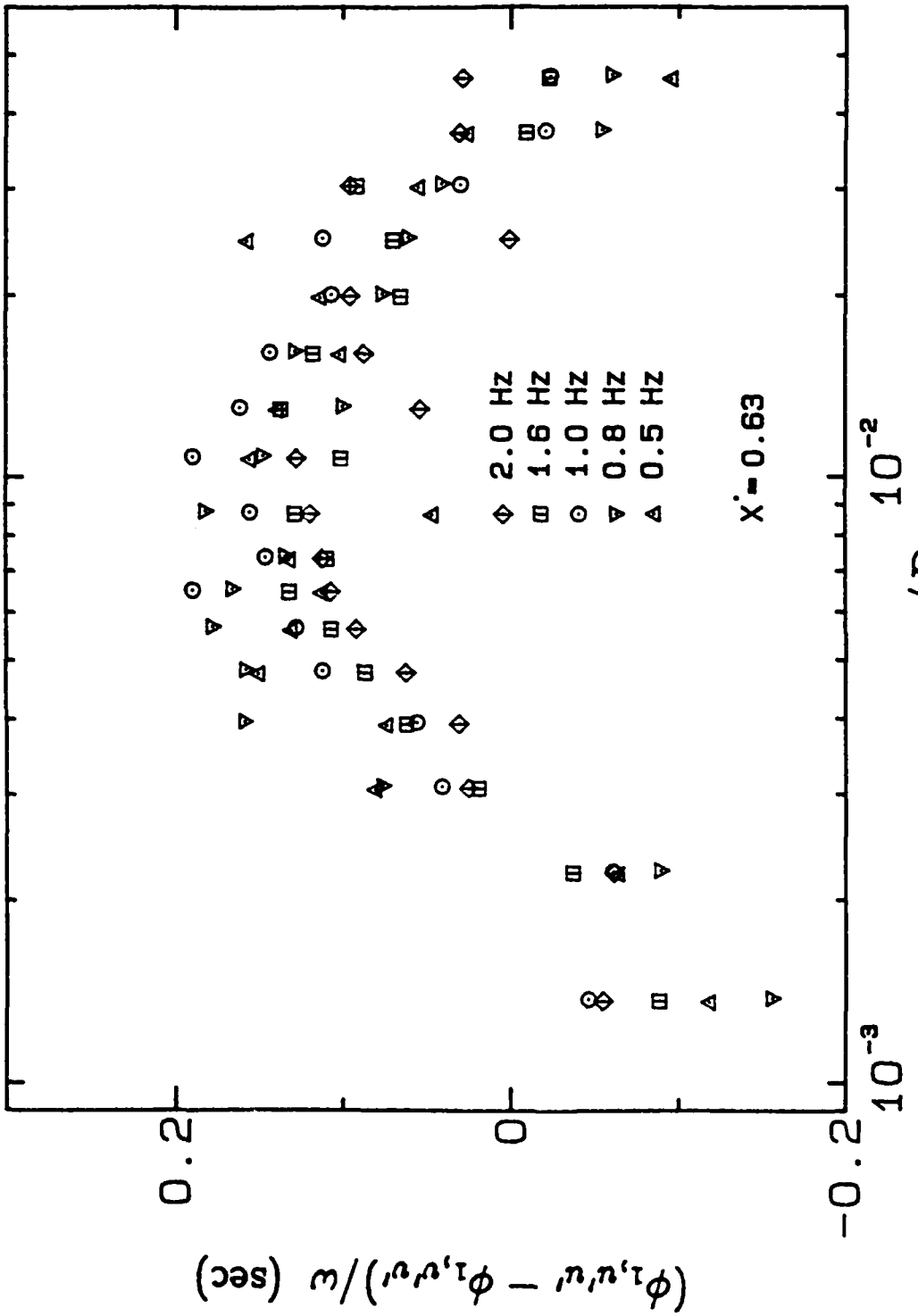

Figure 6.37 Profiles of $(\phi_{1,u'u'} - \phi_{1,v'v'})/\omega$ under unsteady conditions.
$X' = 0.63$

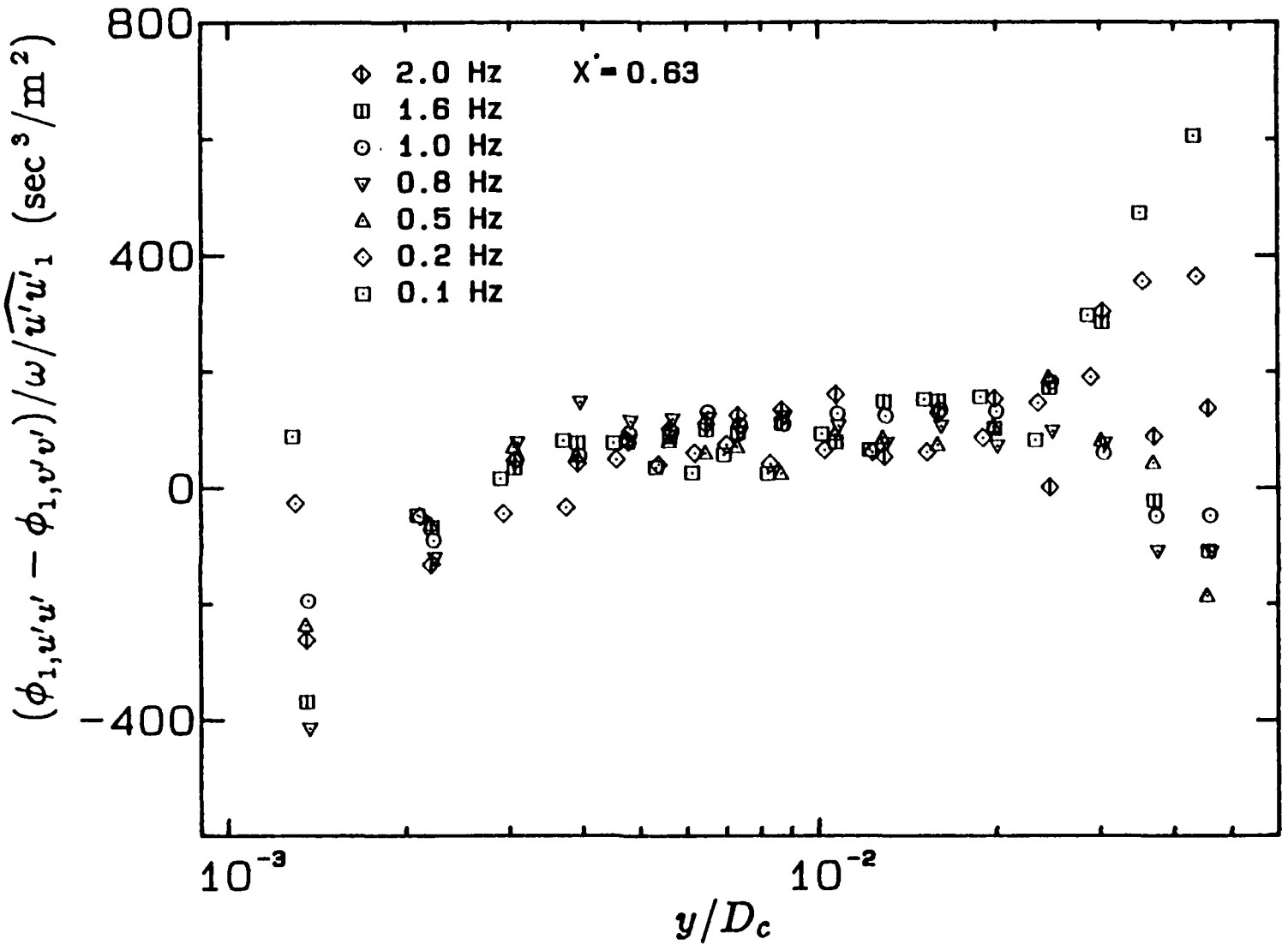

Figure 6.38 Profiles of $(\phi_{1,u'u'} - \phi_{1,v'v'})/\omega/\widehat{u'u'}_1$ under unsteady conditions.
$X' = 0.63$

7. Conclusions and Recommendations

Specific conclusions may be drawn from this study, which focused on new, simultaneous measurements of the u and v components of the velocity field in unsteady, turbulent, boundary layers. Insights concerning: (*i*) the time-averaged behavior of these flows (§5), and (*ii*) their phase-conditioned response and periodic structure (§6), have been developed and the conclusions reached in earlier chapters are recapitulated here. Furthermore, in the course of this study a substantial body of new data was compiled, which spanned a wide range of frequencies of mainstream unsteadiness — it should prove useful as target data for turbulence modelers.

Time-Averaged Unsteady Flow:

(*i*) The velocity measures, U, V, $\overline{u'u'}$, $\overline{v'v'}$ and $-\overline{u'v'}$, which are of importance in the time-averaged momentum equations, were invariant with frequency of forced mainstream unsteadiness throughout the boundary layer.

(*ii*) Profiles of U appeared comparable to their steady-flow counterparts and the familiar linear, log-linear and wake regions could be identified clearly. Likewise, profiles of $\overline{u'u'}$, $\overline{v'v'}$ and $-\overline{u'v'}$ were similar in appearance to their counterparts in steady flow.

(*iii*) In measurements of U, $\overline{u'u'}$, $\overline{v'v'}$ and $-\overline{u'v'}$ at the inlet to the test section, differences between the steady and time-averaged unsteady profiles were evident, particularly near the wall — in computational predictions of these data, initial conditions based on time-averaged unsteady measures would be more appropriate than steady ones.

(*iv*) The periodic, wall-normal component of velocity, $\tilde{v}$, made an important contribution to the $\partial(\overline{\tilde{u}_k\tilde{u}_i})/\partial x_k$ tensor, a term which played a significant role in the mean x-momentum equation. Furthermore, the magnitude of this tensor was dependent on the frequency of forced free-stream unsteadiness.

(*v*) Computational schemes aimed at the accurate prediction of unsteady flows in mean, adverse-pressure gradients should make provision for modeling, or preferably direct calculation, of the $\partial(\widetilde{u}_k\widetilde{u}_i)/\partial x_k$ tensor of the x-momentum equation. In this adverse-pressure-gradient flow, neglect of this tensor would lead to inadequate characterization of the boundary layer.

(*vi*) The important production term, which accounted for transfer of turbulent kinetic energy between the mean and turbulent fields, in a time-averaged sense, was invariant with frequency — its profile was comparable in shape to that of the equivalent steady-flow measure.

(*vii*) While all time-averaged turbulence measures appeared to be invariant with different frequencies of free-stream unsteadiness, a strong frequency dependence was noted in a small, time-averaged production term.

(*viii*) Log-linear descriptions of the instantaneous, phase-averaged profiles of streamwise velocity were not appropriate for unsteady, turbulent boundary layers.

(*ix*) The structural parameters, $-\overline{u'v'}/(\overline{u'u'} + \overline{v'v'})$, $-\overline{u'v'}/(u'v')$, $\overline{\ell}$ and $\overline{\nu_t}$ were invariant with frequency and with different averaging techniques.

Phase-Conditioned Unsteady Flow:

(*i*) The response of the periodic streamwise velocity, $\widetilde{u}$, to forced free-stream unsteadiness was strongly dependent on frequency. It could be described in terms of variation between: (*i*) an asymptotic low-frequency form, which corresponded to the quasi-steady condition of constant phase across the boundary layer, and (*ii*) an asymptotic high-frequency form which matched the analytic solution to the quasi-laminar Stokes equation. As the high-frequency condition was approached, the asymptotic amplitude was matched at lower frequencies than were necessary to satisfy the corresponding phase requirement.

(*ii*) No frequency dependence was obvious in measures of $\tilde{v}$, the wall-normal component of periodic velocity, nor could it be identified with any asymptotic behavior.

(*iii*) The ratio of the leading unsteady and convective terms of the $\tilde{u}$-momentum equation was a suitable parameter for characterizing the response of $\tilde{u}$ to forced free-stream unsteadiness. While the performance of this parameter was adequate, it was barely distinguishable from that of other parameters, the forms of which were based on different premises. This finding was thought to be due to the similarity in the streamwise variation in mean and deterministic velocities which resulted from the design of this particular experiment.

(*iv*) Periodic turbulence measures were strongly dependent on frequency of forced unsteadiness and high frequency behavior was characterized by greatly reduced amplitudes in the deterministic measures: $\widehat{u'u'}_1$, $\widehat{v'v'}_1$ and $-\widehat{u'v'}_1$. At the highest frequencies of forced unsteadiness, these amplitudes were negligible in the outer part of the boundary layer although still significant in the inner part. At low frequencies of forced unsteadiness, the deviation of phase-conditioned turbulence measures from their mean condition appeared similar to the expected quasi-steady response. In contrast to the high-frequency behavior of $\tilde{u}$ (for which an abscissa scaling on a frequency-dependent length scale was appropriate), an abscissa incorporating a mean length scale suited profiles of periodic turbulence measures.

(*v*) The role of second-harmonic quantities in the deterministic momentum equations seemed to be restricted to the characterization of products of first harmonics. No other measures in this study exhibited any appreciable response at this second-harmonic frequency.

(*vi*) Transfer of the streamwise component of the turbulent kinetic energy was from the organized unsteady field ($\widetilde{\tilde{u}\,\tilde{u}}$) to the unorganized unsteady field ($\widetilde{u'u'}$) for all conditions under which these experiments were conducted.

(*vii*) The notion that unsteady effects would not influence turbulence production at high frequencies of forced unsteadiness (which corresponded to thin Stokes layers) was examined but was not supported by the deterministic-production measurements of this study.

(*viii*) Periodic production of turbulent kinetic energy was found to be strongly anisotropic — the energy transfer to $\widetilde{u'u'}$ greatly exceeded that to $\widetilde{v'v'}$. Inter-component transfer of turbulent kinetic energy was recognized as an important feature of periodic turbulence in the unsteady boundary layer.

(*ix*) A simplified high-frequency form of the transport equation for $\widetilde{u'u'}$, the largest of the periodic turbulence components, was proposed — its time derivative was balanced by its production at the highest frequencies of forced unsteadiness of this study.

(*x*) Instantaneous correlations between u' and v' were not maintained at their time-averaged values under organized unsteady conditions.

(*xi*) The variation in phase between periodic measures of streamwise velocity gradient and periodic shear stress was not well organized — it implied that simple modeling of this kind would not be appropriate for organized, unsteady, turbulent flow.

(*xii*) The spatial coincidence of the maxima of periodic and time-averaged measures of production implied that these processes might be closely related.

(*xiii*) The lag in phase of $\widetilde{v'v'}$ behind $\widetilde{u'u'}$ was well organized — it scaled on a local, turbulent time scale (of the same order as the local, turbulent time scale for the time-averaged flow) and a measure of the local, deterministic anisotropy in the Reynolds stress. Since the well organized dependence of this phase lag amounted to a dynamic corollary to Rotta's model for the slow pressure-strain terms in the time-averaged field of flow, the equivalent periodic slow-pressure-strain terms would be important in unsteady boundary-layer flow.

Recommendations for Future Research:

There are several avenues for future research closely related to this study and one leads to investigating the behavior of wall shear in unsteady flow. Although attempts have been made to measure the dynamic response of wall shear to forced unsteadiness, there is still a need for a non-intrusive instrument, capable of making such measurements instantaneously. The time-averaged response is also of considerable interest and might be examined more readily. In time-averaged unsteady flow, the mean shear at the wall might be deduced from near-wall velocity and shear stress data, if the measurement resolution were sufficient. A critical examination of its relationship with the near-wall velocity scale (deduced from fitting a mean, steady velocity profile to the time-averaged profile of streamwise velocity) might then clarify the usefulness of this velocity scale in unsteady flow. Using available data sets, a simple study of this relationship might prove fruitful.

If the difficulties of three-component laser-Doppler anemometry are overcome, there would be considerable scope for extending studies of unsteady flow to include velocity measurements in three dimensions. Initially, such a study might be carried out most usefully in the kinds of experiments better suited to turbulence modeling — fully-developed turbulent channel- or pipe-flow experiments — in order to test and refine prediction schemes for unsteady turbulent flow.

There are also areas in which the imposition of controlled unsteady flow might prove useful. The effectiveness of organized unsteady flow in augmenting surface heat-transfer rates merits careful investigation, as does the notion that boundary-layer flows on the point of separating might be stabilized through local initiation of an organized, unsteady event. A thorough understanding of the behavior of turbulent flow under unsteady conditions would form the basis for such research.

References

ACHARYA, M. & REYNOLDS, W. C. 1975 Measurements and predictions of a fully developed turbulent channel flow with imposed controlled oscillations. *Report TF-8*, Department of Mechanical Engineering, Stanford University, Stanford, California.

ANDERSEN, P.S. 1972 The turbulent boundary layer on a porous plate: an experimental study of the fluid mechanics for adverse free-stream pressure gradients. Ph.D. Thesis (*Report HMT-15*), Department of Mechanical Engineering, Stanford University, Stanford, California.

BARLOW, R. S. & JOHNSTON, J. P. 1985 Structure of turbulent boundary layers on a concave surface. *Report MD-47*, Department of Mechanical Engineering, Stanford University, Stanford, California.

BINDER, G. & KUENY, J. L. 1981 Measurements of the periodic velocity oscillations near the wall in unsteady turbulent channel flow. *Third Symposium on Turbulent Shear Flows*, The University of California, Davis, California.

BINDER, G., TARDU, S., BLACKWELDER, R. F. & KUENY, J. L. 1985 Large amplitude periodic oscillations in the wall region of a turbulent channel flow. *Fifth Symposium on Turbulent Shear Flows*, Cornell University, Ithaca, New York.

BLONDEAUX, P. & COLOMBINI, M. 1985 Pulsatile turbulent pipe flow. *Fifth Symposium on Turbulent Shear Flows*, Cornell University, Ithaca, New York.

BRACEWELL, R. N. 1978 *The Fourier transform and its applications*. McGraw-Hill, New York.

BRERETON, G. J., REYNOLDS, W. C. & CARR, L. W. 1985 Unsteady turbulent boundary layers: some effects of abrupt free-stream velocity changes. *Fifth Symposium on Turbulent Shear Flows*, Cornell University, Ithaca, New York.

BUCHAVE, P., GEORGE, W. K. & LUMLEY, J. L. 1979 The measurement of turbulence with the laser-Doppler anemometer. *Ann. Rev. Fluid Mech.* **11**, 443.

CHOU, P. Y. 1945 On velocity correlations and the solutions of the equations of turbulent fluctuation. *Quart. Appl. Math.* **3**, 38

COLES, D. E. 1968 The young person's guide to the data. *Proc. Computation of Turbulent Boundary Layers - 1968 AFOSR-IFP-Stanford conference* **2**, Department of Mechanical Engineering, Stanford University, Stanford, California.

COOK, W. J., MURPHY, J.D. & OWEN, F.K. 1985 An experimental and computational study of turbulent boundary layers in oscillating flows. *Fifth Symposium on Turbulent Shear Flows*, Cornell University, Ithaca, New York.

COUSTEIX, J., DESOPPER, A. & HOUDEVILLE, R. 1977 Structure and development of a turbulent boundary layer in an oscillatory external flow. *Proc. Symposium on Turbulent Shear Flows*, Penn. State University, University Park, Pennsylvania.

COUSTEIX, J. & HOUDEVILLE, R. 1983 Couches limites instationnaires. *Rapport Technique 53/2259 AND*, Departement d'Etudes et de Recherches en Aerothermodynamique, Centre d'Etudes et de Recherches de Toulouse, Toulouse.

COUSTEIX, J. & HOUDEVILLE, R. 1985 Turbulence and skin friction evolutions in an oscillating boundary layer. *Fifth Symposium on Turbulent Shear Flows*, Cornell University, Ithaca, New York.

CUTLER, A. D. & JOHNSTON, J. P. 1984 Adverse pressure gradient and separating turbulent boundary-layer flows: the effect of disequilibrium in initial conditions. *Report MD-46*, Department of Mechanical Engineering, Stanford University, Stanford, California.

DURST, F., MELLING, A. & WHITELAW, J. H. 1981 *Principles and practice of laser-Doppler anemometry*. Academic Press, London.

EATON, J. K. & JOHNSTON, J. P. 1980 Turbulent flow reattachment: an experimental study of the flow and structure behind a backward-facing step. *Report MD-39*, Department of Mechanical Engineering, Stanford University, Stanford, California.

HINZE, J. O. 1981 *Turbulence*. McGraw-Hill, New York.

HUSSAIN, A. K. M. F. & REYNOLDS, W. C. 1970 The mechanics of an organized wave in turbulent shear flow. *J. Fluid Mech.* **41**, 241.

JAYARAMAN, R., PARIKH, P. & REYNOLDS, W. C. 1982 An experimental study of the dynamics of an unsteady turbulent boundary layer. *Report TF-18*, Department of Mechanical Engineering, Stanford University, Stanford, California.

KARLSSON, S. K. F. 1959 An unsteady turbulent boundary layer. *J. Flui Mech.* **5**, 622.

KEBEDE, W., LAUNDER, B. E. & YOUNIS, B. A. 1985 Large-amplitude periodic pipe flow: a second-moment closure study. *Fifth Symposium on Turbulent Shear Flows*, Cornell University, Ithaca, New York.

KENISON, R. C. 1977 An experimental study of the effect of oscillatory flow on the separation region in a turbulent boundary layer. *AGARD-CP-277* **20**.

KLEBANOFF, P. S. 1955 Characteristics of turbulence in a boundary layer with zero pressure gradient. *NACA Report 1247*.

KLINE, S.J. & McCLINTOCK, F. A. 1953 Describing uncertainties in single-sample experiments. *Mech. Engrg.* **75**, 3.

KLINE, S.J., REYNOLDS, W.C., SCHRAUB, F.A. & RUNSTADLER, P. W. 1967 The structure of turbulent boundary layers. *J. Fluid Mech.* **30**, 741.

KOBASHI, Y. & HAYAKAWA, M. 1981 Structure of a turbulent boundary layer on an oscillating flat plate. *Proc. IUTAM Symposium on Unsteady Turbulent Shear Flows*, Springer Verlag, 67.

LAUFER, J. 1954 The structure of turbulence in fully developed pipe flow. *NACA Technical Note 2954*.

LAUNDER, B. E., REECE, G. J. & RODI, W. 1975 Progress in the development of a Reynolds-stress turbulence closure. *J. Fluid Mech.* **68**, 537.

LIGHTHILL, M. J. 1954 The response of laminar skin friction and heat transfer to fluctuations in stream velocity. *Proc. Roy. Soc. London* A, **224**, 1.

MAO, Z. -X. & HANRATTY, T. J. 1985 Studies of the wall shear stress in a turbulent pulsating pipe flow. *Fifth Symposium on Turbulent Shear Flows*, Cornell University, Ithaca, New York.

MENENDEZ, A.N. & RAMAPRIAN, B. R. 1982 Calculation of unsteady boundary layers. *Report 248*, Iowa Institute of Hydraulic Research, The University of Iowa, Iowa City, Iowa.

MENENDEZ, A. N. & RAMAPRIAN, B. R. 1983 Study of unsteady turbulent boundary layers. *Report 270*, Iowa Institute of Hydraulic Research, The University of Iowa, Iowa City, Iowa.

PATEL, M. H. 1977 On turbulent boundary layers in oscillatory flow. *Proc. R. Soc. London* A, **353**, 121.

PEDLEY, T. J. 1976 Heat transfer from a hot film in a reversing shear flow. *J. Fluid Mech.* **78**, 518.

RAMAPRIAN, B. R. & TU, S. W. 1979 Experiments on transitional oscillatory pipe flow. *Report 221*, Iowa Institute of Hydraulic Research, The University of Iowa, Iowa City, Iowa.

RAMAPRIAN, B. R. & TU, S. W. 1982 Study of periodic turbulent pipe flow. *Report 238*, Iowa Institute of Hydraulic Research, The University of Iowa, Iowa City, Iowa.

REYNOLDS, W.C. & CARR, L. W. 1985 Review of unsteady, driven, separated flows. *AIAA Pap. 85-0527.*

RUCK, B. 1984 LDA-signal triggering and effective particle size range. *Sonderforschungsbereich 210/E/5*, Universität Karlsruhe.

SCHACHENMANN, A. A. & ROCKWELL, D. O. 1976 Oscillating turbulent flow in a conical diffuser. *J. Fluids Eng., Trans. ASME* **98**, 695.

SCHUBAUER, G. B. 1954 Turbulent processes as observed in boundary layer and pipe. *J. Appl. Phys.* **25**, 188.

STOKES, G. G. 1851 On the effect of the internal friction of fluids on the motion of pendulums. *Camb. Trans.* ix **8** [*Papers*, iii. 1].

TENNEKES, H. & LUMLEY, J.L. 1972 *A first course in turbulence.* M.I.T. Press, Cambridge, Mass.

TU, S. W. & RAMAPRIAN, B. R. 1983 Fully developed periodic turbulent pipe flow. Part 1. Main experimental results and comparison with prediction. *J. Fluid Mech.* **137**, 31.

WILCOX, D. C. 1986 Multiscale model for turbulent flows. *AIAA Pap. 86-0029.*

WILCOX, D. C. 1987 Advanced applications of the multiscale model for turbulent flows. *AIAA Pap. 87-0290.*

Appendix A

Estimation of Kolmogoroff Scales

The Kolmogoroff microscales of length, time and velocity are defined as:

$$\eta = (\nu^3/\epsilon)^{1/4} , \qquad \tau = (\nu/\epsilon)^{1/2} \qquad \text{and} \qquad v = (\nu\epsilon)^{1/4} ,$$

where ν is the kinematic viscosity of the fluid and ϵ represents the viscous dissipation of turbulent energy (see, for example, Tennekes & Lumley, §1.5). Their sizes may be estimated by making use of order-of-magnitude assumptions about terms in the turbulent energy budget, which suggest that the production and dissipation terms are of comparable magnitude in many shear flows (*ibid.*, §3.2). The size of the viscous dissipation, ϵ, may then be approximated as $-\overline{u'v'}(\partial U/\partial y)$, which is often the dominant production term.

The estimation procedure adopted here was to supply the velocity-gradient data and a friction-velocity measure from a local profile of the mean streamwise velocity; these measurements were usually not difficult to make and they rarely suffered from deficiencies that would cause appreciable errors when used for order-of-magnitude estimates. The corresponding values of $-\overline{u'v'}$ were taken from the flat-plate, boundary-layer measurements of Schubauer (1954), which were rescaled according to the local value of u_τ.

In Table A–1, the values of $\partial U/\partial y$ are for the steady, flat-plate, turbulent boundary layer measured at $X' = 0.63$; the Reynolds number, based on momentum thickness, was 3115. From a "log-law" fit to the velocity profile (Figure 4.7), u_τ was found to be 28.62 mm/sec. The kinematic viscosity, ν, was 1.1 mm^2/sec. Here f_K is the Kolmogoroff frequency, ν/η^2.

TABLE A-1

Tabulated Data for Microscale Evaluation

y^+	$-\overline{u'v'}/u_\tau^2$	$\partial U/\partial y$	η	f_K
		sec^{-1}	mm	sec^{-1}
4.7	0.12	715	0.11	82
6.0	0.20	690	0.10	106
7.3	0.28	694	0.09	126
8.7	0.34	510	0.09	118
10.0	0.42	453	0.07	193
11.3	0.50	355	0.09	120
13.3	0.61	337	0.09	129
16.7	0.70	248	0.09	123
20.0	0.78	179	0.10	106
24.6	0.86	119	0.10	100

Appendix B

Overview of Two-Component Laser-Doppler Anemometry

Laser-Doppler anemometry is a technique for measurement of turbulent fluid velocities which is still growing in acceptance and popularity. Therefore background information on the technique is provided for the interested reader. This information forms the basis for selection of the particular system used in this study, which is described in §3.2.

Two-component, laser-Doppler anemometry may be treated as an extension of its one-component counterpart. The interference pattern of two intersecting beams of monochromatic light, from a coherent source, is often termed a *fringe pattern*. This interference pattern can be thought of as taking the shape of an ellipsoid, in which wave fronts reinforce and cancel each other to form *fringes* of alternate strong and weak light intensity (Figure B.1). If such an interference pattern were projected in a moving fluid, discrete particles in the fluid would scatter light of alternating intensity as they were convected through the interference region.

The frequency of scattered light may be measured by monitoring the strength of these scattered-light signals with a photo-multiplier tube and a frequency analyzer; it is directly proportional to the velocity of the particle, which may then be obtained from the relationship $\mathbf{u} = f\lambda/(2\sin\kappa)$. Here λ is the wavelength of the monochromatic light and κ is the half angle of intersection of the beams. This system, however, has no directional sensitivity — if it were used in a turbulent reversing flow, the positive and negative parts of its frequency spectrum would overlap. In this context, the frequency spectrum means the velocity distribution function scaled according to the $\mathbf{u}$–f relationship given earlier. It should not be confused with the power spectrum, in which the energy content at different frequencies is expressed through Fourier analysis of a sampled record of data.

The shortcoming in directional sensitivity is resolved by separating the frequency spectra, increasing the frequency of one beam relative to the other (Figure B.2). This operation is termed *frequency shift* and is performed with an acousto-optic modulator, or Bragg cell; it typically changes the frequency of one beam by 40 megahertz, a value which assures efficient refraction of the shifted beam when commercially-available quartz crystals are used in Bragg cells. With the addition of frequency shift to a two-beam anemometer, a stationary particle would then scatter light at the shift frequency. The principles underlying the operation of this kind of dual-beam system are treated rigorously in Durst *et al.* (1981) and Buchave *et al.* (1979).

A one-component system enables velocity measurements to be made in the plane of the two beams, in the direction normal to the bisector of the beams (Figure B.1). To extend this method to measure two components of velocity at a point, a second coincident interference pattern of appropriate orientation must be formed and the scattered light from each pattern must be distinguished easily. It may be done in several ways:

(*i*) Using a monochromatic light source, two pairs of beams, of orthogonal polarity, may be focused to intersect at coincident points. If light scattered from the interference patterns can be assumed to retain its incident polarity, then, by separating the resultant scattered light according to the original, orthogonal components of polarity, the signals from the two interference patterns may be distinguished. The process of light scattering by particles, however, is extremely complex; light is not necessarily scattered at its incident polarity and *cross-talk* problems may result.

(*ii*) Light scattered from two coincident interference patterns, of the same color, may be clearly distinguished by frequency separation if one beam of each pair is shifted in frequency by a different amount. The difference between shift frequencies must be considerably greater than the bandwidths of the

frequency spectra of either scattered-light signal to assure proper separation of the spectra by electronic filtering. In practice, the unshifted beam in each pair is replaced by a single beam.

(*iii*) If the light in each interference pattern is of a different color, the resultant scattered light may be differentiated by color filtering. This technique usually requires a laser which operates in multi-line mode and optics, for separation of the transmitted beam into two pairs of beams of different colors. If a multi-line laser is used, the role of one beam in each pair may be played by a single beam of both colors (*i.e.* a multi-line beam, as produced by the laser). If the separation of light into the desired colors is imperfect, however, cross-talk problems may result.

Of the options described above, the method of color separation was the most practicable for this study and will be considered in greater detail.

The usual choice of coherent, multi-line, continuous wave, light source is an argon-ion laser. It produces visible light at high power levels and has up to ten lasing wavelengths in the blue and green portions of the spectrum. The most prominent and most used wavelengths are the 514.5 nm. green line and the 488.0 nm. blue line. For an argon-ion laser operating in multi-line TEM_{00} mode, with a typical set of reflectors installed, about 50% and 40% of the total power might be produced at these wavelengths respectively.

In the transmitting optics, color separation is commonly achieved either by prisms or by dichroic mirrors. When performed correctly, the prismatic method should result in efficient and complete separation of the green and blue lines of the incident beam into two separate beams of these colors. However, placement of the necessary prisms and mirrors can take up considerable space; where constraints are made on the size of an optical system, color separation by dichroic mirrors may be preferred. The components required for this technique can usually be mounted in line with other optical components and can be much more compact. The levels of

efficiency and quality of color separation achieved by dichroic means, however, are not comparable. While about 80% of the incident light is transmitted, typically 1% of the green beam is blue and 1% of the blue beam is green. When the operation of the laser is not stable, the power levels of the blue and green lines may vary considerably; consequently the proportions of contaminant colors in the blue and green beams may reach disturbingly high values. Highly stable laser performance is therefore critical to the successful separation of colors by dichroic means.

Color separation in the receiving optics is usually carried out in two stages. First a dichroic mirror is employed to transmit most of the scattered green light in one direction and to reflect a large proportion of the blue scattered light in another. Both colors of scattered light will contain some contamination from the other through the imperfections of dichroic separation. In the second stage, color filters of narrow bandwidth are used in an effort to eliminate any cross-talk. If the levels of power in each color are equal, the band-pass filters characteristically transmit 80% of the desired color and less than 1% of the contaminant color. When the power level of one color is much higher than the other, a significant amount of the undesired color may be transmitted and this may cause cross-talk. A disproportionate ratio of power levels in each color may result from unstable laser operation, poor alignment of the transmitting optics, unstable Bragg-cell performance, intermittent obstruction of one beam or from wavelength-dependent reflections or refractions anywhere along the entire optical path. It is therefore advisable to take additional precautions to ensure that the risk of cross-talk is minimized.

A fluid which is perfectly homogeneous in composition will not scatter a significant amount of light as it flows through an optical interference pattern. The processes of Rayleigh scattering, from molecules, and Thompson scattering, from free electrons, are too weak to be useful for these measurement purposes; so is Mie scattering from micron-sized particles. Stronger signals are provided by refraction and reflection of light by larger, discrete, inhomogeneous particles which are either naturally present in the fluid or introduced by design (*i.e.* by seeding). While it

is desirable for these particles to provide as bold a scattered-light signal as possible, it is imperative that they faithfully follow the small-scale motions of the fluid. They must be of sufficiently small size that turbulent forces are not averaged out on their surfaces. Particles in a fluid will usually have a distribution of sizes and the effective signal-to-noise ratios of particles of different sizes will depend upon the signal-processing procedure adopted (Ruck 1984). The suitability of particular seeding particles should therefore be justified by experiment — comparisons between measurements in standard flows and reference data may help to establish whether a particular seeding is satisfactory.

The accuracy with which a laser-Doppler anemometer can make meaningful velocity measurements may depend on the spatial resolution of the system. If the dimensions of the *probe volume* (the interference pattern) are too large, measurements may suffer from spatial-averaging effects. Spatial resolution may be improved in several ways:

(*i*) The *measuring volume* (the image of the probe volume projected through the receiving optics) may be reduced by judicious placement of a pinhole of the desired size in the receiving optics. It may be further reduced by positioning the receiving optics at right angles to the major axis of the probe volume (*i.e.* in side scatter), though the intensity of scattered light in this direction is relatively weak.

(*ii*) The probe volume may be reduced in size, with a corresponding increase in concentration of power, by expanding the diameters and separation of the transmitted beams. When subsequently focused, they will intersect with smaller waists and thus form a smaller probe volume. This technique is known as *beam expansion*.

Barlow & Johnston (1985) reported velocity measurements in turbulent flow for which agreement with reference data could be reached only when the spatial resolution was made comparable to the local Kolmogoroff length scale. Other re-

quirements which had to be satisfied included a data rate and sampling frequency significantly greater than the Kolmogoroff frequency, and a sufficiently large number of samples.

An alternative method for addressing the problem of spatial averaging, without any change in the resolution of the optics, is to selectively process velocity data. Velocities, deduced from the scattered light of the two colors, are considered representative if and only if the signals are detected by both frequency analyzers at times coincident to within a small, selectable interval (in an effort to ensure that both signals are from light scattered by the same particle). If data rates are low, this technique is useful too. Since frequency analyzers "hold" their outputs at the value of the last validated signal, until new data is received, a simultaneous sample of the outputs of two frequency analyzers may not result in simultaneous fluid-velocity measurements unless the signals were detected at coincident times. However, when used with large measuring volumes in which many particles are simultaneously present, signals coincident in time may still be detected from distant particles and so spatial-averaging effects may prevail (Barlow & Johnston 1985).

A signal-conditioning feature incorporated in most systems with frequency shift is a *downmixer*. In the case of turbulent reversing flow, a Bragg cell is often included in a measurement system to enable the direction of the flow to be resolved. The measured frequency spectrum will then usually be centered around the shift frequency (40 megahertz) with a comparatively narrow bandwidth. Since small changes in frequency, relative to 40 megahertz, may be difficult for a frequency analyzer to measure accurately, the frequencies of scattered light are then shifted back down again, or downmixed, by *almost* 40 megahertz — the *downmix frequency*; mixing is achieved through an analog electronic process. The *effective frequency shift* is then the difference between 40 megahertz and the downmix frequency; it must be large enough to separate the positive and negative parts of the frequency spectrum.

To achieve a small, effective shift in frequency, the combination of an acousto-optical shift with a Bragg cell driven at 40 megahertz and an electronic shift with downmixing circuitry of almost equal size may not appear to be an elegant choice. Currently, it is considerably less expensive than other options such as :

(*i*) using two Bragg cells in series to shift the frequency of a beam first up by 40 megahertz and then down by almost 40 megahertz,

(*ii*) using two Bragg cells in parallel to shift one beam up in frequency by 40 megahertz and the other up in frequency by almost 40 megahertz,

(*iii*) using a custom-made Bragg cell which can operate at the desired, effective frequency shift.

This method is also more efficient in producing the desired frequency-shifted output than other means such as diffraction gratings.

Some of the requirements of a reliable, two-component, optical, velocity measurement system may be formulated from these general observations on the art of laser-Doppler anemometry. Many optical parameters and instrument settings must be carefully chosen to suit the individual features of the flow under study. In §3.2 these details are considered and the measurement system is described.

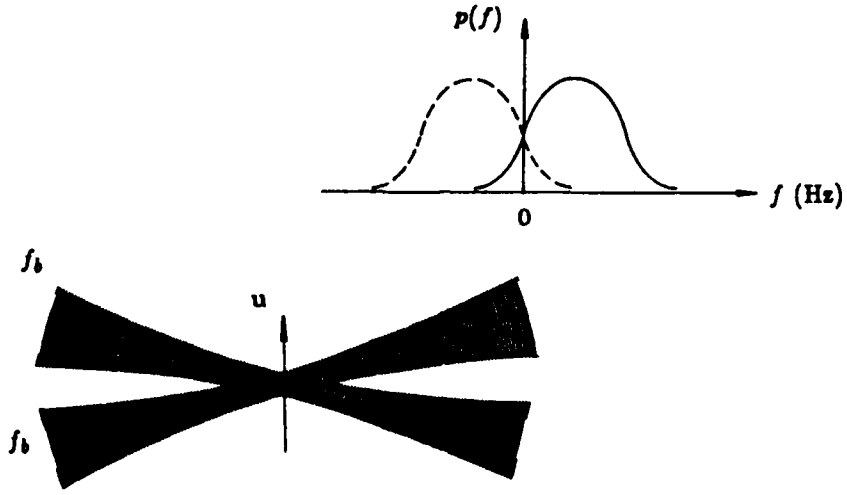

Figure B.1 Two-beam laser-Doppler anemometry system.

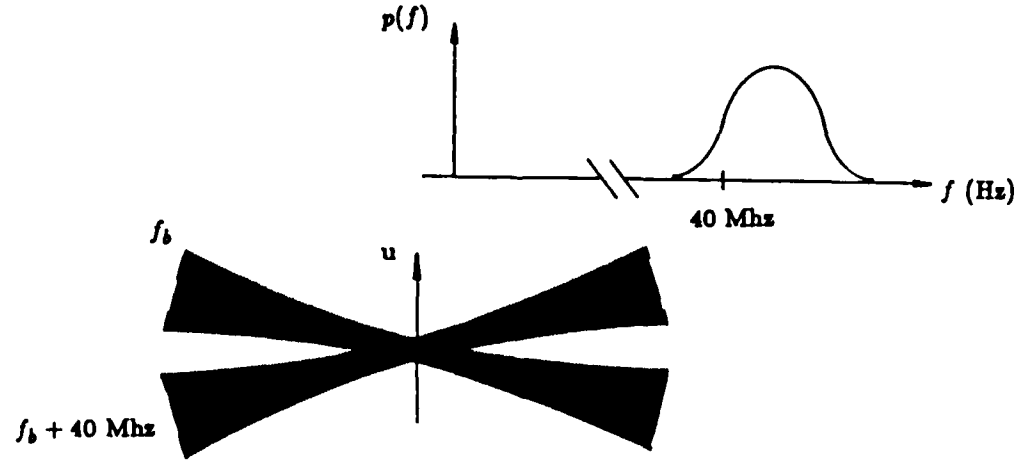

Figure B.2 Two-beam laser-Doppler anemometry system with frequency shift.

Appendix C

Optical System Alignment

Alignment details specific to the TSI components employed in the velocity measurement system are considered in this appendix. Most of the techniques are explained in the manufacturer's manuals, but the particular methods found useful for this study are presented here for completeness.

The initial alignment of the transmitting optics was carried out as recommended — the required optical modules were built onto the transmitting-optics train sequentially, moving along the optical axis away from the laser. As each component was added, the axis of polarization was checked and the power in each beam was measured and recorded for future reference. After the addition of each component to the optical train, the alignment was checked and corrected when adjustment was necessary.

To achieve peak power output from the Bragg cells, a power meter was found to be essential; once all beams but the shifted one had been masked off, the tilt angle of the plate supporting the cell could be adjusted methodically until the highest power level was observed — this peak corresponded to the correct orientation of the cell with respect to the incoming beam. Similarly, the amplitude of the voltage driving the acousto-optic modulator could be tuned to give optimal performance, as measured by the power meter. The correct alignment of the output beam (the shifted one) could then be achieved by adjusting the orientation of the steering wedges in the module.

The remainder of the transmitting optics could then be added in sequence. Two further beam-steering modules were included to allow minor changes in alignment to be made without affecting the color-separation or the frequency-shifting optics. They were positioned to allow steering of the two single-color beams, as the cyan beam could be independently steered by a pair of wedges in the color-separating

module in the optics train. It was necessary to ensure that all components were secured as tightly as possible to one another and to the breadboard. Otherwise, they tended to sag between their supports, with an accompanying degradation in output power as the optimum alignment was disturbed. All exposed mirrors were cleaned frequently and covered when not in use to prevent their gathering dust, which inhibited reflective efficiency.

This particular optical system was designed for making non-intrusive measurements in a water tunnel, the inside of which was not readily accessible when water was flowing. The front lens of the transmitting optics was positioned so that the focused beams would intersect at the desired point of measurement, *in water*. How, then, could one check that the beams intersected at the same point? It was not practical to maneuver a microscope objective to the point of intersection under remote control and thus project a magnified image for inspection. An alternative method was to make any necessary adjustments to the alignment of the transmitted beams to assure coincidence of the probe volumes *in air*. This approximation to the required alignment in water could then be improved upon using the receiving optics and frequency-analysis equipment. Alignment of an optical system in air for subsequent use in water can only be an approximation to the desired alignment in water, in such a two-color system, because of the dependence of the index of refraction on wavelength (dispersion).

The approximate alignment in air was carried out by placing a mirror just beyond the front lens, so that the beams would intersect above the breadboard. The point of intersection could then easily be magnified with a microscope objective and projected against a screen, so that coincidence of the beam intersections could be checked. Lack of coincidence could be remedied by adjustment of the appropriate pairs of wedges in the beam-steering modules. This alignment in air then served as a first iteration in the procedure for obtaining coincidence of the probe volumes in water.

The second stage of the alignment procedure was based on the premise that the optimum alignment produced the best scattered-light signal. Hence the data-validation rate of the frequency trackers could be used as an indication of the quality of alignment at any instant. The trackers used for these experiments could be set to display the current data-validation rate on a meter on the front of the instrument. Once the system was sufficiently well aligned that a Doppler signal could be continually tracked, an increase in the reading of this meter could be taken as an indication that an adjustment to the optical system had resulted in improved alignment.

To meet the requirements of spatial resolution for these experiments, a small pinhole was placed in the field-stop system in the receiving-optics train. By design, this pinhole was the limiting aperture in this part of the optical system. The correct positioning of this component and of the lenses in the receiving optics were then carried out using an alignment eyepiece, according to the manufacturer's instructions. The eyepiece was used to align one channel of the receiving optics (say, the blue channel), so that the resultant downmixed voltage signal from the photomultiplier tube could be tracked. Then adjustments were made methodically to all the alignment features of that channel in the receiving optics, until the best data-validation rate was achieved.

Having optimized the performance of the receiving optics for blue scattered light, a second iteration on the alignment of the transmitting optics could now be made. By careful adjustment of the position of the blue beam, while closely observing the data-validation rate, this beam could be aligned again to try to attain improved coincidence at the point of intersection of the beams and hence an enhanced data rate. The adjustment of the receiving optics could then be refined again and another iteration made, etc. This procedure should assure excellent alignment of the optical components used to transmit blue light in both the transmitting and receiving optics.

The inefficiency of dichroic separation of scattered light could now be used to advantage, to assure coincident interference patterns of both colors. The procedure was as follows:

(*i*) In the transmitting optics, the single-color beam, which had already been fully aligned (the blue beam), was masked off.

(*ii*) In the receiving optics of the blue channel, the color filter, which ostensibly transmitted no green light, was removed. With the equipment used for this study, it could be removed without disturbing the alignment.

(*iii*) The fully aligned (blue) channel of the receiving optics was now correctly positioned to receive only scattered light of the "wrong" color (green), of rather weak intensity but from the correct place. By careful re-alignment of the green beam in the transmitting optics only (the scattered light from which should now be tracked by the tracker for the blue channel), the data rate could again be optimized. In the absence of pronounced wavelength-dependent characteristics in the lenses and mirrors of the receiving optics (other than the color-separation parts), this alignment should correspond to coincidence of the probe volumes of the two colors, in water.

(*iv*) The color filter was then replaced in the receiving optics of the blue channel and a final adjustment was made to the position of the photomultiplier tube on the green channel of the receiving optics, to optimize the data rate of the tracked signal from green scattered light. The masked beam was then unmasked.

In practice, this alignment procedure worked well. Using green and blue light, the difference in wavelengths was small. The length of the optical path from the measuring volume to the photomultiplier tube was short (less than a meter) so that even if wavelength-dependent refraction in the lenses of the system was encountered, its effect might not be noticeable. To judge from the agreement between the

measurements and reference data presented in §4, this method of alignment was quite adequate for the purposes of this study.

Appendix D

Integral Vorticity Analyses for Unsteady Flow

Solutions to approximate forms of the vorticity integral equation may be used to predict the behavior of unsteady, turbulent, boundary-layer flows, when the unsteadiness is organized and can be described in analytic form. In this appendix, the vorticity integral equation is developed for nominally two-dimensional conditions and applied to the flow in reference experiments and in the experiment conducted in this study. The method of solution and the first analysis are modifications of an earlier work by Reynolds (in Reynolds & Carr 1985).

The vorticity equation for an incompressible Newtonian fluid of constant viscosity is (Tennekes & Lumley, §3.3):

$$\frac{\partial \omega_i}{\partial t} + \frac{\partial}{\partial x_k}(u_k \omega_i) = \frac{\partial}{\partial x_k}(\omega_k u_i) + \nu \frac{\partial^2 \omega_i}{\partial x_k \partial x_k} \ . \qquad (D.1)$$

For application to organized, unsteady, turbulent flow, it may be decomposed in the manner of (2.1.1) yielding:

$$\frac{\partial}{\partial t}(\Omega_i + \tilde{\omega}_i + \omega_i') + \frac{\partial}{\partial x_k}\Big[(U_k + \tilde{u}_k + u_k')(\Omega_i + \tilde{\omega}_i + \omega_i')\Big] =$$

$$\frac{\partial}{\partial x_k}\Big[(\Omega_k + \tilde{\omega}_k + \omega_k')(U_i + \tilde{u}_i + u_i')\Big] + \nu \frac{\partial^2}{\partial x_k \partial x_k}(\Omega_i + \tilde{\omega}_i + \omega_i') \ . \qquad (D.2)$$

The deterministic form of this equation is the only one sought and it is found by subtracting the time average of (D.2) from its phase average (as explained for the momentum equations in §2.2). The deterministic vorticity equation is then:

$$\frac{\partial \widetilde{\omega}_i}{\partial t} + \frac{\partial}{\partial x_k}\left(U_k\widetilde{\omega}_i + \widetilde{u}_k\Omega_i + \widetilde{\widetilde{u}_k\widetilde{\omega}_i} + \widetilde{\overline{u'_k\omega'_i}}\right) =$$

$$\frac{\partial}{\partial x_k}\left(\Omega_k\widetilde{u}_i + \widetilde{\omega}_k U_i + \widetilde{\widetilde{\omega}_k\widetilde{u}_i} + \widetilde{\overline{\omega'_k u'_i}}\right) + \nu\frac{\partial^2\widetilde{\omega}_i}{\partial x_k \partial x_k} \,. \qquad \text{(D.3)}$$

The assumption that the flow is uniform in the spanwise (z) direction is now made, together with the constraint that Ω_3 and $\widetilde{\omega}_3$ are the only non-turbulent vorticity terms of significant size. Setting $\Omega_3 = \Omega$ and $\widetilde{\omega}_3 = \widetilde{\omega}$, the deterministic vorticity equation of interest is:

$$\frac{\partial \widetilde{\omega}}{\partial t} + \frac{\partial}{\partial x_k}\left(U_k\widetilde{\omega} + \widetilde{u}_k\Omega + \widetilde{\widetilde{u}_k\widetilde{\omega}} + \widetilde{\overline{u'_k\omega'_3}}\right) = \frac{\partial}{\partial x_k}\left(\widetilde{\overline{\omega'_k u'_3}}\right) + \nu\frac{\partial^2\widetilde{\omega}}{\partial x_k \partial x_k} \,. \qquad \text{(D.4)}$$

This equation may be recast as the sum of the time derivative of deterministic vorticity and the divergence of deterministic vorticity flux:

$$\frac{\partial \widetilde{\omega}}{\partial t} + \frac{\partial}{\partial x_k}\left(U_k\widetilde{\omega} + \widetilde{u}_k\Omega + \widetilde{\widetilde{u}_k\widetilde{\omega}} + \widetilde{\overline{u'_k\omega'_3}} - \widetilde{\overline{\omega'_k u'_3}} - \nu\frac{\partial\widetilde{\omega}}{\partial x_k}\right) = 0 \,. \qquad \text{(D.5)}$$

The flux terms represent three kinds of unsteady convection of vorticity, two kinds of turbulent transport and unsteady viscous diffusion. Expansion of (D.5) from its tensorial form yields:

$$\frac{\partial \widetilde{\omega}}{\partial t} + \frac{\partial}{\partial x}\Big(U\widetilde{\omega} + \widetilde{u}\Omega + \widetilde{\widetilde{u}\,\widetilde{\omega}} + \widetilde{u'\omega_3'} - \widetilde{\omega_1' w'} - \nu\frac{\partial \widetilde{\omega}}{\partial x}\Big)$$

$$+\frac{\partial}{\partial y}\Big(V\widetilde{\omega} + \widetilde{v}\Omega + \widetilde{\widetilde{v}\,\widetilde{\omega}} + \widetilde{v'\omega_3'} - \widetilde{\omega_2' w'} - \nu\frac{\partial \widetilde{\omega}}{\partial y}\Big) = 0\ . \qquad \text{(D.6)}$$

It is now integrated, term by term, across the boundary layer. For the organized unsteady flows considered here, the free-stream boundary condition sets all integrated terms, which were partial derivatives with respect to y in (D.6), to zero (with the obvious exception of the diffusion term). The term, $\nu(\partial^2\widetilde{\omega}/\partial x^2)$, may be neglected on order-of-magnitude grounds leaving the vorticity integral equation as:

$$\frac{\partial}{\partial t}\int_0^\delta \widetilde{\omega}\,dy + \frac{\partial}{\partial x}\int_0^\delta \Big(U\widetilde{\omega} + \widetilde{u}\Omega + \widetilde{\widetilde{u}\,\widetilde{\omega}} + \widetilde{u'\omega_3'} - \widetilde{\omega_1' w'}\Big)\,dy + \nu\frac{\partial \widetilde{\omega}}{\partial y}\Big|_{y=0} = 0\ . \qquad \text{(D.7)}$$

The turbulent transport terms may be simplified further by writing their vorticity terms as gradients of velocity:

$$\widetilde{u'\omega_3'} - \widetilde{\omega_1' w'} = \widetilde{u'\frac{\partial v'}{\partial x}} - \widetilde{u'\frac{\partial u'}{\partial y}} - \widetilde{w'\frac{\partial w'}{\partial y}} = \frac{\partial}{\partial x}(\widetilde{u'v'}) + \frac{\partial}{\partial y}\Big(\frac{\widetilde{v'v'}}{2} - \frac{\widetilde{u'u'}}{2} - \frac{\widetilde{w'w'}}{2}\Big)\ .$$

Integration across the boundary layer removes all the turbulent transport terms except the streamwise derivative of the perturbation Reynolds stress. The vorticity integral equation may then be applied to unsteady, boundary-layer flows in the following form:

$$\frac{\partial}{\partial t}\int_0^\delta \tilde{\omega}\, dy + \frac{\partial}{\partial x}\int_0^\delta \left[U\tilde{\omega} + \tilde{u}\Omega + \widetilde{\tilde{u}\,\tilde{\omega}} + \frac{\partial}{\partial x}(\widetilde{u'v'})\right] dy + \nu\frac{\partial\tilde{\omega}}{\partial y}\Big|_{y=0} = 0\,. \qquad \text{(D.8)}$$

The equation is applied first to the flow in the experiments conducted by Karlsson (1959) and Cousteix & Houdeville (1983). In both studies, a boundary layer was formed at a leading edge in an unsteady mainstream; the boundary layer subsequently developed, bounded by this unsteady mainstream, and strong spatial periodicity in the phase and amplitude of the displacement thickness was observed.

For these experiments, the amplitude of the free-stream perturbation was small compared to the mean, free-stream velocity. By approximating the convective flux terms of (D.8) as $-U(\partial\tilde{u}/\partial x) - \tilde{u}(\partial U/\partial y) - \tilde{u}(\partial\tilde{u}/\partial y) + \widetilde{\tilde{u}(\partial\tilde{u}/\partial y)}$, the relative magnitudes of each term may be compared. Assuming the magnitudes of velocity within the boundary layer are of the same order as their free-stream counterparts, the third and fourth terms are small compared to the first. The convective flux may then be represented by the term $-\partial(U\tilde{u})/\partial y$. If it is further contended that, over the bulk of the boundary layer, the convection velocity (U) of organized unsteady fluid ($\tilde{u}$) is approximately constant (U_c) and that the contribution of the Reynolds stress is negligible, then the vorticity integral equation takes the form:

$$\frac{\partial}{\partial t}\int_0^\delta \tilde{\omega}\, dy + U_c\frac{\partial}{\partial x}\int_0^\delta \tilde{\omega}\, dy + \nu\frac{\partial\tilde{\omega}}{\partial y}\Big|_{y=0} = 0 \qquad \text{(D.9)}$$

where U_c is the mean convection velocity of large eddies. Now the diffusion term may be evaluated by applying the streamwise momentum equation (2.2.8) at the wall. In the experiments of Karlsson and Cousteix & Houdeville, the wall was stationary with no transpiration. The simplified momentum equation is then:

$$0 = -\frac{1}{\rho}\frac{\partial \tilde{p}}{\partial x} + \nu \frac{\partial^2 \tilde{u}}{\partial y \partial y}\Big|_{y=0} \tag{D.10}$$

and obviously $$\nu \frac{\partial^2 \tilde{u}}{\partial y \partial y}\Big|_{y=0} = -\nu \frac{\partial \tilde{\omega}}{\partial y}\Big|_{y=0} .$$

The perturbation velocity in the free stream is given as $\tilde{u}_\infty = A \sin(2\pi f t)$ where A is the amplitude of oscillation and f the frequency. Applying the streamwise momentum equation (2.2.8) in the free stream yields:

$$\frac{\partial \tilde{u}_\infty}{\partial t} = -\frac{1}{\rho}\frac{\partial \tilde{p}}{\partial x} = 2\pi f A \cos(2\pi f t)$$

and hence $$\frac{\partial}{\partial t}\int_0^\delta -\tilde{\omega}\, dy + U_c \frac{\partial}{\partial x}\int_0^\delta -\tilde{\omega}\, dy = 2\pi f A \cos(2\pi f t) . \tag{D.11}$$

Application of the vorticity integral equation at the leading edge yields the boundary condition:

$$U_c \int_0^\delta -\tilde{\omega}\, dy = U_\infty \tilde{u}_\infty = A U_\infty \sin(2\pi f t) . \tag{D.12}$$

The vorticity integral equation, (D.11), with the boundary condition, (D.12), may then be solved for $\int_0^\delta -\tilde{\omega}\, dy$ by the method of characteristics. The solution is:

$$\int_0^\delta -\tilde{\omega}\, dy = A\left[\sin(2\pi ft) + \left(\frac{U_\infty}{U_c} - 1\right)\sin\left(2\pi ft - \frac{2\pi fx}{U_c}\right)\right]. \qquad \text{(D.13)}$$

Since the strongest measures of boundary-layer vorticity would be expected to correspond to the greatest values of boundary-layer thickness, the peak amplitudes of $\int_0^\delta -\tilde{\omega}\, dy$ should correlate with the experimentally measured peaks of boundary-layer thickness. Assuming that a typical convection velocity, U_c , is about $0.8\, U_\infty$, the greatest values of $\int_0^\delta -\tilde{\omega}\, dy$ would occur when:

$$\frac{2\pi fx}{U_c} = 2n\pi \quad \text{for} \quad n = 0,\, 1,\, 2,\, 3, \ldots \qquad \text{or} \qquad \frac{2\pi fx}{U_\infty} \simeq 0,\, 5,\, 10,\, 15, \ldots$$

Reference to Figure D.1 shows that, in the experiments of Karlsson and Cousteix & Houdeville, the peaks of δ_1 and δ_2 are remarkably close to the values predicted by this simple analysis — the spatially periodic nature of the boundary-layer thickness is due to the interaction between the unsteady vorticity convected downstream from the leading edge and the vorticity generated at the surface by the locally unsteady mainstream.

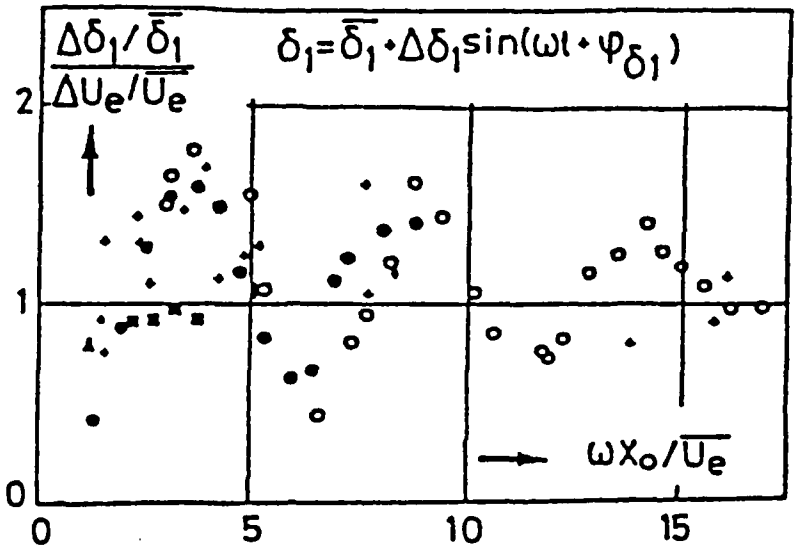

FIG. 8 - HARMONIC ANALYSIS OF DISPLACEMENT THICKNESS

• f = 38 Hz ○ f = 62 Hz ▲■ Earlier experiments f = 40 Hz f = 43 Hz
+ KARLSSON

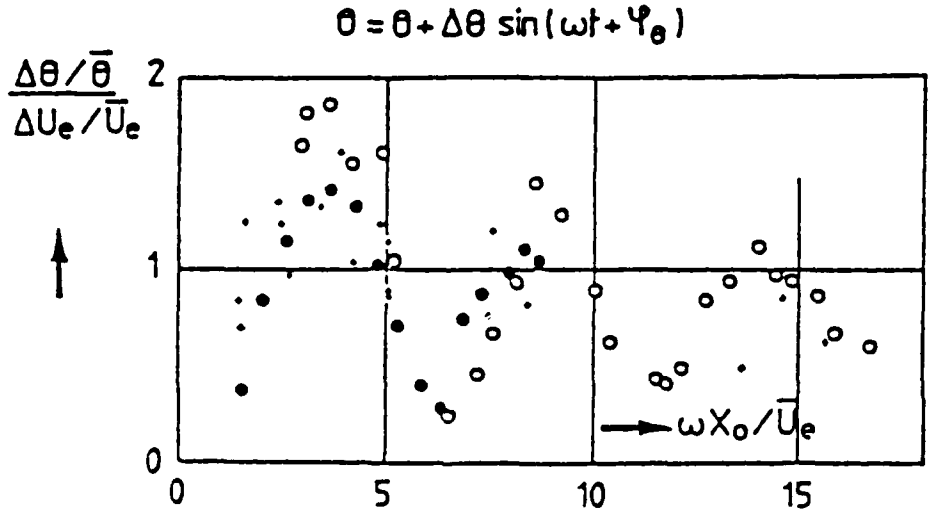

FIG. 9 - HARMONIC ANALYSIS OF MOMENTUM THICKNESS

• f = 38 Hz ○ f = 62 Hz + KARLSSON

Figure D.1 Normalized spatial variation of the amplitudes of δ_1 and δ_2 (from Cousteix & Houdeville, 1983).

The flowfield investigated in this study is now considered. This boundary layer developed under steady conditions and unsteadiness was introduced locally in the test section of the apparatus, as described in §3.1. The unsteady mainstream flow is expressed as:

$$U_\infty = U_0(1 - AX') \qquad \text{and} \qquad \tilde{u}_\infty = U_0 AX' \cos(2\pi f t) \ , \tag{D.14}$$

where U_0 is the steady, free-stream velocity along the development section and A is its amplitude of oscillation at the end of the test section, expressed as a fraction of U_0. Also, X' is defined as the dimensionless distance along the test section (of length L). Since A was reasonably small ($\sim$ 20%), the assumptions which led to the development of (D.9) from (D.8) are made and boundary conditions are sought to the equation:

$$\frac{\partial}{\partial t}\int_0^\delta \tilde{\omega}\, dy + U_c \frac{\partial}{\partial x}\int_0^\delta \tilde{\omega}\, dy + \nu \frac{\partial \tilde{\omega}}{\partial y}\Big|_{y=0} = 0 \tag{D.9}$$

The diffusion of vorticity at the wall is equated to the streamwise pressure gradient (D.10), which is deduced by applying the deterministic momentum equation (2.2.8) in the free stream. These procedures yield:

$$\nu \frac{\partial \tilde{\omega}}{\partial y}\Big|_{y=0} = -\frac{1}{\rho}\frac{\partial \tilde{p}}{\partial x} = \frac{\partial \tilde{u}_\infty}{\partial t} + \frac{\partial}{\partial x}(2\tilde{u}_\infty U_\infty + \widetilde{\tilde{u}_\infty \tilde{u}_\infty}) + \frac{\partial}{\partial y}(\tilde{u}_\infty V_\infty + U_\infty \tilde{v}_\infty + \widetilde{\tilde{u}_\infty \tilde{v}_\infty}) \ .$$

After careful consideration of the role of the v terms, via the continuity equation, (2.2.1), the vorticity-diffusion term is:

$$\nu \frac{\partial \tilde{\omega}}{\partial y}\Big|_{v=0} = \frac{\partial \tilde{u}_\infty}{\partial t} + \frac{\partial}{\partial x}(\tilde{u}_\infty U_\infty) + \frac{\partial}{\partial x}\Big(\widetilde{\frac{\tilde{u}_\infty \tilde{u}_\infty}{2}}\Big) \ . \qquad \text{(D.15)}$$

Substitution of the free-stream velocities, from (D.14), leads to the partial differential equation for $\int_0^\delta -\tilde{\omega}\, dy$:

$$\frac{\partial}{\partial t}\int_0^\delta -\tilde{\omega}\, dy + \frac{U_c}{L}(1 - AX')\frac{\partial}{\partial X'}\int_0^\delta -\tilde{\omega}\, dy = -2\pi f U_0 A X' L \sin(2\pi f t)$$

$$+ U_0^2 A(1 - 2AX')\cos(2\pi f t) + \frac{U_0^2}{2} A^2 X' \cos(4\pi f t) \ , \qquad \text{(D.16)}$$

with the boundary condition: $\displaystyle\int_0^\delta -\tilde{\omega}\, dy = 0 \qquad \text{at} \qquad X' = 0 \ .$

This equation may also be solved by the method of characteristics. By setting $\tilde{G}(X', t) = \int_0^\delta -\tilde{\omega}\, dy$ and choosing transformation characteristics:

$$\xi = t \qquad \text{and} \qquad \eta = \frac{e^{-AU_c t/L}}{1 - AX'} \ ,$$

the solution is: $\widetilde{G}(\xi,\eta) = U_0 L\cos(2\pi f\xi) - \left(\frac{U_0^2 A}{2\pi f}\right)\sin(2\pi f\xi) + \left(\frac{U_0^2 A}{8\pi f}\right)\sin(4\pi f\xi)$

$$+ \frac{e^{-AU_c\xi/L}}{(2\pi f)^2 + (AU_c/L)^2}\left(\frac{2U_0^2 A}{\eta}\right)\left(2\pi f\sin(2\pi f\xi) - \frac{AU_c}{L}\cos(2\pi f\xi)\right)$$

$$- \frac{e^{-AU_c\xi/L}}{(2\pi f)^2 + (AU_c/L)^2}\left(\frac{2\pi f U_0 L}{\eta}\right)\left(\frac{AU_c}{L}\sin(2\pi f\xi) + 2\pi f\cos(2\pi f\xi)\right)$$

$$- \frac{e^{-AU_c\xi/L}}{(4\pi f)^2 + (AU_c/L)^2}\left(\frac{U_0^2 A}{2\eta}\right)\left(4\pi f\sin(4\pi f\xi) - \frac{AU_c}{L}\cos(4\pi f\xi)\right) + \widetilde{F}(\eta)\ .$$

Finally $\widetilde{F}$ is deduced from the boundary condition that $\widetilde{G} = 0$ at $X' = 0$.

The amplitude of the function $\widetilde{G}(X',t)$ was computed and plotted as a function of X' for the various frequencies at which this experiment was conducted. The convection velocity of large eddies, U_c , was again assumed to be $0.8\,U_\infty$. The estimated streamwise variation in amplitude of $\widetilde{G}$ is shown in Figure D.2. From this approximate analysis, it would seem that the amplitude of vorticity generated by oscillation in the local adverse-pressure gradient is much more significant than any spatial variation produced by interaction between convected and locally generated vorticity.

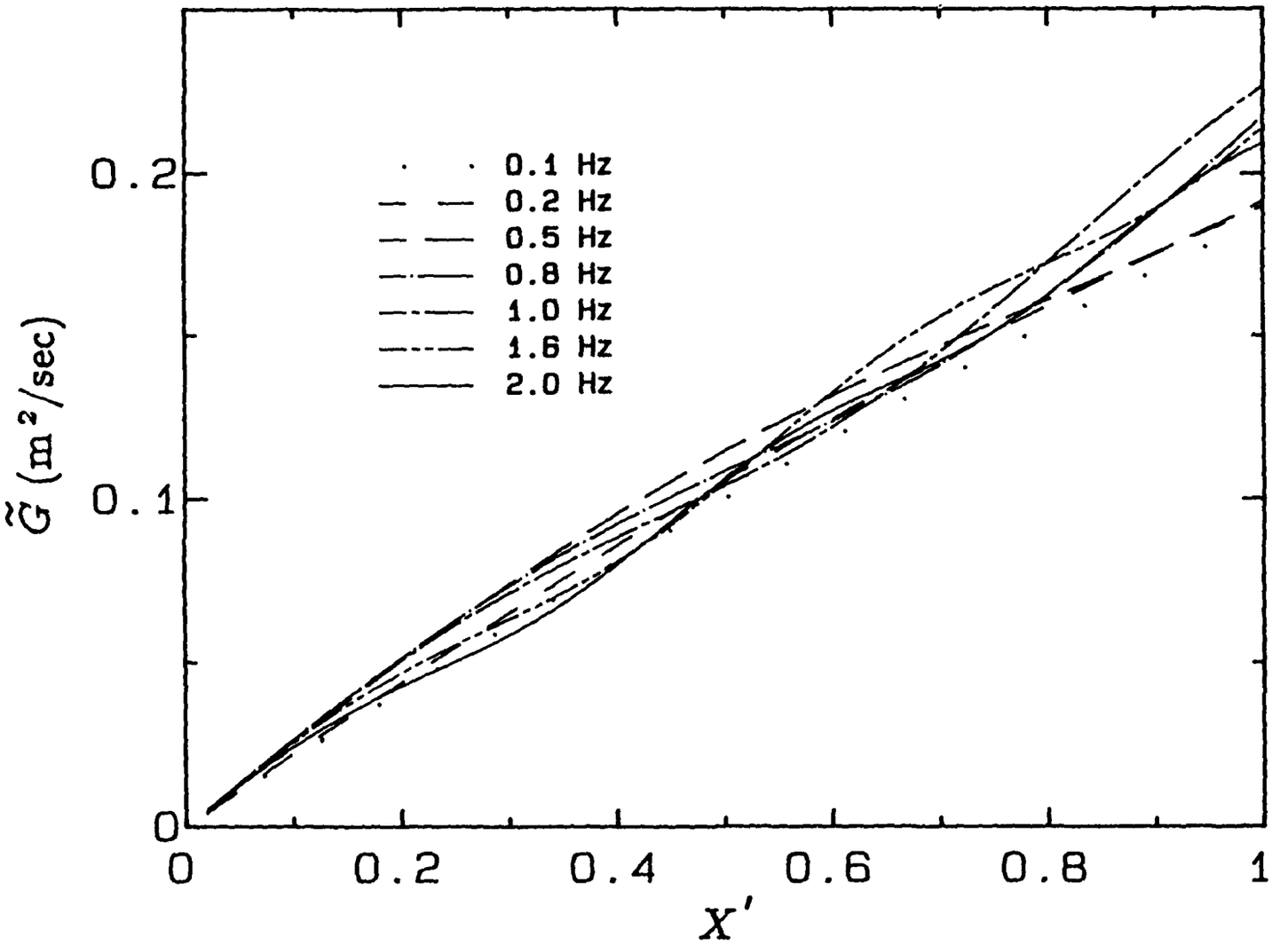

Figure D.2 Spatial variation of the amplitude of the boundary-layer vorticity, for different frequencies of imposed, organized unsteadiness.

Appendix E

Stokes Solution for the Organized Unsteady Flow

A Stokes solution is the name commonly given to a solution of the differential momentum equation which describes the asymptotic, high-frequency behavior of an unsteady flow. For simple boundary conditions the solution often takes an analytic form, from which the high-frequency, organized behavior of the flow may be clearly discerned.

The asymptotic, high-frequency form is first devised through order-of-magnitude considerations of terms of the deterministic momentum equation, which is:

$$\frac{\partial \widetilde{u}_i}{\partial t} + \frac{\partial}{\partial x_k}(U_k \widetilde{u}_i + \widetilde{u}_k U_i) = -\frac{1}{\rho}\frac{\partial \widetilde{p}}{\partial x_i} - \frac{\partial}{\partial x_k}(\widetilde{u'_k u'_i} + \widetilde{\widetilde{u}_k \widetilde{u}_i}) + \nu \frac{\partial^2 \widetilde{u}_i}{\partial x_k \partial x_k} , \qquad \text{(E.1)}$$

as derived in §2.2. The x-momentum equation is considered first and is written as:

$$\frac{\partial \widetilde{u}}{\partial t} + \frac{\partial}{\partial x_k}(U_k \widetilde{u} + \widetilde{u}_k U + \widetilde{u'_k u'} + \widetilde{\widetilde{u}_k \widetilde{u}}) = -\frac{1}{\rho}\frac{\partial \widetilde{p}}{\partial x} + \nu \frac{\partial^2 \widetilde{u}}{\partial x_k \partial x_k} . \qquad \text{(E.2)}$$

For high frequencies of organized unsteadiness, at which the unsteady term, $\partial \widetilde{u}/\partial t$, is much greater than the convective terms, $\partial(U_k \widetilde{u} + \widetilde{u}_k U + \widetilde{u'_k u'} + \widetilde{\widetilde{u}_k \widetilde{u}})/\partial x_k$, the Stokes equation is formed:

$$\frac{\partial \widetilde{u}}{\partial t} = -\frac{1}{\rho}\frac{\partial \widetilde{p}}{\partial x} + \nu \frac{\partial^2 \widetilde{u}}{\partial y \partial y} . \qquad \text{(E.3)}$$

The streamwise dissipation term is negligible compared to its normal component and so has been neglected. This problem may also be viewed as one of unsteady diffusion of vorticity since similar treatment of the deterministic, spanwise, vorticity equation yields:

$$\frac{\partial \tilde{\omega}}{\partial t} = \nu \frac{\partial^2 \tilde{\omega}}{\partial y \partial y} .$$

Before proceeding with the solution to the Stokes equation, the conditions under which the unsteady term greatly exceeds the convective ones are examined. The dominant convective terms are first deduced from order-of-magnitude considerations. Of the four tensors in the expression $\partial(U_k\tilde{u} + \tilde{u}_k U + \widetilde{u'_k u'} + \widetilde{\tilde{u}_k \tilde{u}})/\partial x_k$, the turbulent one may be assumed negligible in comparison to the others (although this assumption might be questionable for $\partial(\widetilde{u'v'})/\partial y$ near the wall). Since the amplitude of $\tilde{u}$ was not expected to exceed about 20% of U_∞ in these experiments, the unsteady correlation of the deterministic velocities, $\partial(\widetilde{\tilde{u}_k \tilde{u}})/\partial x_k$, could be considered small relative to the remaining convective terms: $\partial(U_k\tilde{u} + \tilde{u}_k U)/\partial x_k$. These terms may now be compared with the organized unsteady term to establish a criterion for which the Stokes solution for this flow might be followed.

Although the order-of-magnitude approach may be pursued further for this equation (see, for example, Jayaraman *et al.* 1982), there do not seem to be any obvious ways of estimating characteristic length, velocity or time scales for the unsteady boundary layer, other than to scale them on free-stream or global measures. Now in this experiment, many of the free-stream quantities were prescribed so that estimation of their size and behavior is unnecessary and might amount to discarding useful information. It therefore seemed more profitable to compare the free-stream values of the dominant unsteady and convective terms and to presume that their ratio was maintained, at least approximately, throughout the boundary layer.

In the free stream, the unsteady and convective terms are represented by $\partial\tilde{u}_\infty/\partial t$ and $\partial(U_\infty\tilde{u}_\infty)/\partial x$ respectively. Since $U_\infty = U_0(1 - AX')$ and $\tilde{u}_\infty = U_0 AX' \cos\omega t$, it follows that:

$$\left|\frac{\partial\tilde{u}_\infty}{\partial t}\right| = \omega U_0 AX' \qquad \text{and} \qquad \left|\frac{\partial}{\partial x}(U_\infty\tilde{u}_\infty)\right| = \frac{U_0^2 A}{L}(1 - 2AX') , \tag{E.4}$$

where X' is the dimensionless distance along the test section (of length L). The unsteady term greatly exceeds the convective ones when:

$$\frac{\omega X}{U_0} \gg 1 - 2AX' , \qquad \text{where} \qquad \frac{\omega X}{U_0} \qquad \text{is the relevant Strouhal number.}$$

Since the X dependence of the right-hand side of the inequality is weak ($A \simeq 20\%$), a Stokes solution would be expected when this Strouhal number greatly exceeds one, or alternatively, for the X locations at which data were taken, frequencies of imposed, organized unsteadiness are much larger than ~ 0.3 hertz. It is significant that a Strouhal number incorporating as its length scale X, the distance along the test section, results from this exercise. This dependence on X is a consequence of the design of the experiment such that the amplitude of $\tilde{u}_\infty$ is proportional to distance along the test section. As a criterion for determining whether Stokes flow is to be expected, it obviously has no relevance to flows with dissimilar distributions of velocity — such flows should be characterized according their particular boundary conditions. For example, for the case of unsteady, fully-developed, turbulent channel flow, the ratio of the centerline values of $\partial\tilde{u}/\partial t$ and $\partial(\overline{u'v'})/\partial y$ might serve as a suitable characteristic parameter.

The analytic solution for Stokes flow is now sought. The equation is:

$$\frac{\partial \widetilde{u}}{\partial t} = -\frac{1}{\rho}\frac{\partial \widetilde{p}}{\partial x} + \nu \frac{\partial^2 \widetilde{u}}{\partial y \partial y} \tag{E.3}$$

with boundary conditions: $\widetilde{u}(y,t) = 0$ when $y = 0$ and

$\widetilde{u}(y,t) = \widetilde{u}_\infty(t)$ when $y = \infty$. (E.5)

Order-of-magnitude considerations (Jayaraman *et al.* 1982) require that the deterministic y-momentum equation simplifies to $\partial \widetilde{p}/\partial y = 0$. Therefore, at any given x location, the pressure-gradient term in (E.3) is a function only of time. Moreover, the free-stream boundary condition dictates that the pressure gradient and the time-derivative of deterministic velocity share the same variation with time. Given these restrictions on the pressure-gradient term, a solution may be attempted by the method of separation of variables.

If the y and t dependence of $\widetilde{u}$ are represented by the functions $Y(y)$ and $T(t)$ respectively, such that $\widetilde{u}(y,t) = Y(y)\,T(t)$, then in the free stream:

$$\left.\frac{\partial \widetilde{u}}{\partial t}\right|_{y=\infty} = -\frac{1}{\rho}\frac{\partial \widetilde{p}}{\partial x} = Y(\infty)\,T'(t) \ . \tag{E.6}$$

The Stokes equation (E.3) may then be expressed as:

$$Y(y)\,T'(t) = Y(\infty)\,T'(t) + \nu\,Y''(y)\,T(t) \ . \tag{E.7}$$

Separation of variables yields the ordinary differential equations:

$$\frac{T'(t)}{T(t)} = \nu\,\frac{Y''(y)}{Y(y) - Y(\infty)} = \text{constant} \ . \tag{E.8}$$

As the time dependence may be anticipated as cosinusoidal (from the free-stream condition that $\tilde{u}(\infty,t) = U_0 AX' \cos\omega t$), the constant in (E.8) may be written in complex form as $i\omega$. Since this is a linear problem, the dependent variable, $\tilde{u}$, may expressed as the real part of the same complex variable for which these equations are then solved. The free-stream boundary condition may be written as $\tilde{u}(\infty,t) = U_0 AX'(\cos\omega t + i\sin\omega t)$ and the equation for T may now be integrated, yielding:

$$T(t) = c_0 e^{i\omega t} . \tag{E.9}$$

The ordinary differential equation for Y takes the form:

$$\nu Y''(y) - i\omega Y(y) = -i\omega Y(\infty) , \tag{E.10}$$

and may be integrated to give the solution:

$$Y(y) = Y(\infty) + c_1 e^{y/\sqrt{\nu/i\omega}} + c_2 e^{-y/\sqrt{\nu/i\omega}} , \tag{E.11}$$

where i and $\sqrt{i}$ are defined as $e^{i\pi/2}$ and $e^{i\pi/4}$ respectively. As the free-stream value of Y must be finite, the constant of integration, c_1 , is zero. Furthermore, the boundary condition at the wall dictates that $c_2 = -Y(\infty)$. The constants, c_0 and $Y(\infty)$, are determined by the free-stream boundary condition so that:

$$\tilde{u}(y,t) \qquad \text{is the real part of} \qquad U_0 AX' e^{i\omega t}(1 - e^{-y/\sqrt{\nu/i\omega}}) . \tag{E.12}$$

Separation of (E.12) into real and imaginary parts yields the solution:

$$\tilde{u}(y,t) = U_0 AX' \left[\cos\omega t - e^{-y/\sqrt{2\nu/\omega}} \cos(\omega t - y/\sqrt{2\nu/\omega})\right] . \tag{E.13}$$

Alternatively, (E.13) may be written as the phasor: $\widetilde{u} = |\widetilde{u}|\cos(\omega t + \phi)$

where $|\widetilde{u}| = U_0 A X' \sqrt{1 - 2e^{-\xi}\cos\xi + e^{-2\xi}}$,

$$\tan\phi = \frac{e^{-\xi}\sin\xi}{1 - e^{-\xi}\cos\xi} ,$$

and ξ is defined as $y/\sqrt{2\nu/\omega}$. (E.14)

The phase and amplitude distributions associated with the phasor form of this Stokes solution are shown in Figures E.1 and E.2. By considering the limiting value of ϕ as the wall is approached, it may be shown to be 45° in advance of its free-stream value.

The dimensionless, independent variable of this solution, ξ , is the distance from the wall normalized by the unsteady, viscous length scale; it is useful in estimating the thickness of the near-wall region which accommodates unsteady effects which differ in magnitude from their asymptotic free-stream values. For the purposes of order-of-magnitude estimates, the unsteady, near-wall layer may be considered to be of the order, $\sqrt{\nu/\omega}$, if unsteady, viscous effects are thought to be important this far from the wall. This provision is often tested through comparisons of $\sqrt{\nu/\omega}$ with estimations of the order of the steady, viscous sublayer thickness, ν/u_τ .

When convective effects are unimportant relative to unsteady ones, the Stokes solution may be used to determine the extent of this near-wall layer. If the time and phase dependence in (E.14) are disregarded, the deterministic velocity may be represented by its amplitude alone. If the boundary of this layer is defined as the wall-normal distance beyond which it differs from its asymptotic, free-stream value by less than 1%, the layer extends to $\xi \simeq 4.1$. For unsteady flows with boundary conditions which result in different Stokes solutions (such as unsteady, fully-developed

channel flow), the resulting layers are usually of comparable thickness. If a dynamic representation of this layer is sought for asymptotic, high-frequency flow, then the complete Stokes solution may be used to determine the same thickness estimated with the amplitude of $\widetilde{u}$, only at each discrete phase of the unsteady event.

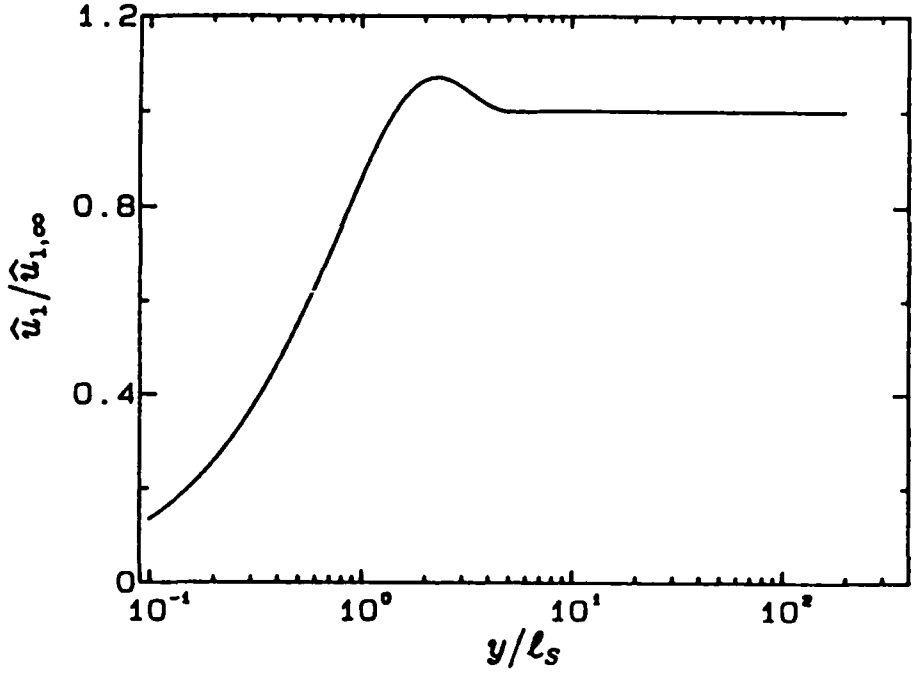

Figure E.1 Variation in velocity phase for the Stokes solution (of the form $\widetilde{u} = |\widetilde{u}|\cos(\omega t + \phi)$).

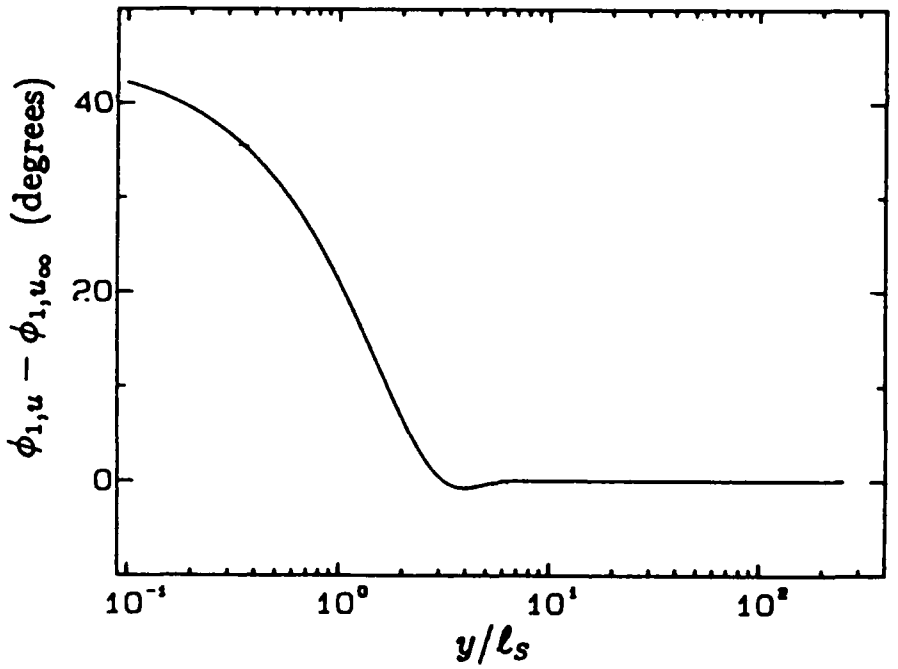

Figure E.2 Variation in velocity amplitude for the Stokes solution (of the form $\widetilde{u} = |\widetilde{u}|\cos(\omega t + \phi)$).

Appendix F

Uncertainty Analysis

The uncertainties in selected measurements made in this study are assessed in this appendix and are reported in terms of the probable error in the measure and an associated confidence level. Since a detailed analysis of the accuracy of every quantity of interest, at each measurement location, was not practical, discussion of additional uncertainties which would be of predominantly local importance is included.

Estimates of the uncertainties in the time-averaged quantities, U, V, $\overline{u'u'}$, $\overline{v'v'}$ and $-\overline{u'v'}$ were made using root-sum-square addition of the errors due to individual effects — a method which has been shown to preserve the statistical probabilities adequately in error-propagation calculations (Kline & McClintock 1953). Of the many possible causes of uncertainty in the laser-Doppler-anemometer measurements of this study, the most significant errors were thought to be due to: (*i*) uncertainty in the precise value of the half angle of intersection of the laser beams, at any given measurement location, and (*ii*) the contribution of electrical and optical noise to uncertainty in individual velocity measurements.

Confidence levels for uncertainty estimates in this study were chosen to be 95% (or 20:1 odds). With this level of confidence, the uncertainty in individual velocity measurements was estimated to be $\pm 0.003\,U_0$ or ± 2 mm/s. This value was deduced from comparisons of the free-stream turbulence measured with the laser-Doppler anemometer used for this study ($\sim 0.8\%$) and with the one used by Jayaraman *et al.* (1982) of $\sim 0.5\%$. These measures were then compared with the noise level detected in measurements of the velocity of a stationary, reflective object positioned on the top wall of the apparatus, using the same equipment ($\sim 0.4\%$), so that an estimate of the order of the noise contribution could be made. The uncertainty in the half angle of intersecting beams of laser light was estimated from their measured

TABLE F.1

Uncertainty Estimates for Mean Measures

Measure	Typical Value	Estimated Uncertainty	Relative Uncertainty
U	300 mm/s	$\pm$ 3 mm/s	$\pm$ 1%
V	12 mm/s	$\pm$ 3 mm/s	$\pm$ 25%
$\overline{u'u'}$	2500 mm^2/s^2	$\pm$ 170 mm^2/s^2	$\pm$ 6%
$\overline{v'v'}$	1000 mm^2/s^2	$\pm$ 110 mm^2/s^2	$\pm$ 10%
$-\overline{u'v'}$	650 mm^2/s^2	$\pm$ 90 mm^2/s^2	$\pm$ 13%

separation, when projected onto a screen adjacent to the apparatus. Variations in the beam separations, at different positions in the boundary layer, were assessed as a relative uncertainty of $\sim 1\%$ of the half angle with 95% confidence (as indicated in Table 3.5).

In first-moment measures such as U, the effects of noise in individual readings were rendered negligible by the large numbers of samples taken. Thus a relative error of $\pm 1\%$, attributable to uncertainties in the half angle of beam intersection, was the most important factor in estimates at this confidence level. Now U was typically of the order of 30 times larger than V, and slight, local misalignment of the optical system was thought to contribute most strongly to errors in V. Since the precision with which the beams used for measurement of the v component of velocity were perpendicular to the top wall of the apparatus was estimated as $\pm 1°$, uncertainty in V was estimated at $\pm 0.01\,U$. Typical values of U, V, $\overline{u'u'}$, $\overline{v'v'}$ and $-\overline{u'v'}$, together with their estimated uncertainties, are shown in Table F.1.

Uncertainties in measures of second moments such as $\overline{u'u'}$, $\overline{v'v'}$ and $-\overline{u'v'}$ were devised in normalized form, using the estimated uncertainties in individual velocity measurements ($\pm 0.003\,U_0$). By applying the root-sum-square addition procedure to individual measurements (as outlined by Eaton & Johnston 1980), the uncertainties in normalized values of $\overline{u'u'}$, $\overline{v'v'}$ and $-\overline{u'v'}$ could be expressed as their local, normalized measure multiplied by an error term representing the uncertainty

TABLE F.2

Uncertainty Estimates for Turbulent Stress Measurements

$\overline{u_i'u_j'}/U_0^2$	$\delta(\overline{u_i'u_j'})/U_0^2$	$\delta(\overline{u_i'u_j'})/\overline{u_i'u_j'}$
0.01	0.0005	± 5%
0.005	0.0003	± 7%
0.001	0.0001	± 15%
0.0001	0.00005	± 50%

in individual measurements. These uncertainties were estimated for a range of normalized values typical of those found throughout the boundary layer and are shown in Table F.2.

Absolute errors in deterministic measures, such as amplitudes and phases of unsteady quantities, would, in general, be of the order of the equivalent time-averaged measures. Obviously the uncertainty of measurements taken at one discrete phase in the cycle would be sensibly larger than that of time-averaged ones, to reflect the reduced number of samples from which these measures were deduced. Now uncertainties in amplitude measures might be significantly larger than those of the corresponding time-averaged quantities if the unsteady component were of sufficiently small size that rounding errors in the Fourier-transformation algorithms became appreciable sources of error. Likewise, phase information deduced from measures, the unsteady components of which were small, would be most untrustworthy. Moreover, the variation of deterministic measures across the boundary layer was such that they fell to negligibly small values in the vicinity of $y/D_c \simeq 0.1$. In this region, relative errors in phase and amplitude results would become extremely large. Consequently, any result which incorporated a deterministic measure would have to be interpreted with great caution in this region.

In the calculation of production terms, additional uncertainty was introduced through estimation of a gradient from neighboring measures of mean velocity. Although uncertainties in these terms were not evaluated explicitly, they would be

sensibly larger than the local turbulent stresses incorporated in these production terms.

An independent check on measures of the mean, streamwise velocity was carried out with a constant-head probe positioned in the free stream. Pressure differences were measured by a transducer which had been calibrated against the differences in pressure due to two columns of water, the difference in heights of which could be gauged accurately by micrometer. Since the free-stream velocity deduced by this technique was within a small percentage of that measured with the laser-Doppler anemometer, the absolute measure of beam half angle (from which the u–f calibration constant for the laser-Doppler anemometer was devised) was considered sufficiently accurate. As no independent check on the corresponding calibration constant for the normal velocity was available, it could only be estimated from measurements of the half angle of intersection of laser beams.

The accuracy of positioning of the probe volume of the laser-Doppler anemometer was estimated as:

(*i*) ± 2 mm in the streamwise (x) direction,

(*ii*) ± 2 mm in the spanwise (z) direction,

(*iii*) ± 0.05 mm in the normal (y) direction, near the wall, and

(*iv*) ± 1 mm in the normal (y) direction, at the measurement locations furthest from the wall,

with the same confidence level used earlier. Two uncertainty estimates are given for the accuracy of the wall-normal position of the probe volume, as only near the wall could it be checked reliably (in the manner described by Jayaraman *et al.* 1982). When measurements were made in the outer parts of the boundary layer, uncertainty in the absolute distance from the wall might result from slight differences between the direction of traversing of the measurement system and the perpendicular to the top wall of the apparatus.

The diameter of the measuring volume (the portion of the probe volume imaged by the receiving optics) was ~ 0.125 mm and this dimension was about 2.5 times larger than the spacing between the eight points nearest the wall at which data were taken. This shortcoming would affect estimations of velocity gradients in the near-wall region. It would also imply that there was interference between the measuring volume and the wall over at least the first two or three points and, in the event of imperfect coincidence of the interference patterns of blue and green light, possibly several more. These uncertainties might provide good grounds for disregarding some near-wall measurements because of untrustworthiness. To judge from the qualification data of §4, measures of V, $\overline{v'v'}$ and $-\overline{u'v'}$ might have suffered from this problem in the six or seven data points nearest to the wall, which corresponded to the region in which $y^+ < 10$. However, it was not apparent from the qualification data that these same shortcomings affected measures of U and $\overline{u'u'}$.

Appendix G

Data

Sets of the phase-averaged raw data of this study have been stored on diskettes and are available to interested researchers on request. The medium on which these data are presently available is 5.25 inch floppy diskettes, 40 tracks per side with 48 tracks per inch, formatted on both sides at double density, with a total capacity of 360 Kbytes — the kind of diskette which is currently most widely used for desk-top computers. This medium was chosen in the hope that no interested researcher would be denied access to these data through hardware limitations; it was also preferred for ease of copying and distribution.

Each diskette contained a complete boundary-layer profile of phase-averaged measurements made at one X location, at one frequency of forced, free-stream unsteadiness. A documentation file describing the structure of the data set and a sample data-reduction program were also included on each diskette.

In the interests of economy of disk space, each boundary-layer profile of phase-averaged measurements was described by two files:

(*i*) A sequential-access file of formatted data containing a title, the frequency of forced unsteadiness, the y locations at which measurements were made and calibration constants. The name of this file took the form: `_____.DT1`.

(*ii*) A direct-access file of unformatted integers representing the phase-averaged values, $\langle u \rangle$, $\langle v \rangle$, $\langle uu \rangle$, $\langle vv \rangle$ and $\langle uv \rangle$, at every one of the 512 discrete phases in each unsteady cycle, for each y location in the profile. The name of this second file was of the form: `_____.DT2`.

The root names of the files containing these sets of measurements, at each X location and frequency of forced unsteadiness, are given in Table G.1.

TABLE G.1

Phase-Averaged Data Files

f (Hz)	$X' = 0.0$	$X' = 0.45$	$X' = 0.63$
0.1			UP0130
0.2	UP0225	UP0228	UP0230
0.5	UP0525	UP0528	UP0530
0.8	UP0825	UP0828	UP0830
1.0	UP1025	UP1028	UP1030
1.6	UP1625	UP1628	UP1630
2.0	UP2025	UP2028	UP2030

Selected graphical and tabular information is also available in microfiche form. For each of the three X stations at which data were taken, profiles of velocity measures made under unsteady conditions are presented at all frequencies of forced perturbation of the free stream. These measures comprise, in part, the time-averaged quantities: U, V, $\overline{u'u'}$, $\overline{v'v'}$ and $-\overline{u'v'}$. They also include the amplitudes: $\widehat{u}_1$, $\widehat{v}_1$, $\widehat{u'u'}_1$, $\widehat{v'v'}_1$ and $\widehat{u'v'}_1$, and the phases: $\phi_{1,u}$, $\phi_{1,v}$, $\phi_{1,u'u'}$, $\phi_{1,v'v'}$ and $\phi_{1,-u'v'}$. The microfiches of graphs and tables of these quantities are available from the authors on request.

END

10-81

DTIC